Reclamation of metal values from TiO_2 production waste residues.

Recovery of vanadium, scandium and niobium

Terence Makanyire

School of Chemical and Process Engineering

The University of Leeds

Submitted in accordance with the requirements for the degree of

Doctor of Philosophy

Institute of Materials
Research

September 2016

Declaration

The candidate confirms that the work submitted is his own, except where work which has formed part of jointly authored publications has been included. The contribution of the candidate and the other authors to this work has been explicitly indicated below. The candidate confirms that appropriate credit has been given within the thesis where reference has been made to the work of others.

List of publications

Some results from this thesis have been published and presented in the following journals and proceedings:

1. Makanyire, T and Jha, A. (*accepted*)*Kinetics of hydrochloric acid leaching of niobium from TiO2 residues*, International Journal of Mineral Processing.

2. Makanyire, T., Sanchez-Segado, S., and Jha, A. (2016) *Separation And Recovery Of Critical Metal Ions Using Ionic Liquids.* Adv. Manuf. 4.1, p.33-46.

3. Sanchez-Segado, S., Makanyire, T., Escudero-Castejon, L., Hara, Y. and Jha, A. (2015). *Reclamation of Reactive Metal Oxides from Complex Minerals Using Alkali Roasting and Leaching - An Improved Approach to Process Engineering.* 46(23), p.2059-2080.

4. Makanyire, T., Jha, A. and Sutcliffe, S. *A Kinetic Analysis of Acid Leaching of Niobium and Zirconium from Titania Waste Residue Stream: An Energy Efficient Methodology for the Reclamation of Metal Values.* Energy Technology 2015: Carbon Dioxide Management and Other Technologies, TMS Annual Meeting & Exhibition, March 15-19, 2015, Orlando, Florida, 115-122.

5. Makanyire, T. and Jha, A. *Chemical Characterization of Transition Metal (Nb, V, Zr) Impurities in Rutile.* Rare Metal Technology, TMS Annual Meeting & Exhibition, February 16-20, 2014, San Diego, California, 121-126.

All the literature and results related to vanadium, scandium, titanium and niobium presented in the papers (and in the thesis) were obtained and analysed by the author of the thesis. The author of thesis wrote the drafts of the papers and the supervisor (Animesh Jha) revised them before sending them for publication. Sections written by other authors were not included in the thesis.

List of potential publications and patents

Patent: Process for the recovery of scandium and vanadium from TiO_2 residue streams

Journal publication Kinetics modelling of thorium dissolution during reclamation of metal values from TiO_2 manufacture waste residue streams

Journal publication The dissolution and chemical properties of vanadium in solvent rutile (TiO_2) lattice

Journal publication Kinetics modelling of vanadium dissolution from TiO_2 plant residues (*Accepted for TMS conference 2017*)

I dedicate this thesis to my loving parents, Farai and Svunurayi Makanyire and to my brother, Eugene Makanyire ...

Acknowledgements

And I am highly grateful to God for His blessings that continue to flow into my life, because of You, I made it through against all odds.

With a great pleasure, I would like to acknowledge the inspirational instruction and guidance of my supervisors, Prof. Animesh Jha and Dr. Stephen Sutcliffe (Huntsman Pigments and Additives). All the training on XRD, XRF and AAS provided by Dr. T. Comyn and Mr. S. Lloyd is highly appreciated, as is the support provided by Mr. M. Javed, Dr. S. Sanchez-Segado and Dr. Y. Hara on a regular basis. I would also like to acknowledge the support and assistance given to me by staff at Huntsman Pigments and Additives, who have contributed ideas and advice on both academic and industrial areas of the project.

I am very grateful to the following colleagues: Steven Parirenyatwa, Lidia Escudero-Castejo, Steven Mudenda and my girlfriend Vikki Mazive, for their support, encouragement and motivation.

Last but not least, I would like to acknowledge the EPSRC and Huntsman Pigments and Additives for the financial support which has made it possible for this project to be carried out.

Abstract

A novel process for recovery of niobium, vanadium and scandium from TiO_2 residues in three stages consisting of acid leaching, selective precipitation and oxidative alkali leaching has been developed using a batch leach test rig. While technologies for recovering these valuable metals from various minerals as co-products or by-products are commercially available, they are not currently used for recovering them in combination. An integrated process for reclamation of the metals could increase the total values recovered while reducing the objectives to their subsequent disposal.

Three batches of TiO_2 filter cake were obtained from Huntsman Pigments and Additives between 2012 and 2014, and were analysed using ICP-OES, TGA, XRD, SEM-EDX and XRF. The samples contained different amounts of unreacted ore and coke, together with hydrated oxides of a wide spectrum of metals such as vanadium, scandium, iron and niobium.

Initially, Pourbaix diagrams were utilised for mapping out when the metals would precipitate or be in solution depending on their concentration, solution pH and electrochemical potential. The information was compared with established metal recovery processes to determine the recovery route. This study showed that the metals could be separated by selectively precipitating and filtering niobium from acidic media at pH $\approx$ 1 followed by controlled co-precipitation of vanadium and iron at pH $\approx$ 2 and scandium at pH $\approx$ 4. It was also determined that further concentration enhancement could be achieved by oxidative alkali leaching after the selective precipitation steps.

Following establishment of the metal recovery route, experiments were carried out to sequentially study the effects of temperature, lixiviant concentration, reaction time, pH, stirring speed, solid-liquid ratio and oxidant concentration on dissolution and precipitation of the metals. The chloride process of TiO_2 production is operated under reducing conditions therefore most hydroxides in the filter cake are in a reduced state. $NaNO_3$ was used as an oxidant for improving metal recovery and selectivity during Na_2CO_3 leaching. Vanadium purification

by salt roasting was investigated and the conventional NH_4VO_3 precipitation route was utilised for vanadium precipitation from pregnant solutions.

Recoveries of over 80 % were achieved for vanadium and niobium, with grades of 99.5 % and 16 % respectively. Zirconium, titanium and thorium were the key impurities in the niobium-rich precipitates. Nearly all the scandium was recovered with a grade of at least 50 % in an alkali solution where rare earths were the main impurities. Adding $NaNO_3$ to the alkali leaching systems significantly improved the extraction of vanadium and scandium, while niobium's selective precipitation at pH 1 was catalysed by sulphate ions.

The random pore model governs the dissolution processes, with all acid leaching kinetics being controlled by pore diffusion and alkali by surface reaction. The developed process opens up opportunities for recovery of other metals, particularly titanium, iron and REE and can be employed for recovery of the metals from filter cake already landfilled.

Table of contents

List of figures

List of tables

Nomenclature

Greek Symbols

α	conversion
ϵ	porosity of particle, ϵ_o initial porosity of particle
λ	wavelength of incident x-rays
ψ	dimensionless structural parameter of random pore model ($\psi > 0$)
ρ_m	molar density (mol cm^{-3})
θ	angle of incidence
Å	Angstrom (10^{-10} m)

Other Symbols

A_g	grain external surface area (cm^2)
A_o	pre-exponential frequency factor
b	stoichiometric coefficient
C_A	concentration of fluid reactant (mol L^{-1})
$C_{A,f}$	bulk concentration of fluid reactant (mol L^{-1})
d	lattice plane spacing
D_e	effective diffusivity of a fluid in porous solid (cm^2 s^{-1})
E_o	activation energy (kJ mol^{-1})
F_g	grain shape factor
L_o	Initial characteristic length of a pore per unit volume

R universal gas constant (8.314 kJ mol^{-1} K^{-1})

r rate of reaction (mol m^{-2} min^{-1})

R_p particle radius (m)

s_o Initial molar surface area

T reaction temperature (K or °C as specified)

t time (minutes)

V volume of solution (ml)

V_g volume of grain (cm^3)

E^o electrochemical potential (volts)

P Pairing energy

Acronyms / Abbreviations

AMV ammonium meta vanadate

CFSE Crystal Field Stabilisation Energy

OSPE Octahedral Site Preference Energy

Chapter 1

Introduction

1.1 Problem statement

Residues from production of pigment grade TiO_2 by the chloride process often have chlorides and oxychlorides of vanadium, scandium and niobium, which if separated and purified, have a very high industrial value. They are used extensively in rapidly growing industries such as the manufacture of mobile phone components, catalysts, HSLA steel, and in energy conversion and storage devices. All three elements are available in higher concentrations in the waste residues than in average mineral concentrates from mine sites, yet there are currently no established technologies for recovery of any metal values from the chloride process waste. This is due to several reasons:

- The chloride process traditionally operates on high grade ores, implying a low iron content with high levels of impurities, hence offers limited value for steel or water treatment.
- The filter cake is wet with chloride solution, making it unattractive for blast furnace use.
- Processing of the waste may concentrate species such as thorium to hazardous levels.
- Limited value from valuable components at historic rates and compositions.
- Capital costs and the potential complexity of a metal recovery process usually deter investors from such projects.

Recovery and use of co-products opens up opportunities for lower quality feedstocks to be used in the TiO_2 production process. The overall research aim of this thesis was therefore to develop and optimise processing steps for the recovery of V, Sc, and Nb oxides from the residues of TiO_2 powder production by the chloride process, for beneficial high-value industrial use. The processing steps developed will greatly enhance the process efficiency by reducing waste volumes and open up opportunities for recovery of other components. The integrated metal recovery process should ideally be a closed loop with all reagents economically regenerated to minimise its environmental impact. The aim of the project was achieved by addressing the following key objectives:

i Chemically analyse the residues (filter cake) from production of pigment grade TiO_2 using the chloride process.

ii Construct Pourbaix diagrams to guide selective leaching and precipitation reactions from thermodynamic considerations.

iii Investigate experimental leaching conditions to obtain a solution of the valuable metals (V, Sc and Nb): vary temperature, solid-liquid ratio, pH, acid concentration and stirring speed.

iv Investigate precipitation variables: temperature, pH and precipitant concentration

v Monitor any changes to concentrations and environmental hazards of metals due to concentrating effects of the recovery processes developed

vi Develop the kinetics models for key reactions taking place in the unit processes.

vii Consider corrosive nature of any chemical solutions used.

To adequately achieve the aforementioned objectives, several challenges had to be addressed:

i The effect of as-received filter cake composition on overall recoveries and purities of the valuable metals.

ii The effect of radionuclides concentrations on separation and purification of valuable metals.

iii The effect of resource recovery on classification of remaining waste.

The process for metal reclamation will be developed by using filter cake from Huntsman Pigments and Additives' chloride process which contains the valuable metals as hydrated oxides.

1.2 Structure of thesis document

The thesis has 7 chapters;

- Chapter 1 is almost over; chapter 2 presents the background information related to mineral extraction, summarises the chloride process for TiO_2 production, justifies the recovery of V, Sc and Nb from TiO_2 production residues and reviews the current processes employed for recovery of V, Sc and Nb from mineral wastes. The theory behind the mineral characterisation techniques employed in this project is also presented as is the theory on kinetics studies.
- Chapter 3 presents the details relating characterisation and handling of the different batches of as-received cake obtained from Huntsman Pigments and Additives' Greatham site between 2012 and 2014.
- Chapter 4 presents the solution chemistry and fundamental theory governing the selection of unit processes and process design for the recovery of vanadium, scandium and niobium values.
- Chapter 5 presents the experimental procedures employed for the dissolution of filter cake, separation of valuable metals by selective precipitation and their purification by roasting and leaching processes.
- Chapter 6 presents the results from batch leaching experiments carried out under various leaching conditions and the kinetics studies for modelling of the dissolution of filter cake and purification of valuable metals. Results from dissolution and chemical properties of vanadium in rutile are also presented.
- Chapter 7 gives the conclusions made from the experimental work and kinetics studies as well as the future work and major achievements.

A bibliography can be found at the back of the thesis and a nomenclature in the preamble.

Chapter 2

Literature review

The global annual consumption of TiO_2 in 2015 was in excess of 6 million tonnes [1]. TiO_2 is predominantly manufactured by either the chloride process (CP) or the sulphate process (SP), with the chloride process being the preferred route for producing high purity TiO_2. TiO_2 produced by the sulphate route is preferred for applications where wear may be a problem since it tends to be less abrasive [2]. Chapter 2 presents an overview of TiO_2 manufacturing by the CP and summarises published literature relevant to recovery of vanadium, scandium and niobium from various mineral processing wastes. Kinetics studies theory and materials characterisation techniques are also presented at the end of the chapter.

2.1 Background

2.1.1 Mineralogy and crystal chemistry

Most rock-forming minerals are ionic compounds which incorporate minor amounts of foreign ions into their crystal lattice. Incoporation of foreign ions is mainly due to ionic substitutions, governed by size and charge of the involved ions. It is well known that there is a preferential association of certain elements in natural assemblages due to factors that allow easy substitutions between the elements. Goldschmidt [3] suggested that a trace ion capable of making a larger contribution to the energy of a crystal structure is capable of substituting the main ion in a crystal structure provided the following rules of substitution are obeyed:

i If two ions have the same radius and charge, they can form a solid solution in a given mineral with equal ease in amounts roughly proportional to their abundances. The ionic radii difference should be less than 15 % otherwise the substitution is limited or rare when radii differ by 15 – 30 % and non-existent for radii differences greater than 30 %.

ii When two ions with same charge but different radii compete for a particular lattice site, the ion with smaller radius would be incorporated preferentially because the smaller ion forms a stronger ionic bond.

iii When two ions with similar radii but different charges compete for a particular lattice site, the ion with higher charge would be incorporated preferentially because it forms a stronger ionic bond.

iv Ions whose charge differs by one unit may substitute for one another provided electrical neutrality is maintained by coupled or compensatory substitution and generally, very little or no substitution occurs when ionic charge difference is greater than one unit.

Fig. 2.1 shows unit cells of rutile (2.1a) and ilmenite (2.1b) where titanium is octahedrally coordinated to six oxygens, with each of the oxygens surrounded by three Ti^{4+} ions as corners of an equilateral triangle. Vanadium ions (V^{5+}

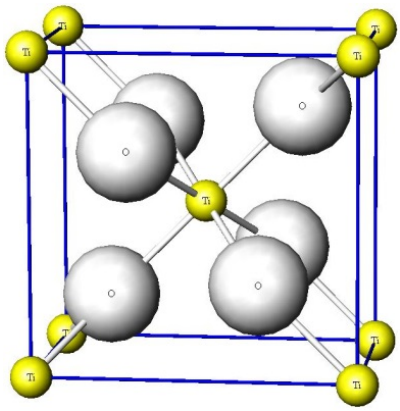

(a) Rutile crystal structure

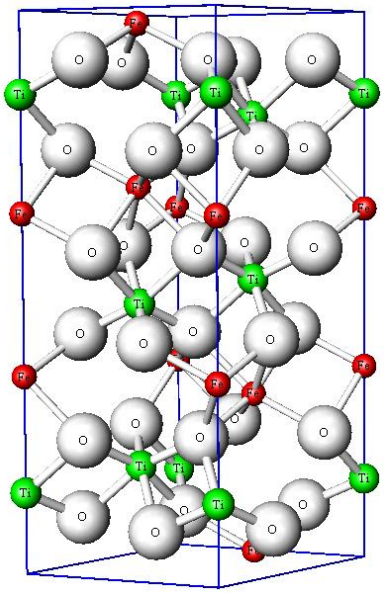

(b) Ilmenite crystal structure

Fig. 2.1 The crystal structures of rutile (2.1a) and ilmenite (2.1b) [4].

= 0.68 Å, V^{4+} = 0.72 Å) are more likely to substitute titanium (Ti^{4+} = 0.74 Å) ions at the octahedral sites in minerals such as natural rutile and ilmenite compared to the bigger niobium ions (Nb^{5+} = 0.78 Å, Nb^{4+} = 0.82 Å, Nb^{3+} = 0.86 Å), and scandium (Sc^{3+} = 0.89 Å).

Although the Goldschmidt rules can explain vanadium substituting titanium in minerals such as natural rutile, they are not adequate for predicting the relative distributions of trace elements in minerals. Mason [5] observed that two elements may be able to substitute for one another in one mineral and not in another. The lack of association between some ions in different minerals can be explained by the crystal field theory, which is based on the effect of crystal structure on *d*-orbitals in transition metals. The crystal field theory describes effects of electrostatic fields on the energy levels of valence electrons of the trace metal (transition metal) when surrounded by negatively charged ligands (oxygen in the case of rutile) [6]. In the absence of the ligands, the electrons in *d*-orbitals are energetically equivalent, with the *d* electrons having equal probability of being located in any of the *d*-orbitals. When ligands are introduced, for example when titanium is in an octahedral coordination, the five $3d$ orbitals do not experience the same interaction due to the difference in their spatial configuration in relation to the ligands [6, 7]. Fig. 2.2 shows the five *d*-orbitals in an octahedral field of ligands.

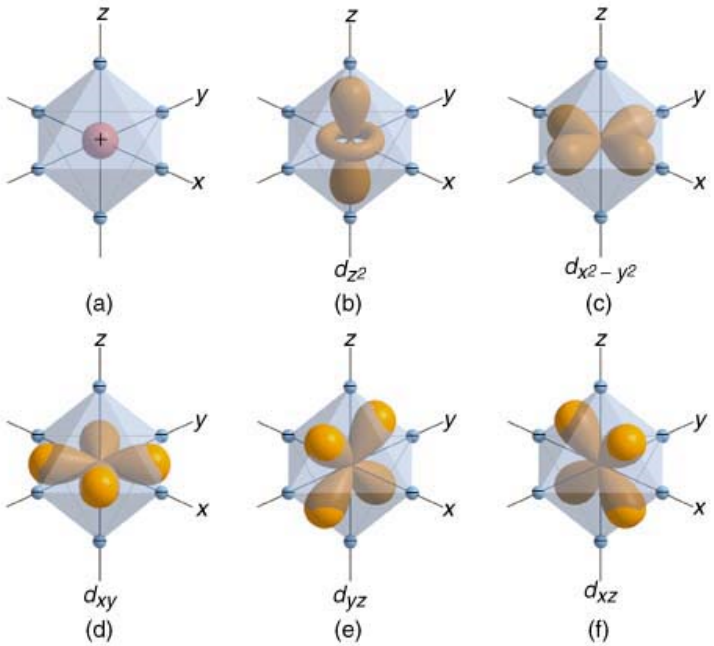

Fig. 2.2 The five d-orbitals in an octahedral field of ligands [8].

The six ligands repel electrons in the lobes of the d_{z^2} and $d_{x^2-y^2}$ orbitals (projecting along the cartesian axes - e_g) to a greater extent than the lobes of the d_{xy}, d_{yz} and d_{xz} orbitals (directed between the axis – t_{2g}), inducing energy separation between the orbital groups.

Fig. 2.3 diagrammatically summarises the splitting of the five normally degenerate d-orbitals.

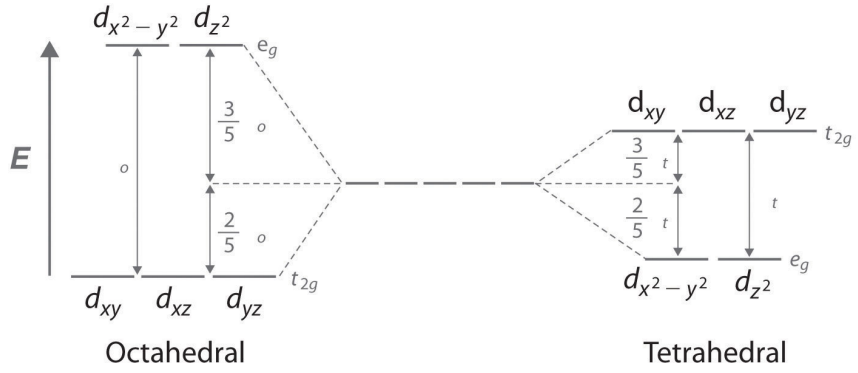

Fig. 2.3 Splitting of the degenerate d-orbitals due to an octahedral ligand field (left) and tetrahedral ligand field (right) [9]

The energy difference between the groups of orbitals is called the crystal-field stabilisation energy (CFSE) and the difference between the stabilisation energies of the octahedral and tetrahedral coordination of the same element is the octahedral site preference energy (OSPE) and is useful in interpretation of cation distributions in mineral forming processes and crystal structures. Nearly all mineral phases contain an abundance of regular octahedral and tetrahedral 'holes' and the concentration of trace ions will be given by their relative crystal field stabilisations in such sites. Ti^{4+} ([Ar] $3d^0$), Sc^{3+} ([Ar] $3d^0$), V^{3+} ([Ar] $3d^2$), V^{4+} ([Ar] $3d^1$), Nb^{5+} ([Ar] $3d^{10}$) and V^{5+} ([Ar] $3d^0$) have no or low octahedral site preference energies and therefore occupy both octahedral and tetrahedral holes in minerals. V^{2+} ([Ar] $3d^3$) has high OSPE, meaning that it is expected to be exclusively found in octahedral positions. Due to its small ionic charge, it can also occupy tetrahedral holes.

Fig. 2.4 and Fig. 2.5 present the curves for uptake of transition metal ions into silicate minerals crystallising from basaltic magma, showing that the cations with highest OSPE tend to enrich early and therefore concentrate in early crystallising minerals compared to cations with zero OSPE, which can occupy both octahedral and tetrahedral sites in different minerals.

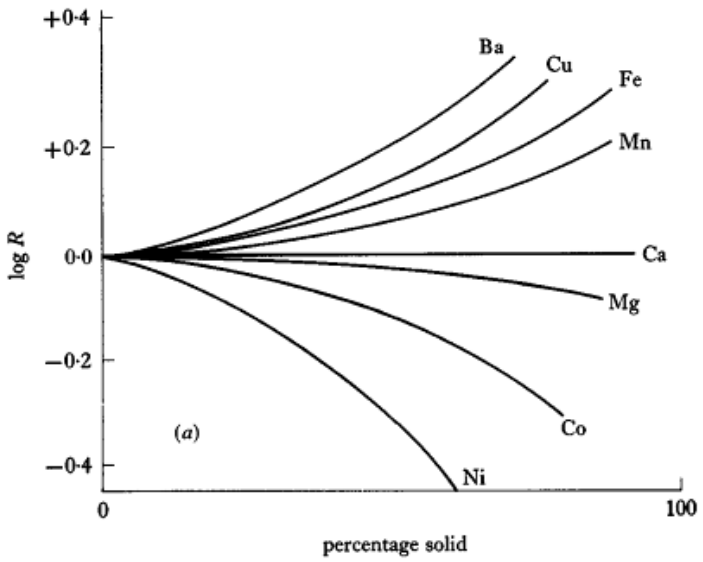

Fig. 2.4 Magmatic differentiation of transition divalent metal ions during crystallisation of silicate minerals from basaltic magma [7]. **R** represents the ratio of ions in magma to the concentration in initial liquid.

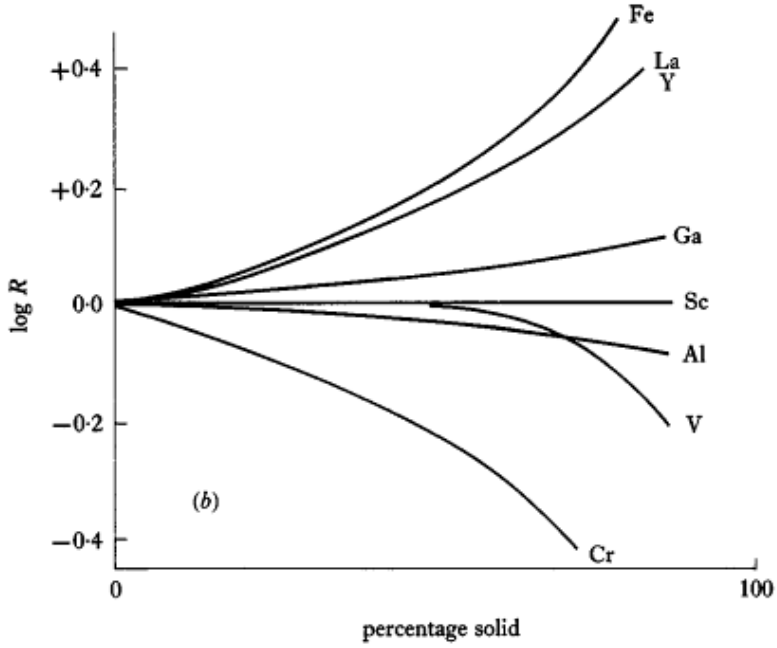

Fig. 2.5 Magmatic differentiation of transition trivalent metal ions during crystallisation of silicate minerals from basaltic magma [7]. **R** represents the ratio of ions in magma to the concentration in initial liquid.

2.1.2 Ore breakdown and process classification

Ore and concentrate extraction is almost wholly carried out by mineral processing, pyrometallurgy, hydrometallurgy or electrometallurgy. Pyrometallurgy involves high temperatures whereas hydrometallurgy is usually carried out at room temperatures in aqueous media. Electrometallurgy on the other hand uses electrolysis for separation at both high and low temperatures [10].

Scandium, vanadium and niobium are electropositive in character and usually occur in nature as refractory minerals. Generally, breakdown of refractory metals is achieved by employing strong chemical reagents which include but not limited to concentrated acids, alkali, fluorides, or gaseous chlorine at high temperature and specialised chemical plants are usually necessary [11]. It is often necessary to beneficiate the ore by initially employing mineral processing techniques to reduce chemical reagent wastage. When iron content of an ore is same as or more than the concentration of desired mineral, iron removal with magnetic separation techniques prior to leaching is beneficial.

Dilute acid and dilute alkali leaching are usually the first choice techniques employed for ore breakdown and other techniques are only ever employed when these cheaper ones cannot break the ore.

2.1.3 Leaching of ions

Cations in a crystal respond to their chemical environment according to their relative stabilities in crystal structures and in hydrated/complex ions in solution. Analysis of thermodynamic data has shown that oxide phases with high standard enthalpies of formation are the least likely to dissolve in aqueous media [12]. This means that cations with high oxidation states, including TiO_2, Nb_2O_5, Fe_2O_3 (compared to FeO) and Sc_2O_3, have large enthalpy of formation values and hence are least soluble. In addition to such thermodynamic analysis, other factors involving the reaction mechanisms and kinetics need to be considered. Detailed thermodynamics and theoretical considerations for process design are presented in chapter 4.

Leaching of ions from octahedral sites takes place through substitution reactions, which depend on kinetic and mechanistic factors. When a mineral is leached, an ion is removed from its site in a crystal structure into the aqueous phase. As illustrated in previous sections, most transition metal ions prefer to be in octahedral sites and in aqueous solutions, they generally form hexahydrated ions with crystal field splitting energies that are comparable to their oxide

crystal structures. Leaching of ions from their octahedral sites depends largely on whether lixiviant molecules can penetrate into the environment about the cation and crystal field theory can provide insights into the substitution reactions involving transition metal cations. Based on the crystal field theory and the transition state theory, it can be argued that cations with the most resistance to leaching/substitution reactions are the ones with the $3d^3$, $3d^8$ and low spin $3d^6$ configurations which have high octahedral site preference energies. These theories also explain the enrichment of cations with high CFSE such as Cr^{3+} and Ni^{2+} during metamorphic recrystallization processes that involve inter-granular aqueous and saline solutions.

Simple agitated batch processes are usually used for carrying out acid leaching. These processes are run under strict conditions including acid concentration, residence time and temperature. When employing batch leaching processes, provision for intermediate storage of at least one batch prior to separation of the liquid from the solid phase is often required [11]. The requirements of intermediate storage and continuous charging and discharging operations can be overcome by using a continuous process.

Industrial scale breakdown of an ore with concentrated acid is only considered feasible if the concentration of the desired mineral is high and the mineral is of environmental or economic importance because high concentration acid leaching presents corrosion problems, which often require expensive materials of construction such as cast iron, tantalum iron or high silicon iron. Acid leaching processes usually use sulphuric acid because it is cheaper, less corrosive and has a higher boiling temperature than most other acids.

Refractory ores can also be broken down using either molten sodium hydroxide or hot concentrated solution to form an oxide, hydroxide or hydrated oxide of the refractory metal. Purification of the ore can further be enhanced by dilute acid washing. Most alkali leaching processes are simple batch operations in mild steel, stainless steel or cast iron vessels. Stirrer design and agitation are not as difficult as with acid leaching since there are no seriously corrosive fumes evolved. Compared to acid leaching, alkali leaching usually requires the particle size of the ore to be much smaller because the alkali is more selective of the material to be leached and therefore does not appreciably react with unwanted gangue [11].

2.1.4 The chloride process

Huntsman Pigments and Additives, from whom we have received filter cake, operates a chloride process for TiO_2 production. The chloride process involves reacting rutile or TiO_2 slag with petroleum coke and chlorine gas at high temperatures to form a vapour of titanium tetrachloride [13]. The impure dry ore is firstly fed into a bed fluidised by an air stream at a temperature of about 650 °C and crushed coke is fed as a reductant. The coke ignites, further increasing the reactor temperature to about 1000 °C and at this point, air is replaced by chlorine gas, allowing formation of gaseous titanium tetrachloride ($TiCl_4$) as shown by equation 2.1.

$$2TiO_2 + 4Cl_2 + 3C \longrightarrow 2TiCl_4 + 2CO + CO_2 \tag{2.1}$$

In equation 2.1, the ratio of CO to CO_2 depends on the reaction temperature, which consequently depends on ore type. A typical CO to CO_2 ratio is in the region of 0.3 - 0.7. Following the chlorination process, cyclonic separation is employed for removal of unreacted components and non-volatile metal chlorides from the $TiCl_4$. Chlorides of vanadium usually follow $TiCl_4$ through the process due to the similarity in their vapour pressures. To separate the vanadium from $TiCl_4$, the $TiCl_4$ gas is condensed and reducing agents such as hydrogen sulphide, powdered copper or organic materials are added to reduce VCl_4 and $VOCl_3$ to the less volatile VCl_3. This permits separation of vanadium and titanium chlorides by fractional distillation [14]. Pure TiO_2 crystals are subsequently produced by oxidation of the purified $TiCl_4$ at a temperature in the region of 800 - 1750 °C as shown by equation 2.2 [15, 16].

$$TiCl_4 + O_2 \longrightarrow TiO_2 + Cl_2 \tag{2.2}$$

The waste stream coming out of the gas cyclone is composed of many hazardous metal chlorides together with unreacted ore, coke and SiO_2. The metal chlorides are made less hazardous by converting them to metal hydroxides using lime. Most of the metal chlorides precipitate as hydroxides at pH 7 upon addition of lime and are part of the filter cake in which vanadium, scandium and niobium are captured. Calcium chloride and some metal chlorides such as those of magnesium and manganese do not precipitate and therefore form the liquid effluent.

Figure 2.6 shows the key processes preceding production of filter cake from which vanadium, scandium and niobium are recovered.

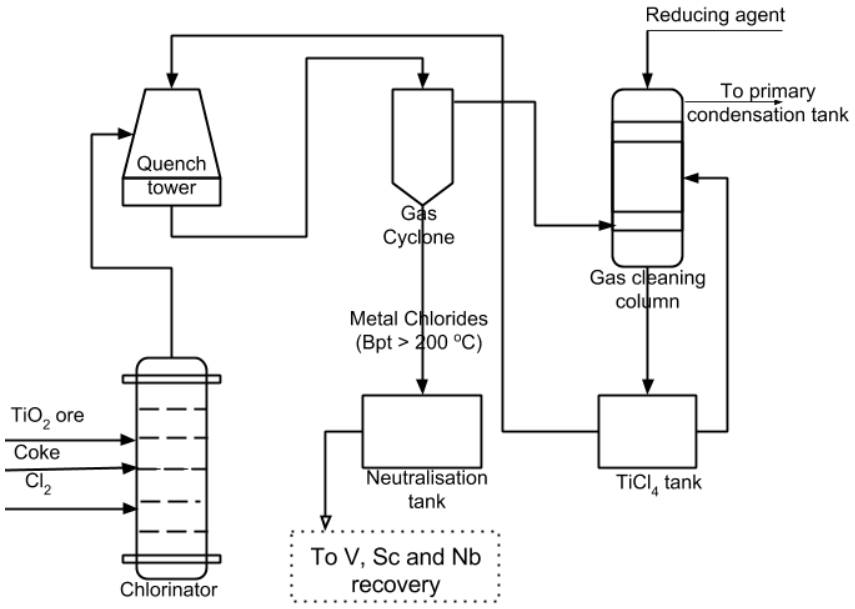

Fig. 2.6 The key steps in the chloride process, highlighting the waste from which V, Sc and Nb are recovered

Table 2.1 shows the typical filter cake composition supplied by Huntsman Pigments and Additives.

Table 2.1 Neutralised filter cake compositions supplied by Huntsman Pigments and Additives

Coke	TiO_2	$Fe(OH)_2$	$Al(OH)_3$	SiO_2	$Ti(OH)_4$	$Nb(OH)_5$	$Si(OH)_4$	$VO(OH)_3$
31.1	27.8	18.5	8.1	2.8	2.2	1.5	1.4	1.4

$Ti(OH)_3$	Al_2O_3	$Cr(OH)_3$	$Zr(OH)_4$	ZrO_2
1.3	1.2	0.6	0.3	0.2

2.1.5 Why recover from TiO_2 residues?

Commercial production of pigment grade TiO_2 using the chloride process generates significant quantities of byproducts, composed of unreacted coke, unreacted ore, and a mixture of metal chlorides and oxychlorides. For disposal in the UK, this material is rendered non-hazardous by neutralising with lime, converting the metal chlorides to stable filterable hydroxides, and the filter cake is then disposed of at high cost at a landfill site. Depending on the type

of feedstock used, 0.6 - 1 tonne of wet, neutralised waste is generated per tonne of pure TiO_2 produced. Clearly, recovery of the metal values could have a positive impact on the economics of TiO_2 production and waste management. Developing a process that provides for the efficient recovery of vanadium and niobium at the same time as scandium would be an advancement in the art. Key benefits of recovering these valuable metals from TiO_2 waste include:

i The metal values that are recovered are increased at the same time that the objectives to subsequent disposal of the material are reduced.

ii Recovery from waste will offer a much more sustainable option than mining these minerals in environmentally sensitive parts of the world, and then transporting them for further beneficiation and purification.

iii Each of the valuable metals is present in the filter cake at a concentration higher than in average mineral concentrates from mine sites.

iv As aforementioned in this chapter, the complex mineralisation of the valuable metals in primary ores, together with the variation in their compositions in different minerals all make economic recovery of the metals very difficult. Since the valuable metals in the filter cake have undergone chlorination and have been precipitated as hydrated oxides, they require much less energy and less harsh lixiviants (niobium recovery usually requires HF leaching) to process than concentrates from mining sites.

2.2 Recovery of vanadium from mineral processing wastes

This section reviews the metallurgical processes employed for dissolving vanadium values as well as the separation and purification techniques used for recovery of vanadium from key sources:

- Fly ash - arguably the most researched source of vanadium at present.
- Titaniferous magnetites wastes - most vanadium is currently extracted as a co-product of iron and titanium from processing of titaniferous magnetites.
- Bauxite - vanadium is produced as a byproduct from Buyer sludge

Fig. 2.7 summarises the key sources of vanadium and distinguishes whether the vanadium is extracted as the main product, coproduct or byproduct. Vanadium is mainly extracted as a coproduct of iron and titanium from titaniferous magnetites and historically, has only ever been recovered as the main/sole product from patronite and Arkansas vanadiferous clay [17]. Titaniferous magnetite became the main commercial supply of vanadium in the mid-1950s, with Finland and South Africa being the major suppliers.

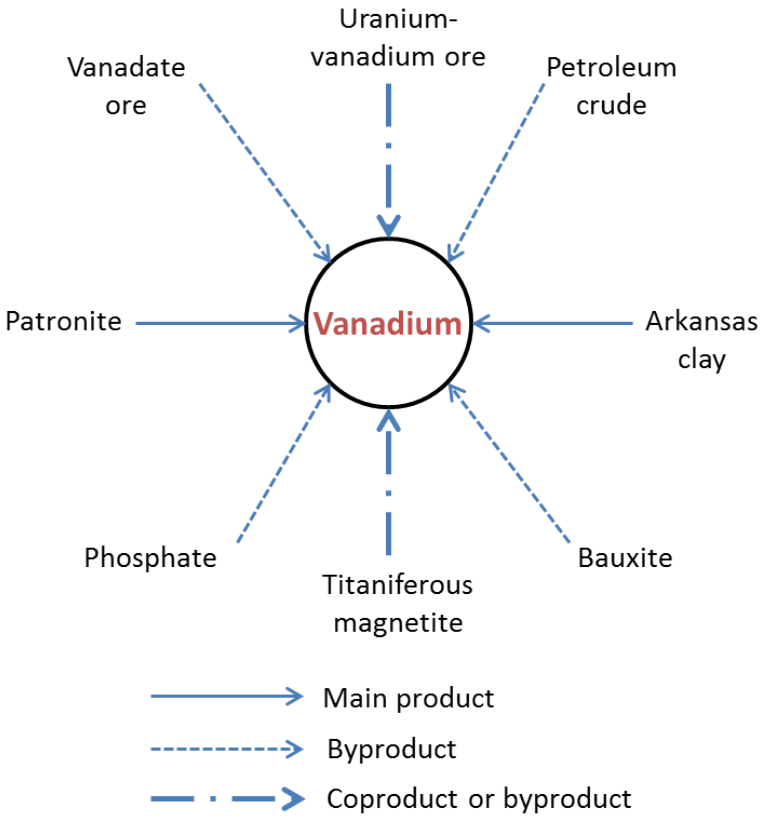

Fig. 2.7 Main product, coproduct and byproduct sources of vanadium [17].

2.2.1 Metallurgical processes

Recovery of vanadium from fly ash

Fly ash is a very fine residue collected in the exhaust gas dust collection systems of fossil fuel power plants and is typically spherical glassy particles. There are two types of fly ash:

1. Oil fly ash - includes lacy, sulphur-rich spheres, smooth alumino-silicate spheres containing either vanadium or nickel and sulphates or carbonaceous particles rich in vanadium or nickel;

2. Coal fly ash - predominantly smooth spheres of alumino-silicate matrix.

Oil fly ashes have higher vanadium content than coal fly ashes and attract most of the attention on vanadium value reclamation research. Published studies on recovery of vanadium from fly ashes have focused on either acid leaching or alkali leaching processes, perhaps because being amphoteric, vanadium oxides can dissolve in both acidic and alkaline media. Mineralogical considerations play a huge role when deciding the type of lixiviant to use for extraction of the vanadium. Acid leaching is not as selective as alkali leaching but in samples high in silica, acid leaching may be better as silica remains in the residues after leaching. When calcium and iron impurities are high, alkali leaching may present a more selective approach to vanadium recovery, usually at the expense of inferior kinetics.

The importance of mineralogy of fly ash on vanadium recovery is clearly reflected by the differing observations and conclusions made by researchers using different lixiviants and fly ashes. For example, studies on the efficiencies of alkali and acid leaching done by Chmielewski et al. [18] and Akita et al. [19] reported that alkali leaching achieves higher extraction rates than acid leaching, whereas Navarro et al. [20] reported otherwise. Despite the higher extraction rates achieved by Navarro et al., acid leaching was found to be less selective for vanadium, with aluminium, iron, silicon and nickel among some of the impurities that dissolved in the 0.5 M H_2SO_4 solutions used. Sulphuric acid is by far the most investigated acid for the recovery of vanadium from fly ash, perhaps because of the high sulphur content of most ashes [21–24]. For both acid and alkali leaching of fly ash, lixiviant concentration and leaching temperature were identified as the key parameters to optimise in order to achieve high vanadium extraction rates [18–20, 25]. Pre-treatment of the fly

ashes for conversion of the largely V^{3+} vanadium to V^{5+} can also significantly improve the vanadium recovery when alkali is used for leaching [19, 25].

Table 2.2 presents a summary of some of the published studies on recovery of vanadium from fly ash by acid leaching processes. Table 2.2 shows that sulphuric acid may be a superior lixiviant for acid leaching of fly ash, with up to 98 % vanadium recovered by leaching fly ash at room temperature for 24 hours.

Table 2.2 Acid leaching of fly ash for vanadium recovery

Lixiviant	**Conditions**			**Recovery (%)**	**Reference**
	T (°C)	**Conc. (M)**	**Time (h)**		
H_2SO_4	Room	0.5	24	98	Navarro et al. [20]
H_2SO_4	100	5	5	66	Stas et al. [26]
H_2SO_4	30	0.5	2	65	Tsai and Tsai [21]
HCl	100	5	5	59	Stas et al. [26]
HNO_3	100	5	5	50	Stas et al. [26]
HCl	50	2	5	23	Akita et al. [19]

Table 2.3 summarises some of the studies carried out on vanadium recovery form fly ash by alkali leaching, indicating the relative importance of alkali concentration, leaching temperature and leaching time on vanadium recovery. There are no clear-cut trends on the influence of parameters, indicating that the mineralogy of the fly ashes also play a critical role on vanadium recovery.

Table 2.3 Alkali leaching of fly ash for vanadium recovery

Lixiviant	**Conditions**			**Recovery (%)**	**Reference**
	T (°C)	**Conc. (M)**	**Time (h)**		
NaOH	100-110	7.5	2	94	Chmielewski et al. [18]
NaOH	Room	2	24	90	Navarro et al. [20]
NaOH	30	2	2	80	Tsai and Tsai [21]
Na_2CO_3	Room	0.66	24	80	Navarro et al. [20]
NaOH	100	8	5	77	Stas et al. [26]
NaOH	90	3	9	64	Font et al. [25]
Na_2CO_3	50	2	7	60	Akita et al. [19]

Chlorination [27] and smelting [28, 29] are among some of the alternative methods studied over the last few decades with recoveries in the range 85 - 90 % being achieved in up to 12 hours of processing.

Recovery from titaniferous magnetite wastes

Titaniferous magnetites contain approximately 1.6 % vanadium, which is feasible for commercial extraction as a byproduct or co-product, for example to iron in the iron and steel making process. Vanadium produced from titaniferous magnetites represent approximately 80 % of the world's present vanadium production.

Linz-Donawitz (LD) converter slag may contain between 3 - 10 wt% vanadium, and in some cases, as much as 20 % as V_2O_5 [17, 30]. This vanadium is conventionally recovered by roasting the slag in a multiple hearth furnace or rotary kiln using NaCl and/or Na_2CO_3 as additives. Salt roasting has long been established as a refractory metal recovery process and is economically attractive for vanadium recovery when the vanadium content is more than 1 wt% [17]. Lower grade ores (less than 1 wt%) require a hydrometallurgical process, and sometimes, a combination of hydrometallurgical and pyrometallurgical processes since large amounts of energy are required to melt gangue minerals if pyrometallurgy is employed. The salt roasting process renders the metal values water soluble and converts the refractory metals to their maximum valence state oxidic anions.

Generally, 8 - 10 wt% NaCl is added to the LD slag and roasted at 750 - 850 °C for 60 - 120 minutes in a multiple hearth roaster or rotary kiln. The roasted mixture is then water leached to dissolve the formed sodium vanadate, leaving the insoluble gangue in the residues. To produce a soluble pentavalent vanadate, both the oxidation and salt reaction become important. These reactions can be summarised by equation 2.3

$$2NaCl + O_2 + H_2O + V_2O_3 \longrightarrow 2NaVO_3 + 2HCl \tag{2.3}$$

When roasting the slag with NaCl, it is important to ensure there is some water vapour present to supply the hydrogen for forming the gaseous HCl, otherwise the reaction proceeds at a much slower rate, following equation 2.4

$$2NaCl + \frac{3}{2}O_2 + V_2O_3 \longrightarrow 2NaVO_3 + Cl_2 \tag{2.4}$$

Depending on the ratio of vanadium to NaCl, other water soluble vanadates such as orthovanadates and hexavanadates can form. Insoluble 'bronzes' could form if insufficient sodium chloride is used for roasting. 'Bronzes' can also form due to insufficient water vapour since the reaction will be proceeding at a very slow rate.

Water soluble sodium vanadates can also be formed by roasting the vanadium-containing slag with Na_2CO_3 or $Na2SO_4$ as shown by reactions 2.5 and 2.6. When Na_2CO_3 or $Na2SO_4$ are used for roasting, water vapour is not needed as the reactions are relatively faster than with NaCl.

$$Na_2CO_3 + V_2O_5 \longrightarrow 2NaVO_3 + CO_2 \tag{2.5}$$

$$Na_2SO_4 + V_2O_5 \longrightarrow 2NaVO_3 + SO_3 \tag{2.6}$$

Sodium chloride roasting requires temperatures in the region of 800 - 900 °C for effective vanadium recovery and is very selective for vanadium. Sodium carbonate roasting is carried out in the temperature range 900 - 1200 °C and is not selective for vanadium. As well as the sodium vanadates, soluble compounds of silica, phosphorous, and alumina, which always interfere with vanadium recovery [17] are also formed. Although selective on its attack on vanadium, sodium sulphate requires a much higher temperature, in the range of 1200 - 1230 °C. For this reason, as well as the higher cost compared to the sodium chloride, sodium sulphate is limited to certain iron ores.

Silica can form low melting sodium iron silicates upon roasting with a sodium salt. These compounds incorporate and retain vanadium in a water insoluble solid solution. Acmite, $Na_2O.Fe_2O_3.4SiO_2$ is one example of such sodium iron silicate. Generally, vanadium extraction can be conducted satisfactorily provided the initial material has less than 3% silica and less than 1.5 % calcium. Historic recoveries in the range 60 - 85 % vanadium have been reported in literature [31–33]. The reported recoveries have been improving with improving roasting technologies.

Mahdavian et al. [34] investigated the recovery of vanadium from Esfahan steel company slag by roasting the slag with Na_2CO_3 at 1000 °C and leaching in a mixture of sodium carbonate and sodium hydroxide to achieve a recovery of more than 80 %. Acid leaching of the alkali roasted LD converter slag can significantly improve the overall vanadium recovery at the expense of vanadium selectivity. Aarabi-Karasgani et al. [35] recovered 95 % vanadium by roasting

LD converter slag with 20 % Na_2CO_3 at 1000 °C for 120 minutes and leaching in 3 M H_2SO_4 for 150 minutes at 70 °C. Sulphuric acid leaching of the roasted slags ensures that the water-insoluble vanadates of calcium, magnesium and iron are dissolved.

Bioleaching processes have also been investigated for selective removal of vanadium from titaniferous magnetite wastes. Mirazimi et al. [36] investigated the use of microbial systems for removal of vanadium from LD converter slag using *Acidithiobacillus thiooxidans* (autotrophic bacteria), *Pseudomonas putida* (heterotrophic bacteria) and *Aspergillus niger* (fungi). Despite claiming that conventional processes that include salt roasting or acid leaching are inferior to bioleaching, their proposed process does not seem to have any significant benefits. In fact, they had to roast the slag at 1000 °C for 120 minutes with 20 % Na_2O_3 before introducing the bacteria and this is more energy and resource intensive than the conventional processes which normally employ a temperature of 850 °C and 7 - 10 % NaCl for 60 - 180 minutes. The bacteria removed up to 80 % of the $NaVO_3$ present in solution, but the authors did not provide any information on the selectivity of the bacteria and fungi they used. Based on the amount of vanadium removed from solution, the bioleaching process may be useful for selective removal of vanadium from solutions provided biological and engineering constraints such as the endurance to toxic metals in the solutions and kinetics of vanadium uptake are optimised. Liu et al. [37] developed a process for selectively recovering vanadium from slag using a molten NaOH - $NaNO_3$ binary system and recovered nearly 94 % of the vanadium after a residence time of six hours at 400 °C. Helge and Rolf [38] patented a process for production of ferrovanadium directly from slag obtained from vanadium-containing pig iron. Despite directly producing ferrovanadium with as much as 50 % vanadium, the process involved two high temperature steps (in the region of 1600 °C) making it unattractive from an energy consumption perspective.

Although established, recovery of vanadium from titaniferous magnetites is quite energy intensive as it often requires high temperatures for breakdown of the ores and research is ongoing to find a less energy intensive route.

Vanadium recovery from red mud

Red mud is a toxic waste generated in the industrial production of aluminium oxide or alumina from raw aluminium ore (bauxite). The mineralogy of red mud is largely dependent on the composition of the bauxite ore and the processing

techniques employed in preceding stages. Red mud can contain up to 20 % V_2O_5 [39], which is a significant amount considering the high production volumes currently in the region of 120 million tonnes per year. Moreover, there is a huge global inventory of over 3 billion tonnes of red mud [40], presenting a potentially important secondary source of metals and minerals. Despite significant amount of research on recovery of vanadium and other valuable metals from red mud being carried out over the last few decades, usage of conventional processes has been reported to be uneconomical [41].

Due to the high sodium content of red mud, several authors have managed to dissolve its vanadium fraction by slurrying the sludge in hot water [39, 42, 43]. Gladyshev et al. [42] investigated the recovery of vanadium from red mud containing more than 14 % V_2O_5 by leaching in water and obtained vanadium with a purity of nearly 99 %. ‚No value was reported for the overall recovery therefore their results could not be directly compared to other researchers', and the water leaching process they developed was not optimised, meaning that a better recovery and/or purity could be achieved with appropriate optimisation. Okudan et al. [43] extracted nearly 80 % of the vanadium content in Bayer residues by leaching in distilled water at 80 °C and achieved a maximum recovery of 96 % when the water leaching stage was followed by an H_2SO_4 leaching step. In their investigation, H_2SO_4 did not have any significance on vanadium leachability, yet the authors did not investigate the influence of a second water leaching stage as opposed to leaching in a mixture of H_2SO_4 and Na_2CO_3. Having used a pulp density of 60 %, it may well be that their solution was saturated due to the huge amount of water solubles in the sludge, limiting vanadium dissolution to just under 80 %. Leaching of red mud in an autoclave at 90 °C and 20 atm for 240 minutes in the presence of lime can extract as much as 65 % of the vanadium content. Abdulvaliyev et al. [44] suggested that the autoclave leaching process minimises alkali and alumina loses, and reduces energy consumption and material costs in comparison to the conventional Bayer-sintering processing of aluminium containing raw materials. The process may be generally economical for recovery of several metal values in combination. For recovering vanadium alone, a process that can utilise a lower temperature and pressure such as the one reported by Okudan et al. [43] can suffice.

2.2.2 Separation and purification technology

Once vanadium is in solution, often as sodium vanadate or vanadium oxy-sulphate, the separation and purification processes can be divided into three categories depending on the solution chemistry:

i Direct selective precipitation from the pregnant solution;

ii Recovery by solvent extraction and/or ion exchange followed by selective precipitation;

iii Recovery by adsorption

Solvent extraction, ion exchange and adsorption process often employ an ammonium meta vanadate (AMV) precipitation step in the later stages. AMV precipitation is one of the key steps in recovery of vanadium from various kinds of sources.

Selective precipitation

AMV precipitation is the most widely used method for selective precipitation of vanadium from sodium vanadate solutions [17–19, 26, 45, 46]. When the vanadium containing solution is relatively pure, AMV precipitation is usually employed instead of solvent extraction as it is very selective for vanadium.When alkali leaching is employed for initially dissolving vanadium from various residues, the sodium vanadate solutions, usually produced at pH >12, are often contaminated by impurities such as silica, aluminium and phosphorous. The impurities need to be removed before precipitation of vanadium. This is achieved by reducing the pH of the sodium vanadate solution to 8, where nearly all the impurities including aluminium are precipitated [17, 46]. Once the precipitated impurities are removed from the sodium vanadate solutions, the pH of the solution is adjusted to about pH 7 and an ammonium salt is added. Ammonium sulphate and ammonium chloride are by far the most widely used salts. The pH is then further reduced to about pH 5 and solution is mixed for up to six hours for complete ammonium vanadate precipitation. Equation 2.7 shows the AMV formation reaction:

$$2NaVO_3 + (NH_4)_2SO_4 \longrightarrow 2NH_4VO_3 + Na_2SO_4 \tag{2.7}$$

Vanadium pentoxide of over 99 % purity can be obtained from thermal decomposition of the AMV at 450 °C. The thermal decomposition reaction is represented by equation 2.8.

$$2NH_4VO_3 \longrightarrow V_2O_5 + 2NH_3 + H_2O \tag{2.8}$$

To achieve higher vanadium grades, the metavanadate is recrystallised by slurrying in water followed by dissolution in sulphuric or hydrochloric acid at pH 2. Ammonium hydroxide is then added at room temperature and at about pH 8, ammonium metavanadate is once again crystallised and processed to obtain V_2O_5 with 99.9 % purity.

Selective precipitation can also be employed for recovery of vanadium from acidic liquors. The vanadium is firstly oxidised to the pentavalent state using oxidising agents such as sodium chlorate or sodium nitrate. The pH of the solution is then adjusted to between 2 and 3 using sodium hydroxide or ammonium hydroxide and sulphuric acid.

The temperature of the solution is then adjusted to 95 - 100 °C to precipitate a red-brown flocculate widely known as red cake. Technical grade vanadium is subsequently produced by air drying the red cake. Purity of the V_2O_5 produced this way can be improved by reacting the red cake with Na_2CO_3 solution in the presence of $NaClO_3$ followed by removal of impurities by filtration and slurrying the pregnant liquor with $(NH_4)_2SO_4$ at pH 8 - 9 and room temperature. AMV crystallises over a reaction time of six hours and constant mild agitation. The crystallisation of AMV follows reaction 2.7 and up to 99 % of the vanadium initially present in red cake is recovered as AMV crystals, which can be filtered off from the residual liquor and washed with 5 % ammonium chloride solution [17] ready for drying and calcination.

When the vanadium bearing solutions are too lean, vanadium can be quantitatively recovered by selectively precipitating it as calcium vanadates of different $CaO:V_2O_5$ mole ratios using $CaCl_2$ or $Ca(OH)_2$ [17, 47, 48]. $2CaO.V_2O_5$ is the most economical form of the calcium vanadates for precipitating and processing. Dissolution of the dicalcium vanadate in acid yields a solution suitable for conversion of the vanadium content to red cake whereas alkali dissolution yields a concentrated vanadium solution suitable for ammonium metavanadate crystallisation.

Solvent extraction

When the solutions from the leaching processes are lean in vanadium, solvent extraction processes are preferred to direct crystallisation as ammonium vanadate [19]. The most popular extractants for vanadium recovery are amines [45], and Di(2ethylhexyl) phosphoric acid (D2EHPA). Both mineral acids and bases can be used for stripping vanadium from the loaded organic phases. From an aqueous solution, D2EHPA can extract pentavalent vanadium ions (VO_2^+) as well as the four valent form, VO^{2+} with the four valent vanadium much easier to extract than the V(V) [49]. Li et al. [50] and Deng et al. [51] investigated solvent extraction of vanadium from acid leach liquors and achieved a maximum vanadium recovery of about 85 %. Both authors used a system of 10 % P_2O_4, 5 % TBP and 85 % sulphonated kerosene for extraction, and 15 % sulphuric acid for stripping the vanadium from organic phase.

The extraction reaction can be represented by equation 2.9

$$nVO^{2+} + m(HA)_{2(org)} \rightleftharpoons (VO)_n(A)_{2n}(HA)_{2(m-n)} + 2nH^+ \tag{2.9}$$

where D2EHPA is denoted by HA. In practice, extractant concentration is kept between 0.2 and 0.4 M while maintaining the pH at about 2 [17]. The major drawback of these conditions is the strong co-extraction of iron (III) when it is present in the solution. Reduction of the Fe (III) to Fe (II) using agents such as iron, sodium sulphide or sodium hydrosulphide can circumvent the coextraction of iron. Moreover, reduction of the Fe (III) to Fe (II) is coupled with reduction of pentavalent vanadium to the more extractable V(IV).

An alternative to vanadium extraction using the D2EHPA system is usage of anionic amines [20, 52–54]. When using amines for extraction, all the vanadium has to be present as V (V) because only pentavalent vanadium can form anionic complexes with amines. Hydrogen peroxide is usually used to oxidise the vanadium in solution when not present in the pentavalent state. Equation 2.10 shows the oxidation reaction of vanadium:

$$2VO^{2+} + H_2O_2 \longrightarrow 2VO_2^+ + 2H^+ \tag{2.10}$$

Anionic vanadium complexes are stable over a wide pH range, therefore, amines have a much larger flexibility in terms of extraction medium and pH than D2EHPA, which can only extract vanadium in strong acidic solutions

[55]. Equation 2.11 shows the vanadium extraction mechanism when a tertiary amine is used:

$$H_2V_{10}O_{28}^{4-} + 4R_3N_{HSO_4}^{H-} \rightleftharpoons 4R_3N_{H_2V_{12}O_{28}}^{H-} + 4HSO_4^- \tag{2.11}$$

Tertiary amines such as alamine 336 and quaternary amines such as aliquat 336 have been reported to be more efficient in vanadium extraction than other amines [26, 55, 56]. Despite only extracting 18 % vanadium at pH 1, alamine 336 reportedly extracts up to 92 % vanadium at pH 2.4 [56]. Vanadium extraction rate increases from 55 % to 95 % when aliquat 336 is used for vanadium recovery in the pH range 1 - 5. Higher recoveries are achieved with increasing pH up to pH 9.5. To minimise oxidation of the amines by V(V), the solvent extraction residence time has to be kept at a minimum. Phase disengagement and third phase formation problems are the major causes of concern when using amines, particularly tertiary amines, for extraction of vanadium. Moreover, quaternary amines are very expensive.

Ion exchange resins can also be employed for recovery of vanadium from various types of solutions [57–59]. Ion exchange recovery of vanadium relies on the ion exchange reactions where reversible interchange of ions between the solid ion exchanger and the vanadium containing solution occurs. As a general example, if an ion exchanger of the form M^-A^+ carrying A^+ cations as the exchanger ions is placed in a solution phase containing B^+ cations, an ion exchange reaction represented by equation 2.12 may take place.

$$M_{solid}^- A^+ + B_{solution}^+ \rightleftharpoons M_{solid}^- B^+ + A_{solution}^+ \tag{2.12}$$

Similarly, anionic exchange reactions can occur according to the general equation:

$$M_{solid}^+ A^- + B_{solution}^- \rightleftharpoons M_{solid}^+ B^- + A_{solution}^- \tag{2.13}$$

In equations 2.12 and 2.13, an ion can be defined as a vanadium molecule carrying a net positive (cation) or net negative (anion) electrical charge. Ion exchange resins present a cost effective and relatively easy to operate processes. They are very sensitive to metal ion concentrations, therefore their usage in processes where the vanadium concentration varies is limited [57, 59]. Moreover, the loading of vanadium on ion exchange resins typically used for vanadium recovery, such as the strong base quaternary ammonium anionic resins is low,

leading to low concentrations of vanadium in eluate, usually about 50 gL^{-1}. De-bottlenecking of the engineering barriers to vanadium loading on the ion exchange resins may make ion exchange processes very attractive as they are more environmentally friendly than the conventional solvent extraction and ammonium vanadate precipitation processes.

Adsorption processes

Adsorbents for removal/recovery of vanadium from aqueous solutions range from activated carbon [39, 60, 61] to zirconium impregnated collagen fibres [62]. Commercially established processes for purification of vanadium from mineral waste effluents by adsorption are not reported in published literature, perhaps due to the popularity of the well-established ammonium vanadate precipitation and solvent extraction processes. Moreover, adsorbents reported in literature such as activated carbon are also used for removal of heavy metal ions from aqueous solutions [63–66], indicating that they are not as selective for vanadium as the ammonium vanadate precipitation process. Vanadium can also be removed from waste water by adsorption on iron hydroxides [67, 68]. Usage of iron hydroxides for selective recovery of vanadium from TiO_2 residues will be explored in this work since the filter cake from Huntsman Pigments and Additives has significant quantities of iron.

2.2.3 Summary of vanadium recovery processes

Four key observations can be made from review of published literature on recovery of vanadium from industrial wastes:

i There is currently no process for vanadium recovery from chloride waste generated during TiO_2 production.

ii All recovery processes focus on selective leaching and/or roasting of vanadium values, perhaps because waste effluents are too lean for selective precipitation of vanadium.

iii Lixiviant concentration and reaction temperature are the most influential parameters on selective leaching of vanadium values.

iv Although the procedure for AMV precipitation is well documented, no relevant kinetics data is available in the published literature that can be

used for designing the reactors needed for an industrial AMV precipitation process.

Fig. 2.8 summarises the processes employed for vanadium recovery from various sources.

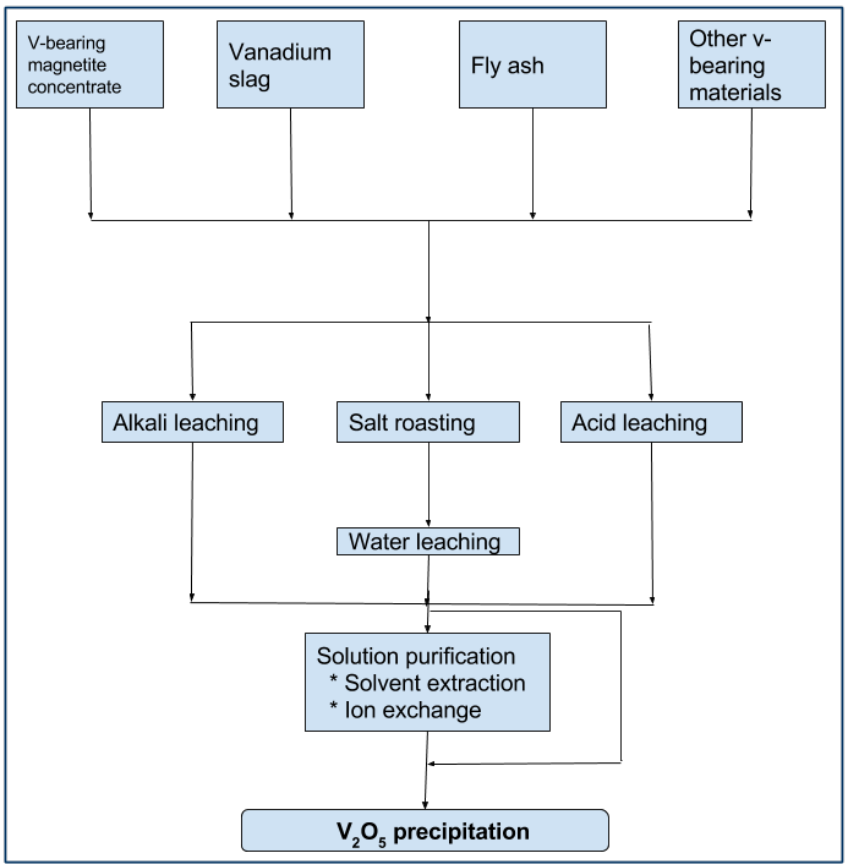

Fig. 2.8 Summary of conventional vanadium recovery processes [17].

2.3 Recovery of scandium from mineral processing wastes

Red mud from the Bayer process presents one of the largest sources of scandium, where the scandium is nearly doubly enriched compared to the original bauxite ore [69]. Treatment of the red mud for scandium recovery is very difficult due to the high levels of major impurities, particularly iron, titanium and aluminium. Other notable sources of scandium are uranium ores, wolframite, titanium ores and zirconium ores.

2.3.1 Metallurgical processes

Recovery from bauxite wastes

Scandium is often associated with aluminium in nature and its recovery from red mud is by far the most studied area on reclamation of scandium values from wastes [70, 71]. Most published literature focuses on scandium recovery from the red mud by leaching using mineral acids. There is no published literature on recovery of scandium from any sources by alkali leaching, perhaps because scandium is a very basic oxide. There are two main drawbacks to usage of acids for scandium recovery from red mud:

i The red mud is highly alkaline, implying a high acid consumption process

ii The high level of impurities requires precise operating conditions for minimisation of contamination.

Sulphuric acid is commonly used for recovery of valuable metals, including scandium, from red mud [70–73], and other sources such as uranium ores, wolframite, titanium and zirconium ores due to its availability at a reasonable price. As with recovery of vanadium from fly ash and red mud, the recovery of scandium depends on the mineralogy of the red mud. The influence of mineralogy of red mud on extraction of scandium can be observed from the variation in recoveries and conflicting conclusions that have been reported in published literature.

Wang et al. [70] investigated the extraction rates of scandium from red mud using the mineral acids H_2SO_4, HNO_3 and HCl and concluded that H_2SO_4 is more effective. This conclusion contradicts Ochsenkühn et al. [74] who found that both nitric acid and hydrochloric acid are superior to sulphuric acid, implying that the mineralogical differences of the two red muds used led to the different conclusions. The difference between HNO_3 and H_2SO_4 extraction rates is 10 %, hence may be insignificant. Wang et al. found that leaching Australian red mud in 0.5 M H_2SO_4, 0.5 M HCl or 0.5 M HNO_3 for 120 minutes at 23 °C results in poor scandium extraction rates of 32 %, 18 % and 22 % respectively. On the other hand, by leaching Greek red mud at 25 °C for 24 hours, Ochsenkuhn et al. extracted up to 80 % scandium in 0.5 M HNO_3 and 68 % in 0.5 M HCl. As well as the relatively high extraction rates, extraction of scandium from red mud using HNO_3 was also found to be more selective for scandium as only 3 % iron was co-extracted. Zhou et al. [75] reported

complete scandium extraction from red mud by leaching in 6 M HCl at 60 °C for 4 hours, suggesting that lixiviant concentration and residence time have a significant impact on scandium extraction. Ochsenkühn et al. [71] described a scandium recovery process where red mud is fused with a borate/carbonate salt at 1100 °C for 20 minutes and leached in 1.5 M HCl for dissolution of the scandium values together with a significant amount of impurities including iron, aluminium and titanium. Despite high extraction rates being achieved when concentrated acids are used for scandium recovery from bauxite wastes, the level of impurities in the scandium solution suggest that trade-offs between extraction rate and cost of impurity removal need to be considered.

Table 2.4 summarises the key studies that have been published on recovery of scandium from red mud.

Table 2.4 Acid leaching of bauxite for scandium recovery

Lixiviant	**Conditions**			**Recovery (%)**	**Reference**
	T (°C)	**Conc. (M)**	**Time (h)**		
H_2SO_4	23	0.5	2	32	Wang et al. [70]
HNO_3	23	0.5	2	22	Wang et al. [70]
HCl	23	0.5	2	18	Wang et al. [70]
H_2SO_4	50	1	2	48	Wang et al. [70]
HNO_3	25	0.5	24	80	Ochsenkühn et al. [71]
HCl	25	0.5	24	68	Ochsenkühn et al. [71]

Recovery from rare earth and uranium ores

Scandium and the rare earth elements are very similar in their chemical properties and are therefore often found together in nature. Most metallurgical processes employed for extraction of rare earths, particularly yttrium and lanthanum, also dissolve scandium. Due to the close association of scandium and rare earths, their separation typically involves more than one processing step [76]. Published literature on scandium recovery from rare earth ores is very scarce, perhaps due to the relatively low concentrations of scandium in key rare earth minerals such as bastnasite and monazite (20 - 50 ppm) compared to other sources such as red mud [77]. Nevertheless, Li et al. [78] described a process for production of scandium as a co-product during production of rare earths from bastnasite mineral. Almost all rare earths and scandium were solubilised by baking the bastnasite in concentrated sulphuric acid at 250 - 300

°C and leaching in water. Iron, thorium, calcium, fluorine and phosphorous were among the main impurities that needed to be separated for efficient recovery of both the rare earths and scandium.

Trace amounts of scandium are often present in uranium ores such as uranite and with a global annual uranium production of more than 50 000 tonnes [79], recovery of scandium as a byproduct form uranium ores can provide a relatively significant amount of scandium into the supply chain. Despite the high interest shown in recovery of scandium from uranium ores in the 1960s [80, 81], commercialisation of the developed processes was very limited and published literature on the technologies is very scarce. Sulphuric acid is once again the lixiviant of choice for recovery of scandium from uranium ores. Lash and Ross [80] described a process for recovery of scandium from uranium ores by leaching the ground ore in sulphuric acid followed by a solvent extraction process, precipitation of scandium as a fluoride and re-dissolution of the precipitate in HCl. The scandium-rich HCl solution had significantly lower levels of impurities, mainly titanium, zirconium and iron. Scandium oxalate could then be precipitated from the pregnant liquor by adding oxalic acid and scandium oxide with a grade of 99.5 % subsequently obtained by calcining the oxalate. The complexity of scandium recovery from uranium ores can be observed from the multiple precipitation and dissolution steps reported in the very limited publications available. The need for several stages of concentration enhancement may be the reason for lack of interest in recovery of scandium values from uranium ores. Rourke [82] attempted to circumvent the need for several precipitation and dissolution stages by using an iminodiacetic acid cationic ion exchange resin to recover scandium from uranium ores. The process, involves extracting the scandium, along other ions, on a cationic resin, washing off most of the impurities selectively and finally eluting the scandium in an aqueous solution for selective precipitation of the oxalate or fluoride. No information was given on either the achieved recovery or purity of final product therefore the feasibility of such a process cannot be compared with other aforementioned scandium recovery routes.

Recovery from titanium and zirconium ores

Feuling [83] described a process for recovery of scandium, yttrium and lanthanides from the solid residues produced titanium ore processing by the chloride process. Scandium is recovered from the residues by dissolving the

residues in 6 M HCl for 24 hours and selectively extracting the scandium from solution using TBP, eluting the scandium using 0.1 M HCl and precipitating scandium hydroxide by adding ammonium hydroxide to the solution. Scandium with a purity of more than 99 % can be achieved by using this process. Considering that global TiO_2 production by the chloride process is in excess of 3.5 million tonnes annually [84] and that typical TiO_2 residues contain more than 130 ppm [85] scandium oxide, TiO_2 waste can potentially supply over 460 tonnes of Sc_2O_3 per annum. To put this into perspective, the global supply and consumption of scandium is estimated to be about 10 - 15 tons per year [1]. Feuling [83] patented a similar process for scandium recovery, the only difference being that the residues from which scandium is recovered are from a zirconium chlorination process.

Scandium can also be recovered from sulphate tailings produced during TiO_2 production by the SP. The 2 M sulphate tailings landfilled annually reportedly contain between 15 - 20 ppm scandium, contaminated with impurities such as Zr, Ti, Fe and Si [86]. Scandium can be extracted from the sulphate solution using solvent extraction as described in section 2.3.2.

Recovery from other ores

The residues from processing of tungsten ores contain between 0.03 - 0.1 % scandium [87–90]. In tungsten residues, scandium is predominantly in the hydroxide form and can therefore be dissolved in mineral acids such as HCl, H_2SO_4 and HNO_3. Hydrochloric acid leaching of the residues has historically been the preferred approach for dissolving the scandium values [87, 90–93] from tungsten residues and the preference can be attributed to HCl's selective dissolution of scandium by formation of stable scandium complexes [91]. Despite the high dissolution rates of scandium in HCl, some authors [82, 85, 94] prefer H_2SO_4 because the HCl leach method is susceptible to HCl evaporation, leading to increased operating costs and pollution [79]. Scandium extraction rates in the region of 95 % can be achieved by leaching tungsten residues in either H_2SO_4 or HCl at high temperatures (100 - 120 °C). When a solvent extraction process is to be employed for the recovery of scandium from acidic solutions, iron (III) has to be reduced to iron (II) since Fe^{3+} tends to be co-extracted by the organic phase during scandium extraction. Reduction of the iron (III) to Fe^{2+} is therefore a key intermediate step and can be achieved using SO_2.

Kimura et al. [95] described an acid leaching based process for recovery of scandium from nickel containing oxide ores. The process selectively leaches scandium and nickel from the ore by maintaining a leaching temperature of 220 - 260 °C and pressure in the range 23 - 47 bars to restrain dissolution of iron and aluminium. As much as 95 % scandium is extracted under the aforementioned conditions when the acid used is HNO_3, H_2SO_4 or HCl.

Sulphating tantalum waste residues at 150 °C for 60 minutes and leaching in water has been shown to achieve a 95 % scandium extraction rate [96]. Trace amounts of scandium have also been recovered quantitatively from niobium ores by leaching the ores in 45 % NaOH to convert the scandium values into hydroxides which are subsequently leached with HCl leaving niobium and titanium in the residues [97].

2.3.2 Separation and purification technology

A typical process for separation and purification of scandium from aqueous solutions involves selectively transferring the scandium ions from the aqueous phase to an organic phase, scrubbing the loaded organic phase with an acidic solution and stripping the scandium ions from the loaded organic phase into an aqueous phase before separating the scandium ions from the aqueous solution, usually by employing an anion exchange apparatus [98] or selective precipitation. Precipitation of scandium compounds from enriched aqueous solution is the easiest method for scandium recovery. Due to the low concentration of scandium (usually parts per million) in the solutions and the high levels of impurities such as iron and aluminium, impurity co-precipitation makes the selective precipitation approach nearly impossible to use for scandium purification. Consequently, the recovery of scandium from solutions by solvent extraction is by far the most widely adopted method. Solvents used depend on the types and amounts of impurities present as well as the type and molarity of the aqueous phase from which scandium is extracted.

Acidic organic-phosphorus extractants such as di-(2-ethylhexyl) phosphoric acid (HDEHP) and 2-ethylhexyl phosphoric acid mono-2-ethylhexyl ester (HEHEHP, PC-88A) are among the most popular solvents for scandium recovery from HCl and H_2SO_4 solutions respectively [79, 99–101]. HDEHP and HEHEHP require high extracting and stripping acidities [79, 102] and are arguably the most commercially established solvents for scandium recovery due to their superior selectivity. Research is ongoing to find new extractants

with properties superior to HDEHP and HEHEHP [102]. Other commercially exploited extractants include bis(2 ethylhexyl)hydrogen phosphate (DEHPA), 2-ethylhexyl phosphonic acid mono-2-ethylhexyl ester (Ionquest 801), di-2,4,4-trimethylpentyl phosphinic acid (Cyanex 272) and tri-butyl phosphate (TBP) [103–105].

Ion exchange based methods have also been reported in literature but the approach is not as established as the solvent extraction methods [71, 73, 106–108]. Zhou et al. [75] reported a method for recovering scandium from red mud using activated carbon modified by TBP. The process nearly achieved a complete absorption of scandium from solution, with co-adsorption of titanium being stated as the cause for incomplete recovery of the scandium.

Overall scandium recoveries in the range 50 - 94 % have been reported in the literature, with typical grades in the region 95 - 99 %. Due to the high level of impurities and the low concentrations of scandium in residue streams, several extraction stages may be needed. Li and Wang [86] reported a process for scandium recovery from TiO_2 production residues where 6 - 8 stages of extraction, 7 - 9 stages of scrubbing and 1 - 2 stages of stripping are required to obtain a scandium product with up to 96 % purity at 94 % recovery.

Scandium precipitation from leach solutions is normally carried out for one of two reasons, depending on the chemistry of the solution:

1. Selective precipitation of scandium for concentration enhancement - after acidic leaching of scandium-containing ores

2. As the penultimate step of a scandium value recovery system - when the scandium containing solutions are relatively pure, usually after a solvent extraction or ion exchange process, scandium is precipitated and calcined to the pure oxide.

The selective precipitation of scandium is a key step in the scandium recovery process and is widely reported in literature. In fact, all the literature on scandium recovery reported herein has at least one selective precipitation step employed. Scandium is exclusively precipitated as an oxalate, fluoride or hydroxide and depending on the grade, the precipitate is either calcined to the pure oxide or re-dissolved for further purification. Scandium hydroxide precipitation is achieved by adjusting the pH of the solution to between 4 and 6, usually using sodium hydroxide solution. The oxalate is precipitated by adding oxalic acid to the solution while the fluoride is usually precipitated by addition of concentrated hydrofluoric acid.

2.3.3 Summary of scandium recovery processes

Red mud and TiO_2 residues contain significant amounts of scandium. A lot of studies are currently being carried out to develop processes for recovery of scandium from residues and effluents. There are no alkali leaching processes for scandium extraction reported in the published literature and this has been attributed to the basic nature of Sc_2O_3. Once scandium has been dissolved, there are three main purification routes reported in literature:

1. Solvent extraction
2. Selective precipitation - as a hydroxide, fluoride or oxalate
3. Ion exchange

Solvent extraction is by far the most adopted method for the separation and concentration of scandium from leach solutions. This is because even after several purification stages, scandium is present in solutions in very small concentrations compared to the impurities.

Fig. 2.9 summarises the processes employed for scandium recovery from various sources.

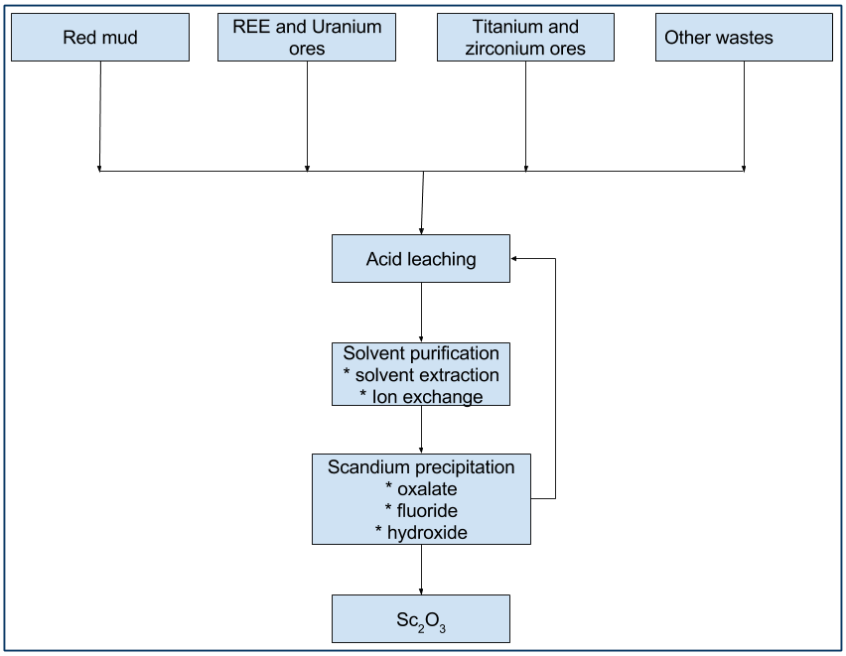

Fig. 2.9 Summary of conventional scandium recovery processes

2.4 Recovery of niobium from mineral processing wastes

Of all the niobium-containing mineral wastes, cassiterite slag (tin smelter waste) is considered the most important one due to the concentration of niobium and supply potential [109–114]. There is low interest in recovery of niobium from secondary sources, perhaps because the recovery processes require same extraction steps as in niobium recovery from primary ores [112, 113]. Niobium extraction typically involves HF leaching or smelting in electric furnaces, both of which are limited by economic or by environmental considerations. Shaw et al. [115] reported that as little as 2 % of total global niobium production is produced as a byproduct.

2.4.1 Metallurgical processes

Leaching of niobium containing materials in an HF - H_2SO_4 system is arguably the most established method [112, 113, 116] for processing ores and concentrates with more than 10 % Nb_2O_5. An alternative method involves fusing the niobium containing ores with acidic or alkaline fluxes such as $KHSO_4$ and NaOH before leaching in water or HCl [112, 117, 118].

Tin slags contain 1 - 3 % niobium as Nb_2O_5 and are one of the most researched secondary sources of niobium [119]. Leaching of tin slags with common mineral acids such as HCl does not dissolve niobium values [111, 114] therefore chlorination or carbochlorination processes have been studied as modern alternatives to leaching of the slags with a mixture of HF and H_2SO_4. Recent literature on recovery of niobium from tin slags is focusing on substitution of the HF leaching processes with chlorination and carbochlorination processes. Of particular interest is the efficiency of chlorination on separation of niobium from impurities present in the slags. Published literature on chlorination-based processes is very scarce but two key approaches to impurity minimisation are repeatedly reported by various authors:

1. Pretreatment of the tin slags prior to the chlorination reactions - concentration enhancement can be achieved by leaching of the slag in mineral acids and/or alkali.

2. Precise control of chlorination conditions to minimise the amount of impurities that get chlorinated and/or condensed with the niobium.

Leaching tin slags in HCl can double the niobium concentration at the expense of some niobium loss (nearly 5 %). Brocchi and Moura [114] studied the effectiveness of leaching tin slags in HCl at 80 °C for 6 hours on niobium concentration enhancement. Oxides of iron and calcium dissolved, reducing the slag weight by nearly 60 % but the niobium-containing residues were not considered attractive for chlorination as they still had key impurities such as oxides of titanium, silica, aluminium, manganese and residual iron, all of which interfere with the chlorination process.

To determine the influence of impurities and chlorination method, Brocchi and Moura [114] studied the chlorination of as-received tin slag by gaseous chlorine in presence of either carbon or carbon tetrachloride vapour. Nearly all the niobium was chlorinated at 900 °C after 40 minutes of chlorination by gaseous chlorine and about 40 % was chlorinated when carbon tetrachloride was used. The chlorinated niobium was highly contaminated by the aforementioned impurities, suggesting that further treatment is required.

Gaballah et al. [111] also studied the influence of pretreatment on contamination of final niobium product and concluded that leaching of the tin slags to concentrate niobium before chlorination or carbochlorination improves the overall recovery and purity of the niobium. Chlorination of low grade concentrates (LGC) produced by leaching tin slags in HCl achieves a higher niobium extraction efficiency of 95 % compared to chlorination of high grade concentrates (HGC) produced by leaching LCG in NaOH (84 % efficiency). Despite the higher extraction efficiency, the LGC chlorination was not favoured due to the high level of impurities present in the condensate. It was also observed that complete extraction of LGC could only be achieved by carbochlorination at 1000 °C, compared to 500 °C when HGC were used, indicating that HGC should be used for niobium recovery by carbochlorination as nearly pure niobium could be obtained at temperatures as low as 500 °C.

Existing hydrometallurgical processing of niobium containing slags is considered economical only if the niobium content is greater than 10 % due to the costs of HF and reactors that can withstand the highly corrosive acid.

Subramanian and Suri [120] described a hydrometallurgical process similar to the one suggested by Gaballah et al. [111] for producing HGC. They produced a residue containing nearly 11 % Nb_2O_5 from an initial niobium concentration of 3.4 %, allowing the conventional HF - H_2SO_4 niobium recovery route to be economically employed.

Some of the most recently published studies have been on recovery of niobium from chloride residues produced during production of TiO_2. The residues typically contain between 0.5 - 3 % niobium as Nb_2O_5 and present an important source of niobium [121, 122]. The residues contain a lot of impurities, including iron, titanium, aluminium thorium and uranium, and such a high level of impurities may be one of the reasons for lack of interest in recovering niobium from the residues. Gireesh et al. [121] concentrated niobium from 0.5 % to over 50 % by using a simple selective precipitation process and Makanyire et al. [122] presented the dissolution kinetics of such residues in HCl, showing that the conventional HF-H_2SO_4 lixiviant system is not needed for dissolution of niobium from TiO_2 residues.

2.4.2 Separation and purification technology

After concentration enhancement, the niobium concentrates from tin slags are conventionally leached with a combination of hydrofluoric and sulphuric acid at an elevated temperature [123] to form the complex heptafluorides H_2NbOF_5 and H_2NbF_7 in solution with most of the accompanying elements [124]. From these solutions, niobium and tantalum are selectively extracted using organic solvents, prior to their separation for producing pure niobium and tantalum oxides. Solvent extraction is by far the most exploited technique for separation and purification of niobium. More than 200 combinations of organic solvents and mineral acids have been investigated for extraction and separation of niobium and tantalum. Only four of the solvents; methyl iso-butyl ketone (MIBK), TBP, cyclohexanone (CHN) and 2-Octanol (2-OCL), are commercially exploited [125] for niobium extraction. MIBK is the most commonly used of the four extractants due to its low density, relatively low viscosity and availability at a reasonable cost. When commercially separating and purifying niobium from solution, the presence of fluoride ions is a notable prerequisite. There is need for research into alternative extraction processes that do not require use of the environmentally harmful fluorides.

Mayorov and Nikolaev [126] investigated the recovery of niobium and tantalum from natural ores using octanol-1 (OCL) and found its efficiency to be comparable to that of MIBK. OCL has the advantage of being less fire and explosion hazardous compared to MIBK and is readily soluble in aqueous solutions. Other promising extractants include tertiary amines such as Alamine 336, which has shown promising results for purification of niobium and tantalum

in very low HF concentrations or oxalic acid solutions where HF is not present [125].

Once sufficient niobium and tantalum oxides have been extracted into the organic phase, sulphuric acid of normality 6-15 N is used for washing the organic phase. Water or dilute sulphuric acid is then added to extract niobium, leaving fluorotantalite in the organic phase. Any remaining traces of tantalite are removed from the niobium by re-extraction using MIBK. Niobium oxide hydrate is finally precipitated from the aqueous solution using ammonia in gaseous or aqueous form.

Gireesh et al. [121] and Bowerman [127] demonstrated that niobium can be selectively precipitated from chloride media below pH 2. In both cases, sulphuric acid is added to facilitate the niobium precipitation process but the mechanism by which the sulphuric acid accelerates the precipitation process could not be ascertained. Niobium can also be precipitated from chloride media without adding the sulphuric acid, but long residence times are required to achieve the same level of precipitation as when sulphate ions are present in solution. The precipitates formed when sulphuric acid is added to facilitate the reaction contain about 16 % sulphate ions, indicating that the precipitation process is not solely due to precipitation of insoluble sulphates. Phosphate ions can also facilitate the precipitation of niobium at low pH [128] and the precipitation conditions suggest that the sulphate and phosphate ions facilitate niobium precipitation through a similar mechanism.

2.4.3 Summary of niobium recovery processes

At present, tin smelter wastes are by far the most important secondary source of niobium due to the concentration of niobium and supply potential. Established hydrometallurgical processes for recovery of niobium from both primary and secondary sources exclusively employ an HF-H_2SO_4 system for dissolution of the niobium values. Usage of HF for leaching leads to high capital and operating costs. As a result, most niobium sources have to be upgraded to obtain concentrates containing at least 10 % Nb_2O_5 before leaching in HF. Conventional recovery of niobium from both primary and secondary sources involves four key stages:

i Concentration enhancement (to achieve $Nb_2O_5 > 10$ %)

ii Dissolution of the niobium values

iii Selective extraction of niobium and tantalum by solvent extraction

iv Separation and purification of niobium and tantalum - niobium and tantalum have very similar chemical properties and are difficult to separate

Fig. 2.10 summarises the processes employed for niobium recovery from various sources.

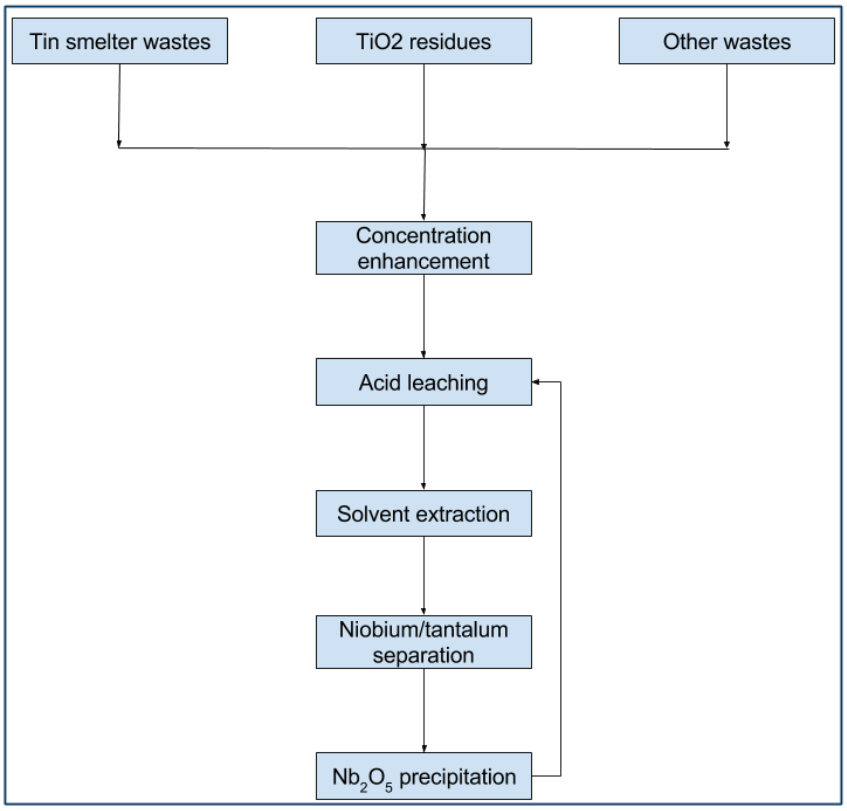

Fig. 2.10 Summary of conventional niobium recovery processes

Processes for selectively precipitating niobium from solutions obtained by leaching TiO_2 residues in HCl have been reported in recent literature. Sulphate and phosphate ions catalyse the selective precipitation of niobium from the chloride media at pH lower than 2.

2.5 Kinetics studies

Understanding the thermodynamic stability of various species is very critical for any process development work and for practical applications, an understanding of the rate of reactions is of equally great importance. Reactions that are too slow have no economic importance and those that are too fast are potentially dangerous. Chemical kinetics is the study of how fast a chemical reaction occurs. The measurement of kinetics of metal dissolution provides key knowledge necessary for the design and optimisation of reactors. Observing how changing a certain parameter affects the rate of reaction allows a scientist to infer what is going on at the molecular level and hence allow them to know how long to hold the reaction at one stage before moving on, ensuring that the reactions are finished before moving on to the next ones. Leaching processes usually involve several simultaneous elementary reactions, with each subject to mass action kinetics. This means simplifying assumptions are used to develop closed-form rate equations and such assumptions include:

Pseudo-steady-state - assuming that concentration of unstable intermediates does not change during reaction.

Equilibrium for certain fast reversible reactions and completion of very fast irreversible steps.

Rate determining step - assumes that the reaction rate is determined by the slowest steps in the reaction network composing the overall reaction.

Assuming that the rate-determining step is the slowest step in the leaching process and it controls the overall leaching kinetics, several steps in the leaching process can be eliminated in deriving the kinetic equations. The rate-limiting step can either be:

1. Diffusion in the liquid film surrounding the solid particles (film diffusion).
2. Diffusion within the particles – in pores or through the solid phase itself (particle diffusion).
3. Chemical reaction at the surface of the particle (surface reaction).

2.5.1 Modelling of fluid-solid reactions

The shrinking core model

The shrinking core model (SCM) is the most widely used model for describing fluid-solid reaction kinetics of non-porous particles. The shrinking core model assumes that the acid diffuses through the film surrounding a cake particle (pellet) and reacts at the interface, which consequently moves inwards leaving a shell of exhausted solid as the reaction progresses.

The homogeneous model

For porous filter cake, the dissolution reaction occurs throughout the pellet, with no sharp interface. If diffusion can be considered to be fast, the lixiviant concentration throughout the cake pellet can be assumed to be uniform, leading to the so-called homogeneous model. The model assumes that an inert product layer forms as the reaction progresses.

The uniform pore model

The uniform pore model assumes that the porous solid has completely wetted cylindrical pores which increase in size as the reaction progresses. The model also assumes that the physical size of the solid body does not change with leaching time but the whole structure can collapse due to the continuous enlargement of pores.

The random pore and grain models

The random pore model assumes that the filter cake has void elements of similar geometry, such as cylindrical pores or spherical voids with random intersections. The grain model visualises cake particles as pellets consisting of individual dense grains compacted together and each grain reacts individually following an unreacted shrinking core pattern where the lixiviant diffuses through the interstices of the solid grains while undergoing reaction, progressively reducing the amount of unreacted filter cake. According to Bhatia and Perlmutter [129], the random pore and grain models are similar in their descriptions and solutions. Only graphical solutions exist for the random pore model when pore diffusion controls therefore the grain model can be employed to get an

analytical solution.For chemically controlled reactions, the analytical expression derived by Bhatia and Perlmutter [129] is:

$$\alpha = 1 - \exp[-kt - \psi(kt/2)^2] \tag{2.14}$$

where

$$k = rs_0 \tag{2.15}$$

$$\psi = \frac{4\pi L_o(1-\epsilon_o)}{S_o^2} \tag{2.16}$$

s_o is the initial molar surface area (m^2 mol^{-1}), L_o is the initial characteristic length of a pore per unit volume (m m^{-3}) and S_o is the initial reaction surface area per unit volume (m^2 m^{-3}).

When pore diffusion controls the leaching process, the analytical expression suggested by Bhatia and Perlmutter [129] is:

$$1 - 3(1-\alpha)^{2/3} + 2(1-\alpha) = \frac{t^*}{\sigma^2} \tag{2.17}$$

where

$$t^* = (\frac{bkC_{a,f}}{\rho_m}\frac{A_g}{F_g V_g})t \tag{2.18}$$

$$\sigma = \frac{R_p}{3}(\frac{3k(1-\epsilon)}{2\mathscr{D}_e}\frac{A_g}{F_g V_g})^{1/2} \tag{2.19}$$

F_g represents the grain shape factor, with a value of either 1, 2 or 3 for grain shapes of flat plate, cylinder or sphere respectively. A_g and V_g represent the external surface area (cm^2) and volume (cm^3) of grains respectively. ρ_m is the molar density of the cake particles (mol cm^{-3}, R_p is the radius of the cake particles (cm), ϵ is the porosity of cake particles, b is the stoichiometric factor and k is the reaction rate constant (mol m^{-2} min^{-1}).

2.5.2 Calculation of activation energy

When the rate constants are calculated using any of the aforementioned rate equations, the activation energy can be calculated by employing the linearised form of the Arrhenius equation (equation 2.20).

$$\ln k = \ln A_o - \frac{E_a}{RT} \tag{2.20}$$

A_o represents the pre-exponential frequency factor, computed from the intercept of the $\ln k$ against $^1/_T$ plot. R is the universal gas constant (8.314 kJ mol $^{-1}$ K^{-1}) and T is the reaction temperature (K).

Plotting $\ln k$ against $^1/_T$ for all temperatures gives a linear relationship and activation energy(E_a) can be determined from the slope.

2.6 Material characterisation techniques

2.6.1 Liquid samples

Atomic absorption spectroscopy

Atomic absorption spectroscopy (AAS) is a spectroanalytical procedure that relies on the Beer - Lambert law [130] to determine the concentration of a particular analyte in a sample using the absorption of optical radiation by free atoms in the gaseous state. Fig. 2.11 presents the simplified drawing of a basic AAS system. The electrons of the atoms (vanadium, niobium and scandium

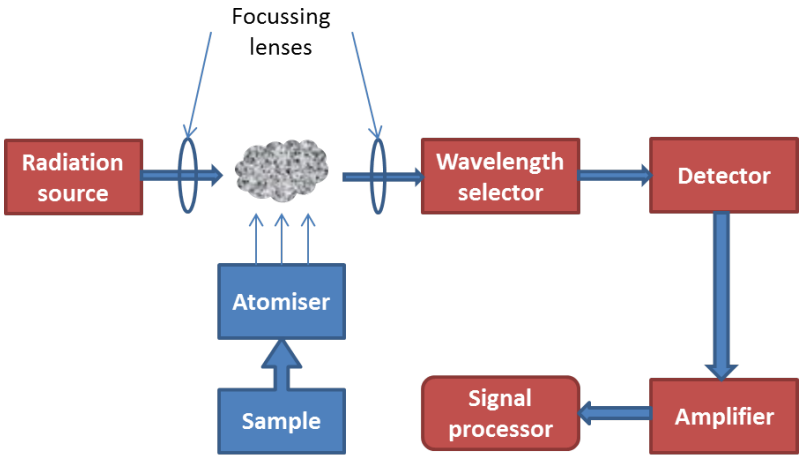

Fig. 2.11 Schematic arrangement of an atomic absorption spectrometer

atoms) in the atomizer are excited to higher orbitals for a short period of

time by absorbing a defined quantity of radiation of a given wavelength. The energy is specific to a particular electron transition in a particular element and each wavelength generally corresponds to only one element. The width of an absorption line is only of the order of a few picometers (pm), giving the technique its elemental selectivity. The radiation flux without a sample and with a sample in the atomizer is measured using a detector, and the ratio between the two values represents the absorbance, which is converted to analyte concentration or mass using the Beer-Lambert Law.

Inductively coupled plasma - optical emission spectrophotometer

Inductively coupled plasma - optical emission spectrometry (ICP - OES) is an analytical technique that uses the inductively coupled plasma to produce excited atoms and ions that emit electromagnetic radiation with energies specific to particular elements and is used for the determination of trace metals in a variety of different sample matrices [131]. Fig. 2.12 presents a schematic of the ICP - OES arrangement.

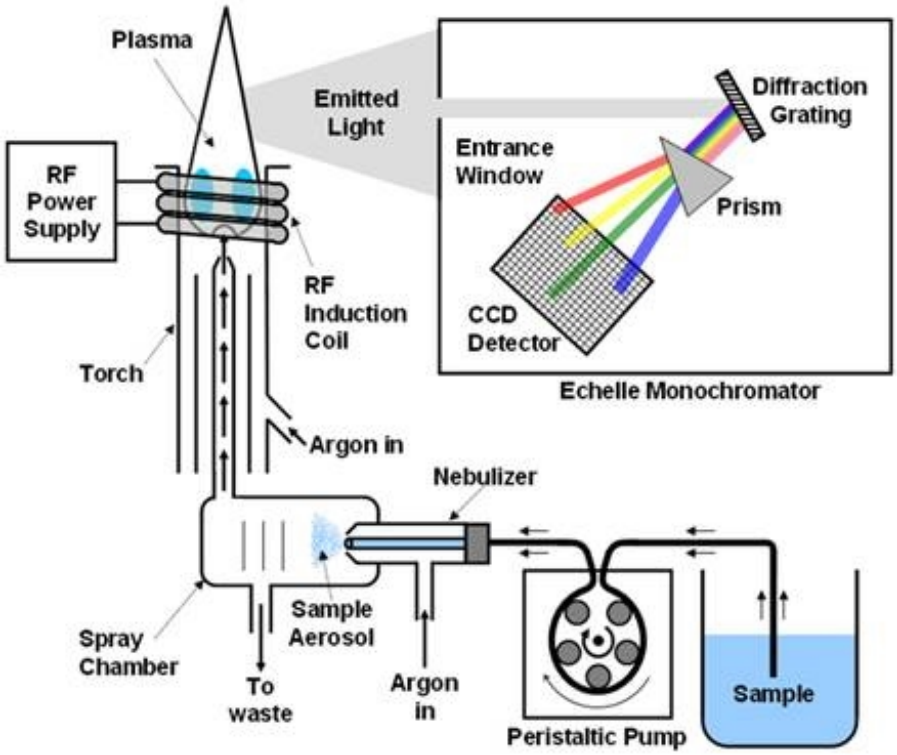

Fig. 2.12 Schematic arrangement of an Inductively coupled plasma - optical emission spectrophotometer [132].

The filtrates from cake leaching are injected into a radiofrequency- induced argon plasma using a nebuliser or other sample introduction techniques and the sample mist reaching the plasma is quickly dried, vapourised, and energized through collisional excitation at high temperature [133]. The atomic emission emanating from the plasma is viewed in either a radial or axial configuration, collected with a lens or mirror, and imaged onto the entrance slit of a wavelength selection device where the intensity for each wavelength is indicative of the concentration of the element within the sample [134].

2.6.2 Solid samples

X-ray powder diffraction (XRD) analysis

Crystalline phases in a sample have many planes, with each parallel set having a definite spacing referred to as the d-spacing. Diffraction occurs when X-rays interact with electrons meeting certain conditions as defined by the Bragg's Law, which states:

$$n\lambda = 2d\sin\theta \tag{2.21}$$

where d is the inter-planar spacing (lattice plane spacing), θ is the angle of incidence/reflection, λ is the wavelength of the incident x-rays and n is the order of reflection [135, 136].

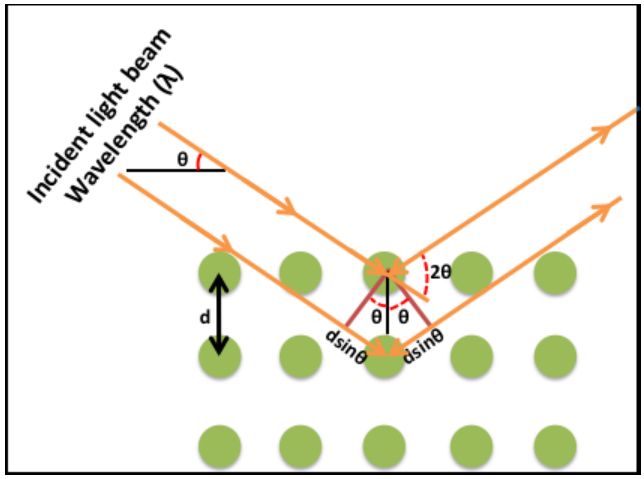

Fig. 2.13 Schematic representation of Bragg's Diffraction Law [137]

According to Bragg's Law [138], beams reflected from adjacent crystal planes undergo constructive interference when the path difference between them is an integer multiple of the x-ray's wavelength. The constructive interference

generated over time is recorded as several peaks for polycrystalline materials with numerous planes. Due to the difference in atomic arrangements in different materials, the planes are specific to each material and hence the diffraction peaks produce a pattern that is specific to each material.

Scanning electron microscopy with energy dispersive X-ray spectroscopy

Fig. 2.14 illustrates the interactions of the beam electrons with sample material [139] where backscattered and secondary electrons are used for imaging and the x-rays give characteristic chemical information of the emitting atoms.

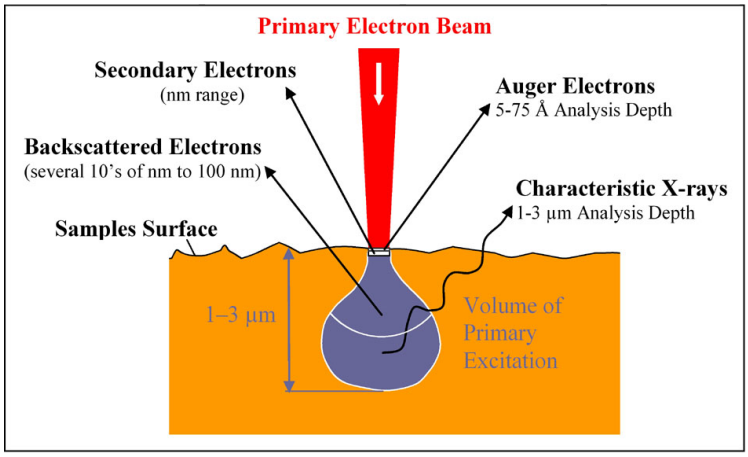

Fig. 2.14 Schematic drawing of the electron and x-ray optics of a combined SEM-EDX [139].

Backscattered electrons are high energy reflected electrons with varying energies which depend on the atomic number of elements in the sample [140]. As a consequence, elements with high atomic numbers appear brighter than those with lower atomic numbers, making backscattered electron imaging good for showing phase contrast in a sample with different compositions or multiphase sample. Secondary electrons are most valuable for showing morphology and topography since a change in surface topography changes the yield of secondary electrons. X-rays are generated as a result of inelastic collisions of the incident electrons with electrons in discrete orbitals of atoms in the sample, creating temporary electron vacancies [141]. As the excited electrons return to lower energy states, they lose part of their energy in the form of x-rays, hence, characteristic x-rays are produced for each element in a mineral that is 'excited' by the electron beam.

X-ray fluorescence spectroscopy

The fundamental principles for XRF method of analysis are very similar to other methods such as SEM-EDX and XRD, which involve interactions between electron beams and x-rays with samples. XRF spectroscopy is capable of analysing phases that are in much smaller concentrations (ppm) compared to both SEM-EDX and XRD analysis.

2.7 Chapter summary

Chapter 2 presented the background chemistry relevant to recovery of vanadium, scandium and niobium from various sources, highlighting the importance of mineralogy of the sources on overall recoveries and grades achieved. The mineralogy of the residues determines the processing conditions required for recovery of the valuable metals, as observed in the recovery of vanadium from fly ash and recovery of both vanadium and scandium from red mud. Any changes in the feedstocks or chloride plant operating conditions that affect the composition of the residues will influence the recovery and purity of the products. Sophisticated process control schemes may be required to maintain satisfactory recoveries.

Residues from the CP have a lot of impurities, the major ones being iron, titanium and aluminium. The impurities need to be removed/restricted in order to economically recover the values contained without wasting reagents and energy. This entails a selective precipitation based recovery process. Although literature demonstrates selective leaching and selective precipitation work in individual systems of V, Sc and Nb, a combined system for recovery of the three metal values from any sources is yet to be demonstrated. Moreover, the only published literature on recovery of vanadium and niobium from TiO_2 residues focuses on concentration enhancement rather than a complete recovery process. Further processing of the concentrates for obtaining saleable products needs to be established. There is no literature on recovery of scandium from waste produced by the CP.

There is also no published literature on the chemical kinetics of dissolution of the three elements in either acidic or alkaline media. Leaching kinetics information is a prerequisite of any process design or process selection work.

Chapter 3

Materials characterisation

Chapter 3 describes the materials used in the experiments conducted for recovery of vanadium, scandium and niobium from TiO_2 residues. Samples were analysed by XRD, SEM-EDX, TGA and XRF to ascertain the phases present, microstructure, amount of volatiles and the chemical composition.

3.1 Materials

3.1.1 Chemical reagents

The list of main chemicals used in the investigations is presented in Table 3.1.

Table 3.1 List of chemicals used in the investigations

Chemical	Supplier	Grade
HCl	Sigma-Aldrich	ACS Grade
H_2SO_4	Sigma-Aldrich	ACS Grade
$(NH_4)_2SO_4$	Sigma-Aldrich	99+ wt%
NH_4Cl	Alfa Aesar	98+ wt%
NaOH	Alfa Aesar	98+ wt%
Na_2CO_3	Alfa Aesar	98+ wt%
NaCl	Alfa Aesar	99+ wt%
$NaNO_3$	Alfa Aesar	98+ wt%
TiO_2	Alfa Aesar	99.9+ wt%
V_2O_5	Alfa Aesar	99.5+ wt%

3.1.2 Filter cake

Three batches of filter cake were obtained from the Greatham plant on three different occasions as prompted by the requirements of the test work. The coning and quartering sampling method described in the Appendix (section A.1) was employed for obtaining representative samples for materials characterisation and leaching experiments.

1. About 15 kg of wet neutralised filter cake (B1), used mainly for small scale leaching experiments to determine physical and chemical properties of the cake.

2. About 50 kg of wet neutralised filter cake (B2), used mainly for identifying effects of key parameters such as leaching temperature, slid-liquid ratio and stirring rate on dissolution of filter cake in HCl.

3. About 10 kg of wet neutralised filter cake (B3), used for continuation of pre-oxidation experiments and reproducibility studies. The data from this study was used for a patent application.

For initial characterisation, neutralized TiO_2 filter cake was oven dried to constant weight at 80 °C, ground using a motor and pestle, and sieved through a 100 micron sieve. Five samples from each batch were then collected using the coning and quartering sampling method and characterised by XRD, XRF, SEM-EDX and TGA.

3.1.3 Sample preparation for analysis

XRD analysis

A representative portion of the sample was ground into a homogeneous powder using a motor and pestle and mounted into a sample holder for analysis in the Institute of Materials Research's XRD suite using a Bruker D8.

Unless stated otherwise, the scanning conditions for all samples were:

- Continuous scan between 15 and 70° 2θ
- Step size of 0.030 and scan rate of 2° 2θ min^{-1}
- Long fine-focus ceramic copper target anode (2.2 kW) producing Cu kα radiation

Results were stored in digital format and manipulated using the X'pert High Score Plus software, which is supported by the JCPDS PDF-4+ database.

AAS/ ICP - OES analysis

Several liquid samples were analysed using atomic absorption spectroscopy and the results were very comparable to those obtained using the inductively coupled plasma - optical emission spectrophotometer (ICP - OES) technique therefore the ICP - OES technique was employed when several metals needed to be analysed in a single sample. AAS analysis was carried out at the University of Leeds and ICP - OES at Huntsman Pigments and Additives' analytical chemistry laboratories.

SEM-EDX analysis

Representative samples were mounted in a mixture of 3 parts epoxy resin and 1 part hardener and cured for 16 hours before gentle grinding on silicon carbide paper and polishing to 1 μm. The polished samples were then coated with a 5 nm layer of platinum to prevent charge build-up on electrically insulating samples and analysed using a Carl Zeiss Evo MA 15 at an accelerating voltage of 20 kV, working distance of 8 mm and magnifications in the range 50 - 6 000X. An EDX detector was present for semiquantitative elemental analysis and elemental mapping (using Oxford Instruments' INCA software), making it especially useful for analysis of phases that are present in quantities too small for XRD analysis (< 3 %).

XRF analysis

Samples were analysed by the pressed pellet method, which required them to be ground to homogeneous powders, mixed with EPM resin before pressing into pellets in aluminium cap supports. The compositions were reported as oxides, for example, $NaVO_3$ would be expressed as Na_2O and V_2O_5.

3.1.4 Phase analysis using XRD

Fig 3.1 shows the X-ray diffraction patterns for the as-received filter cake sample from batch 3. Only TiO_2 and SiO_2 phases were identified using XRD because the other components of the filter cake such as iron, aluminium and zirconium were present as amorphous hydrated oxides, which are poorly ordered and do

not have sharp peaks in their XRD patterns. The crystalline TiO_2 and SiO_2

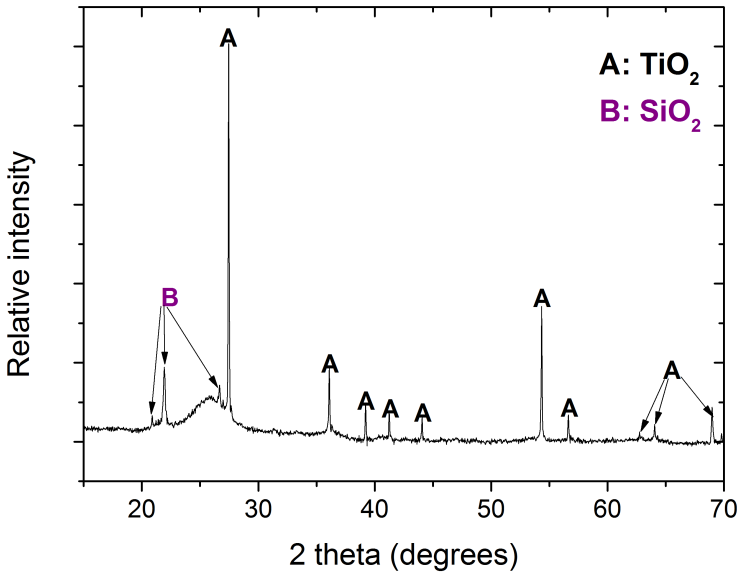

Fig. 3.1 XRD pattern of the dried as-received filter cake

phases identified in Fig. 3.1 are primarily from unreacted ore and silica.

3.1.5 XRF quantitative analysis

Table 3.2 shows the average compositions[1] of key elements in three different batches of filter cake obtained from Huntsman Pigments and Additives between 2012 and 2014. All three batches had different composition due to different feedstocks and/or operating conditions being utilised in the preceding TiO_2 recovery process. The compositions presented in Table 3.2 do not add to 100 % as less important and minor elements such as chlorine are not included. Full analysis of the various samples is presented in the appendix (section B.1).

Table 3.2 Compositions of three batches of neutralised chloride process waste - as oxides.

	TiO_2	Fe_2O_3	CaO	Al_2O_3	ZrO_2	Nb_2O_5	V_2O_5	ThO_2	Sc_2O_3	LOI(%)
B1	27.6	36.8	9.6	5.2	1.3	1.6	1.7	0.1	747*	31
B2	33.7	25.4	9.9	4.8	2.4	2.3	2.1	980*	890*	28
B3	29.2	24.3	10.6	5.7	5.8	2.2	2.1	0.1	352	27

*= ppm

[1] An average of five samples for each batch, determined by XRF

Nearly 50 % of the dry mass is unreacted ore (TiO_2), SiO_2 and coke, all insoluble in 4 M HCl.

3.1.6 Examination of microstructure by SEM-EDX

Fig. 3.2 shows the elemental maps of the as-received filter cake (Batch 1). The elemental maps show that some vanadium is dissolved in the unreacted rutile matrix. Zirconium is evenly distributed across the analysed area, whereas aluminium and iron are concentrated in one area. The compositions of areas highlighted in image 3.2b were determined by EDX and are presented in table B.4. More SEM micrographs from analysis of the three batches are presented in the appendix.

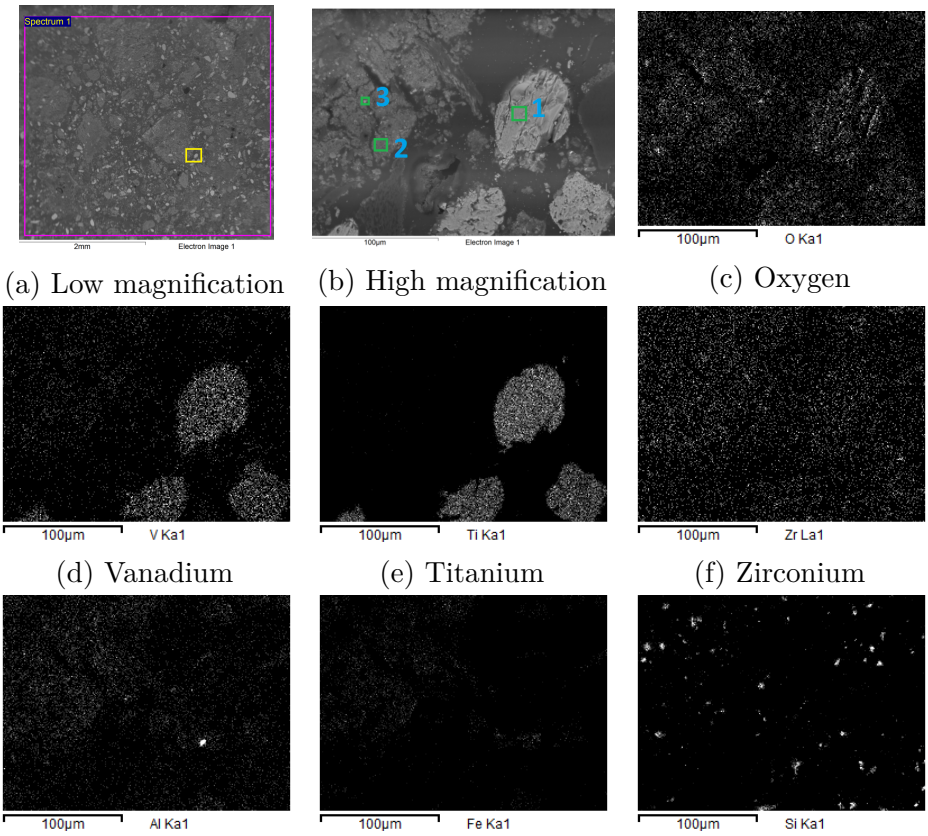

(a) Low magnification (b) High magnification (c) Oxygen

(d) Vanadium (e) Titanium (f) Zirconium

(g) Aluminium (h) Iron (i) Silicon

Fig. 3.2 Elemental mapping of the as-received filter cake, 3.2a (low magnification) and 3.2b (high magnification) show the analysed area under backscattered electron imaging

3.1.7 Determination of volatile constituents by loss on ignition

To determine the weight of volatile constituents in the filter cake, water washed cake was heated to constant weight (250 minutes) at 950 °C. The plot of fraction of weight lost against time (for B2) is presented in Fig. 3.3.

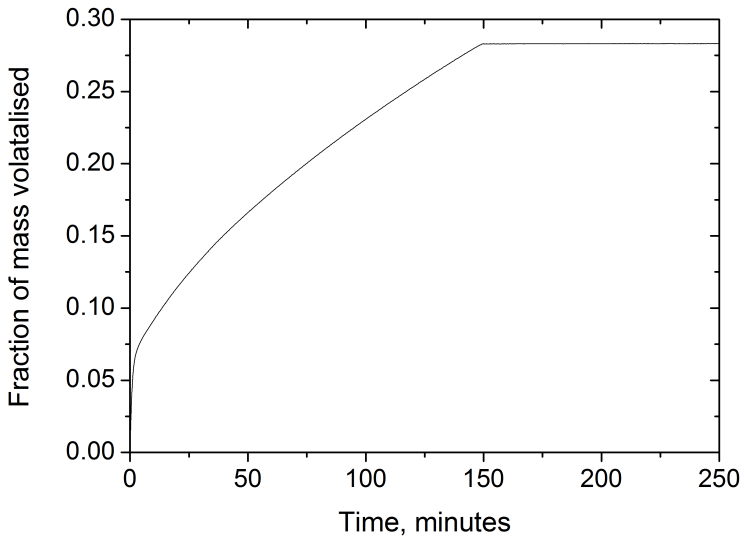

Fig. 3.3 Estimation of the volatile fraction of the as-received filter cake (dried) by LOI at 950 °C

Fig. 3.3 shows that about 5% of the cake weight is lost within a few minutes of heating the filter cake and a total of just under 30 % of the cake weight is lost after heating for about 150 minutes. The initial weight loss is mostly due to loss of water from the sample because:

1. Some moisture remains in the filter cake after drying
2. Most of the metals are present in the samples as hydrated oxides which lose the water of hydration upon heating (as shown in equation 3.1).

An example of the reaction for water loss by heating is given by equation 3.1:

$$2Al(OH)_3 \leftrightharpoons Al_2O_3 + 3H_2O \tag{3.1}$$

The weight loss observed after the initial rapid water loss is due to combustion of the coke present in the filter cake as well as loss of any remaining water and residual chlorine.

3.2 Chapter summary

Phase characterization, micro-structural and compositional analyses of the as-received filter cake were carried out using XRD, SEM-EDX and XRF respectively. All three batches have different chemical compositions due to different feedstocks and/or operating conditions used in the preceding chlorination process. SEM-EDX analysis of the filter cake shows that due to favourable Gibbs energy of dissolution, vanadium ions occupy octahedral sites in TiO_2 rutile. Experiments using synthetic V_2O_5 - TiO_2 binary mixtures can be carried out to further understand the dissolution and chemical characteristics of vanadium in the rutile phase and allow an informed decision on recovery of the vanadium. Loss on ignition analysis has shown that nearly 30 % of the dry filter cake volatilise at 950 °C and this gave an indication of the amount of residual coke in the filter cake. The information obtained from analysis of as-received filter cake was very crucial for the designing, implementation and development of the experimental techniques.

Since the filter cake consists of nearly 50 % water, a largely hydrometallurgical approach could be utilised for recovery of metals from TiO_2 filter cake. Review of the published literature showed that vanadium recovery usually involves a combination of hydrometallurgical and pyrometallurgical processing stages therefore both systems could be investigated. Hydrometallurgical processes are typically used for small scale operations since they have a lower capital investment sensitivity to plant size in lower plant capacity ranges and can be used for separating closely related metals [17].

Chapter 4

Process design

4.1 Introduction

Chapter 4 presents the solution chemistry and fundamental theory that governs the unit process selection for the recovery of vanadium, scandium and niobium. The chemistry of various soluble and insoluble species of vanadium, scandium, niobium and thorium are also summarised. To determine the feasibility of recovering the three metals in combination, it is critical to study the system thermodynamics. Thermodynamics calculations can map out when the metals would precipitate or be in solution depending on their concentration, solution pH and electrochemical potential. Understanding process chemistry, particularly chemical thermodynamics and chemical kinetics helps engineers design efficient metal recovery processes. As well as ascertaining process limitations, thermodynamics analysis can also provide valuable information during the experimental planning, and process selection and evaluation stages of process development. Information obtained by a thorough thermodynamics analysis include:

1. The solubility of metals and their loading limits in different lixiviants.
2. Estimates of vapour pressures of volatile compounds
3. The extent of reaction under various conditions

4.2 Solution chemistry

The first stage when determining the conditions for leaching the filter cake and selectively precipitating the valuable metals is identification of various

soluble species which may be formed in the system. This allows for the range of potentials, pH and concentration of other ionic species over which the metal ions remain in solution to be identified [142]. Two fundamental parameters that can be used to control the behaviour of metals in aqueous solutions are pH and oxidation potential of the system. Metal valencies in an aqueous system are determined by the oxidation potential of the solution and determine whether the metal species are soluble or not. All metals and alloys need to be oxidised in order to be soluble and therefore require addition of oxidising agents such as H_2O_2, $NaNO_3$ or oxygen when being leached.

4.2.1 Equilibrium potential

When a metal solution is at equilibrium, the electrode potential depends on the concentrations of all species in the system. Filter cake form TiO_2 processing plants is mainly composed of iron, titanium, aluminium and residual calcium chloride. The influence of ions of these metals on aqueous chemistry of niobium, vanadium and scandium is therefore of critical importance when developing the processing steps for metal recovery. Equilibrium potential is usually measured with respect to the standard hydrogen electrode (SHE), which has a defined and reproducible potential. Standard electrode potentials for half cell reactions are available in published literature, quoted for for standard conditions of 25 °C and an activity of unity for all species. When the activity of the metal ions is not equal to unity, as expected in most systems, the value of the standard potential $E°$ can be corrected using the Nernst equation Eq. 4.1:

$$xX + bB + ne^- \longrightarrow cC + dD$$

$$E_e = E^o + \frac{RT}{nF} \ln \frac{(a_X)^x (a_B)^b}{(a_C)^c (a_D)^d} \tag{4.1}$$

In Eq. 4.1, E_e is the equilibrium potential, R the universal gas constant, T the system temperature, F the Faraday's constant, n the number of electrons and a the activity coefficient of the metal ions.

4.2.2 Pourbaix diagrams

Thermodynamics calculations can be employed for determining and mapping of metal ion distribution in aqueous medium as a function of either concentration

or electrochemical potential and pH. The relative stabilities of metals and metal compounds in aqueous solutions are conveniently represented on Pourbaix diagrams. The diagrams clearly show when a metal is in solution, insoluble as well as the species it exists as. This means that leaching and precipitation conditions for selective recovery of metals can be predicted, reducing the amount of practical work required to determine the best processing route. In general, an electrochemical reaction can be written:

$$xX + cH_2O + ne^- \longrightarrow cC + mH^+$$

On a Pourbaix diagram, horizontal lines represent regions where only electrochemical potential has influence on the equilibrium phases, vertical lines represent regions where only pH has influence on the equilibrium phases and slopes are for regions where both pH and electrochemical potential have an influence.

As well as showing soluble species in an aqueous system and leaching conditions, Pourbaix diagrams allow predictions to be made on potential for metal recovery by adsorption/coprecipitation. Amorphous iron oxyhydroxides precipitate at low pH [143] and exhibit a great potential to remove oxyanions from solutions by adsorption/coprecipitation due to their high surface area per unit volume. This means some species of niobium, vanadium and scandium that would normally be soluble at a given pH could coprecipitate from the chloride solution and/or adsorb onto the high surface area of precipitated iron oxyhydroxides [144]. Iron adsorption/coprecipitation is an established process for removal of heavy metals from wastewater, reducing the metal content of the solutions to parts per billion levels. During adsorption, the titanium, calcium, aluminium or iron oxide surface can act as a weak acid or base and undergo protonation or deprotonation. Depending on the solution pH, cation adsorption reactions can be generalised as:

$$\overline{\mathrm{SOH}} + M^{n+} + m\mathrm{H_2O} \rightleftharpoons \overline{\mathrm{SO} \cdot M(\mathrm{OH})_m^{n\text{-}m-1}} + (m+1)\mathrm{H}^+ \tag{4.2}$$

and anion adsorption reactions can be generalised as:

$$\overline{\mathrm{SOH}} + A^{n-} + m\mathrm{H}^+ \rightleftharpoons \overline{\mathrm{SOH}_{m+1}A^{m\text{-}n-1}} \tag{4.3}$$

where M and A represent the cationic and anionic adsorbates respectively and $\overline{SOH}$ represents a singly protonated calcium, titanium, aluminium or iron oxide

site. A close analysis of equations 4.2 and 4.3 shows that increasing the pH increases the adsorption of cations while decreasing adsorption of anions [143]. Titanium hydroxide precipitation has been shown to coprecipitate vanadium, where 200 mg of titanium can completely precipitate 50 mg of vanadium when ammonium hydroxide is used for adjusting the solution pH. Aluminium hydroxide has been shown to be a strong adsorbent of vanadium. In fact, vanadium adsorption on aluminium hydroxide is much stronger than on iron oxides [145].

4.3 Vanadium chemistry

4.3.1 Oxides

Vanadium pentoxide (V_2O_5), a yellowish solid with a melting point of 690 °C, is arguably the most important oxide of vanadium. It gives vanadates upon reacting with alkali metal hydroxides or ammonium hydroxide and can be reduced in solution by sulphate ions, forming vanadyl ions VO^{2+} or by ferrous iron in acidic solutions. Vanadium (IV) oxide reacts with sulphuric, hydrofluoric and hydrochloric acid to form salts which when dissolved in water, give blue solutions [146]. The trioxide, V_2O_3, has a melting point of 1977 °C and is usually in the form of a black powder formed by thermal decomposition of ammonium vanadates at 600 - 900 °C in a reducing atmosphere. Vanadium (III) behaves similarly to chromium (III) and iron (III) and forms soluble salts with most common acids. Vanadium (II) is similar to divalent states of chromium and iron and forms soluble salts with most acids and can form soluble complexes with cyanide, fluoride, sulphate and ammonia. In aqueous solutions, vanadium in all oxidation states undergoes hydrolytic, acid-base, condensation and redox reactions, with the chemistry of each oxidation state remarkably different from others [147].

4.3.2 Vanadates

Fig. 4.1 shows the distribution of various vanadate and polyvanadate species in aqueous medium as a function of vanadium concentration and solution pH. In highly alkaline solutions with no reducing agents, discrete anions of the fully oxidised orthovanadates (VO_4^{3-}) are the most stable vanadium species and in strong basic solutions, vanadium atoms only occur in a tetrahedral

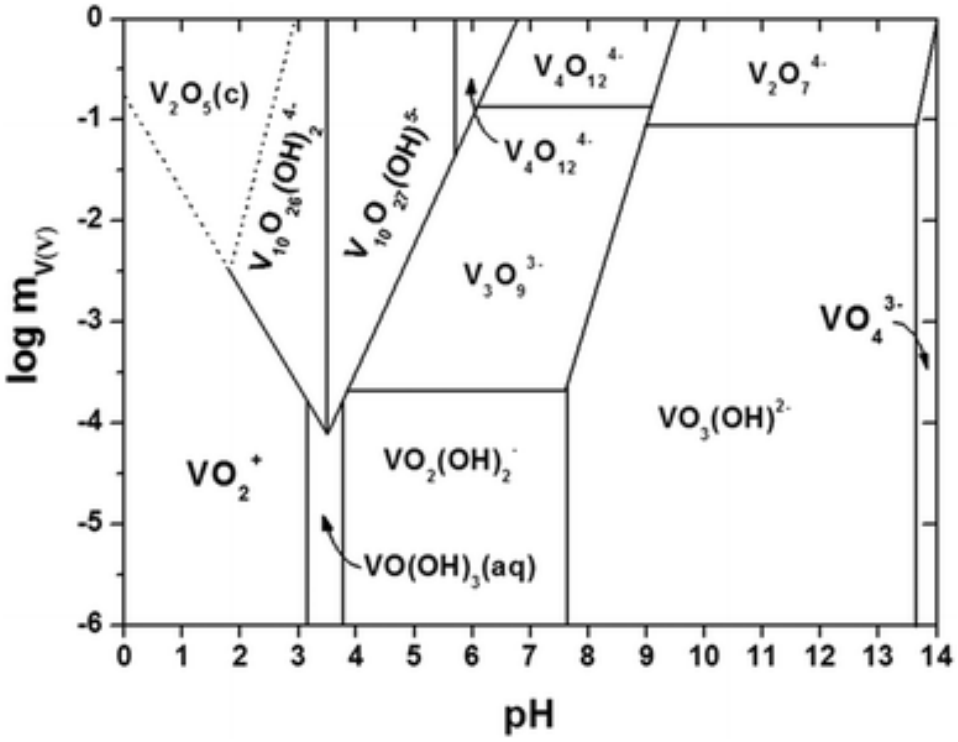

Fig. 4.1 Distribution of various vanadate and polyvanadate species in aqueous medium as a function of both concentration of vanadium and pH of the solution [148]

geometry. When pH is reduced to between 9 and 13.5, the orthovanadate is protonated to form $VO_3(OH)^{2-}$. Further reduction in pH leads to protonation of the species and geometry changes to trigonal bipyramid, square pyramid or octahedral. Below pH 2, the hydrated vanadium molecules deprotonate to form pervanadyl cations (VO_2^+). If there are no reducing agents in the solution, further decrease in pH leads to oligomeric or polyoxovanadate anionic clusters [147]. In the presence of reducing agents, vanadium can be reduced to lower valence oxidation states as shown by reactions 4.4 - 4.6:

$$VO_2^+ + 2H^+ + e^- \rightleftharpoons VO^{2+} + H_2O \qquad E^o = +1.00V \tag{4.4}$$

$$VO^{2+} + 2H^+ + e^- \rightleftharpoons V^{3+} + H_2O \qquad E^o = +0.34V \tag{4.5}$$

$$V^{3+} + e^- \rightleftharpoons V^{2+} \qquad E^o = +0.26V \tag{4.6}$$

Equations 4.4 and 4.5 show that both pH of the solution and electrochemical potential may influence the conversion of VO_2^+ to VO^{2+} and VO^{2+} to V^{3+}, while equation 4.6 shows that only electrochemical potential affects the reduction of V^{3+} to V^{2+}. This can be observed in Fig. 4.2, which also maps out the theoretical equilibrium phases of the iron-vanadium-water electrochemical system. Fig. 4.2 can be used together with Fig. 4.1 to aid in the identification of species in the complex solution.

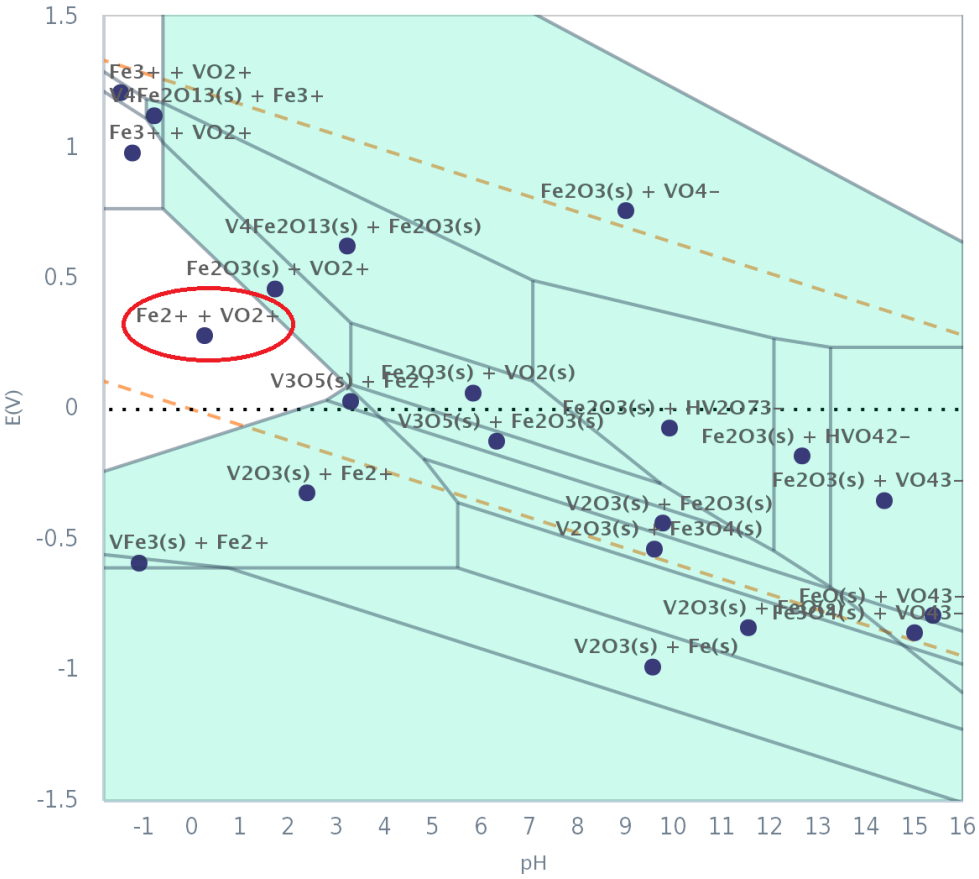

Fig. 4.2 Pourbaix diagram for an Fe - V - H_2O system at 25 °C [149]

Fig. 4.2 highlights that VO^{2+} is stable in the same region as Fe^{2+} up to nearly pH 2 (species circled in red). Depending on the pH of the system, VO^{2+} will exist in solution with Fe^{2+} in the potential range -0.25 - 0.75 V. Separation of iron and vanadium is therefore a key part of the vanadium recovery process. From acidic media, this can be achieved by either increasing the pH of the system using alkali or by changing the electrochemical potential of the solution by adding either a reductant or an oxidant. Adding an oxidising agent such as $NaNO_3$ to the system could allow separation of Fe_2O_3 precipitates from

vanadium which remains in solution as VO_4^-. Iron is insoluble in highly alkaline media and could be separated from vanadium by selective alkali leaching (above pH 12).

Fig 4.3 presents the Pourbaix diagram for the Ti - V - H_2O system. A close comparison of Fig. 4.2 and Fig. 4.3 shows that separation of vanadium and titanium should be relatively easier than of iron and vanadium species since TiO_2 precipitates at low pH. A selective precipitation process could be utilised in the pH range -1 – 3 and potentials of -0.25 – 1.25 V for effective separation of vanadium and titanium (as species circled in red).

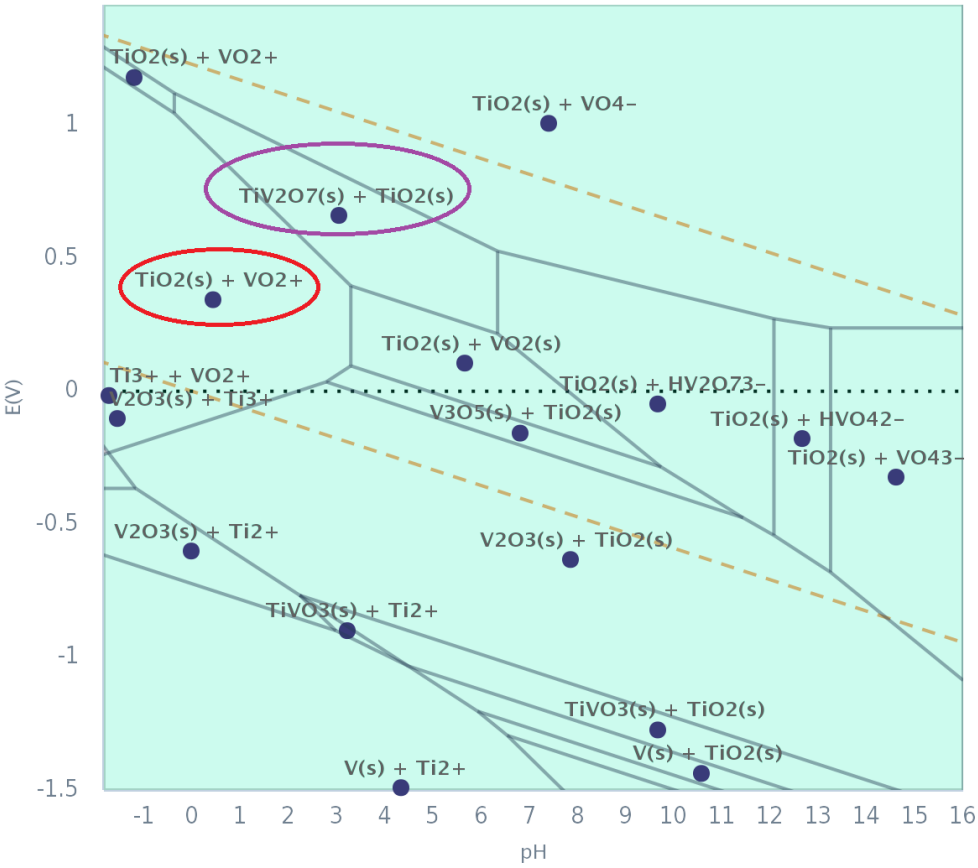

Fig. 4.3 Pourbaix diagram for a V - Ti - H_2O system at 25 °C [149]

Alkali leaching of the filter cake or leaching under oxidising conditions can also allow separation of vanadium and titanium. Separation of the TiO_2 and vanadium could be complicated by coprecipitation of vanadium on hydrated TiO_2, as observed by Brownlee [146]. This is highlighted in Fig. 4.3 in the region between pH 0 and pH 5 and potentials of 0.5 - 1.1 V (species marked in purple circle). Vanadium forms soluble vanadates at high pH and under

oxidising conditions, allowing for potentially easy separation from TiO_2 provided coprecipitation is kept at a minimum.

The aluminium - vanadium - H_2O electrochemical system is another important system for separation of vanadium from samples containing relatively large amounts of aluminium, such as the TiO_2 residues and red mud. Fig. 4.4 presents the Eh-pH diagram for the V-Al-H_2O system, highlighting that Al^{3+} and VO^{2+} are stable in the same region (species circled in red). From Fig. 4.4, it can be seen that separation of aluminium and vanadium may be easier from alkaline media than from acids. Below pH 3, vanadium and aluminium can most conveniently be separated by utilising electrochemical potential to precipitate V_2O_3. Most commercial vanadium extraction processes use the differences in solubilities of vanadium and aluminium in alkaline media for separation and purification of vanadium [26].

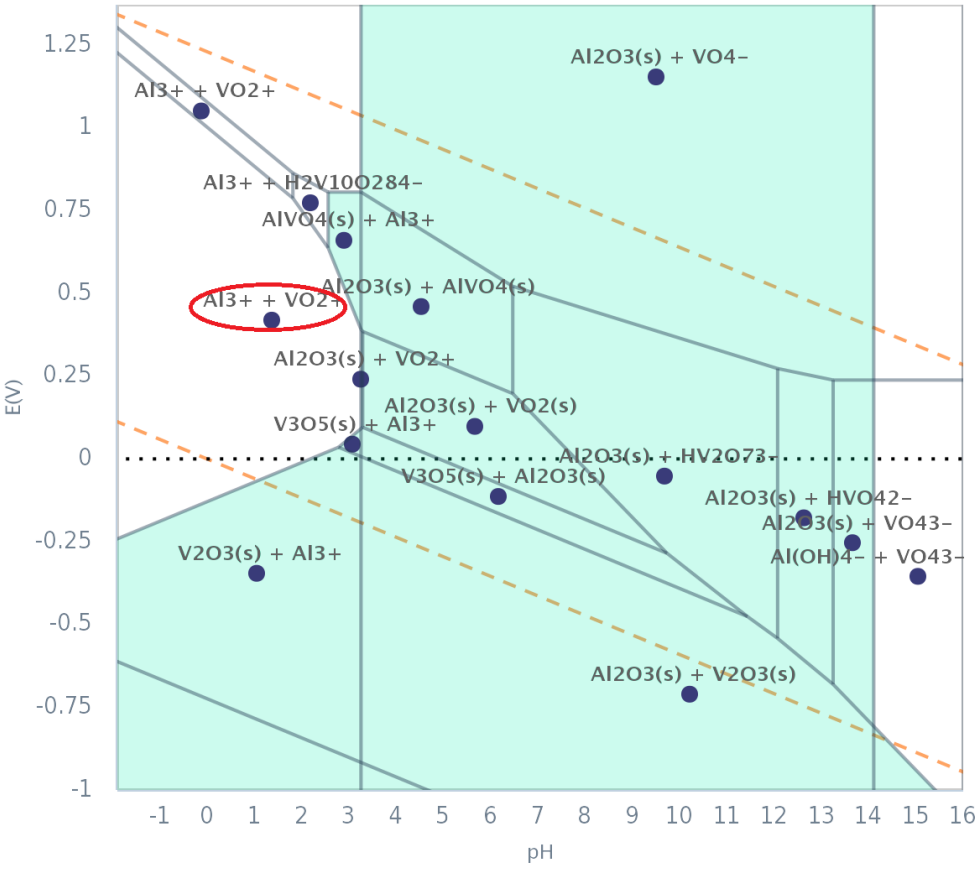

Fig. 4.4 Pourbaix diagram for a V - Al - H_2O system at 25 °C [149]

Between pH 3.5 and 14, high electrochemical potentials (above 0.8 V at pH 3 and above 0.4 V at pH 14) can be utilised for separation of vanadium and

aluminium. It is clear from Fig. 4.4 that vanadium is more stable in solution under those conditions than aluminium is.

Vanadates of ammonia, lithium, and the alkali metals are more or less soluble in aqueous solutions [146] and can condense to form poly-compounds. All vanadates of calcium are insoluble in water, meaning that the water soluble calcium chloride residues need to be washed from the filter cake for effective selective precipitation of vanadium. Ammonia metavanadate is a key intermediate in the manufacturing of various vanadium products. Its thermal decomposition starts at 70 °C and is sparingly soluble in cold water but readily soluble in mono and di-ethanolamine and can be precipitated from alkali metal vanadate solutions by addition of ammonium chloride or ammonium sulphate. Ammonium metavanadate is readily converted to V_2O_5 and other vanadium oxides at high temperatures under oxidising conditions. Another key intermediate product in the production of vanadium pentoxide is ammonium polyvanadate, $(NH_4)_2V_6O_{16}$, an orange powder produced by adding a mineral acid and ammonium salts to alkali metal vanadates at pH 2-3 [150].

4.3.3 Other vanadium compounds

In aqueous media, vanadium pentoxide reacts with sulphur dioxide to form blue soluble crystals of vanadyl sulphate, $VOSO_4.5H_2O$. The chlorides, oxychlorides, fluorides, oxyfluorides and bromides of vanadium are all fairly soluble in aqueous solutions [146]. Of all vanadium halides, only $VOCl_3$ (yellow liquid, melting point of 79.5 °C and boiling point of 126.7 °C), VCl_4 (red-brown liquid, boiling point of 148 °C) and vanadium trichloride, VCl_3 (boiling point between 300-400 °C) are of commercial interest. $VOCl_3$ is stable but VCl_4 slowly decomposes into solid VCl_3 and chlorine gas. $VOCl_3$ is produced by the reaction of vanadium pentoxide and carbon with chlorine gas and VCl_4 can be produced from reaction of oxygen-free vanadium with chlorine gas.

4.4 Scandium chemistry

Although strictly not a rare earth, scandium is often included in rare earth discussions due to its very similar chemical behaviour to that of the lanthanide group of metals. Scandium exists in aqueous solutions, under normal conditions, only as the Sc^{3+} ion. The trivalent cation has a strong affinity for water and forms the hexa aqua-complex $[Sc(H_2O)_6]^{3+}$.

Most scandium salts are soluble in acids including HCl, HNO_3, and H_2SO_4 and can undergo extensive hydrolysis [151] as:

$$[Sc(H_2O)_6]^{3+} \rightleftharpoons [Sc(OH)(H_2O)_5]^{2+}_{aq} + H^{+}_{aq} \tag{4.7}$$

When bonded with water, the Sc (III) ion forms a divalent ion which polymerizes as:

$$[Sc(OH)(H_2O)_5]^{2+}_{aq} \rightleftharpoons [Sc(OH)(H_2O)_5]^{2n+}_{n\,aq} \qquad n = 1, 2, 3... \tag{4.8}$$

Some research has been done on the solubility of $Sc(OH)_3$ in ammonium hydroxide and in carbonate and bicarbonate solutions [88]. In NH_4OH solutions, the general understanding is that the increase in solubility of $Sc(OH)_3$ on increasing NH_4OH concentration is due to formation of $[Sc(OH)_6]^{3-}$ complex ions. In carbonate and bicarbonate solutions, complex carbonates and hydroxocarbonates are formed. The dissolution reactions have been reported as:

$$Sc(OH)_3 + OH^- \rightleftharpoons [Sc(OH)_4]^- \tag{4.9}$$

$$Sc(OH)_3 + 2OH^- \rightleftharpoons [Sc(OH)_5]^{2-} \tag{4.10}$$

$$Sc(OH)_3 + 3OH^- \rightleftharpoons [Sc(OH)_6]^{3-} \tag{4.11}$$

Scandium hydroxide has been reported to dissolve in carbonate solutions as the complex ion $[Sc(CO_3)_4]^{5-}$ [88]. The sulphate, $Sc_2(SO_4)_3{\cdot}5H_2O$ dissolves in concentrated sulphuric acid, precipitating very hygroscopic crystals of $Sc_2(SO_4)_3{\cdot}3H_2SO_4$ when allowed to stand [88]. Solubility of the anhydrous sulphate decreases with increasing concentration of sulphuric acid [88].

Fig. 4.5 illustrates the stable phases in an Sc - Fe - H_2O system.It can be seen from the diagram that scandium will exist in solution (Sc^{3+}) with iron (Fe^{2+}) up to pH 4 under reducing conditions (potential ≈ -0.5 V). Scandium

could be separated from the iron at pH as low as zero by raising the system potential to 0.75 for Fe_2O_3 precipitation. When no potential is applied to the system, separation of scandium and iron can be achieved by raising the pH of the solution to between 4 and 5, allowing Fe_2O_3 to precipitate leaving hydrated scandium ($Sc(OH)_2^+$) in solution.

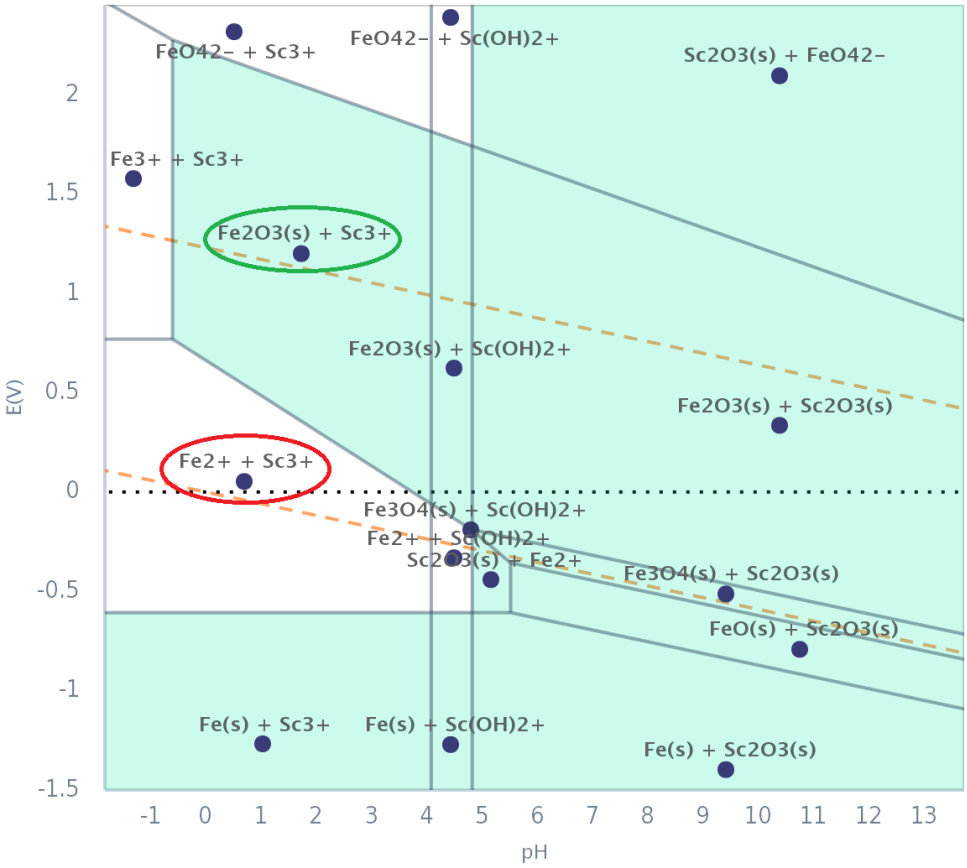

Fig. 4.5 Pourbaix diagram for the Sc - Fe - H_2O system at 25 °C [149]

Fig. 4.6 shows the stable phases in a Sc - Al - H_2O system. It can be seen that there is a very small window for separation of scandium from aluminium containing solutions by selective precipitation (highlighted in olive on the Pourbaix diagram). Since aluminium dissolves as AlO_2^- above pH 8, it may be possible to selectively leach it from the hydroxide mixture in strong alkaline solutions (such as NaOH), leaving scandium in the residues for further purification. The same principle is used for extraction of aluminium using the Bayer process [69, 75, 152].

Analysis of Fig. 4.5 and 4.6 shows that scandium may be selectively precipitated from solution by firstly removing Fe_2O_3 from solution under

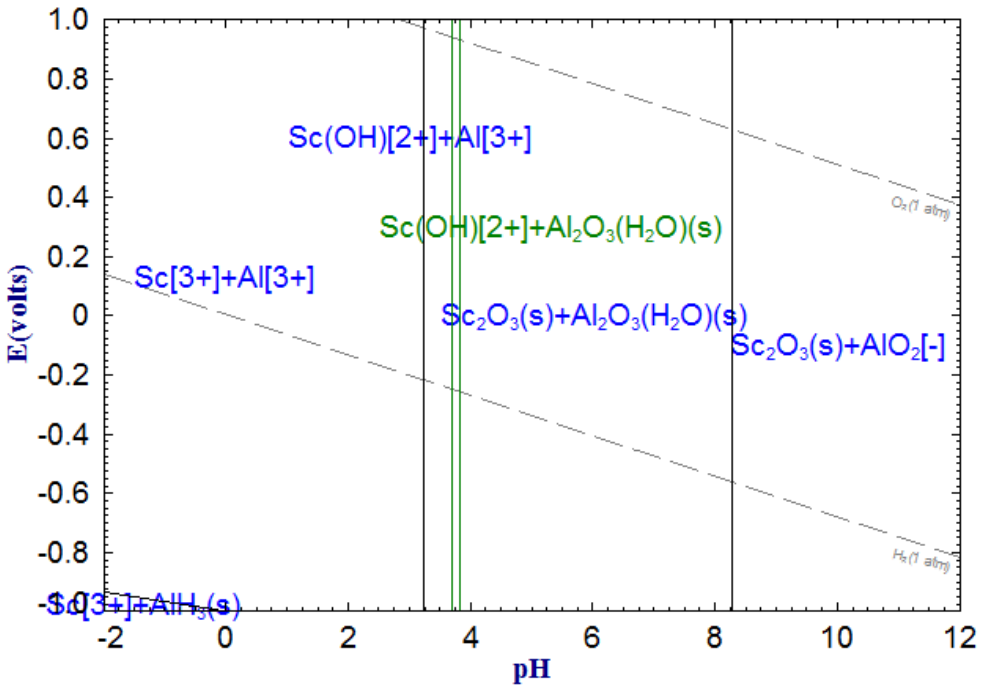

Fig. 4.6 Pourbaix diagram for the Sc - Al - H_2O system at 25 °C. Generated using FactsSage version 6.4

oxidising conditions and then precipitating the scandium at pH 5 as the hydrated oxide. The scandium-rich precipitate is likely to be contaminated by hydrated aluminium oxide which precipitates from pH 3, and any residual iron. According to Fig. 4.6, changing the potential of the system has no influence on the separation of scandium and aluminium. This entails a selective leaching based process for scandium concentration enhancement and subsequent recovery.

4.5 Niobium chemistry

The most characteristic niobium compound is the very insoluble and unreactive Nb_2O_5, which can only be dissolved by acids and bases in the presence of complex forming ions or by fusion with acidic or alkaline fluxes such as NaOH or $KHSO_4$ or in hydrofluoric acid [116]. Niobium pentoxide has a melting point of 265 °C and a boiling point of 1495 °C. Fig. 4.7 shows the predominance area diagram for niobium in an aqueous solution. The influence of solution temperature on the stability regions is also presented in the diagram.

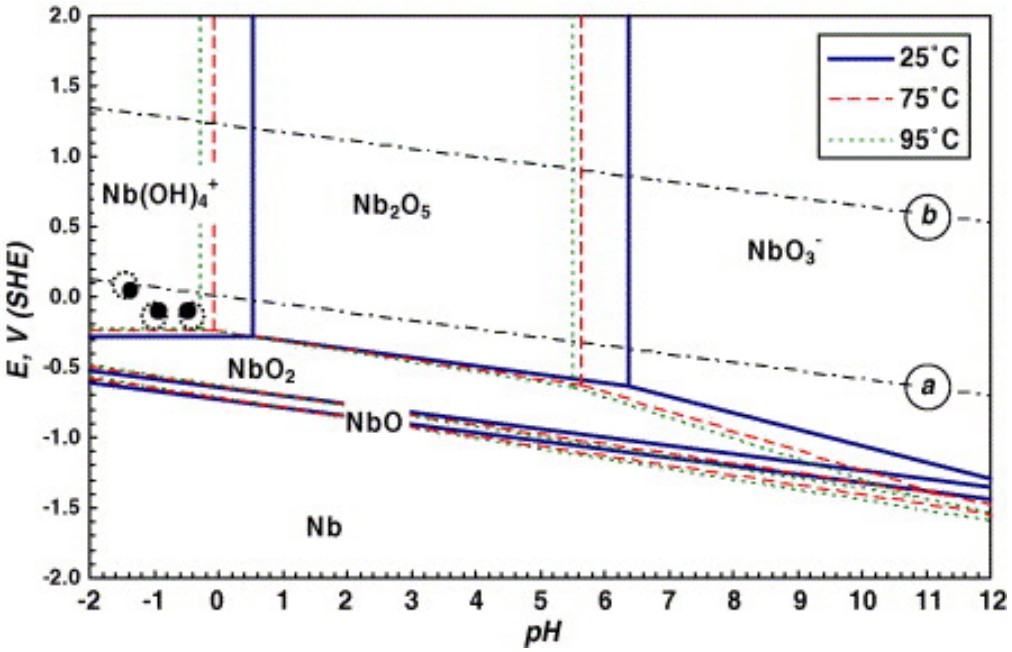

Fig. 4.7 Pourbaix diagram for the Nb - H_2O system at 25, 75 and 95 °C [153]

When an acid is added to a solution of a niobate, hydrated niobium oxides are precipitated [154]. In strongly acidic environments, the dissolution of niobium can be explained by formation of niobium tetrahydroxide ($Nb(OH)_4^+$) [153]. There are limited data to suggest that niobium ions exist as the hydrated pentavalent ions however there is some evidence of the $Nb(OH)_4^+$ ions being present in acidic solutions [155]. At temperatures above 75 °C, hydrated niobium pentoxide can be precipitated from solutions at pH as low as zero.

Chemical dissolution of Nb_2O_5 in acidic solutions, below pH 0.5 at a temperature of 25 °C proceeds as shown in equation 4.12:

$$Nb_2O_5 + 3H_2O + 2H^+ \rightleftharpoons 2Nb(OH)_4^+ \tag{4.12}$$

and electrochemical dissolution of niobium dioxide follows equation 4.13 [155]:

$$NbO_2 + 2H_2O \rightleftharpoons Nb(OH)_4^+ + e^- \tag{4.13}$$

As presented in both Eq. 4.12 and Fig. 4.7, the dissolution of pentavalent niobium when no potential is applied to the system is dependent on the pH of the system and independent of the system potential. Electrochemical potential only affects the dissolution of lower valence niobium oxides.

Niobium is strongly adsorbed by many precipitates, including sulphides and hydroxides. The pentoxide, Nb_2O_5, can be prepared by hydrolysis of alkali-metal niobates, niobium alkoxides, niobium pentachloride or by precipitation from hydrofluoric acid using ammonia or alkali metal hydroxides [109]. The pentachloride, $NbCl_5$, has a melting point of 209.5 °C and a boiling temperature of 249 °C and can be produced by chlorination of ferroniobium, niobium metal or niobium scrap. Upon reacting with water, the yellow strongly hygroscopic crystals of niobium form the colourless crystalline $NbOCl_3$ or hydrated niobium pentoxide. Niobium pentachloride is also very soluble in dry ethanol, tetrahydrofuran and benzene. Fluorination of niobium pentachloride or niobium metal in fluorine or anhydrous hydrofluoric acid can form niobium pentafluoride, which has a melting point of 72 °C and a boiling point of 236 °C. Various fluoroniobics can be formed by reacting niobium pentoxide with aqueous hydrofluoric acid, with the type of fluoroniobic formed depending on the concentration of the hydrofluoric acid. Fluoroniobics are soluble in organic solvents and are very important in niobium separation chemistry.

4.6 Radionuclides

From the three batches of filter cake supplied for this research, thorium is the only radionuclide requiring close monitoring, and therefore its aqueous chemistry needs to be understood in order to minimise the risk of concentrating it to hazardous levels.

Fig. 4.8 presents a Th - Fe - H_2O Pourbaix diagram, showing that thorium precipitates from highly acidic solutions at pH 0.5. The precipitation of ThO_2 is independent of system potential.

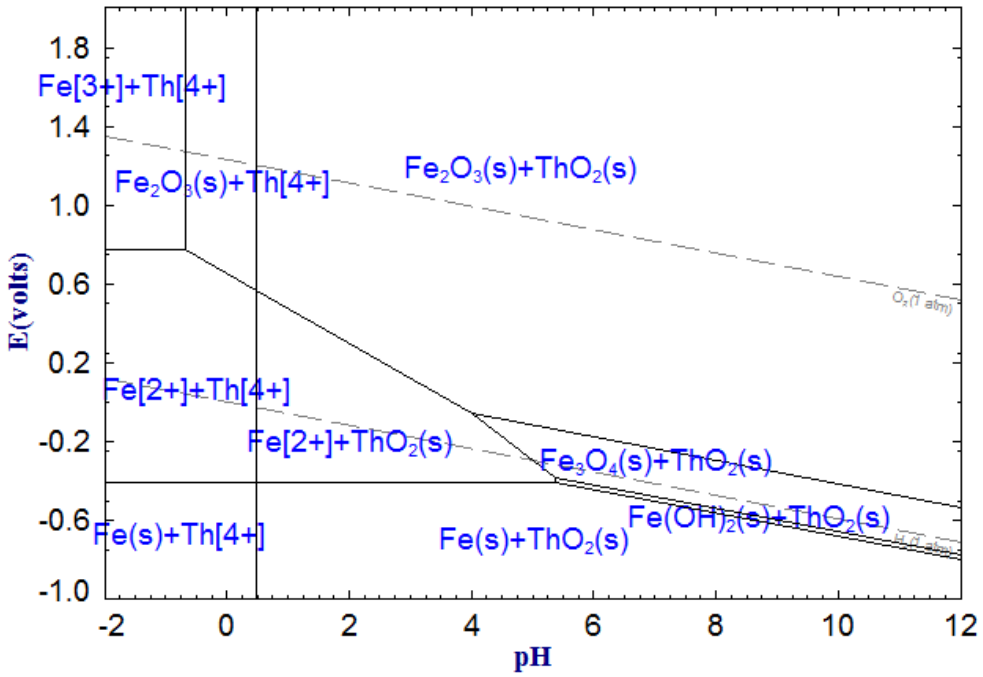

Fig. 4.8 Pourbaix diagram for the Th - Fe - H_2O system at 25 °C. Computed using FactSage software, version 6.4

Thorium exists in solution as a comparatively small highly charged cation, hence undergoes extensive interaction with water as well as a wide range of anions [156]. It only has one oxidation state and therefore oxidation - reduction reactions need not be considered. The nitrate, chloride, sulphate and perchlorate of thorium are all soluble in water and the fluoride, iodide and phosphate are very insoluble in water. Adding alkali or ammonium hydroxide to an aqueous solution of Th^{4+} leads to formation of a highly insoluble, gelatinous thorium hydroxide ($Th(OH)_4$). $Th(OH)_4$ is amphoteric and only dissolves in aqueous

solutions containing ions such as citrate, carbonate, or sulfosalicylic acid, which complex the thorium ion [156] and in acids.

Fig. 4.9 presents a Th - Nb - Sc - H_2O Pourbaix diagram, showing that Th^{4+} ions are stable in same regions as $Nb(OH)_4^+$ and Sc^{3+} ions (species circled in red) and could interfere with recovery of the metals from the TiO_2 residues. Thorium

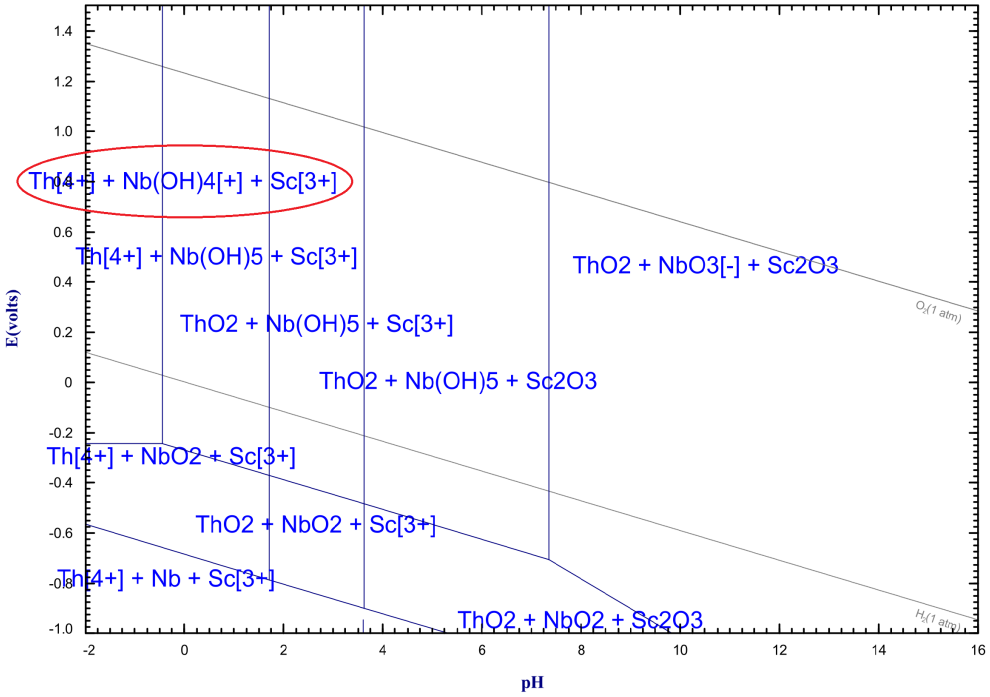

Fig. 4.9 Pourbaix diagram for the Th - Nb - Sc - H_2O system at 25 °C. Computed using FactSage software, version 6.4

can coprecipitate quantitatively with a wide range of insoluble hydroxides including lanthanum, ferric and zirconium hydroxide [156]. This means that although thorium ions are meant to stay in solution at pH < 2, they could still coprecipitate with hydroxides of niobium and iron which can precipitate at as low as zero. When hydrogen peroxide is added to a dilute mineral acid containing thorium ions, the highly insoluble thorium peroxide precipitates.

If filter cake is leached with hydrochloric acid, hydrated thorium oxide reacts with the acid to form oxychlorides as shown by equation 4.14.

$$Th(OH)_4 + 2Cl^- \longrightarrow ThOCl_2 + 3OH^- \tag{4.14}$$

Based on an analysis of a $NaHCO_3$-Na_2CO_3-NaCl aqueous system [157], the dissolution of hydrated thorium oxide in carbonate follows equation 4.15:

$$Th(OH)_4 + zCO_3^{2-} \longrightarrow Th(OH)_y(CO_3)_z^{4-y-2z} + (4-y)OH^- \tag{4.15}$$

Abdel-Rehim (2002) [158] found that thorium hydroxide can be leached in ammonium carbonate solutions in the form of ammonium-thorium carbonate complexes as shown in equation 4.16.

$$Th(OH)_4 + 5(NH_4)_2CO_3 \longrightarrow (NH_4)_6[Th(CO_3)_5] + 4NH_4OH \tag{4.16}$$

4.7 Chapter summary

This chapter has introduced the chemistry that governs the dissolution and precipitation processes used for recovery of vanadium, scandium and niobium from various sources. The thermodynamically stable phases under various conditions have been highlighted and target pH ranges for selective precipitation identified. Niobium can be precipitated first (below pH 1), followed by vanadium (likely to coprecipitate with iron and/or titanium) and finally scandium (above pH 4).

The presence of large quantities of iron and relatively large amounts of titanium and aluminium in the multi-metal solutions means any developed metal separation process will require a sophisticated process control scheme to minimise coprecipitation and contamination. Fig. 4.8 shows that thorium is likely to precipitate below pH 1 together with titanium, niobium and any oxidised iron. A process for selective precipitation of the valuable metals therefore requires considerable amount of process control to minimise contamination of valuable metals by undesirable ions, which would increase the costs associated with purification. Aluminium may be problematic in recovery of vanadium and scandium. It coexists with both scandium and vanadium in solution and precipitates over a wide pH and potential range. Based on the Pourbaix diagrams presented in this chapter, oxidative alkali leaching can provide a good separation of vanadium and aluminium (between pH 3 and 14 and Eh $>$ 0.25 V). Aluminium can be selectively leached from scandium under highly alkaline conditions. Fig. 4.1 summarises the key observations made from analysis of Pourbaix diagrams. Published literature has shown that scandium forms

Table 4.1 Summary of selective precipitation studies

Metal	Precip. pH	Comments
Niobium	0.5	• Can precipitate at lower pH (≈ 0) when temperature of the system is raised above 75 °C.
Vanadium	2	• Can coprecipitate with titanium and iron hydroxides from pH 0 under oxidising conditions or as V_2O_3 under reducing conditions.
Scandium	4-5	• Precipitates from acidic solutions at pH 4.
Iron	0	• Can precipitate from pH 0 under oxidising conditions (Eh > 0.75). • Can precipitate at higher pH (4) if the system is kept at a potential in the region -0.5 – 0.2 V
Titanium	< 0	• Any titanium in solution will likely interfere with niobium precipitation and could coprecipitate with vanadium under oxidising conditions (between pH 1 - 6 at potentials in the range 0.25 - 1.25).
Thorium	0.5	• Will precipitate with niobium at pH ≈ 0.5
Aluminium	3.5	• Closely follows vanadium and scandium in acidic and alkaline media. • Under oxidising conditions (Eh 0.5 - 0.8 between pH 2 and 3), vanadium may coprecipitate with aluminium.

soluble carbonate solutions therefore could also be separated from aluminium by oxidative leaching in carbonate solutions.

A potential metal separation route is presented in Fig. 4.10:

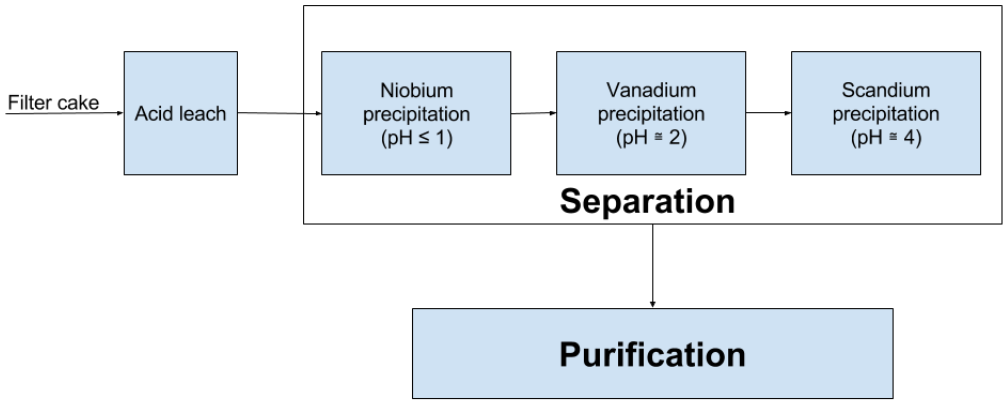

Fig. 4.10 The three stages that can be employed for recovery of vanadium, scandium and niobium from TiO_2 residues.

The pH of the solution, the electrochemical potential as well as the concentration of ionic species are the main parameters controlling the solubility of oxidised or hydrolysed metal species, and determine the acid-base character of the system. Deliberate addition of acid or alkali can be used for pH control, where acid addition consumes the hydroxyl group, lowering the pH and alkali addition consumes hydrogen ions, raising the pH.

Water has a relatively high heat capacity, therefore heating dilute solutions above ambient temperature requires considerable amounts of energy to be expended. It is therefore important that the dissolution of filter cake is performed at a modest temperature. The influence of temperature on leaching and precipitation processes needs to be studied in order to determine conditions that allow reactions to occur at a relatively fast rate without using too much energy on heating the reactants. The collision theory of reactions suggests that increasing the concentration of lixiviant or filter cake increases the filter cake leaching rate [159]. There has to be a good balance between the amount of lixiviant used to achieve a reasonable filter cake dissolution rate and the lixiviant cost. In view of this, the effect of acid/alkali concentration on extraction rates of the key metals also needs to be investigated.

Other parameters that need to be investigated to obtain important information for process development include solid - liquid ratio, stirring speed, precipitation temperature, pH and reaction temperature.

Chapter 5

Experimental

5.1 Introduction

In this chapter, the experimental setup and protocols common to the work presented in this thesis are discussed. The techniques form four distinct groupings which are:

- Synthesis, leaching and analysis of TiO_2 - V_2O_5 binary samples
- Dissolution of as-received cake in acid
- Selective precipitation of valuable metals
- Purification of valuable metals from precipitates

The first group describes the procedures used for synthesising binary oxides of vanadium and titanium used for studying dissolution of vanadium in rutile. The second group describes the dissolution of as-received filter cake in HCl, focusing on dissolution of vanadium, scandium and niobium values (studied using samples from batch 1). The third group describes the partial separation of valuable metals from impurities by selective precipitation (studied using samples from batch 2) and the fourth group describes the investigations on purification of vanadium, scandium and niobium from their respective precipitates (studied using samples from batch 2). The leaching, selective precipitation and purification investigations were done incrementally and parameter optimisation for each stage was done sequentially.

5.2 Dissolution and chemical properties of V_2O_5 in TiO_2.

5.2.1 The effect of vanadium mole fraction and leaching on rutile lattice parameters

Six TiO_2 - V_2O_5 (1 - 2 μm powder particles) binary mixtures of varying compositions as shown in table 5.1 were prepared by mixing 10 grams of the pure oxides using a motor and pestle for about five minutes. The mixtures were then pelleted using a 13 mm evacuable pellet die and a pellet press.

Table 5.1 Amounts of pure TiO_2 and V_2O_5 used for synthesising the binary mixtures

Mixture	Amount of TiO_2 (g)	Amount of V_2O_5 (g)
1	9.7	0.3
2	9.5	0.5
3	9.0	1.0
4	8.5	1.5
5	8.2	1.8
6	7.9	2.1

The mixed samples were sintered at 1100 °C for 24 hours before being taken out of the furnace to quickly cool in open air. The sintered samples were analysed using SEM-EDX and the Rietveld refinement method (XRD). For each binary mixture composition, two gram samples were ground and passed through a 53 μm sieve. The ground samples were then leached in 100 ml of 2 M NaOH solution at 60 °C on a multi plate heated stirrer. After one hour of leaching, the samples were filtered, washed and dried ready for analysis by SEM-EDX, XRD and AAS.

5.2.2 The effect of sintering temperature on microstructure and lattice parameters

The effect of sintering temperature on microstructure and lattice parameters was investigated by sintering 10 g samples (similar to mixture 5 in table 5.1) at 700, 800, 900, 1000 and 1100 °C for 24 hours before cooling in air and characterising by SEM-EDX and XRD.

5.3 Experimental set-up for dissolution of filter cake

Cake dissolutions were conducted batch-wise in a closed 1500 mL Pyrex reaction flask, as depicted in Fig. 5.1. Agitation was provided by a magnetic stirrer that allowed adequate dispersion of the particles without evaporation loss of the solution and heating by a thermostatically controlled hot plate.

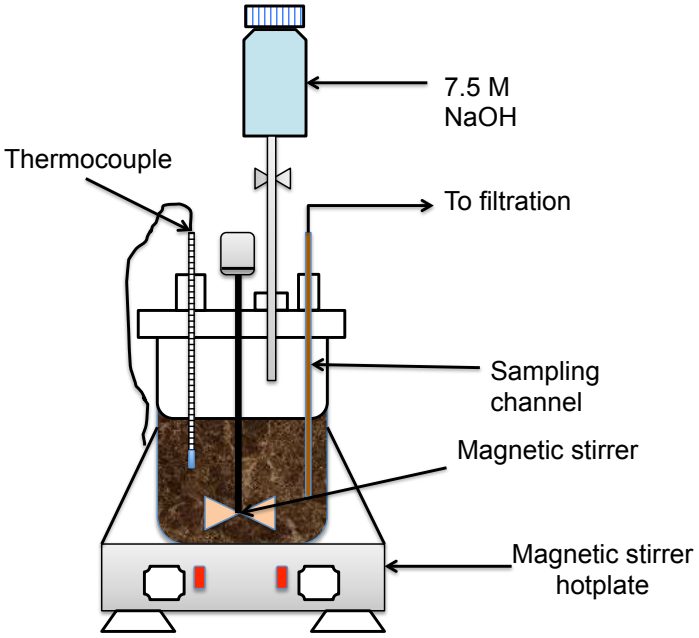

Fig. 5.1 Schematic representation of the leaching reactor

Studies on dissolution kinetics were carried out using a sequential optimisation process rather than a factorial method due to the large number of experiments required to adequately investigate all process variables and make mathematical interpretations. Chapter 2 showed that leaching temperature and mineralogy of residues have the most significant influence on recovery of vanadium, scandium and niobium, therefore, the influence of leaching temperature was investigated first in the four-stage sequential optimisation method described herein:

1. **Effect of leaching temperature and time:** To investigate the influence of leaching temperature on rate of dissolution of valuable metals from the filter cake, 50 g of dried cake was mixed with a pre-calculated amount of deionised water (876.82 mL) and placed in the reactor. The slurry was then heated to a predetermined temperature (25, 50, 60, 70,

80 or 90 °C) under continuous agitation at 300 rpm. Once temperature was stabilised, a pre-calculated amount of concentrated hydrochloric acid (123.18 mL) was injected into the reactor to make 1000 mL of 1.5 M HCl solution.

2. **Effect of HCl concentration and time:** 50 g of the filter cake was mixed with a pre-calculated amount of deionised water and placed in the reactor. The slurry was then heated to 70 °C and predetermined amounts of concentrated HCl were injected into the reactor to make 1000 mL of 0.5, 1.5, 2.5, 3 or 4 M HCl solution.

3. **Effect of solid - liquid ratio and time:** The influence of mass of filter cake to volume of acid used during the cake dissolution stage was investigated by mixing 50 g of the filter cake with a pre-calculated amount of deionised water and placing in the reactor. The slurry was then heated to 70 °C and predetermined amounts of concentrated HCl were injected into the reactor to make a 4 M HCl solution corresponding to required solid - liquid ratios (0.04, 0.05, 0.07, 0.10, 0.20 g mL^{-1}).

4. **Effect of stirring speed and time:** To investigate the influence of stirring speed, 50 g of filter cake was mixed with 671.53 mL of distilled water and heated to 70 °C in the leaching reactor. Once temperature was stable, 328.47 mL of HCl stock solution was slowly added to the reactor to make 1000 mL of 4 M HCl and leached at stirring speeds of 0, 100, 200, 300, 400 and 500 rpm for 60 minutes.

In all leaching experiments, 10 mL samples of the slurry were drawn from the reaction flask at selected time intervals using a syringe and quickly filtered to prevent further reaction between the filter cake and acid in the slurry sample[1]. Filtration was done using a Buchner funnel connected to a vacuum pump and Whatman 541 filter paper was used to produce clear solutions for ICP - OES and/or AAS analysis.

To determine the errors associated with the instrument and sampling techniques, four cake samples from batch 3 (B3) were leached at 70 °C for 60 minutes and filtered immediately while hot. Five samples from each of the leached batches were then drawn and analysed by ICP OES.

[1]Except for studies on effect of pH where residues were analysed after leaching for 60 minutes

5.4 Selective precipitation studies

Precipitation studies were conducted using samples from batch 2 (B2) and the same reaction vessel utilised for leaching experiments. Similarly to the leaching studies, samples of the precipitates formed during the selective precipitation studies were drawn from the reaction flask at selected time intervals using a syringe and quickly filtered for analysis by ICP - OES, AAS and XRF. Fresh cake samples (pre-oxidation) from batch 2 and 3 (B2 and B3) were used for selective precipitation studies. Representative samples were washed with distilled water to remove residual water soluble chlorides, mainly $CaCl_2$ before carrying out the leaching and selective precipitation steps. About 100 g of fresh cake was washed in 1000 mL distilled water using a set up similar to the leaching reactor.

5.4.1 Niobium precipitation

1. **Effect of precipitation temperature and time:** 10 mL of concentrated H_2SO_4 was added to 990 mL of solution from optimised leaching of filter cake. The mixture was then heated to 50, 60, 70, 80 or 90 °C and pH adjusted to 1 using 7.5 M NaOH solution and stirred at 200 rpm for 240 minutes.

2. **Effect of precipitation pH:** 10 mL of concentrated H_2SO_4 was added to 990 mL of solution from optimised leaching of filter cake, heated to 90 °C and pH was adjusted to 0.5, 1, 1.5, 2 or 2.5 using 7.5 M NaOH and stirred at 300 rpm for 180 minutes before filtering for residue analysis.

3. **Effect of SO_4^{2-} ions concentration:** 2.5, 5, 10, 15 or 20 mL concentrated H_2SO_4 was added to the solution containing metal chlorides (to make up 1000 mL solutions) at 90 °C and pH adjusted to 1 while stirring at 300 rpm for 180 minutes before filtering for residue analysis.

5.4.2 Vanadium precipitation

The pH 1 filtrates from optimised niobium precipitation stage were used for studying the effects of precipitation temperature and pH on vanadium precipitation rate. A solution of 7.5 M NaOH was used for adjusting precipitation pH. The investigations were carried out as follows:

1. **Effect of precipitation temperature and time:** 1000 mL of solution filtered from optimised niobium precipitation stage was heated to 50, 60, 70, 80 or 90 °C and pH was adjusted to 2 using 7.5 M NaOH solution. Air was then sparged through the reactor at a rate of 5 L min^{-1} while stirring at 300 rpm for 120 minutes before filtering and analysing the filtrates and precipitates.

2. **Effect of precipitation pH:** 1000 mL of solution filtered from optimised niobium precipitation stage was heated to 90 °C and 7.5 M NaOH was carefully injected into the reactor to achieve a pH of 0.5, 1, 1.5, 2 or 2.5. Once the pH was set, air was bubbled through the reactor at a rate of 5 L min^{-1} while stirring at 300 rpm. After 180 minutes, precipitation was ceased and the precipitates were filtered for analysis.

5.4.3 Scandium precipitation

1. **Effect of precipitation temperature:** 1000 mL of the solution from the optimised vanadium precipitation stage was heated to 50, 60, 70, 80 or 90 °C and pH was adjusted to 5 using 7.5 M NaOH solution. The solution was then stirred at 300 rpm for 60 minutes before filtering the precipitates and washing with hot water ready for analysis.

2. **Effect of precipitation pH:** 1000 mL of solution filtered from optimised vanadium precipitation stage was heated to 90 °C and 7.5 M NaOH was carefully injected into the reactor to achieve a pH of either 2.5, 3.5, 4.5, 5.5 or 7. Once the pH was set, the solution was stirred at 300 rpm for 60 minutes before filtering the precipitates and washing with hot water ready for analysis.

5.5 Purification studies

Purification studies were done sequentially, following the order of metal precipitation (niobium, then vanadium and finally scandium). Batch 2 (B2) was used for the studies.

5.5.1 Purification of niobium from pH 1 precipitates

To investigate the removal of zirconium from pH 1 precipitates by alkali leaching, the following parameters were studied sequentially:

1. **Effect of leaching temperature and time:** A 20 g sample of water washed pH 1 residues was introduced to 1000 mL of a 1 M Na_2CO_3 solution at temperatures of 25, 50, 60, 70, 80 or 90 °C and leached for 60 minutes while stirring at 300 rpm. 50 gL^{-1} $NaNO_3$ was added in all investigations.

2. **Effect of Na_2CO_3 concentration:** 1000 mL of Na_2CO_3 at concentrations of 0.5, 1, 1.5 and 2 M was introduced to the reactor and mixed with 50 gL^{-1} $NaNO_3$ before heating to 90 °C. Once temperature was stable, 20 g of water washed pH 1 precipitates were added to the reactor and stirred at 300 rpm for 60 minutes.

3. **Effects of $NaNO_3$ concentration and stirring speed:** 1000 mL of 2 M Na_2CO_3 solution was mixed with 0, 2, 5, 10, 15 or 20 gL^{-1} $NaNO_3$. The mixture was then heated to 90 °C and a 20 g sample was introduced to the reactor. The mixture was stirred for 60 minutes at 100, 200, 300, 400 or 500 rpm and filtered for analysis.

5.5.2 Purification of vanadium from pH 1.5 precipitates

Two approaches were investigated for purification of vanadium from pH 1.5 precipitates:

1. Salt roasting of vanadium concentrates followed by water leaching

2. Re-dissolving vanadium values from selective precipitation stage in Na_2CO_3 solutions

Salt roasting

The effects of salt - cake ratio, roasting temperature, roasting time (for both oxidising and NaCl roasting), leaching temperature, and leaching time were investigated. The studies on salt roasting process can be divided into three stages:

1. Pre-water leaching studies

2. Water leaching studies

3. Post water leaching studies

The pre-water leaching studies focused on the salt roasting of the cake and were sequentially investigated in four stages. Unless stated otherwise, the cake was roasted for 30 minutes at 550 °C before any investigations were carried out.

1. **Effect of oxidation temperature and time:** 25 g samples were roasted at 250, 350, 450, 550, 650 and 750 °C in open air for 10, 20, 30, 40, 50 and 60 minutes before mixing with 2.5 g NaCl and roasting again at 850 °C for 60 minutes. The roasted samples were water leached for 60 minutes at 60 °C while stirring at 300 rpm and filtered for analysis.

2. **Effect of roasting temperature and time:** The effects of roasting temperature on vanadium recovery were investigated at 750, 800, 850, 900 and at 950 °C. 25 g samples were mixed with 2.5 g of NaCl in a motor and pestle and roasted for up to 120 minutes at the appropriate temperature. The roasted samples were water leached for 60 minutes at 60 °C while stirring at 300 rpm and filtered for analysis.

3. **Effect of salt - cake ratio:** 25 g cake samples were roasted with 0, 2.5, 5, 10, 15, 20 and 25 wt. % NaCl at 850 °C for 60 minutes before water leaching in 500 mL distilled water for 60 minutes and analysing.

4. **Effect of leaching temperature and time** 50 g samples were oxidised at 550 °C for 60 minutes, roasted at 850 °C for another 60 minutes with 15 % NaCl and water leached at 25, 50, 60, 70, 80 or 90 °C for up to 60 minutes.

Alkali leaching

Alkali leaching of the pH 1.5 precipitates was studied as an alternative method for vanadium recovery for purification. The following parameters were studied sequentially:

1. **Effect of leaching temperature:** A 50 g sample of water washed pH 1.5 residues was introduced to 1000 mL of a 1 M Na_2CO_3 solution at temperatures of 25, 50, 60, 70, 80 or 90 °C and leached for 60 minutes while stirring at 300 rpm. 50 gL^{-1} $NaNO_3$ was added in all investigations.

2. **Effect of Na_2CO_3 concentration:** 1000 mL of Na_2CO_3 at concentrations of 0.5, 1, 1.5 and 2 M was introduced to the reactor and mixed with 50 gL^{-1} $NaNO_3$ before heating to 90 °C. Once temperature was stable, 50 g of water washed pH 1.5 precipitates were added to the reactor and stirred at 300 rpm for 60 minutes.

3. **Effects of $NaNO_3$ concentration and stirring speed:** 1000 mL of 2 M Na_2CO_3 solution was mixed with 0, 2, 5, 10, 15 or 20 gL^{-1} $NaNO_3$. The mixture was then heated to 90 °C and a 20 g sample was introduced to the reactor. The mixture was stirred for 60 minutes at 100, 200, 300, 400 or 500 rpm and filtered for analysis.

4. **The influence of solid-liquid ratio:** 20 gL^{-1} $NaNO_3$ was added to a 1000 mL solution of 2 M Na_2CO_3 at 90 °C. 40, 50, 70, 100 or 200 g of pH 1.5 precipitates samples were added to the reactor and the mixture was stirred at 300 rpm for 60 minutes.

All the investigations were carried out using a reactor set up similar to the one illustrated in Fig. 5.1 and samples for determining the influence of leaching time were drawn at 5, 10, 15, 20, 30, 40, 50 and 60 minutes.

5.5.3 Precipitation of vanadium from pregnant solutions

Vanadium was precipitated from the vanadium-rich solutions by employing the ammonium vanadate precipitation method [17, 46]. The effects of precipitation pH, precipitation temperature, time and NH_4Cl - V_2O_5 ratio on yield of precipitated vanadium were investigated. The mother liquor from alkali leaching of pH 5 precipitates was contaminated by aluminium, which had to be removed from the solution before precipitation of vanadium. This was achieved by adjusting the pH of the sodium carbonate solution from pH > 12 to pH 8. The precipitated aluminium was filtered and the solution treated in a similar way to the solution from NaCl roasting process for recovery of the vanadium values. The following parameters were sequentially studied:

1. **Effect of precipitation pH and temperature:** The pH of a 500 mL sodium vanadate solution at 20, 25, 30, 40 or 50 °C was adjusted to pH 7 and NH_4Cl was added to maintain an NH_4 to vanadium ratio of 0.6 (0.6 g NH_4 per gam vanadium). The solution pH was further reduced to 4,

4.5, 5, 5.5 or 6 using HCl and the mixture was stirred at 200 rpm for 6 hours before filtering and washing the precipitates in distilled water.

2. **Effect of NH_4Cl - V_2O_5 ratio and time** 0.4, 0.5, 0.6, 0.7 or 0.8 g ammonium chloride calculated as NH_4, per gram of vanadium pentoxide was added to 1000 mL sodium vanadate solutions at pH 7 before further reducing the pH to 4.5 using HCl. The mixture was then stirred at 200 rpm for 6 hours and 10 mL samples were drawn from the solution at regular intervals and quickly filtered for analysis.

5.5.4 Purification of scandium from pH 5 precipitates

Purification of scandium present in the pH 5 precipitates was achieved by leaching the precipitates in a mixture of Na_2CO_3 and $NaNO_3$. The following parameters were optimised sequentially:

1. **Effect of leaching temperature and time:** A 50 g sample of water washed pH 5 residues was introduced to 1000 mL of a 1 M Na_2CO_3 solution at temperatures of 25, 50, 60, 70, 80 or 90 °C and leached for 60 minutes while stirring at 300 rpm. 50 gL^{-1} $NaNO_3$ was added in all investigations.

2. **Effect of Na_2CO_3 concentration:** 1000 mL of Na_2CO_3 at concentrations of 0.5, 1, 1.5 and 2 M was introduced to the reactor and mixed with 50 gL^{-1} $NaNO_3$ before heating to 90 °C. Once temperature was stable, 50 g of water washed pH 5 precipitates were added to the reactor and stirred at 300 rpm for 60 minutes.

3. **Effects of $NaNO_3$ concentration and stirring speed:** 1000 mL of 2 M Na_2CO_3 solution was mixed with 0, 2, 5, 20, 30 or 50 gL^{-1} $NaNO_3$. The mixture was then heated to 90 °C and a 50 g sample of pH 5 precipitates was introduced to the reactor. The mixture was stirred for 60 minutes at 100, 200, 300, 400 or 500 rpm and filtered for analysis.

5.6 Integrated recovery process

1 kg of wet as-received cake (Batch 3) was washed in 2000 mL distilled water in a 4000 mL closed reactor similar to the one in Fig. 5.1. The washed sample was used in all stages of the process:

1. Dissolved in 1500 mL of 4 M HCl and stirred at 300 rpm for 60 minutes at 70 °C.

2. Sample from step 1 was filtered while hot and filtrates were mixed with 150 mL concentrated H_2SO_4.

3. The mixture temperature was raised to 90 °C and maintained for 180 minutes while stirring at 200 rpm to precipitate niobium at pH 1.

4. The precipitates formed in step 3 were filtered off and solution was re-heated to 90 °C and pH raised to 1.5 using 7.5 M NaOH.

5. Air was sparged through the reactor at a rate of 7.5 $L \cdot min^{-1}$ for vanadium precipitation.

6. The vanadium-rich precipitates from step 5 were filtered hot and the filtrates were again heated to 90 °C and pH adjusted to 5 while stirring at 200 rpm for scandium precipitation.

7. The scandium-rich precipitates were then water-washed and leached for 60 minutes in a mixture of 1M Na_2CO_3 and 50 gL^{-1} $NaNO_3$ at 90 °C and stirring speed of 300 rpm. The filtrates and precipitates from all stages were weighed and analysed by XRD, XRF and SEM-EDX.

The different stages employed for metal recovery were repeated using batches 2 and 3 to determine influence of cake mineralogy on metal recovery.

Chapter 6

Results and discussion

6.1 Introduction

Chapter 6 presents results from batch leaching, selective precipitation and metal purification experiments as well as results from experiments conducted using synthetic oxides of TiO_2 and V_2O_5. The influence of temperature, lixiviant concentration, leaching time, stirring speed, solid-liquid ratio and pH on the leaching and precipitation characteristics of vanadium, scandium and niobium are reported herein:

- Section 6.2 presents the effects of composition of binary mixtures and sintering temperature on dissolution of vanadium in solvent rutile phase as well as the vanadium dissolution model for NaOH leaching of the solid solutions formed.
- The effects of parameters temperature, HCl concentration, leaching time, stirring speed, solid-liquid ratio and pH on dissolution of vanadium, scandium and niobium in HCl are presented in section 6.3. These are used in developing the kinetics models for the leaching processes and can be used to predict the behaviour of the valuable metals when cake already landfilled is leached.
- Section 6.4 presents the effects of parameters on recovery and purity of the valuable metals when selective precipitation processes are employed for separation.
- The purification of metals from their respective precipitates is presented in section 6.5 and the behaviour of thorium in acidic and alkaline media is presented in section 6.6.

Section 6.7 presents a diagramatic illustration of the integrated processing steps and mass balance based on a 1 kg batch experiment and all results are summarised in section 6.9.

6.2 Dissolution and chemical properties of vanadium in TiO_2 lattice

6.2.1 The effects of vanadium mole fraction and NaOH leaching on rutile lattice parameters

Figures 6.1 and 6.2 show that increasing V_2O_5 concentration leads to a decrease in both the *'a'* and *'c'* lattice parameters, suggesting that the smaller V^{5+} ions (0.54 Å)[1]are substituting Ti^{4+} ions (0.61 Å)[1] at the octahedral sites.

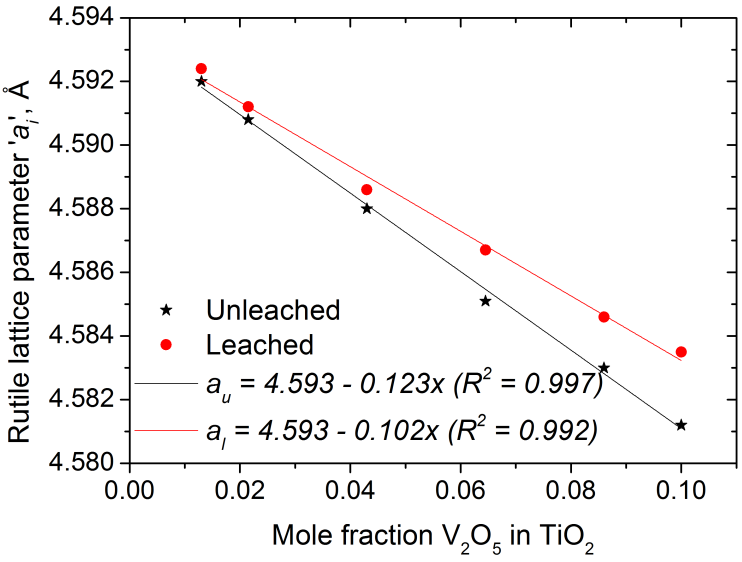

Fig. 6.1 The influence of leaching and V_2O_5 mole fraction on tetragonal rutile lattice parameter *'a'*. Constants: Sintering temperature (1100 °C), leaching temperature (60 °C), stirring speed (300 rpm), NaOH concentration (2 M). Lattice parameters determined using the Rietveld refinement method

Leaching the solid solutions in NaOH increases the lattice parameters due to dissolution of some vanadium from the octahedral sites. For all compositions, '*c*' parameters follow the same trend as the '*a*' parameters. Lattice changes parallel to the *'c-axis'* are not as marked as in the *'a-axis'*, suggesting structural

[1]six-fold ionic radii

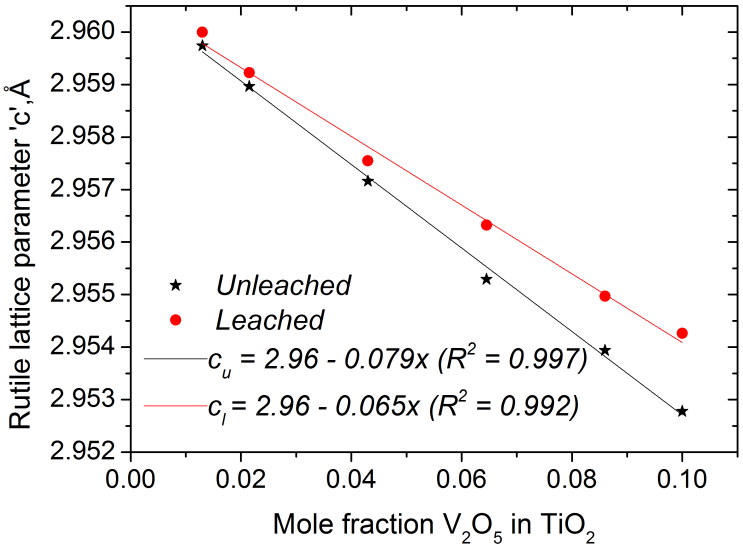

Fig. 6.2 The influence of leaching and V_2O_5 mole fraction on tetragonal rutile lattice parameter *'c'*. Constants: Sintering temperature (1100 °C), leaching temperature (60 °C), stirring speed (300 rpm), NaOH concentration (2 M). Lattice parameters determined using the Rietveld refinement method

implications and this agrees with Sanghera and Williamson's work on TiO_2 – Nb_2O_5 solid solutions [160].

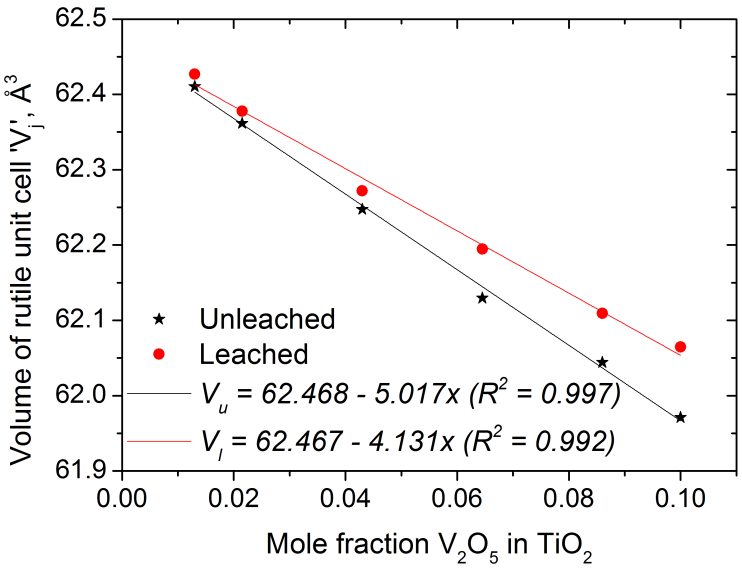

Fig. 6.3 The influence of leaching and V_2O_5 mole fraction on rutile unit cell volume *'V'* determined using the Rietveld refinement method

The solid lines for lattice parameters are linear fits that follow Vegard's law [161] very well (R^2 values >0.99) and are represented by equations 6.1 and 6.2 for the unleached and leached samples respectively. The solid lines for cell

volumes, V_i, are also linear fits and are represented by equations 6.3 and 6.4 for the unleached and leached samples respectively.

$$a_u = 4.593 - 0.123x \tag{6.1}$$

$$a_l = 4.593 - 0.102x \tag{6.2}$$

$$V_u = 62.468 - 5.017x \tag{6.3}$$

$$V_l = 62.467 - 4.131x \tag{6.4}$$

a_u and a_l represent the 'a' lattice parameters for the unleached and leached binary mixtures respectively, and similarly, V_u and V_l represent the unit cell volumes for the unleached and leached binary mixtures respectively.

6.2.2 Effects of sintering temperature on microstructure

Fig. 6.4 and Fig. 6.5 show the SEM micrographs and XRD patterns of the sintered binary mixtures respectively.

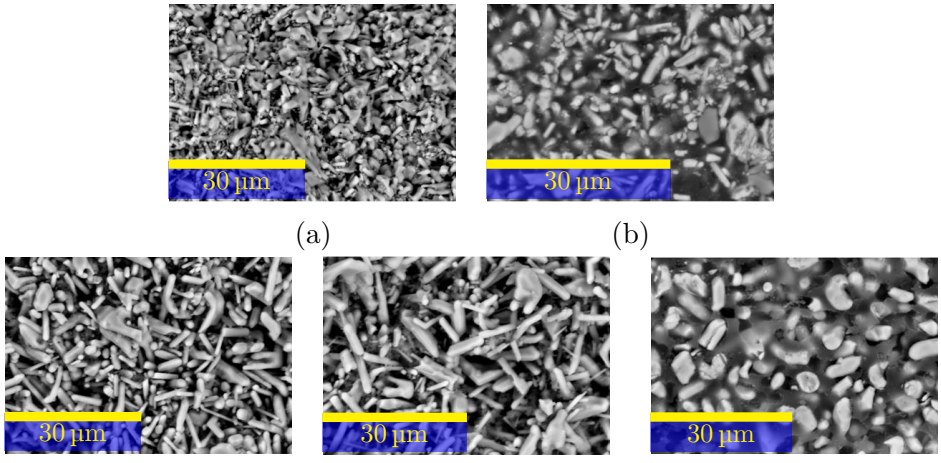

Fig. 6.4 SEM micrographs of TiO_2 - V_2O_5 binary mixtures sintered at 700 °C (a), 800 °C (b), 900 °C (c), 1000 °C (d) and 1100 °C (e) for 24 hours.

No V_2O_5 phases are present in both the XRD patterns and SEM micrographs, suggesting that the minor V_2O_5 is completely dissolved in the TiO_2 matrix to form a complete solid solution.

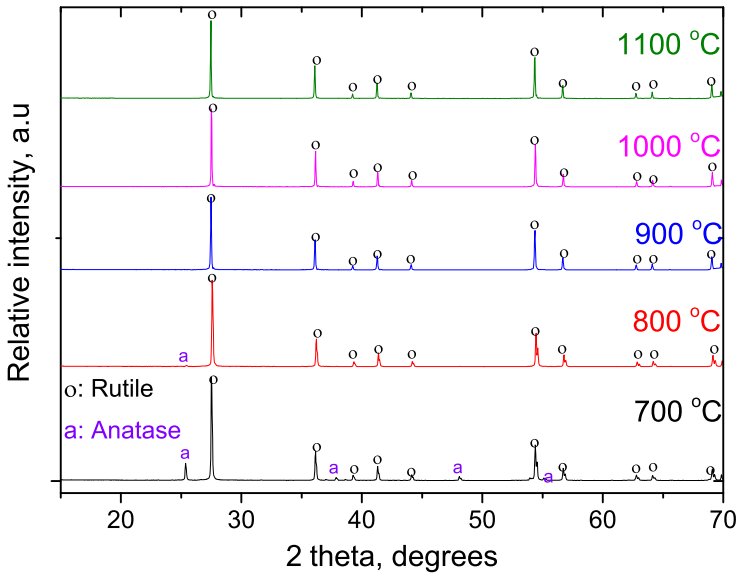

Fig. 6.5 Powder X-ray diffraction patterns measured at room temperature for TiO_2 - V_2O_5 binary mixtures sintered at various temperatures and rapidly quenched. The diffraction data compares well with the ICDD references: 04-008-7811 (TiO_2 rutile) and 04-006-9240 (TiO_2 anatase)

Fig. 6.4 also shows that the average grain size increases with sintering temperature, with a clear preferential orientation of the rod-like particles, typical of rutile [162], suggesting that the crystals and particles may be growing preferentially along *'a-axis'*.

6.2.3 Effect of sintering temperature on TiO_2 lattice parameters

Figures 6.6 and 6.7 show a decrease in rutile lattice parameters with increasing sintering temperature, indicating that more vanadium ions occupy the octahedral sites with increasing sintering temperature. Equations 6.5 and 6.6 represent the decrease in parameter *'a'* and *'c'* respectively, for the unleached samples.

$$a_u = -0.00121x^2 + 0.000916x + 4.591 \tag{6.5}$$

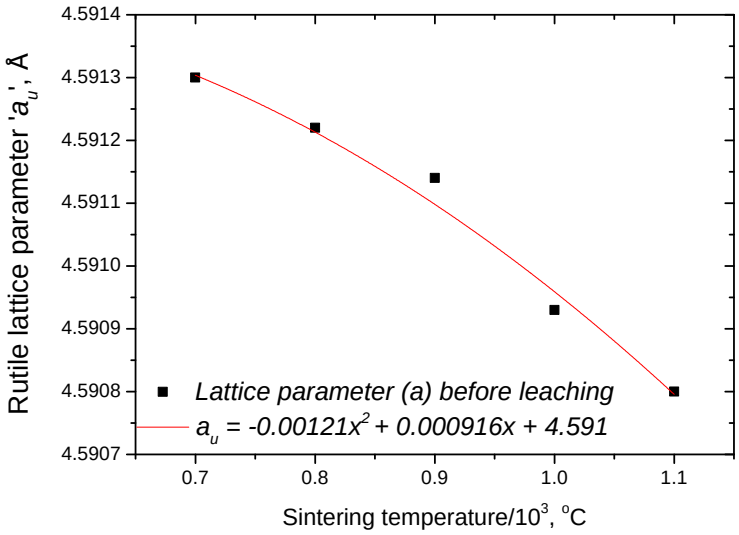

Fig. 6.6 Effect of sintering temperature on lattice parameter 'a'. All samples sintered for 24 hours at the required temperature. Vanadium concentration was maintained at 2 mol% as V_2O_5 in all samples.

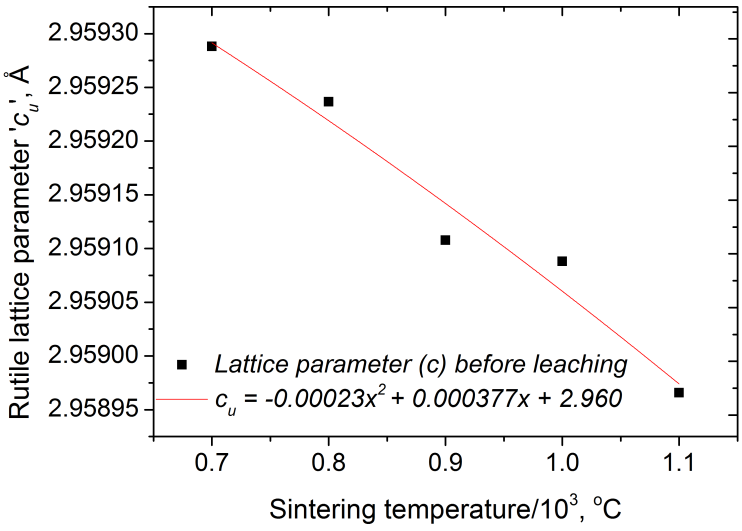

Fig. 6.7 Effect of sintering temperature on lattice parameter 'c'. All samples sintered for 24 hours at the required temperature. Vanadium concentration was maintained at 2 mol% as V_2O_5 in all samples.

$$c_u = -0.00023x^2 + 0.000377x + 2.960 \tag{6.6}$$

6.2.4 Effect of leaching temperature

Effect of leaching temperature and time on vanadium dissolution

Fig. 6.8 presents the influence of temperature on the dissolution of vanadium for binary mixtures sintered at 700, 800, 900, 1000 and 1100 °C.

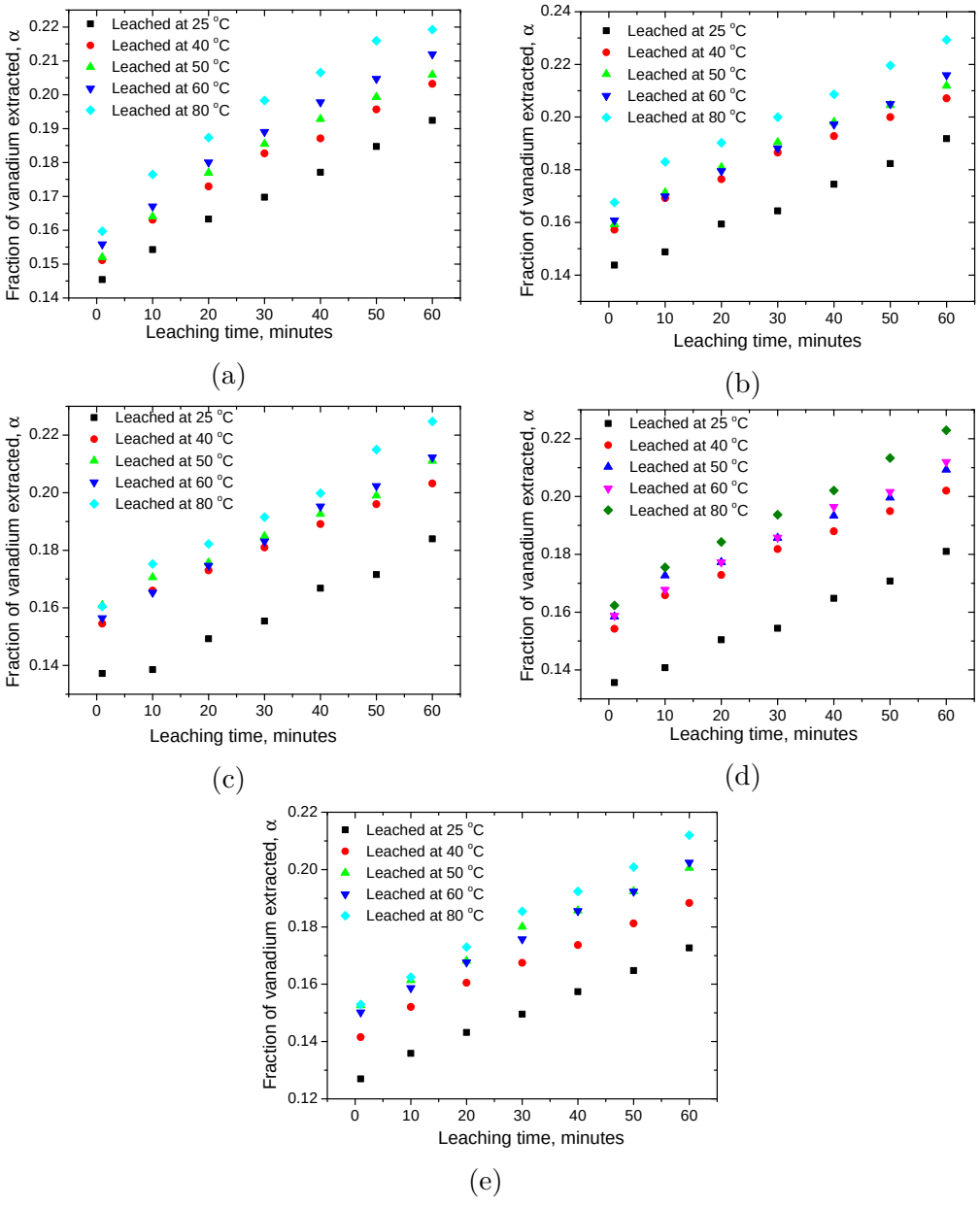

Fig. 6.8 The effects of leaching temperature and time on the dissolution of vanadium from TiO_2 - V_2O_5 binary mixtures sintered at 700 °C (a), 800 °C (b), 900 °C (c), 1000 °C (d) and 1100 °C (e) for 24 hours and leached in 2M NaOH mainintaining a pulp density of 20 g L^{-1} and a stirring speed of 300 rpm

The effects of leaching temperature and time on dissolution of vanadium from rutile solid solutions were investigated by leaching the sintered binary mixtures in 2 M NaOH solution for 60 minutes at 25, 40, 50, 60, 70 and 80 °C. The results indicate that vanadium extraction increases with increasing leaching temperature, with best recoveries observed when the samples are leached at 80 °C for 60 minutes. Fig. 6.8 also shows a small decrease in recovery with increasing sintering temperature.

From the investigations carried out on synthetic TiO_2 - V_2O_5 solid solutions, it was observed that:

1. Although V_2O_5 has high solubility in NaOH, extraction from rutile solid solutions using 2M NaOH is poor (less than 25 % after 60 minutes of leaching), meaning that extraction of vanadium from the rutile lattice requires a different lixiviant.

2. Increasing V_2O_5 concentration in the solid solution leads to a decrease in rutile lattice parameters and unit cell volumes. The decrease in rutile lattice parameters with increasing vanadium concentration in the solid solutions follow Vegard's law very well (R^2 values >0.99).

3. Leaching the solid solutions in NaOH leads to an increase in unit cell volumes.

6.3 Dissolution of metal values in HCl

6.3.1 Effect of leaching temperature

Figures 6.9 - 6.11 present the influence of leaching temperature on extraction of niobium, vanadium and scandium from as-received filter cake. Batch 1 (B1) was used for all the investigations carried out on influence of leaching temperature. Fig. 6.9 shows that increasing the leaching temperature from 25 °C to 80 °C raises niobium extraction rate from nearly 30 % to just under 50 % within 60 minutes of leaching. Raising the temperature further to 90 °C lowers the extraction rate to about 35 %. The decrease in niobium extraction rate is due to precipitation of hydrous oxides of niobium [163]. Marczenko and Kloczko [164] have reported a method of separation and pre-concentration of niobium, where an acidic solution is heated to hydrolyse and coagulate niobium, forming niobium oxides. A similar phenomenon has been observed on other transition

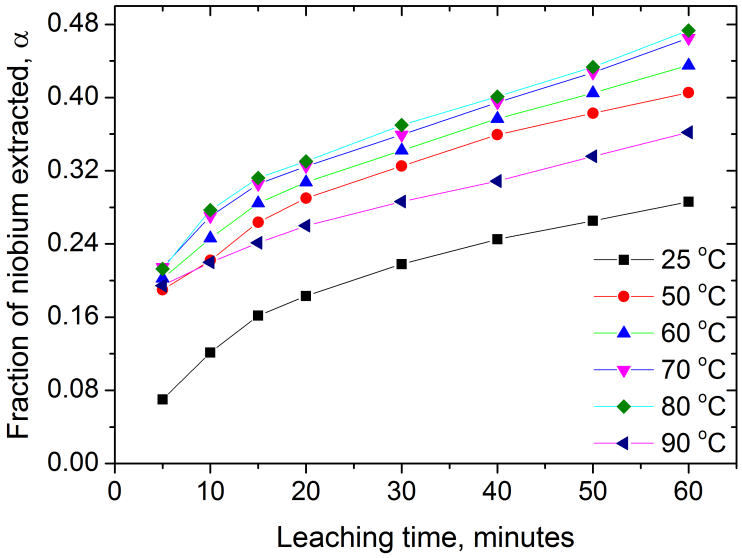

Fig. 6.9 Effect of leaching temperature on niobium dissolution. Constant parameters were: Stirring speed (300 rpm), solid-liquid ratio (50 g L^{-1}) and HCl concentration (1.5 M).

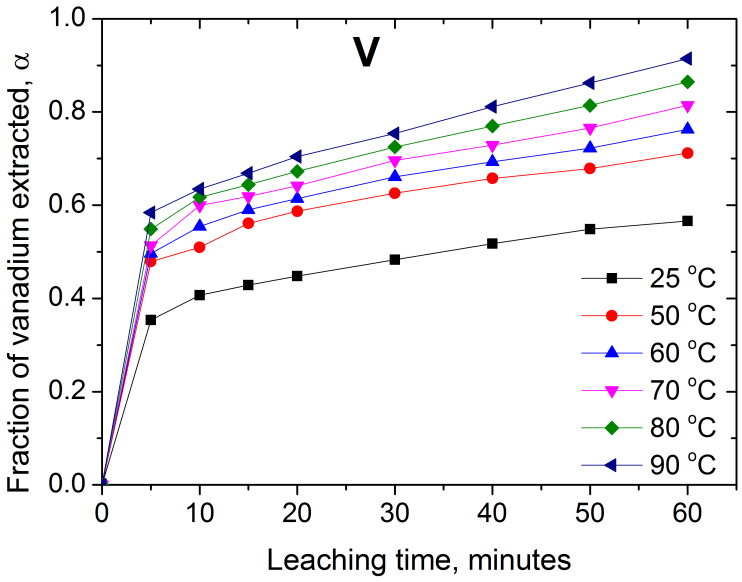

Fig. 6.10 Effect of leaching temperature on vanadium dissolution. Constant parameters were: Stirring speed (300 rpm), solid-liquid ratio (50 g L^{-1}) and HCl concentration (1.5 M).

metals such as zirconium [165], nickel [166], which precipitates as an oxalate at temperatures above 50 °C and titanium, which precipitates as hydrous titanium dioxide at temperatures above 70 °C [167].

Fig. 6.10 shows a better extraction rate of vanadium compared to niobium (Fig. 6.9) in the same temperature range. Vanadium extraction rate doubled

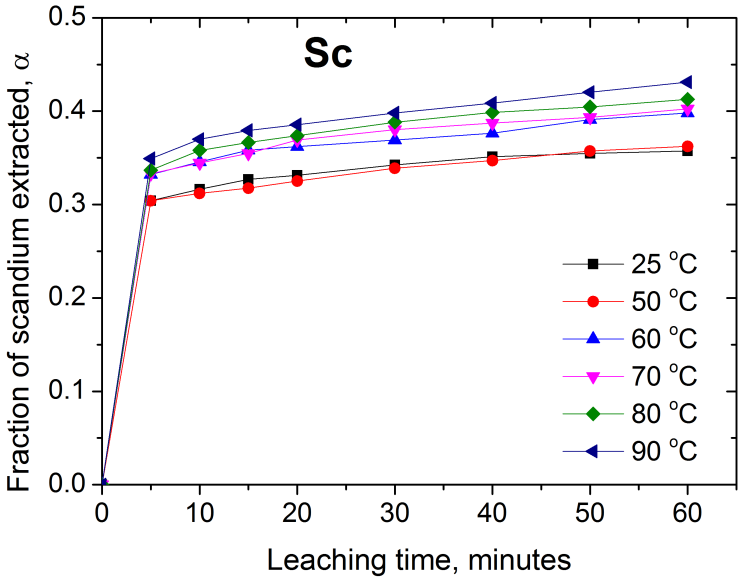

Fig. 6.11 Effect of leaching temperature on scandium dissolution. Constant parameters were: Stirring speed (300 rpm), solid-liquid ratio (50 g L^{-1}) and HCl concentration (1.5 M).

from about 40 % at 25 °C to 80 % at 90 °C. Unlike with the dissolution of niobium, which reduces above 80 °C, the degree of vanadium dissolution gradually increases over the temperature range investigated. Fig. 6.11 shows that scandium leaching rate gradually increases with temperature over the investigated temperature range. Less than 45 % scandium is dissolved over a leaching time of 60 minutes when 1.5 M HCl is used for leaching the as-received cake.

A leaching temperature of 70 °C was employed for all remaining investigations on metal extraction rates as both the filtration and leaching rates were similar to those observed at 80 °C. Leaching at 90 °C lowers niobium extraction rate.

6.3.2 Effect of HCl concentration

The influence of HCl concentration on extraction rates of niobium, vanadium and scandium is shown in figures 6.12 - 6.14. Batch 1 (B1) was used for all studies on influence of HCl concentration on dissolution of metals.

Fig. 6.12 shows the effects of HCl concentration and leaching time on niobium dissolution. Increasing the HCl concentration from 0.5 M to 4 M raises the fraction of niobium extracted from under 5 % to more than 90 % after 60 minutes.

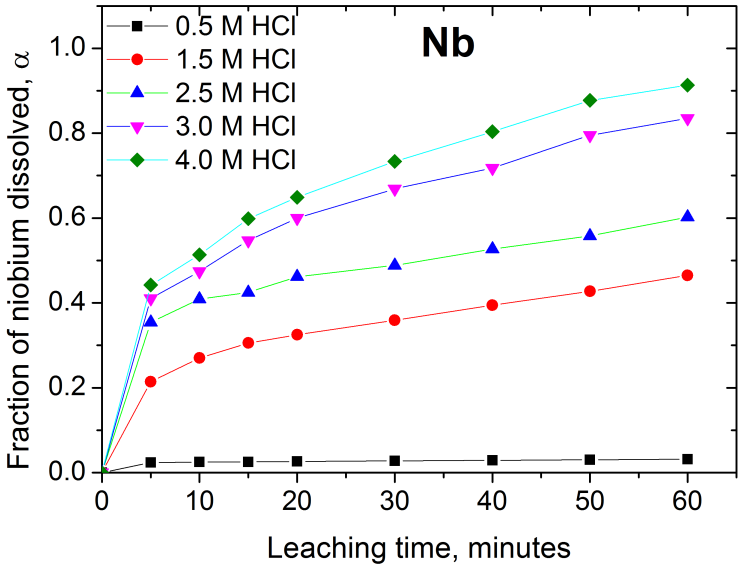

Fig. 6.12 Effect of HCl concentration on niobium dissolution. Constant parameters were: Stirring speed (300 rpm), solid-liquid ratio (50 g L^{-1}) and leaching temperature (70 °C).

Fig. 6.13 shows that nearly all vanadium is leached after 60 minutes in 4 M HCl and more than 50 % is leached after 60 minutes in 0.5 M HCl. Under the

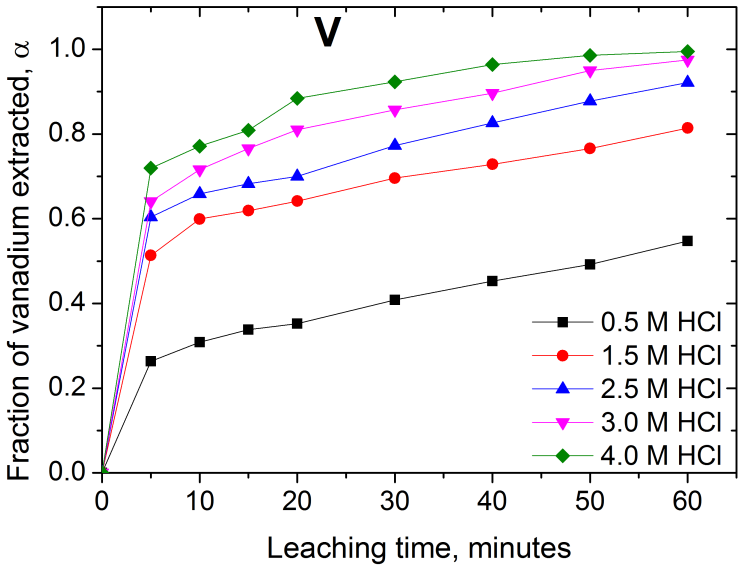

Fig. 6.13 Effect of HCl concentration on vanadium dissolution. Constant parameters were: Stirring speed (300 rpm), solid-liquid ratio (50 g L^{-1}) and leaching temperature (70 °C).

same leaching conditions, vanadium extraction rate is less sensitive to changes in HCl concentration compared to niobium dissolution.

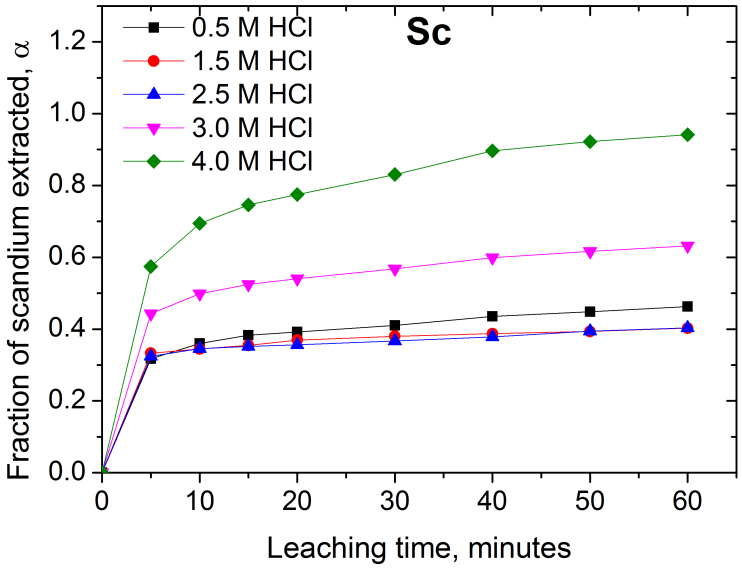

Fig. 6.14 Effect of HCl concentration on scandium dissolution. Constant parameters were: Stirring speed (300 rpm), solid-liquid ratio (50 g L^{-1}) and leaching temperature (70 °C).

The influence of HCl concentration on scandium extraction is shown in Fig. 6.14. The scandium extraction rate is higher when 0.5 M HCl is used compared to leaching in either 1.5 M or 2.5 M HCl, although the difference is less than 5 %. Raising the HCl concentration to 3 M and 4 M significantly increases the degree of scandium extraction, with an extraction efficiency of nearly 100 % when 4 M HCl is used for leaching.

Increasing HCl concentration significantly increases extraction rates of niobium, vanadium and scandium. This is because increasing the concentration of reactants increases the concentration gradient, hence the flow rate across the interfacial boundary layer [168]. Although there is no significant difference in extraction rates of vanadium and niobium when either 3 M or 4 M HCl is used, the difference in scandium extraction means that all remaining investigations were carried out using 4 M HCl for cake dissolution. Filtration of residues from leaching of as-received cake using 4 M HCl is also much faster compared to samples leached in 3 M HCl.

6.3.3 Effect of solid - liquid ratio

Figures 6.15 - 6.17 present the influence of solid - liquid ratio on extraction rates of niobium, vanadium and scandium. Batch 1 (B1) was utilised for studying the influence of solid-liquid ratio on dissolution rate of metals.

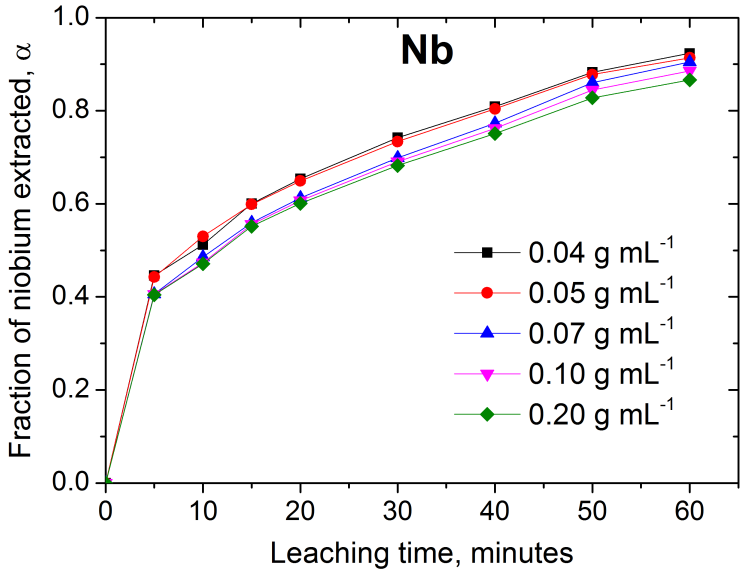

Fig. 6.15 Effect of solid - liquid ratio on niobium dissolution. Constant parameters were: Stirring speed (300 rpm), HCl concentration (4 M) and leaching temperature (70 °C).

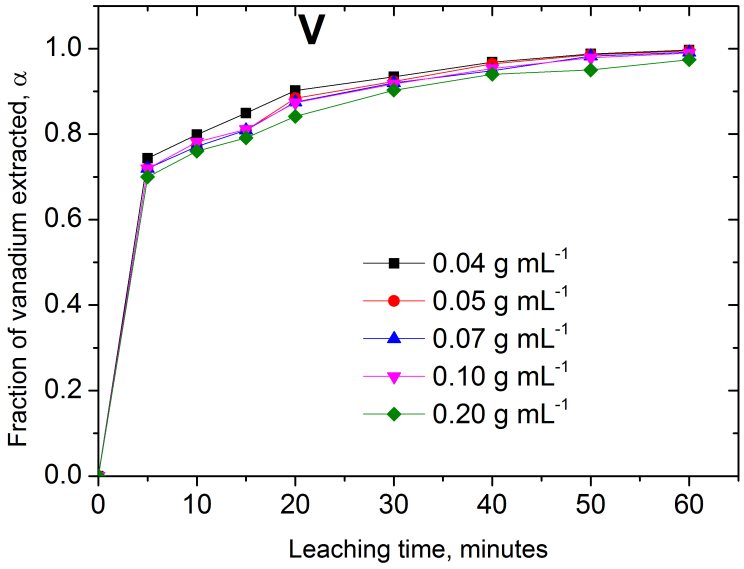

Fig. 6.16 Effect of solid - liquid ratio on vanadium dissolution. Constant parameters were: Stirring speed (300 rpm), HCl concentration (4 M) and leaching temperature (70 °C).

In the range of solid - liquid ratios investigated, there is no significant difference in extraction rates of all the metals investigated, meaning that the decrease in association between the HCl and filter cake is not significant.

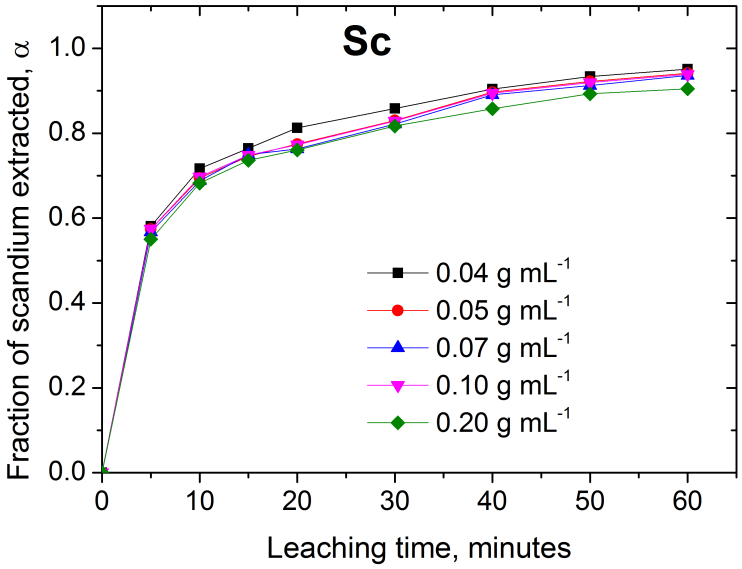

Fig. 6.17 Effect of solid - liquid ratio on scandium dissolution. Constant parameters were: Stirring speed (300 rpm), HCl concentration (4 M) and leaching temperature (70 °C).

6.3.4 Effect of stirring speed

The influence of stirring speed and leaching time on extraction rates of niobium, vanadium and scandium from the filter cake (B1) is presented in figures 6.18 - 6.20.

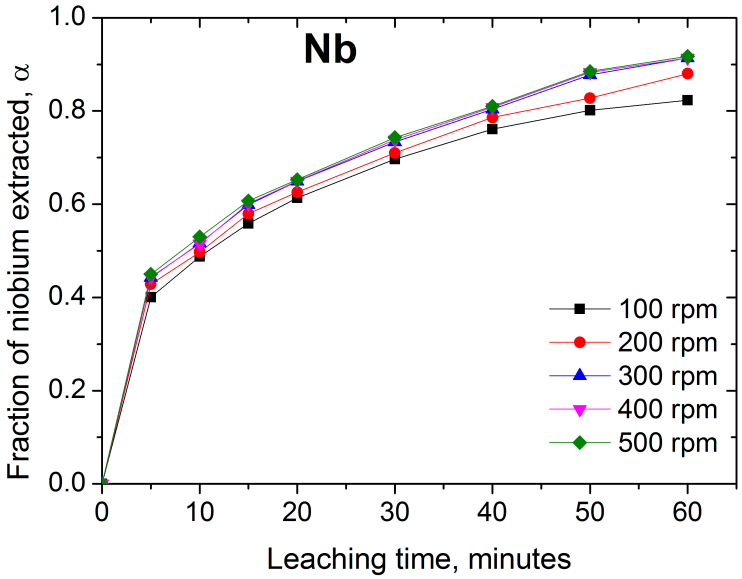

Fig. 6.18 Effect of stirring speed on niobium dissolution. Constant parameters were: Solid - liquid ratio (50 g L^{-1}), HCl concentration (4 M) and leaching temperature (70 °C).

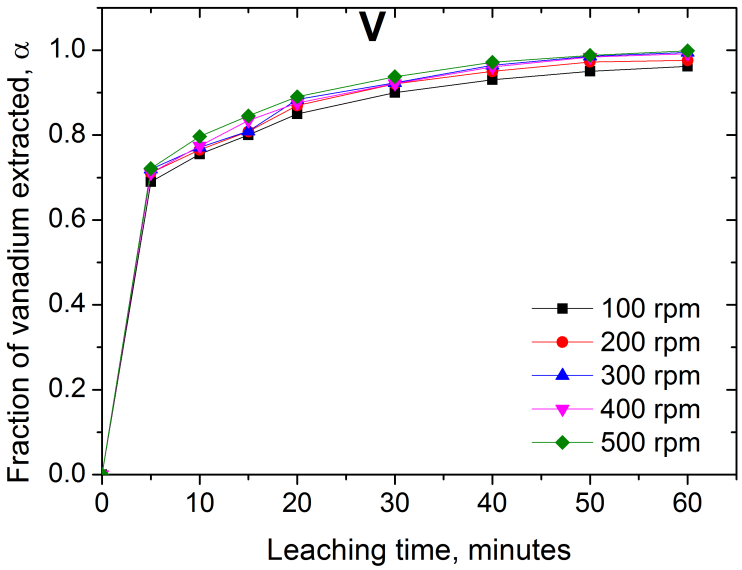

Fig. 6.19 Effect of stirring speed on vanadium dissolution. Constant parameters were: Solid - liquid ratio (50 g L^{-1}), HCl concentration (4 M) and leaching temperature (70 °C).

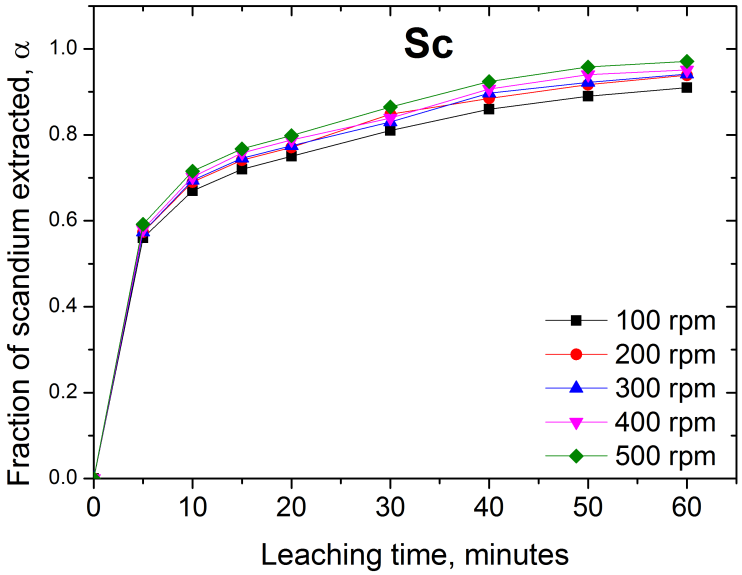

Fig. 6.20 Effect of stirring speed on scandium dissolution. Constant parameters were: Solid - liquid ratio (50 g L^{-1}), HCl concentration (4 M) and leaching temperature (70 °C).

The film thickness around filter cake particles suspended in a reaction vessel varies with the stirring speed. Increasing the stirring speed minimises the diffusion layer thickness, hence increases the mass transfer rates through the diffusion layer. The sensitivity of metal extraction rates to stirring speed can be used for distinguishing between film diffusion and particle diffusion

controlled reaction kinetics. For intraparticle diffusion controlled reactions, the ion-exchange rates are independent of the stirring speed. Figures 6.18-6.20 show that the influence of stirring speed is minimal for extraction of the metals from filter cake. Niobium extraction rate has the biggest sensitivity to stirring speed (Fig. 6.18), with only about 10 % difference in extraction rate when stirring speed is increased from 100 to 500 rpm. Vanadium and niobium extraction rates are independent of stirring speed above 300 rpm, and scandium extraction increased by 3 % when stirring speed was increased from 300 rpm to 500 rpm. Thus 300 rpm is the optimum stirring rate for simultaneous extraction of the metals from the filter cake.

6.3.5 Optimum leaching conditions

Based on the overall recoveries for all metals and the leaching characteristics of the residues, the ideal conditions for leaching of filter cake are:

Table 6.1 Conditions for dissolution of filter cake

Temperature	[HCl]	pH	Solid-liquid ratio	Stirring speed	Time
70 °C	4 M	-0.6	0.05 g mL^{-1}	300 rpm	60 minutes

Leaching the filter cake under these conditions minimises hydrothermal precipitation of hydrated niobium oxide (typically occurs at about 90 °C) without impacting on extraction rates of the valuable metals.

6.3.6 Analysis of the HCl leach residues

Residues from the optimised HCl leach process were analysed by SEM-EDX and XRD to help understand the leaching process. Filter cake was leached utilising the conditions summarised in Table 6.1 and filtered before water washing the residues ready for analysis. Analysis of residues helps with monitoring of radionuclides to ensure that they are not concentrating to levels hazardous for landfilling at current landfill sites.

A summary of phase analysis by XRD and Loss on ignition (LOI)

An average of 85 % TiO_2 and nearly 10 % SiO_2 was observed from XRF analysis of the HCl leach residues (metal oxides only). The X-ray diffraction analysis of calcined residues shown in Fig. 6.21 also confirms that the residues consist of TiO_2 and SiO_2. The residues have a LOI of nearly 30 % at 950 °C.

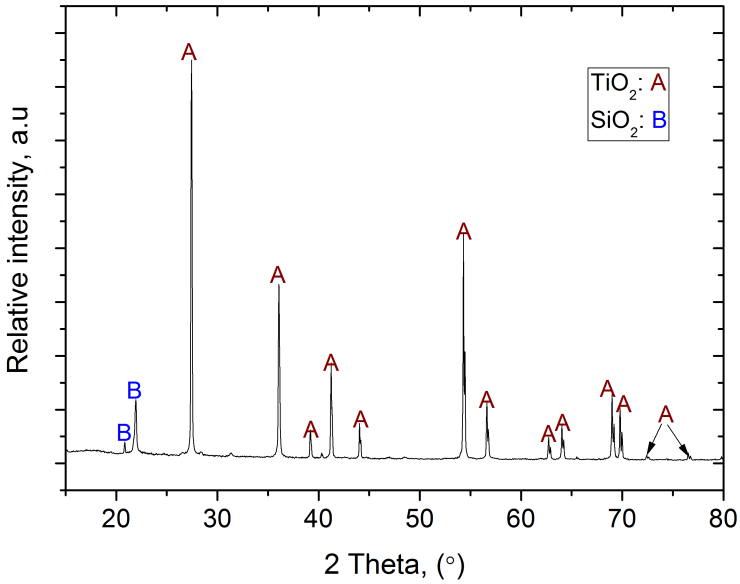

Fig. 6.21 The XRD pattern of HCl leach residues from leaching of filter cake at 70 °C with a solid-liquid ratio of 0.05 and a stirring speed of 300 rpm in 4 M HCl

A summary of phase analysis by SEM-EDX

Figure 6.22 presents the SEM phase analysis of the residues formed from optimised leaching of filter cake.

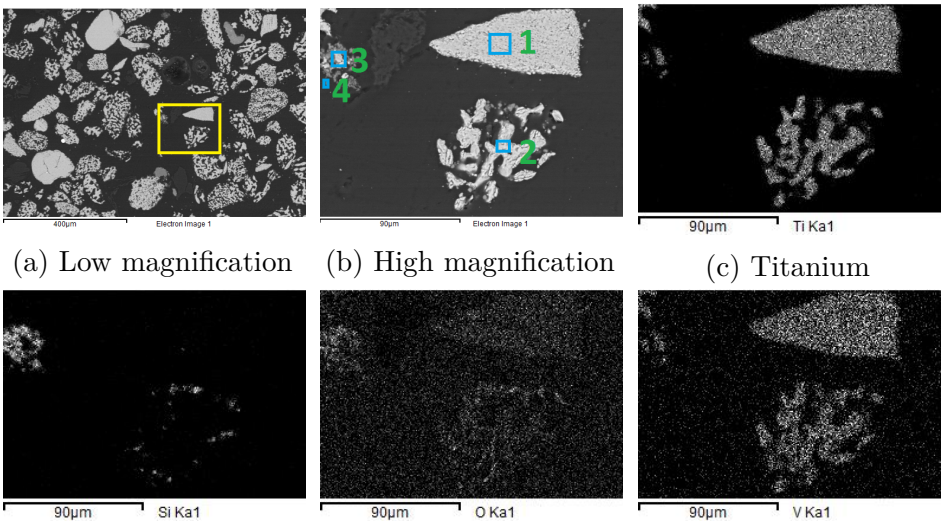

(a) Low magnification (b) High magnification (c) Titanium

(d) Silicon (e) Oxygen (f) Vanadium

Fig. 6.22 SEM analysis of residues from leaching of filter cake at 70 °C with a solid-liquid ratio of 0.05 and a stirring speed of 300 rpm in 4 M HCl

Unreacted ore (TiO_2) and silica are the main components of the residues. By comparing Fig. 6.22c and Fig. 6.22f, it can be concluded that most of the

vanadium that cannot be leached under optimum leaching conditions is trapped in rutile solid solution. Elemental mapping of the residues shows no evidence of niobium, scandium or thorium but EDX chemical analysis presented in Table B.5 corroborates the presence of niobium in rutile solid solution.

6.4 Selective precipitation of valuable metals

6.4.1 Selective precipitation of niobium

Effect of precipitation temperature

Fig. 6.23 shows that niobium precipitation significantly increases with increasing precipitation temperature.

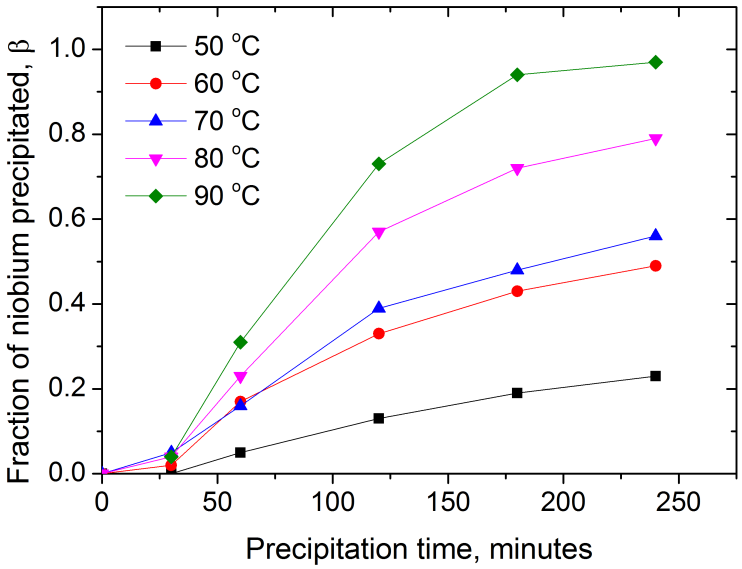

Fig. 6.23 The effect of temperature on niobium precipitation. Stirring speed (200 rpm), pH (1) and Solid - liquid ratio (50 g L^{-1})

The conclusion drawn from analysing Fig. 6.9 was that hydrated niobium oxides precipitate when filter cake is leached at 90 °C and this is supported by the increasing niobium precipitation rate observed as precipitation temperature is increased to 90 °C in Fig. 6.23. When precipitation is carried out at 90 °C, nearly all the dissolved niobium is precipitated.

Table 6.2 Compositions of final precipitates after precipitating for 120, 180 and 240 minutes at 90 °C and pH 1.

	TiO_2	Fe_2O_3	Nb_2O_5	ZrO_2	ThO_2
120 minutes	27.8	9.6	19.4	20.3	0.8
180 minutes	21.9	12.5	15.7	18.1	0.7
240 minutes	21.7	14.1	15.2	17.8	0.7

Similar recoveries were observed by Gireesh et al. [121], who had to wait for 5 hours before achieving optimum recovery. The reason for such a relatively long precipitation time being needed has not been established. There is a

strong possibility that in this research, niobium and other metals coprecipitated/adsorbed on hydrated TiO_2 and Fe_2O_3, which both precipitated relatively fast at pH 1.

Effect of precipitation pH

Fig. 6.24 shows the influence of pH on precipitation of niobium at 90 °C and a precipitation time of 180 minutes.

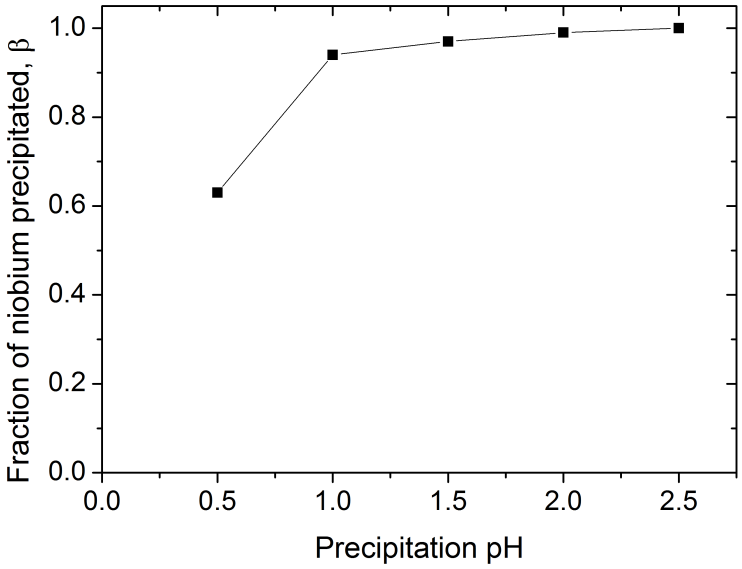

Fig. 6.24 The effect of pH on niobium precipitation. Constant parameters were: Solid - liquid ratio (50 g L^{-1}), Stirring speed (200 rpm) and leaching temperature (90 °C).

As shown in Fig. 6.24, niobium precipitation is favoured by high pH. Table 6.3 shows that at higher pH, the precipitated niobium is contaminated by other species, mainly iron therefore an optimum pH has to be determined.

Table 6.3 Compositions of precipitates formed at 90 °C and pH values of 0.5, 1, 1.5, 2 and 2.5 over a total time of 180 minutes.

pH	TiO_2	Fe_2O_3	Nb_2O_5	ZrO_2	ThO_2
0.5	39.2	5.6	21.6	22.3	0.8
1.0	21.9	12.5	15.7	18.1	0.7
1.5	18.2	27.5	14.5	15.7	0.6
2.0	14.0	35.5	11.3	12.1	0.5
2.5	13.7	38.1	11.0	11.9	0.5

Based on Table 6.3 alone, pH 0.5 seems to be the ideal precipitation pH for subsequent niobium recovery as it has the least amount of contaminants.

Fig. 6.24 is in contrast to utilising pH 0.5 since it only achieves about 60 % niobium precipitation after a precipitation time of 180 minutes. Consequently, pH 1 has been chosen as the optimum precipitation pH despite having slightly inferior niobium concentration.

Effect of catalyst (H_2SO_4) volume

The effect of catalyst volume on niobium precipitation is presented in Fig. 6.25.

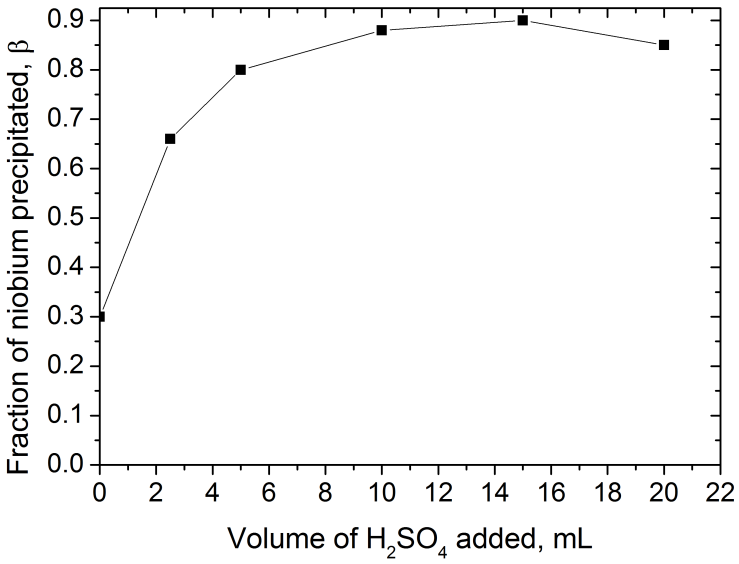

Fig. 6.25 The effect of amount of H_2SO_4 catalyst added on niobium precipitation at pH 1 and 90 °C.

Increasing the H_2SO_4 volume from 2 mL to 15 mL increases the amount of niobium precipitated while increasing further to 20 mL leads to a slight decrease in amount of niobium precipitated. There is no significant difference in the quality of niobium precipitated using different volumes of catalyst.

A summary of phase analysis by SEM-EDX

Fig. 6.26 and Table B.6 show that titanium, iron and zirconium are the main impurities in pH 1 precipitates and they precipitate as sulphates. Thorium also coprecipitates with other sulphates, concentrating to levels which may be hazardous if the stream is not mixed with other waste streams coming from the process.

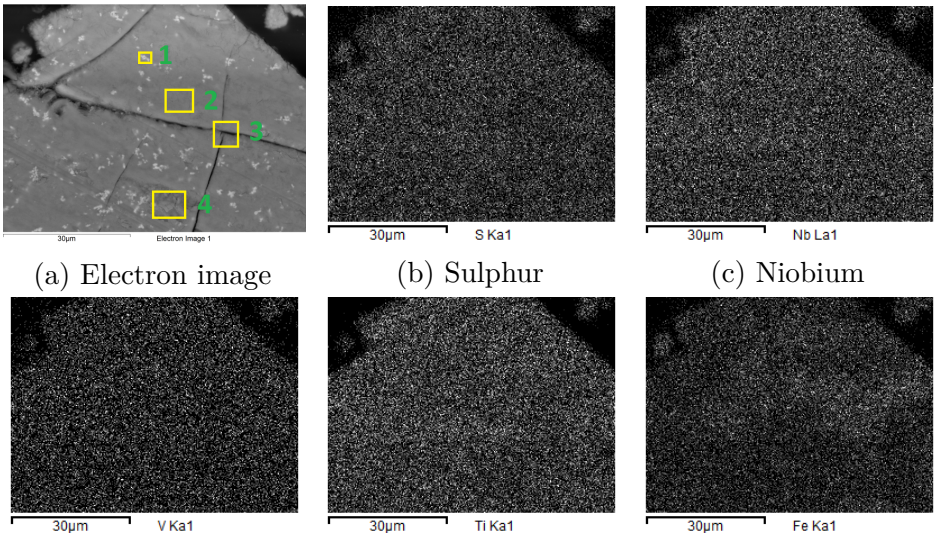

(a) Electron image (b) Sulphur (c) Niobium

(d) Vanadium (e) Titanium (f) Iron

Fig. 6.26 SEM analysis of niobium-rich precipitates from precipitation of niobium at 90 °C at pH 1

A summary of phase analysis by XRD

As with the as-received filter cake, the pH 1 precipitates were mainly hydrated oxides with poor crystal ordering hence could not produce sharp peaks when analysed by XRD. In some samples, calcium sulphate peaks were observed. The appearance and intensity of the peaks varied and depended on the efficiency of the water washing stage where residual $CaCl_2$ was washed from the filter cake. The amount of calcium that slips through the processing steps has to be minimised as it forms stable vanadates that could limit the extraction efficiency of the valuable metals, particularly vanadium [17]. Fig. B.4 presents the XRD analysis of the pH 1 precipitates, highlighting the importance of minimising slipping of residual calcium through the process.

Optimum conditions for precipitation of niobium

Table 6.4 summarises the optimised conditions for precipitation of niobium from the HCl leach filtrates.

Table 6.4 Conditions for precipitation of niobium

Temperature	H_2SO_4	pH	Time	Solid-liquid ratio
90 °C	15 mL	1	180 minutes	0.05 g mL^{-1}

The volume of the H_2SO_4 required was found to be dependent on the amount of niobium present in solution as well as the amount of residual calcium. For most investigations, the H_2SO_4 requirement was in the region of 10 - 15 mL for 50 g filter cake dissolved in 1000 mL HCl.

6.4.2 Selective precipitation of vanadium

Effect of precipitation temperature

Fig. 6.27 shows the influence of temperature on selective precipitation of vanadium. As shown in Fig. 6.27, precipitation temperature has no significant

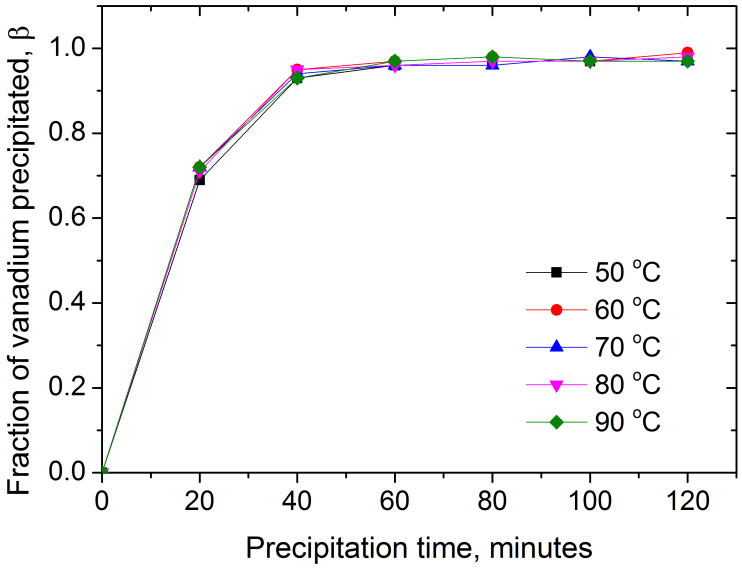

Fig. 6.27 The effects of temperature on vanadium precipitation. Stirring speed (200 rpm), pH (2) and Solid - liquid ratio (50 g L^{-1})

influence on vanadium precipitation. Filtration of cake precipitated at low temperature is very difficult, therefore, 90 °C has been chosen as the preferred precipitation temperature for further studies. At low temperatures, vanadium coprecipitates with ferrihydrite ($Fe(OH)_3$) which is very difficult to filter and at higher temperatures (> 70 °C), goethite precipitation is favoured [169–171].

Effect of precipitation pH

Fig. 6.28 illustrates the influence of precipitation pH on vanadium precipitation. More than 90 % of the vanadium in solution is precipitated at pH 1.5 and nearly all the vanadium is precipitated at pH.

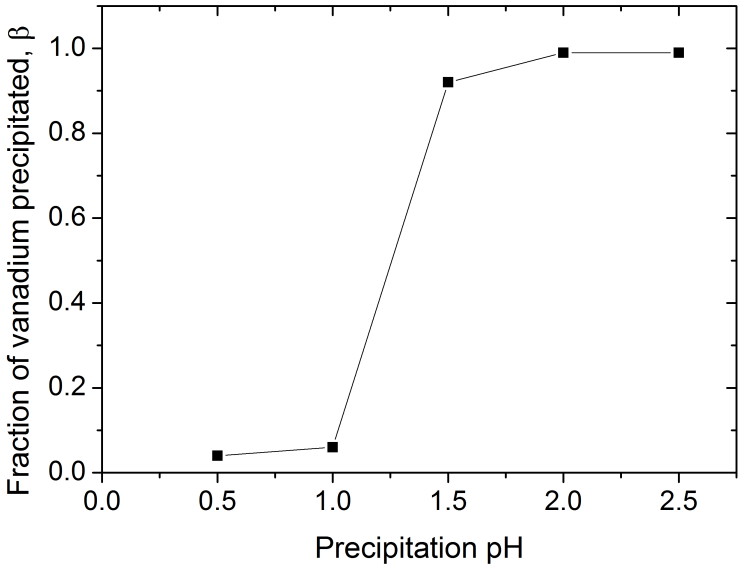

Fig. 6.28 The effect of precipitation pH on vanadium precipitation. Solid - liquid ratio (50 g L^{-1}), Stirring speed (200 rpm), leaching temperature (90 °C).

A summary of phase analysis by SEM-EDX

The precipitates from leaching of fresh cake were analysed by SEM-EDX and the elemental mapping is shown in Fig. 6.29.

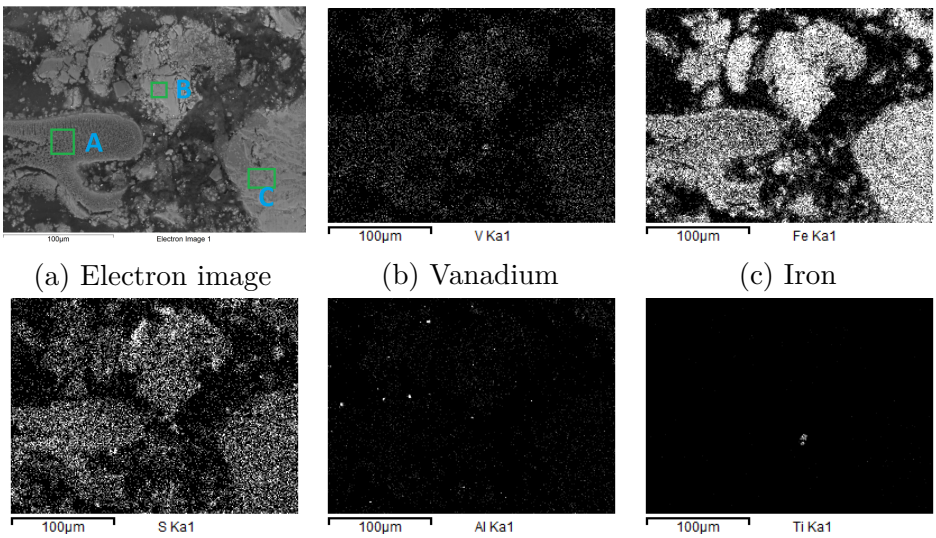

(a) Electron image (b) Vanadium (c) Iron

(d) Sulphur (e) Aluminium (f) Titanium

Fig. 6.29 SEM analysis of vanadium-rich precipitates - precipitated at 90 °C and a pH of 1.5

For comparison, the elemental mapping of pH 0.5 precipitates is shown in Fig. 6.30.

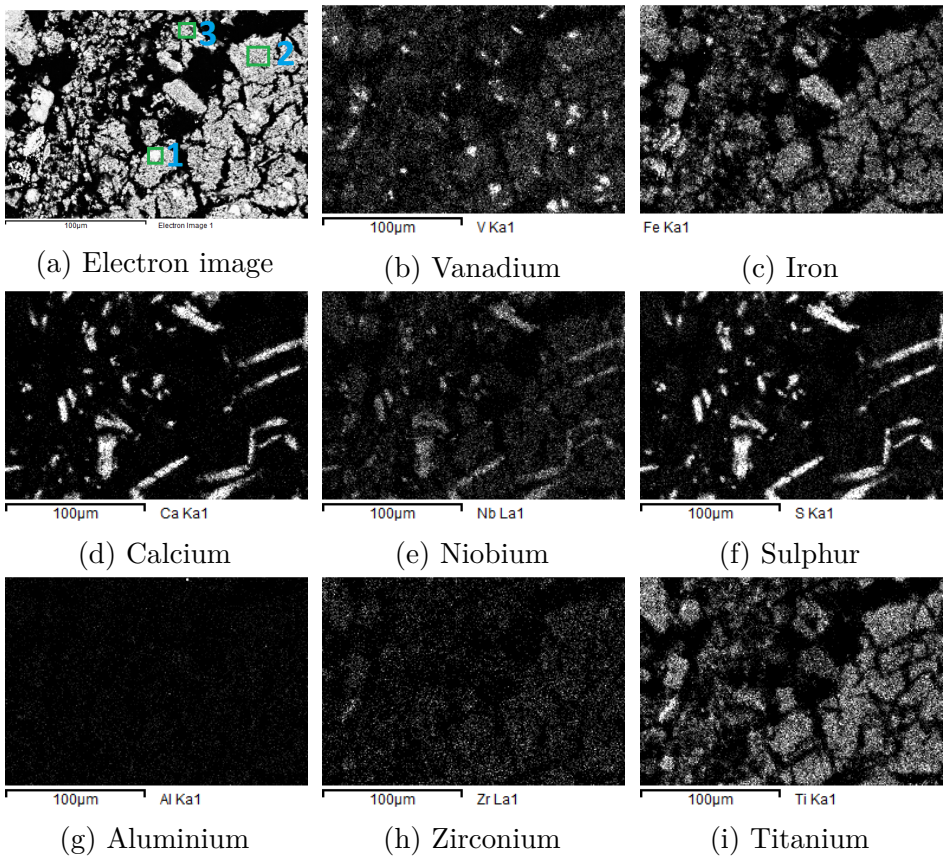

(a) Electron image (b) Vanadium (c) Iron

(d) Calcium (e) Niobium (f) Sulphur

(g) Aluminium (h) Zirconium (i) Titanium

Fig. 6.30 SEM analysis of vanadium-rich precipitates - precipitated at 90 °C and a pH of 0.5

There is a difference between precipitates formed from cake that is pre-oxidised by drying in air before HCl leaching and cake that is leached while fresh (not oxidised). Oxidation of the cake prior to acid leaching leads to conversion of Fe (II) to Fe (III) and as a result, iron precipitation starts at a pH as low as 0.5. Fig. 6.30 shows that niobium precipitates with calcium and sulphur. The niobium-calcium-sulphur precipitates are rod-shaped, showing that the nucleation occurs preferentially along one axis, whereas vanadium nucleates in spherical clusters within the iron and titanium matrix. Nearly all the vanadium and niobium are precipitated from solution at pH 0.5 when the filter cake is oxidised before leaching, leaving a solution containing aluminium and iron together with scandium and rare earth elements. Oxidation of the filter cake before acid leaching therefore complicates the subsequent steps for niobium reclamation as it introduces more species to the niobium-rich precipitates. Table B.7 presents the compositions of three points chosen from the elemental maps presented in Fig. 6.30a and three points chosen from the elemental maps

presented in Fig. 6.29a. Table B.5 confirms that precipitation of vanadium at pH 1.5 provides more selectivity. Consequently, all investigations on selective precipitation were carried out using fresh cake.

The average compositions of pH 0.5 and pH 1.5 precipitates obtained from five batches are presented in table 6.5. The full XRF analysis results for each of the samples is in the Appendix (B.11 and B.12). The major impurities in pH 0.5 precipitates are the oxides of iron, zirconium and titanium whereas only iron is the major impurity in pH 1.5 precipitates. Thorium is also concentrated in pH 0.5 precipitates but is not detected in pH 1.5 precipitates.

Table 6.5 Average compositions of pH 0.5 and pH 1.5 precipitates.

pH	TiO_2	Fe_2O_3	Nb_2O_5	ZrO_2	V_2O_5	Al_2O_3	ThO_2
0.5	16.5	33.1	12.6	12.9	5.7	0.5	0.5
1.5	ND	73.9	0.7	0.4	9.5	2.0	ND

ND= Not Detected

Fig 6.31 shows an image of the pH 1.5 precipitates. To encourage goethite precipitation, air was bubbled through the system. The colour of the precipitates suggests that the pH 1.5 precipitates are a mixture of the red goethite and yellowish sodium jarosite. Sodium jarosite forms due to the residual sulphate ions present in the solution after niobium precipitation.

Fig. 6.31 Precipitates formed at pH 1.5 - after filtration and washing

When air/oxygen is not bubbled through the system and there are no sulphate ions to promote jarosite precipitation, gelatinous $Fe(OH)_3$ which is very difficult to filter precipitates. Fig 6.32 shows an image of the gelatinous ferrihydrite.

Fig. 6.32 Ferrihydrite precipitation - pH 1.5 in the absence of sulphate ions and air/oxygen bubbling

A summary of phase analysis by XRD

X-ray diffraction analysis of the pH 1.5 precipitates is presented in Fig. 6.33 and shows that NaCl is the only crystalline phase present in the residues. Sodium chloride is the product of the neutralisation reaction of sodium hydroxide and hydrochloric acid and is present due to the residual Na^+ and Cl^- ions trapped in the precipitates after filtration.

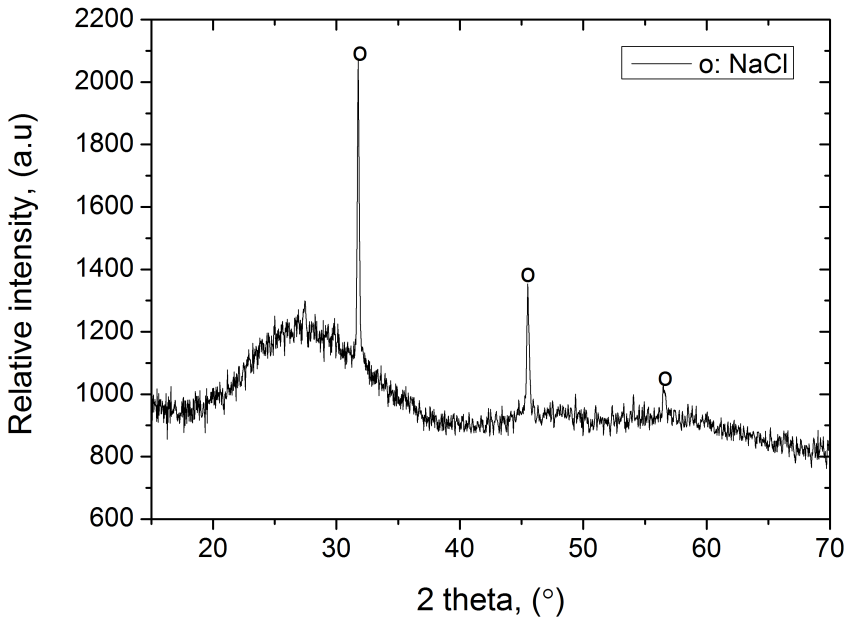

Fig. 6.33 XRD analysis of precipitates formed at pH 1 and 90 °C.

Optimum conditions for precipitation of vanadium

The optimised conditions for selective precipitation of vanadium from HCl leachates are summarised in table 6.6.

Table 6.6 Conditions for precipitation of vanadium from HCl solutions

Temperature	Air/O_2	pH	Time
70 °C	6 L min^{-1}	1.5	30 minutes

The Air/O_2 flow rate assumes an HCl volume of one litre is utilised for vanadium recovery. Preliminary studies showed that when the oxygen flow rate is too high, the gelatinous ferrihydrite ($Fe(OH)_3$) precipitates instead of the more filterable goethite.

6.4.3 Selective precipitation of scandium

Effect of precipitation temperature

Fig. 6.34 presents the fraction of scandium precipitated against precipitation time, showing that scandium precipitation is rapid at pH 4.5. Temperature has

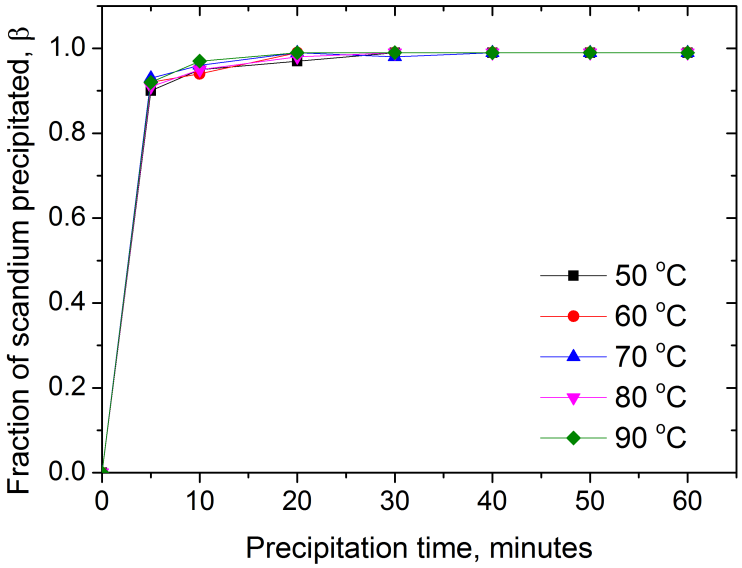

Fig. 6.34 The effects of precipitation temperature and time on scandium recovery. Stirring speed (200 rpm), pH (4.5)

minimal influence on precipitation of scandium and nearly all the scandium is precipitated within the first five minutes for all the investigated temperatures. Cake filterability was again dependent on precipitation temperature therefore a temperature of 70 °C was chosen for the scandium precipitation process.

Effect of precipitation pH

Table 6.7 presents the compositions of filter cake precipitated at pH 3.5, 4.5 and 5.5 at a precipitation temperature of 70 °C.

Table 6.7 Compositions of precipitates formed at 70 °C over a total time of 30 minutes.

pH	Na_2O	Fe_2O_3	Sc_2O_3	Al_2O_3	ThO_2
3.5	4.5	27.6	0.4	23.3	ND
4.5	4.4	31.8	0.4	20.8	ND
5.5	5.0	36.1	0.3	17.3	ND

ND= Not Detected

As shown in table 6.7, the amount of iron precipitated significantly increases with increasing pH. It was also noted that the filtration properties of the precipitates improved significantly with increasing pH, indicating that a trade-off between impurities and filterability has to be determined for efficient scandium recovery.

Fig. 6.35 presents the influence of pH on scandium precipitation from solution, showing that the fraction of scandium precipitated increases in the pH range 2.5 - 4.5.

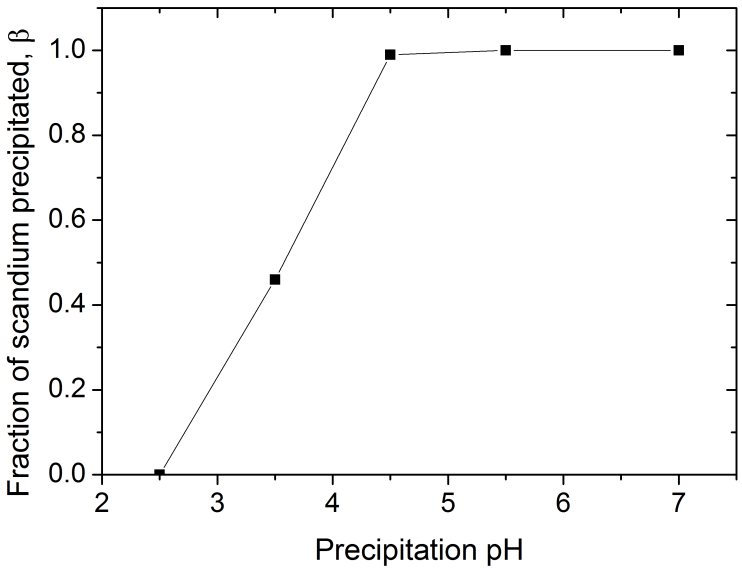

Fig. 6.35 The effects of precipitation pH and time on scandium precipitation. Precipitation temperature (70 °C), stirring speed (200 rpm), solid-liquid ratio (0.05 g mL^{-1})

Increasing the precipitation pH above 4.5 has no influence on precipitation of scandium, but improves the filtration characteristics of the cake. Consequently,

subsequent experiments utilised a precipitation pH of 5 and temperature of 70 °C for scandium recovery from solution.

6.4.4 A summary of phase analysis by SEM-EDX

Fig. 6.36 presents the SEM micrographs of the pH 5 precipitates. Scandium was not detected because its theoretical concentration in the pH 5 precipitates is between 0.3 - 0.5 wt.%, which is relatively small for positive identification by microscopy. Iron and aluminium are the main impurities.

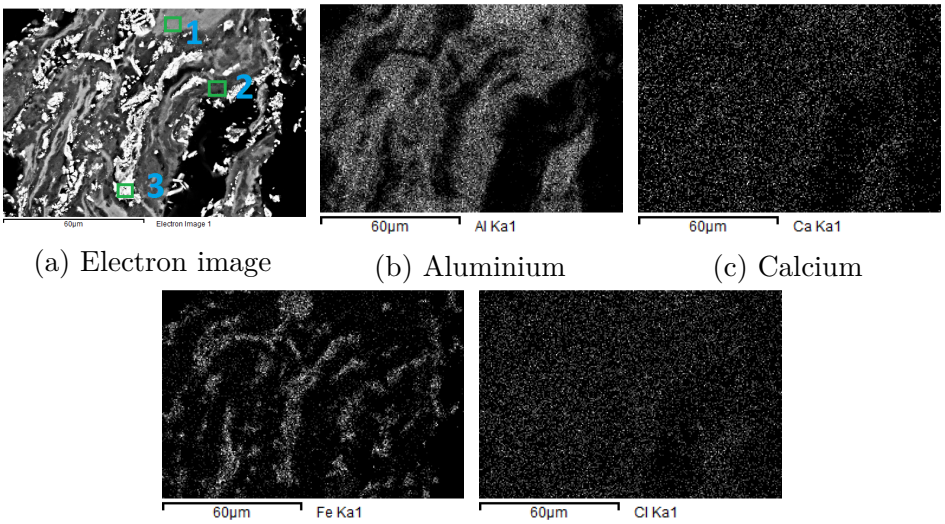

(a) Electron image (b) Aluminium (c) Calcium

(d) Iron (e) Chlorine

Fig. 6.36 SEM analysis of scandium-rich precipitates - precipitated at pH 5 and temperature of 90 °C

The compositions of three points highlighted on the electron image (Fig. 6.36a) are presented in Table B.8. A close analysis of Fig. 6.36 and table B.8 shows that pH 5 precipitates consist of aluminium rich and iron rich areas, all containing evenly distributed scandium. The distribution of scandium evenly between iron and aluminium sorbents has also been reported by the American Geological Institute [172].

The average composition of the pH 5 precipitates was determined by XRF analysis and is presented in table 6.8.

Table 6.8 Average composition of pH 5 precipitates - from 5 batches.

pH	TiO_2	Fe_2O_3	Y_2O_3	CeO_2	Sc_2O_3	V_2O_5	Al_2O_3	ThO_2
5	ND	34.7	0.2	0.4	0.4	ND	18.4	ND

Table 6.8 confirms that aluminium and iron oxides are the major impurities in the relatively scandium-rich precipitates. CeO_2 and Y_2O_3 are also present in the precipitates as they have a very similar chemistry to that of scandium. Separation of the CeO_2 and Y_2O_3 from Sc_2O_3 is typically achieved by solvent extraction, liquid membranes or ion exchange as well as a combination of the techniques [79, 88, 101, 173].

A summary of phase analysis by XRD

Fig. 6.37 presents the XRD pattern for residues selectively precipitated at pH 5 for scandium recovery. There are no distinguishable patterns due to the amount of highly amorphous $Al(OH)_3$ and $Fe(OH)_3$ [76, 174–176], which both coprecipitates with the scandium.

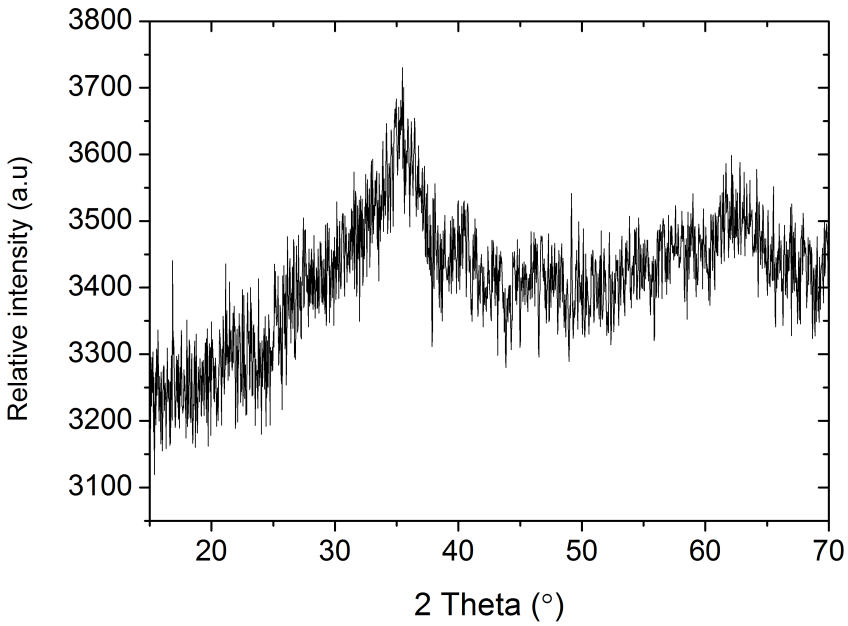

Fig. 6.37 XRD analysis of pH 5 precipitates - precipitated at 70 °C

6.5 Purification of valuable metals

6.5.1 Purification of niobium from pH 1 precipitates

Effect of leaching temperature and time on zirconium dissolution

Fig. 6.38 presents the effect of leaching temperature on zirconium extraction from the niobium-rich precipitates. Zirconium poorly dissolves in the lixiviant

system, with a maximum extraction rate of less than 15 % after 60 minutes of leaching at 90 °C.

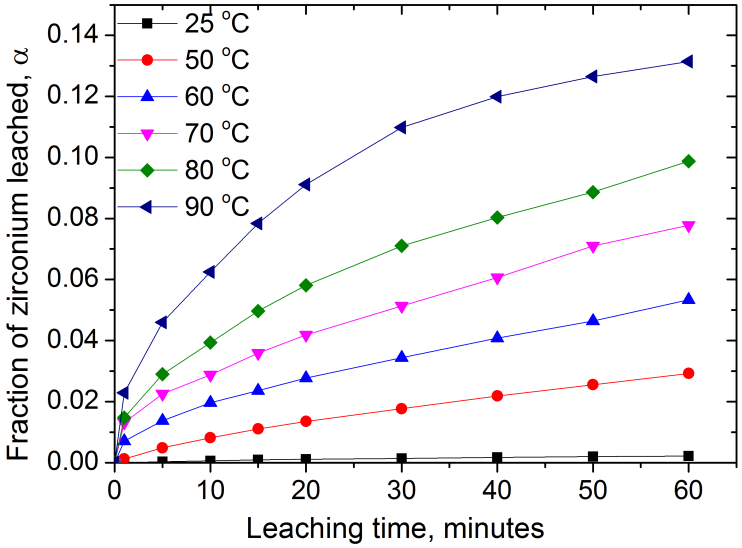

Fig. 6.38 The effect of leaching temperature on zirconium dissolution. Constants: 1 M Na_2CO_3; 50 g L^{-1} $NaNO_3$; stirring speed (300 rpm) and solid-liquid ratio (50 g L^{-1})

Fig 6.38 also shows that leaching temperature influences the dissolution rate of zirconium. Unlike in the acid leaching process where both zirconium and niobium dissolution rates decreased at 90 °C, zirconium dissolution rate increases continuously with temperature in the alkali system.

Effect of Na_2CO_3 concentration and time

Fig. 6.39 presents the effect of Na_2CO_3 concentration on zirconium dissolution, showing that Na_2CO_3 concentration has a significant effect between 0.5 and 1 M Na_2CO_3 and little influence above 1 M. It is not clear yet why there is such a difference between the fraction of zirconium dissolved when 0.5 M Na_2CO_3 is used as opposed to 1 - 2 M Na_2CO_3. It is worth mentioning that less than 15 % zirconium is dissolved under best conditions hence more research is needed to fully understand the dissolution mechanism and make an informed decision on the suitability of the approach.

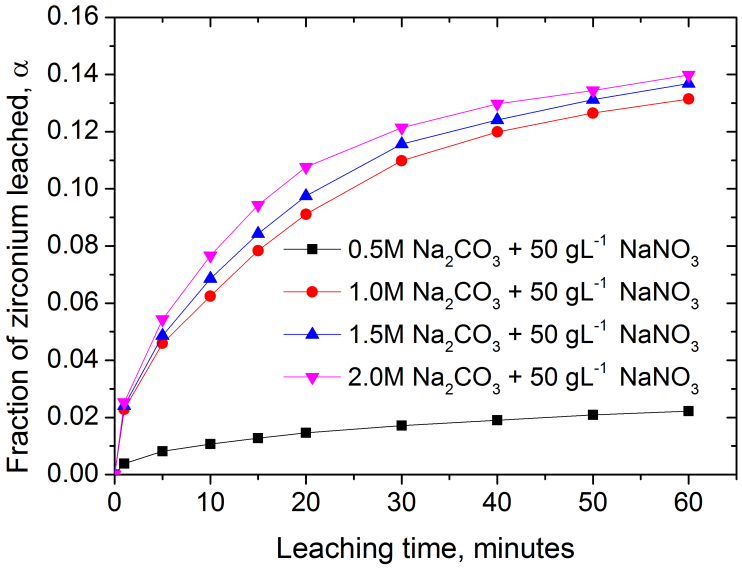

Fig. 6.39 The effect of Na_2CO_3 concentration on zirconium dissolution. Constants: Temperature (90 °C); 50 g L^{-1} $NaNO_3$; stirring speed (300 rpm) and solid-liquid ratio (50 g L^{-1})

Effects of $NaNO_3$ concentration and stirring speed

The effects of $NaNO_3$ concentration and stirring speed on zirconium dissolution are summarised in Fig. 6.40. Stirring speed has negligible influence on zirconium

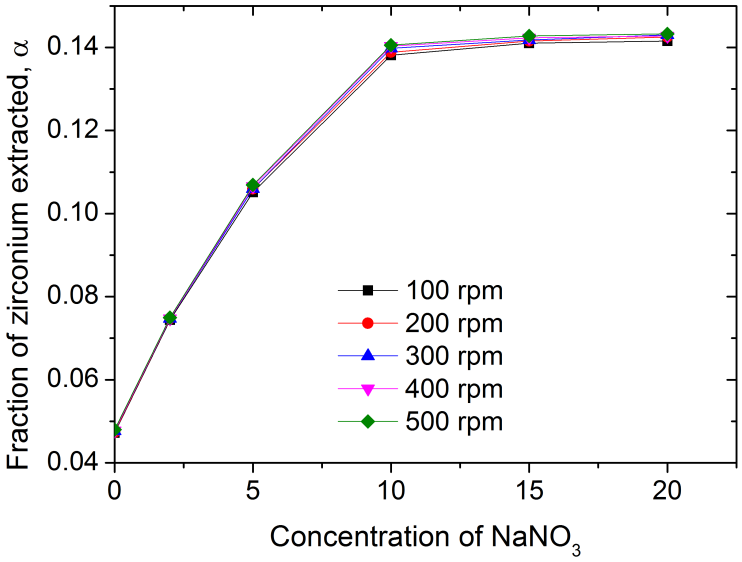

Fig. 6.40 The effects of $NaNO_3$ concentration and stirring speed on zirconium extraction. Constants: Temperature (90 °C), Na_2CO_3 concentration (2 M) and solid-liquid ratio (50 g L^{-1})

dissolution rate and zirconium dissolution increases with increasing $NaNO_3$

concentration up to 15 g L^{-1}, beyond which an increase in $NaNO_3$ concentration has negligible influence on zirconium dissolution rate.

6.5.2 Purification of vanadium from pH 1.5 precipitates - Salt roasting

Effect of oxidation temperature and time on vanadium recovery

Fig 6.41 presents the effects of roasting temperature and time on vanadium extraction rate. Vanadium leaves the chloride process in a reduced state and therefore needs to be oxidised to the pentavalent state before salt roasting.

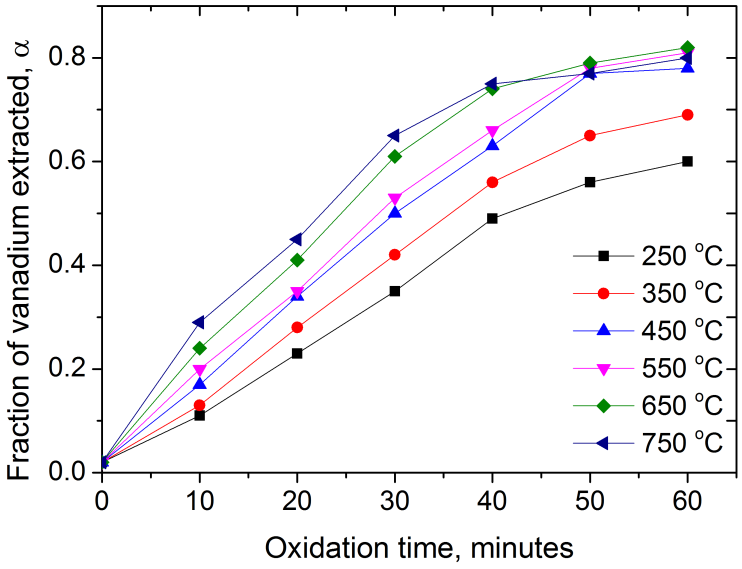

Fig. 6.41 The effects of oxidation temperature and time on vanadium recovery. Constants: Leaching temperature (60 °C); salt-precipitate ratio (10 %); salt roasting (60 minutes at 850 °C)

Increasing the oxidation time increases the vanadium recovery rate as more vanadium gets exposed to oxygen with increasing time. Vanadium extraction rate also increases with oxidation temperature up to 60 minutes. After 60 minutes of oxidation, there is negligible difference in vanadium extraction rates when oxidation is carried out above 450 °C. An optimum oxidation temperature of 450 °C was utilised for all subsequent vanadium recovery investigations that employed salt roasting.

Effect of salt roasting time and temperature on vanadium recovery

Fig. 6.42 presents the effect of roasting temperature and time on recovery of vanadium from pH 1.5 precipitates.

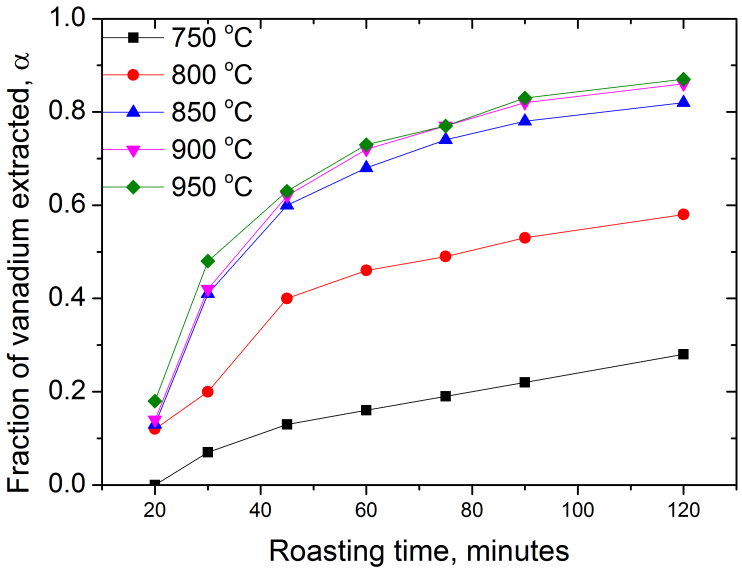

Fig. 6.42 The effects of roasting temperature and time on vanadium recovery from pH 1.5 precipitates. Constants: Leaching temperature (60 °C); salt-precipitate ratio (10 %); oxidation (60 minutes at 450 °C)

Fig. 6.42 shows an increase in vanadium recovery as roasting temperature is increased from 750 °C to 850 °C. Above 850 °C, the increase in vanadium recovery with roasting temperature is negligible. For all roasting temperatures investigated, vanadium recovery also increases with roasting time. A roasting temperature of 850 °C over 90 minutes has been chosen as optimum for further investigations.

Effect of salt-precipitate ratio on vanadium recovery (pH 1.5 precipitates)

The effect of salt to vanadium-rich precipitate ratio on vanadium recovery is presented in Fig. 6.43. Vanadium recovery increases from nearly 0 % when there is no NaCl added to a maximum of nearly 80 % when NaCl makes up 15 % of the roasted mixture. Increasing the salt - cake ratio further has no significant influence on the amount of vanadium recoverable, in fact, there is a small decrease in the total amount of vanadium recovered as the ratio of NaCl is increased above 15 %. A salt - precipitate ratio of 15 % was therefore utilised for all subsequent investigations.

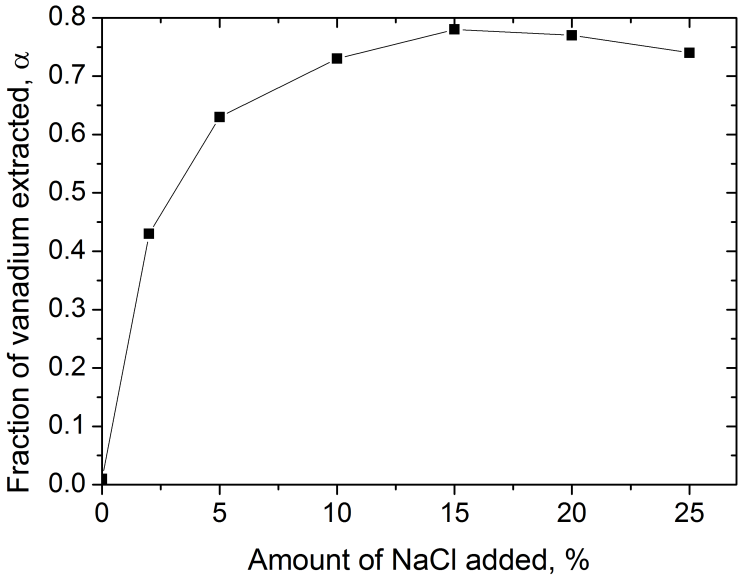

Fig. 6.43 The effect of salt-precipitate ratio on vanadium recovery. Constants: Leaching temperature (60 °C); roasting temperature (90 minutes at 850 °C); oxidation (60 minutes at 450 °C)

Effect of leaching temperature on vanadium recovery

Fig 6.44 shows the influence of leaching temperature and time on the fraction of vanadium recovered from the optimised salt roasting process.

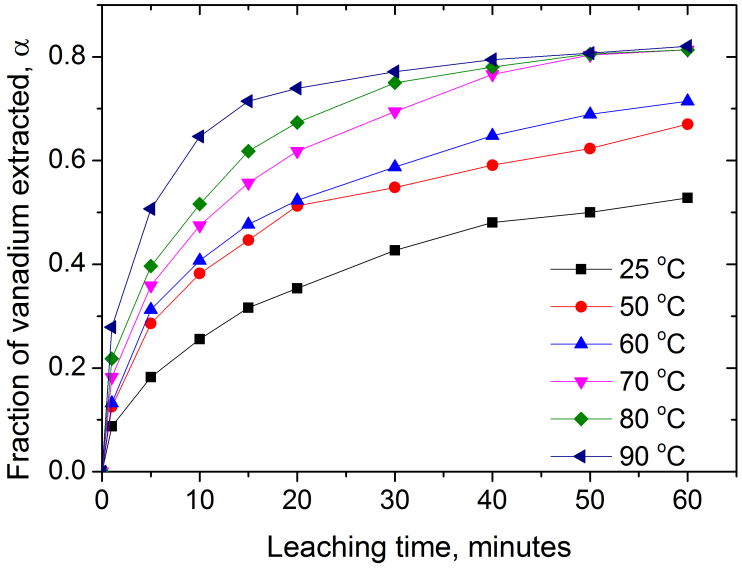

Fig. 6.44 The effects of leaching temperature and time on vanadium recovery. Constants: Salt-precipitate ratio (15 %); roasting temperature (90 minutes at 850 °C); oxidation (60 minutes at 450 °C)

As shown in Fig. 6.44, vanadium recovery increases with leaching temperature between 25 and 70 °C, increasing the leaching temperature further has negligible influence on recovery after 50 minutes of leaching. Vanadium extraction rate generally increases with time for all leaching temperatures. When leaching at temperatures above 80 °C, leaching time has little influence after 30 minutes. At leach temperatures below 60 °C, vanadium extraction rate may be increased by increasing the leaching time beyond the investigated 60 minutes. An optimised leaching temperature of 70 °C was employed for all subsequent vanadium recovery investigations.

6.5.3 Purification of vanadium from pH 1.5 precipitates - Alkali leaching

Effect of leaching temperature

The effects of leaching temperature and time on vanadium recovery from pH 1.5 precipitates by oxidative alkali leaching are presented in Fig. 6.45.

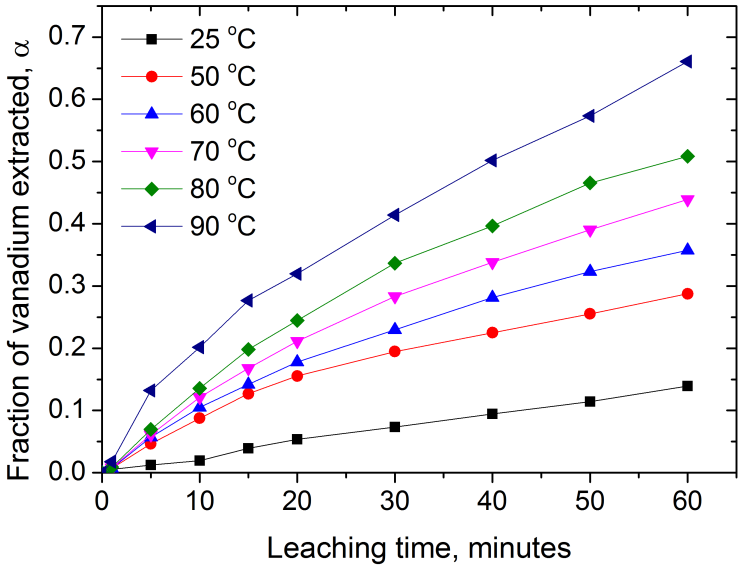

Fig. 6.45 The effects of leaching temperature and time on vanadium recovery by alkali leaching. Constants: Na_2CO_3 (2 M); $NaNO_3$ oxidant (50 g L^{-1}); solid-liquid ratio (0.05 g mL^{-1}) and stirring speed (300 rpm).

The amount of vanadium extracted by leaching the pH 1.5 precipitates in Na_2CO_3 increases with increasing leaching temperature. The amount of vanadium extracted also increases continuously with leaching time for all investigated temperatures.

Effect of Na_2CO_3 concentration

The sensitivity of the vanadium extraction reaction to alkali concentration is presented in Fig. 6.46.

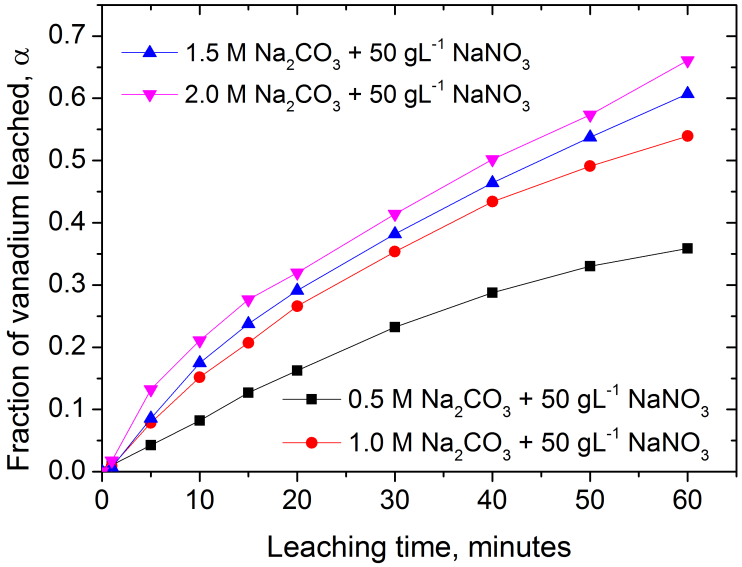

Fig. 6.46 The effects of alkali concentration and time on vanadium recovery. Constants: Leaching temperature (90 °C); $NaNO_3$ oxidant (50 g L^{-1}); solid-liquid ratio (0.05 g mL^{-1}) and stirring speed (300 rpm).

Vanadium leaching rate increases with increasing alkali concentration. When the Na_2CO_3 concentration is doubled from 0.5 M, vanadium recovery increases from about 35 % to nearly 55 %. Doubling the concentration further to 2 M only increases recovery by a further 10 %, showing that although alkali concentration has an influence on recovery for all investigated concentrations, its effect above 1 M Na_2CO_3 is reduced.

Effect of solid - liquid ratio

The influence of solid - liquid ratio on vanadium recovery is presented in Fig. 6.47. Solid - liquid ratio has negligible influence on vanadium recovery as a four-fold increase in solid - liquid ratio reduces the amount of vanadium recovered by less than 2 %.

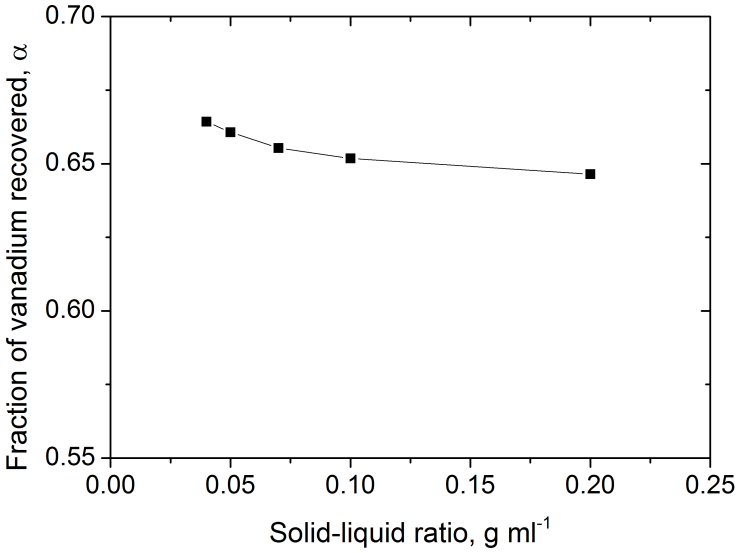

Fig. 6.47 The effects of solid - liquid ratio on vanadium recovery. Constants: Na_2CO_3 (2 M); $NaNO_3$ oxidant (50 g L^{-1}); leaching temperature (90 °C) and stirring speed (300 rpm).

Effect of stirring speed and $NaNO_3$ concentration

The effects of stirring speed and $NaNO_3$ concentration are presented in Fig. 6.48. Stirring speed has negligible influence on vanadium recovery. Increasing

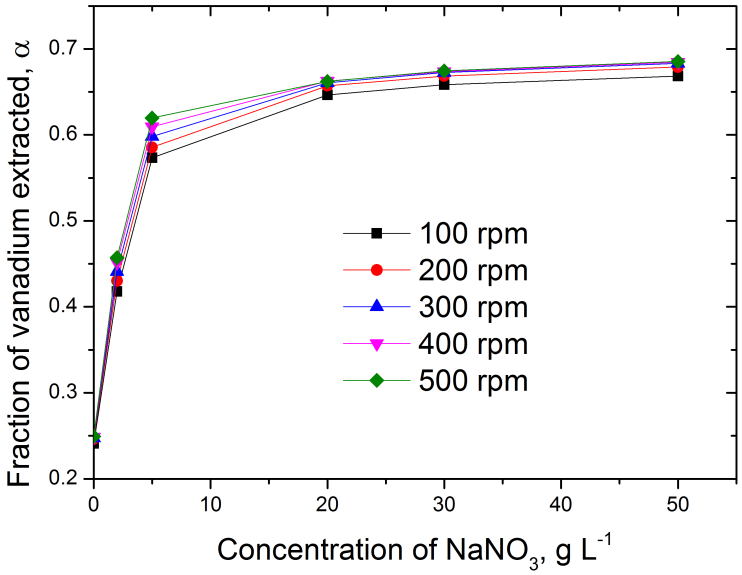

Fig. 6.48 The effects of stirring speed and $NaNO_3$ concentration on vanadium recovery from pH 1.5 precipitates. Constants: Temperature (90 °C), Na_2CO_3 concentration (2 M) and solid-liquid ratio (50 g L^{-1})

the concentration of $NaNO_3$ between 0 and 20 g L^{-1} leads to an increase in

vanadium recovery, while increasing the concentration further has negligible influence on amount of vanadium recoverable.

6.5.4 Precipitation of near-pure vanadium

The removal of impurities from solutions produced by alkali leaching of pH 1.5 precipitates led to vanadium losses of nearly 30 % as a lot of vanadium coprecipitated with impurities. Apart from the lower recoveries achieved by the alkali leaching route, the two processes had very similar results for the parameters investigated (precipitation temperature, pH, time and NH_4-V_2O_5 ratio).

Effects of precipitation pH and temperature

The effects of precipitation pH and temperature are presented in Fig. 6.49. As reported in literature [17, 46, 48], precipitation of ammonium vanadate was very high in the pH range 4 - 6, with a maximum yield of 99 % achieved for precipitation at pH 4.5 and a precipitation temperature of 20 °C.

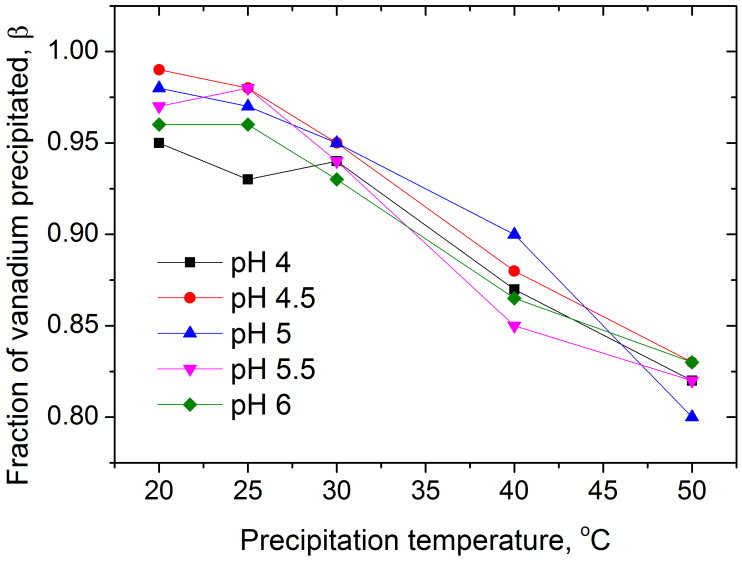

Fig. 6.49 The effects of precipitation pH and temperature on precipitation of ammonium vanadate. Constants: NH_4 - V_2O_5 ratio (0.6), precipitation time (6 hours) and stirring rate (200 rpm)

Fig. 6.49 also shows that amount of ammonium vanadate precipitated generally decreased with increasing precipitation temperature. This is because the solubility of ammonium vanadate in water increases with increasing temperature [46, 48].

Effects of precipitation time and NH_4 - V_2O_5 ratio

The influence of precipitation time on amount of ammonium vanadate precipitated from the sodium vanadate solution is presented in Fig. 6.50.

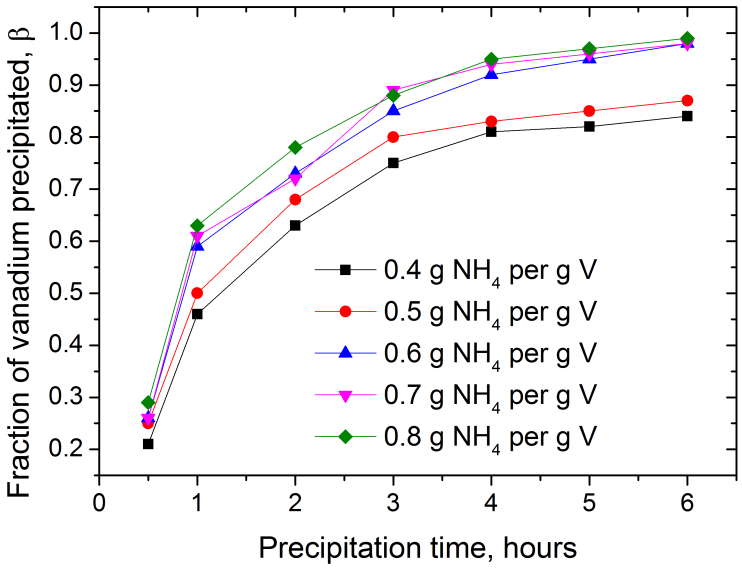

Fig. 6.50 The effects of NH_4 - V_2O_5 ratio and precipitation time on NH_4VO_3 precipitation from $NaVO_3$ solutions. Constants: Precipitation temperature (25 °C), pH (4.5) and stirring rate (200 rpm)

From Fig. 6.50, it can be deduced that precipitation times greater than 3 hours are needed for recoveries > 90% to be achieved. Precipitation times greater than 2 hours have been recommended in literature [46]. In this work, a maximum of just under 80 % recovery could be achieved in this work after 2 hours of ammonium vanadate crystallisation. The lower precipitation time reported in literature may be for solutions much richer in vanadium, which encourages the crystallisation reactions. The amount of ammonium vanadate precipitated generally increased with increasing NH_4 - V_2O_5 ratio up to 0.6 g NH_4 per gram V. There is negligible improvement for ratios greater than 0.6 g NH_4 per gram V. In view of this, the conditions chosen for the precipitation of vanadium are as presented in table 6.9.

Table 6.9 Conditions for precipitation of ammonium vanadate

Temperature	NH_4-V_2O_5 ratio	pH	Time
25 °C	0.6 g NH_4 per g V	4.5	4 hours

The precipitated ammonium vanadate was calcined at 450 °C for 30 minutes to make V_2O_5 with 99.5 % purity, majority of the impurities being sodium and residual Cl.

Summary of phase analysis by SEM

Following the re-dissolution of vanadium in Na_2CO_3 solution from pH 1.5 precipitates, impurities were removed from the solution by adjusting the pH to 8. The aluminium-rich precipitate (impurities) were analysed by SEM-EDX to determine the phases of impurities precipitated and amount of vanadium coprecipitated.

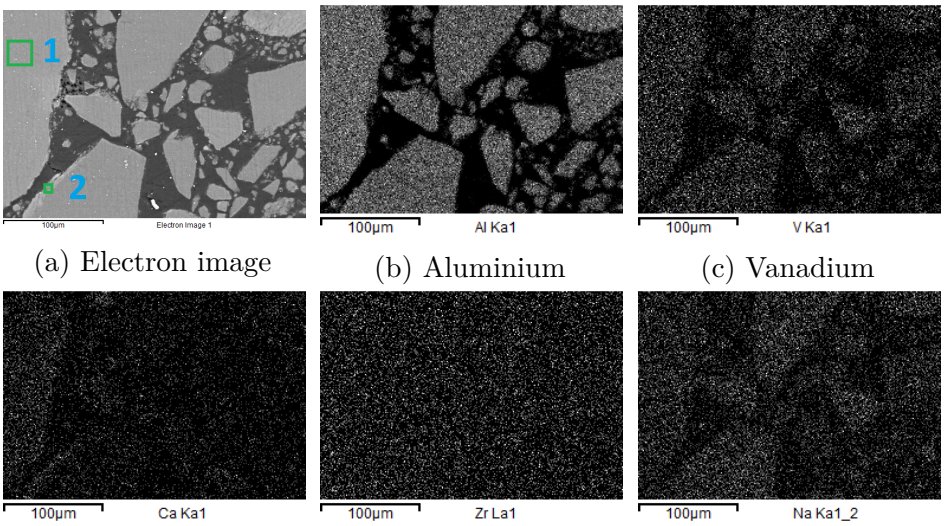

(a) Electron image (b) Aluminium (c) Vanadium

(d) Calcium (e) Zirconium (f) Sodium

Fig. 6.51 SEM analysis of precipitates from purification of vanadium rich solutions for NH_4VO_3 precipitation

Fig. 6.51 confirms that some vanadium precipitates with the impurities during the purification of solutions from alkali leaching of pH 1.5 precipitates. Re-dissolving the precipitate and re-precipitating the impurities slightly improved the vanadium retention in solution. The vanadium remaining in solution was too lean for ammonium vanadate precipitation and needed the solutions to be heated to get rid of water before precipitating ammonium vanadate. Solutions for ammonium vanadate precipitation should ideally have between 10 - 30 g L^{-1} vanadium as V_2O_5 [17, 46, 48].

Table B.9 presents the EDX semiquantitative analysis results for the areas highlighted in Fig. 6.51a, confirming that the impurity removal step for the ammonium vanadate precipitation leads to co-precipitation and eventual loss

of vanadium. The salt roasting approach does not require an impurity removal step as it is highly selective for vanadium, hence is a superior route in that respect.

Summary of phase analysis by XRD

Analysis of the precipitated ammonium vanadate and the V_2O_5 from calcination of the precipitates are presented in figures 6.52 and 6.53 respectively. As expected, there are no patterns of impurities such as aluminium, confirming that both the ammonium vanadate and final V_2O_5 are of very high purity.

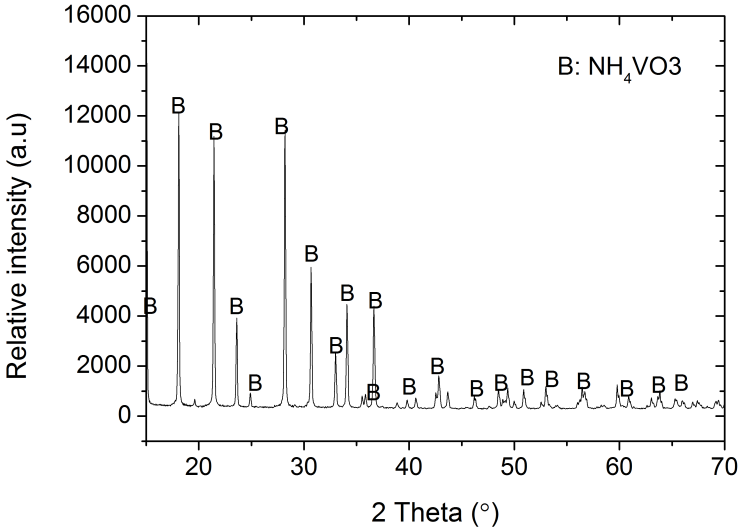

Fig. 6.52 Precipitated NH_4VO_3

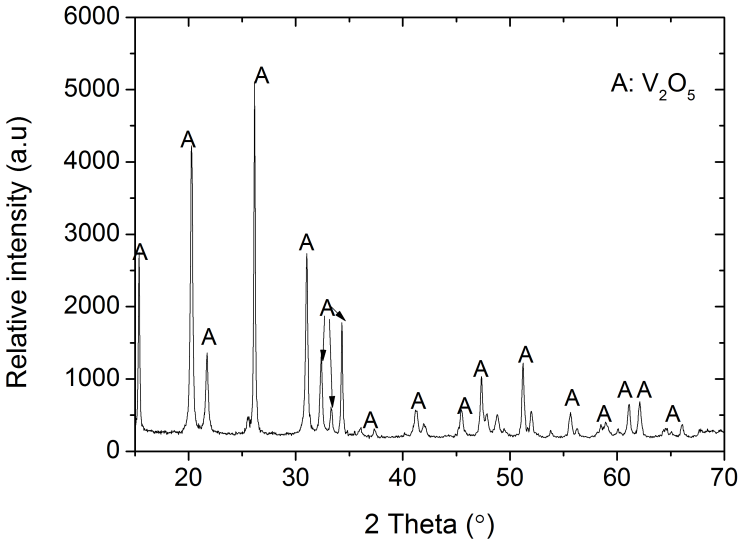

Fig. 6.53 Final V_2O_5 product

6.5.5 Purification of scandium from pH 5 precipitates

Due to the low concentration of scandium in the pregnant solutions compared to the sodium content, the sodium salts of the organic acids precipitated when selective alkali leaching and re-precipitation using organic acids was investigated for purification of scandium in pH 5 precipitates.

Effect of leaching temperature

The effects of leaching temperature and time on scandium dissolution in 2 M Na_2CO_3 re presented in Fig. 6.54. Temperature has a significant influence on scandium recovery in alkaline media.

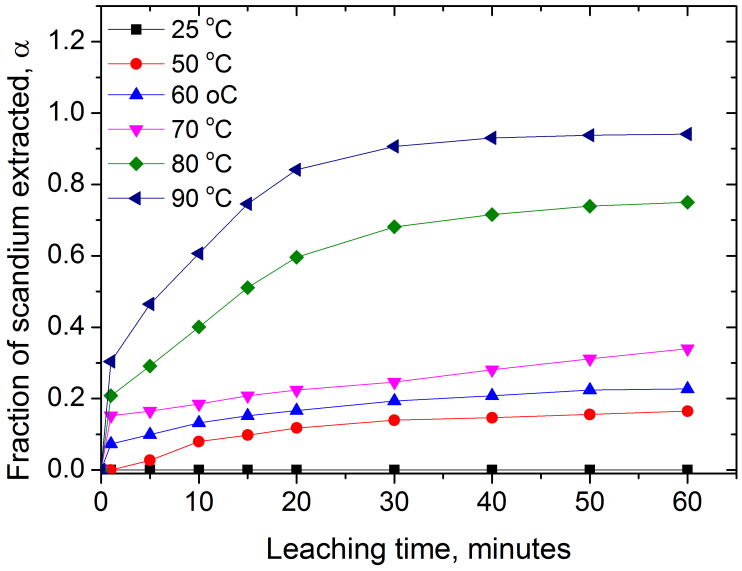

Fig. 6.54 The effects of leaching temperature and time on scandium recovery. Constants: Solid - liquid ratio (50 g L^{-1}), Na_2CO_3 concentration (2 M), $NaNO_3$ concentration (50 g L^{-1}) and stirring rate (300 rpm)

At 25 °C, scandium is not recovered from the precipitates and doubling the temperature leads to scandium recovery of nearly 20 % after 60 minutes of leaching. There is a notable increase in scandium recovery when temperature is increased from 70 to 80 °C, with a further increase to above 90 % when temperature is further increased to 90 °C. At 90 °C, at least 80 % of the scandium is dissolved within the first 20 minutes of leaching. A leaching temperature of 90 °C was therefore chosen as the ideal leaching temperature for all subsequent scandium dissolution investigations.

Effect of Na_2CO_3 concentration on scandium extraction

Fig. 6.55 presents the relationship between fraction of scandium dissolved and leaching time for the different lixiviant concentrations.

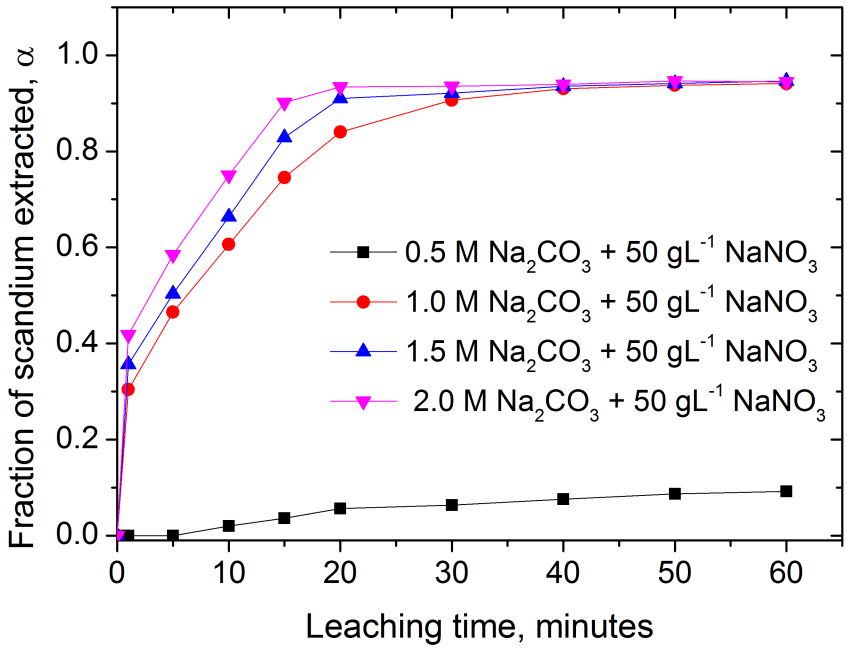

Fig. 6.55 The effects of Na_2CO_3 concentration and time on scandium recovery. Constants: Temperature (25 °C, solid - liquid ratio (50 g L^{-1}), $NaNO_3$ concentration (50 g L^{-1}) and stirring rate (300 rpm)

As shown in Fig. 6.55, Na_2CO_3 concentration has negligible influence on scandium dissolution when a concentration above 1 M is used for leaching. Less than 10 % scandium is recovered when a 0.5 M Na_2CO_3 solution is used for leaching the pH 5 precipitates for 60 minutes. Doubling the Na_2CO_3 concentration leads to a recovery above 90 %. After a leaching time of about 30 minutes, there is negligible difference between the scandium extraction rates obtained by leaching in 1, 1.5 or 2 M Na_2CO_3. For this reason, 1 M Na_2CO_3 was chosen as the ideal molarity for alkali leaching of scandium-rich residues.

Effect of solid - liquid ratio on scandium extraction

Fig. 6.56 presents the effect of solid-liquid ratio on scandium extraction from pH 5 precipitates when Na_2CO_3 is used for leaching. Just like with alkali leaching of vanadium from pH 1.5 precipitates, the dissolution of scandium from pH 5 precipitates is not influenced by solid - liquid ratio in the investigated

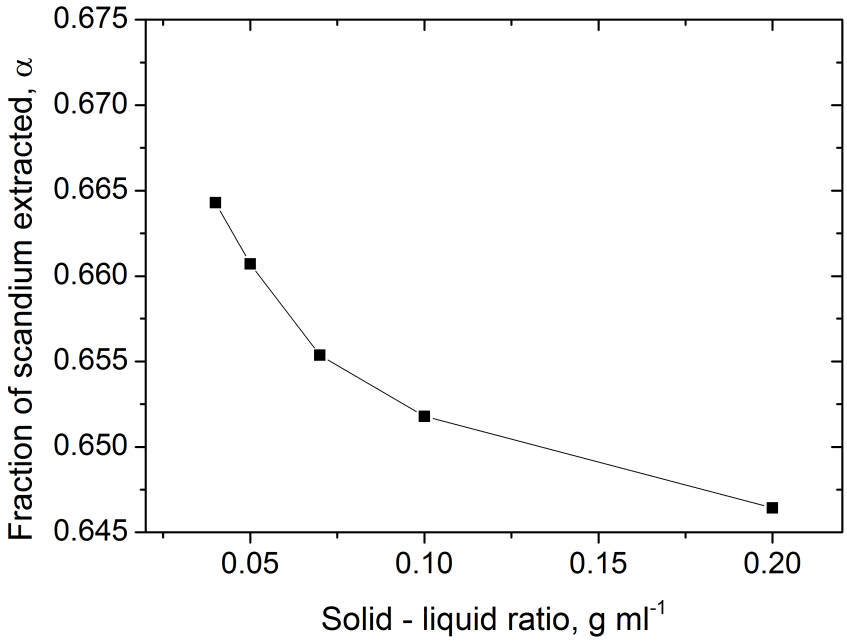

Fig. 6.56 The effect of solid - liquid ratio on scandium recovery. Constants: Temperature (90 °C, Na_2CO_3 concentration (1 M), $NaNO_3$ concentration (50 g L^{-1}), leaching time (60 minutes) and stirring rate (300 rpm)

ranges. Increasing the ratio from 0.05 to 0.2 g mL^{-1} leads to less than 2 % decrease in scandium recovery.

Effect of stirring speed and $NaNO_3$

Fig. 6.57 presents the relationship between $NaNO_3$ concentration and fraction of scandium extracted in Na_2CO_3 for a given stirring speed. Stirring speed has negligible influence on scandium extraction from pH 5 precipitates and recovery increases with $NaNO_3$ concentration up to 20 g L^{-1}. Increasing the $NaNO_3$ concentration further has no influence on the amount of scandium recovered, much like the influence of $NaNO_3$ concentration on vanadium recovery from pH 1.5 precipitates. The optimised leaching conditions for selective re-dissolution of scandium from pH 5 precipitates are presented in table 6.10:

Table 6.10 Conditions for re-dissolution of scandium hydroxide in Na_2CO_3

Temperature	$[Na_2CO_3]$	Solid-liquid ratio	Stirring speed	$[NaNO_3]$	Time
90 °C	1 M	0.2 g mL^{-1}	300 rpm	20 g L^{-1}	0.5 hours

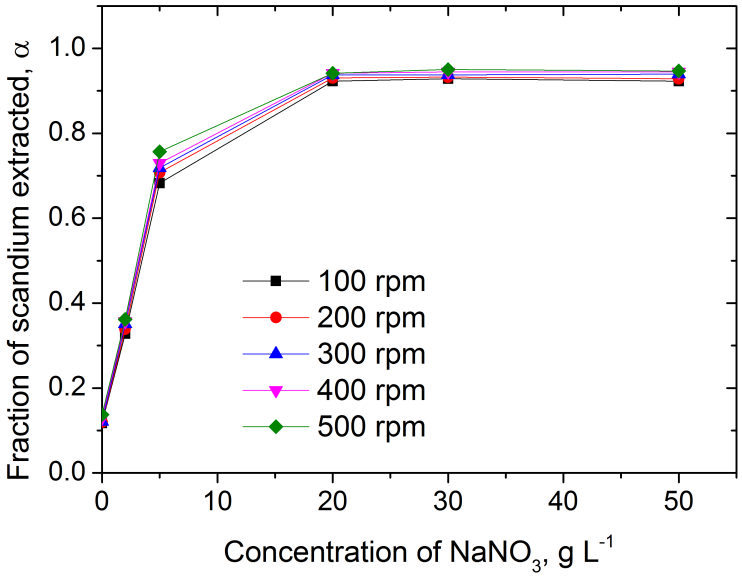

Fig. 6.57 The effects of stirring speed and $NaNO_3$ concentration on scandium extraction. Temperature (90 °C), Na_2CO_3 concentration (1 M), solid-liquid ratio (50 g L^{-1}) and leaching time (60 minutes)

Precipitation of scandium from Na_2CO_3 solution

Fig.6.58 shows SEM images of sodium-rich precipitates formed when oxalic acid was employed for precipitating scandium from sodium-rich solutions.

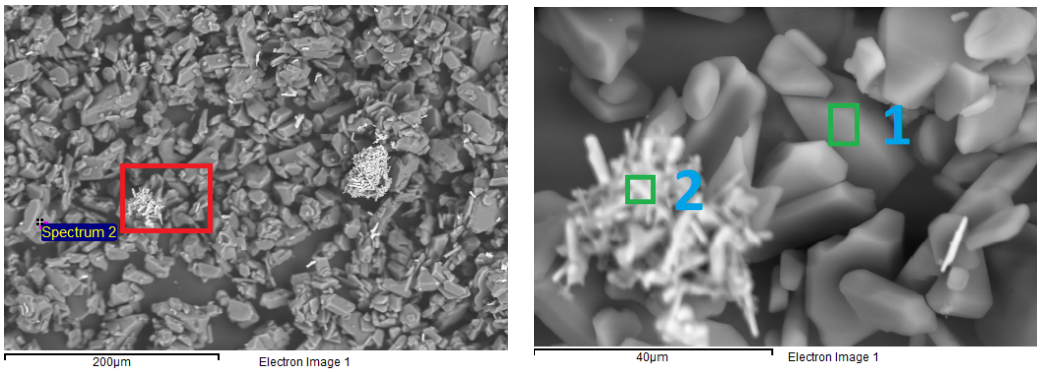

(a) Low magnification (b) High magnification

Fig. 6.58 SEM analysis of precipitates formed during scandium oxalate precipitation attempts. Conditions: Temperature (25 °C), pH (1), stirring-speed (200 rpm) and precipitation time (30 minutes).

No insoluble organic salts of scandium were observed in the sodium-rich precipitates formed at pH 1 and no other precipitates were observed up to pH 12. This may have been due to either the low concentration of scandium in the solution or the high sodium concentration. Horovitz [88] reported that the

solubility of scandium is considerably affected by the presents of other ions in the solution and this may explain the difficulty in precipitating the scandium below pH 5 where pH was adjusted using HCl. Vickery [177] investigated the solubility of scandium oxalates in water and found that presents of HCl and H_2SO_4 significantly increase the solubility of scandium oxalate. Table B.10 shows the compositions of points 1 and 2 from Fig 6.58b, confirming that the oxalate precipitates are of sodium. Neither the titanium-rich nor the sodium phases had scandium, indicating that it remained in solution. A different approach for the precipitation of scandium is thus needed.

6.6 Radionuclides

6.6.1 Dissolution of thorium in HCl

Effect of leaching temperature and time

The relationship between leaching temperature and fraction of thorium extracted from as-received filter cake (B1) is presented in Fig. 6.59.

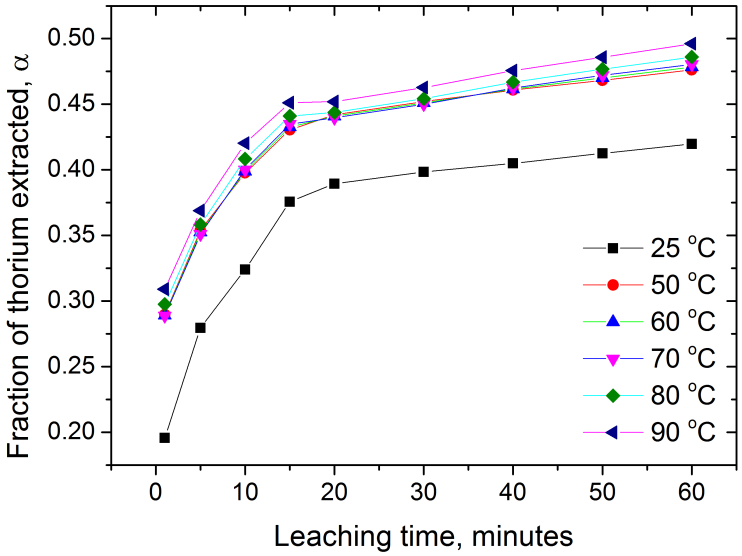

Fig. 6.59 The effects of leaching temperature and time on thorium extraction. Constants: Solid-liquid ratio (50 g L^{-1}), HCl concentration (1.5 M) and stirring rate (300 rpm)

For all leaching temperatures, thorium dissolution in HCl is very rapid in the first 15 minutes but quite slow between 15 and 60 minutes, suggesting that the leaching behaviour is controlled mainly by kinetics in the first 15 minutes and then approached equilibrium as free acid is consumed. Consequently, analysis

of the effect of temperature on thorium leaching rate in HCl is divided into two parts, where 1 - 15 minutes is the first stage and 15 - 60 minutes is the second stage. Fig. 6.59 shows that the influence of temperature on thorium dissolution above 50 °C is negligible, indicating that thorium dissolution in HCl is most likely controlled by diffusion processes.

Effect of HCl concentration and time

The influence of HCl concentration and leaching time on thorium extraction is presented in Fig. 6.60. HCl concentration has considerable influence on

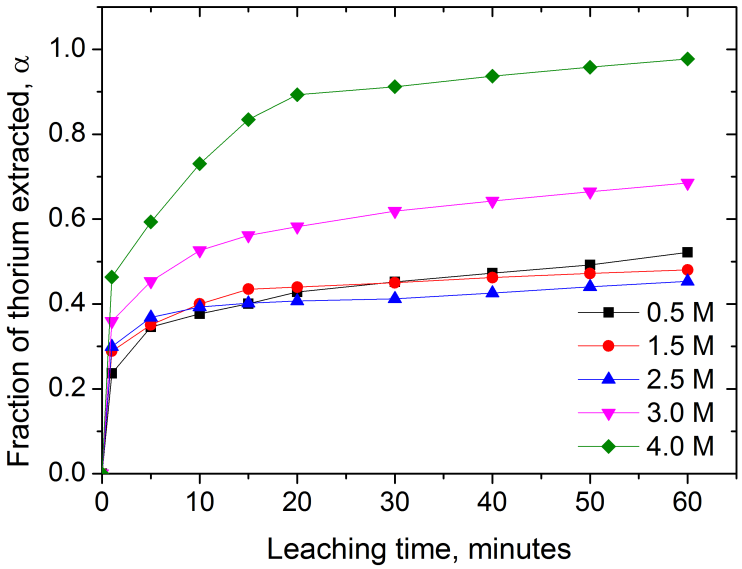

Fig. 6.60 The effects of HCl concentration and leaching time on thorium extraction. Constants: Solid-liquid ratio (50 g L^{-1}), temperature (90 °C) and stirring rate (300 rpm)

thorium extraction rate. Below HCl concentration of 2.5 M, a maximum of about 50 % thorium is extracted from the filter cake and the influence of acid concentration on extraction is not significant. A significant increase in thorium extraction is observed upon increasing the concentration from 2.5 to 3 M, where nearly 65 % of the thorium is solubilised. Increasing the concentration further to 4 M increases the thorium extraction rate to nearly 98 %. Fig. 6.60 also shows that the influence of HCl concentration on thorium dissolution is complex. When an HCl concentration of lower than 2.5 M is used for leaching, thorium dissolution decreases with increasing acid concentration where as above 2.5 M HCl, thorium dissolution rapidly increases. The reason for reduction in thorium extraction rates with increasing acid concentration below pH 2.5 has not been

ascertained. It is likely a consequent of thorium adsorption on colloidal iron hydroxide which was observed below pH 2.5. As acid concentration is increased from 0.5 M to 2.5 M, the volume of iron hydroxides in colloidal form may be increasing faster than the dissolution rate of thorium, meaning more dissolved thorium re-precipitates by an adsorption mechanism and when iron is fully in solution (above pH 2.5), there is no surface for thorium to adsorb on hence will remain in solution. Thorium's strong affinity for iron hydroxide surfaces is well documented [178].

Effects of solid - liquid ratio and stirring speed

The effects of solid - liquid ratio and stirring speed on thorium dissolution are presented in figures 6.61 - 6.63.

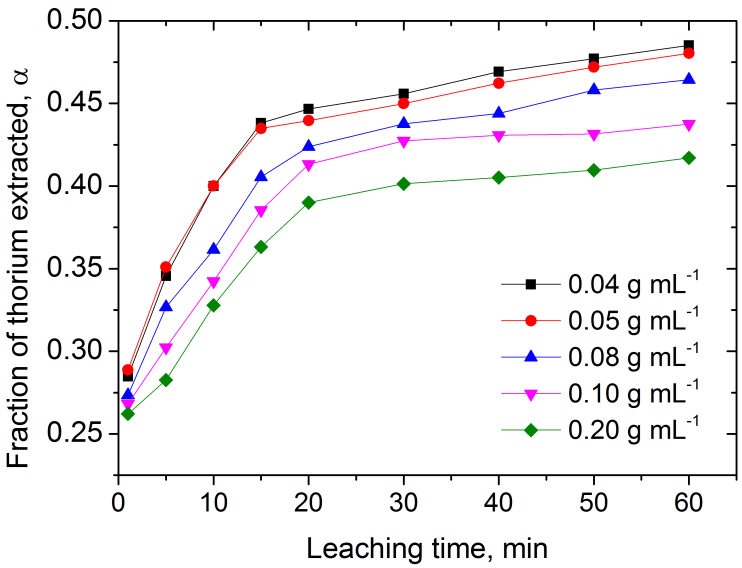

Fig. 6.61 Effect of solid - liquid ratio on thorium extraction. HCl concentration (1.5 M), temperature (70 °C) and stirring rate (300 rpm)

As shown in figures 6.61 and 6.62, solid - liquid ratio and stirring speed show some influence on thorium extraction when 1.5 M HCl is used for leaching. Increasing the solid - liquid ratio from 0.04 g mL^{-1} to 0.20 g mL^{-1} raises the total extraction rate from about 42 % to 49 % while increasing stirring speed from 100 rpm to 500 rpm leads to a 10 % increase in thorium extraction. On the contrary, both parameters have insignificant influence on thorium extraction rate when 4 M HCl is used for leaching (Fig. 6.63). An increase in extraction with increasing stirring speed is a typical behaviour of diffusion

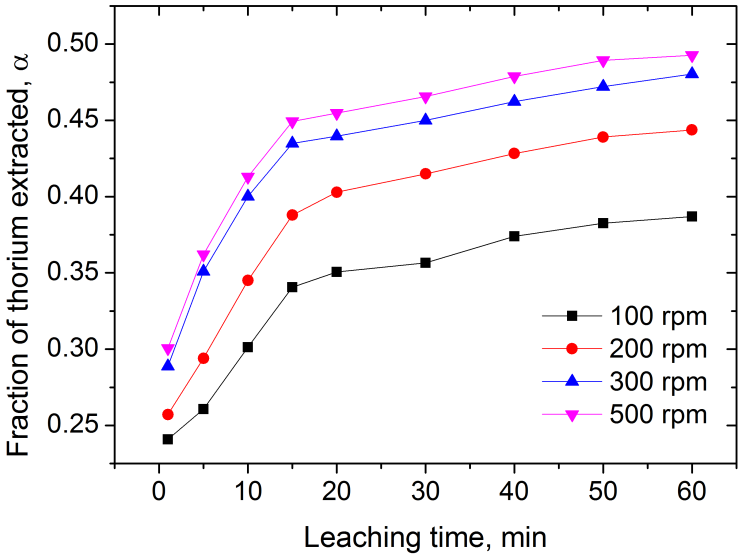

Fig. 6.62 Effect of stirring speed on thorium extraction. Solid-liquid ratio (0.05 g mL^{-1}), temperature (70 °C) and HCl concentration (1.5 M)

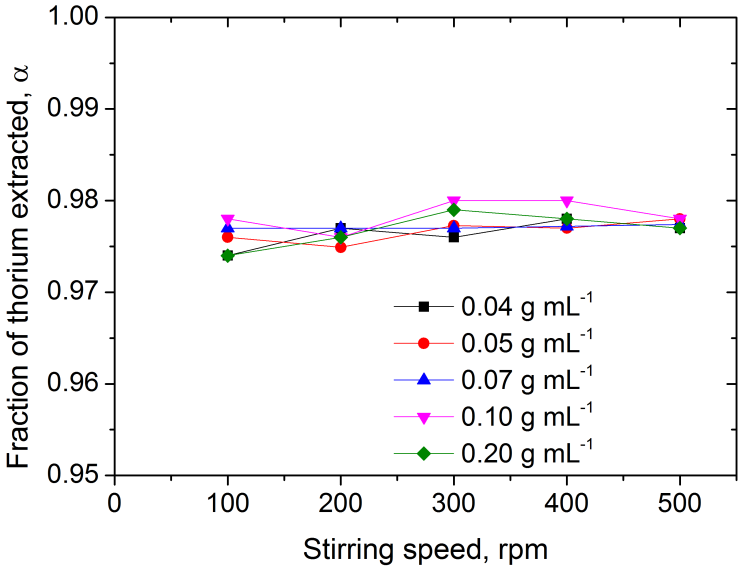

Fig. 6.63 Effects of stirring speed and solid - liquid ratio on residues leached in 4 M HCl at 70 °C

controlled reaction kinetics [179] where increasing the stirring speed increases the interfacial area and hence the mass transfer rate.

From the results obtained during the thorium dissolution investigations, it can be inferred that thorium will dissolve when filter cake is digested in HCl for recovery of valuable metals. It is therefore of paramount importance that the precipitation characteristics of thorium from HCl media be studied further to

enable prediction of conditions that minimise contamination of valuable metals to be identified.

6.6.2 Dissolution of thorium in alkaline media

Effect of leaching temperature

Fig. 6.64 presents the influence of leaching temperature on dissolution of thorium from as-received filter cake (B3). The dissolution of thorium in Na_2CO_3 increases rapidly with increasing temperature, with a maximum of 35 % being dissolved after leaching for 60 minutes at 90 °C.

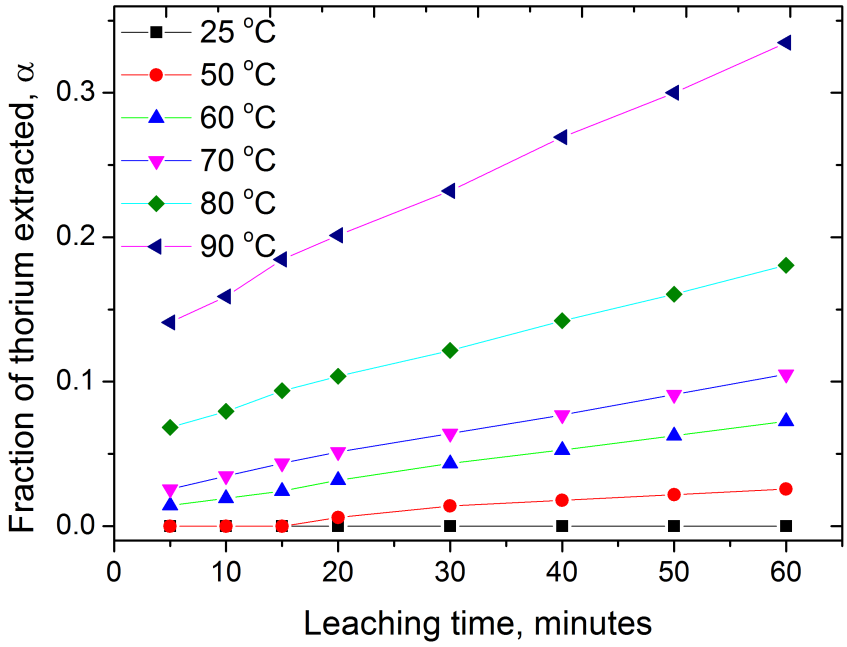

Fig. 6.64 The effect of leaching temperature on thorium extraction. Solid-liquid ratio (0.05 g mL^{-1}), Na_2CO_3 concentration (1 M Na_2CO_3), stirring speed (300 rpm) and $NaNO_3$ concentration (50 g L^{-1} $NaNO_3$)

Fig. 6.64 also shows that dissolution of thorium is more dependent on temperature in alkaline media compared to acidic media.

Effect of Na_2CO_3 concentration on thorium dissolution

The influence of Na_2CO_3 concentration on thorium dissolution from filter cake is presented in Fig. 6.65, showing that a maximum of 10 % thorium was dissolved at 70 °C in 1 M Na_2CO_3 mixed with 50 g L^{-1} $NaNO_3$, and no extraction occurred when 0.5 M Na_2CO_3 solution was used for leaching. Since thorium

is expected to dissolve from the residues by means of complexation, the low dissolution rates may be a result of slow reaction/complexation.

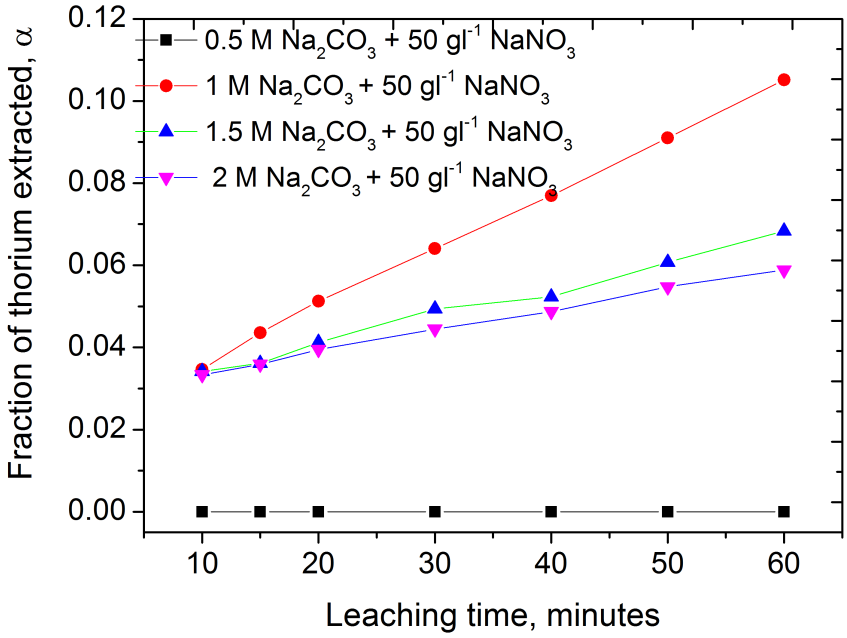

Fig. 6.65 The effect of Na_2CO_3 concentration on thorium extraction. Solid-liquid ratio (0.05 g mL^{-1}), temperature (70 °C), stirring speed (300 rpm) and $NaNO_3$ concentration (50 g L^{-1} $NaNO_3$)

Effect of solid - liquid ratio on thorium dissolution

Fig. 6.66 presents the effects of solid - liquid ratio on dissolution of thorium from as-received filter cake. Solid - liquid ratio has negligible influence on the extraction rate of thorium in the range investigated and once again, just over 10 % of the thorium dissolves in the alkali system.

The studies on alkali dissolution of thorium show that thorium dissolves poorly in a Na_2CO_3 - $NaNO_3$ system. This implies that thorium will remain concentrated in the residues if the Na_2CO_3 - $NaNO_3$ system is employed for recovery of metals at 70 °C.

6.6.3 Precipitation of thorium

Thorium tends to be scavenged from solutions by particles with high surface area such as those of hydrated iron oxides [178, 180]. Harris and Kratochvil [181] reported that thorium hydroxide has a tendency to adsorb on iron (III) hydroxide, with more than 95 % precipitating from acidic solutions by this

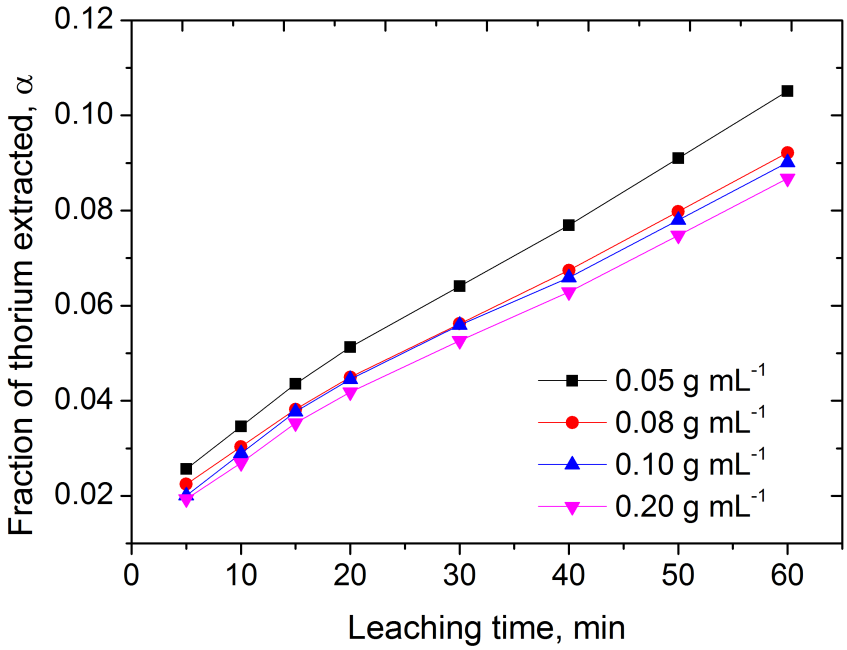

Fig. 6.66 The effect of solid - liquid ratio on thorium extraction. Na_2CO_3 concentration (1 M), temperature (70 °C), stirring speed (300 rpm) and $NaNO_3$ concentration (50 g L^{-1} $NaNO_3$)

means and remaining there even after filtration and washing. All the dissolved thorium was removed from solution by adsorption on hydrated iron (III) oxide below pH 1, hence contaminated the niobium concentrate.

6.7 Integrated metal oxide monitoring

Table 6.11 presents the compositions of key materials present in the streams highlighted in Fig. 6.67. Streams 1 - 11 are for dissolution of filter cake in acid and subsequent selective precipitation while streams 12 - 18 are for the purification of the precipitates for recovery of valuable metals. The compositions do not add to 100 % as some minor and trace elements such as chlorine are not included. XRF analysis of some samples was repeated to determine the errors associated with the instrument and sampling techniques. The measurement uncertainty varies between each metal oxide. The errors observed from analysis of dissolved Nb_2O_5, Sc_2O_3 and V_2O_5 are all less than 5 % (see B.6).

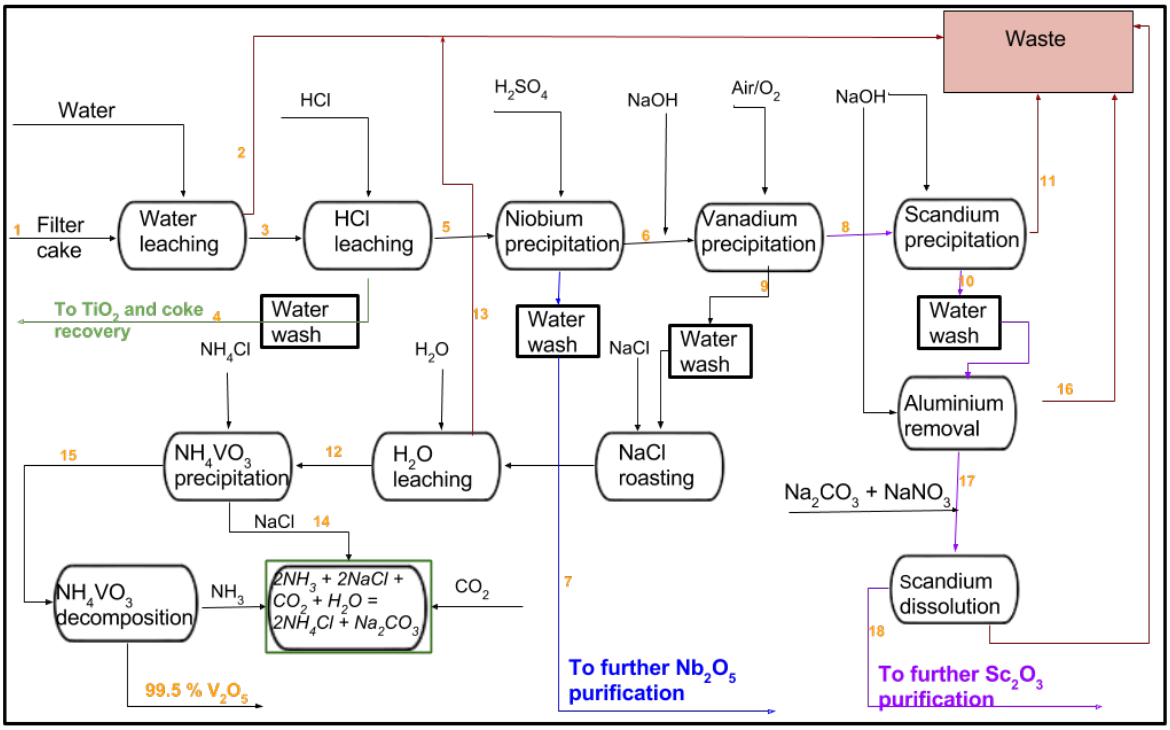

Fig. 6.67 Processing steps for the integrated metal recovery process.

Table 6.11 Composition of key elements in the streams numbered in Fig. 6.67

Stream	TiO_2	ZrO_2	Nb_2O_5	Fe_2O_3	CaO	ThO_2	Sc_2O_3	V_2O_5	Al_2O_3	Total (g)
1	115.8	8.2	7.9	86.1	33.4	0.3	0.3	7.1	16.3	339.0
2	ND	ND	ND	0.1	31.5	ND	ND	ND	0.3	51.0
3	120.0	8.4	7.8	85.8	1.9	0.3	0.3	7.4	16.0	288.0
4	106.9	0.4	0.6	1.1	0.3	ND	ND	0.1	0.7	125.1
5	8.0	7.8	7.2	84.5	1.7	0.3	0.3	7.2	15.1	162.9
6	ND	0.2	0.8	79.8	ND	ND	0.3	7.0	15.1	148.1
7	8.1	7.5	6.5	5.2	1.5	0.3	ND	0.3	0.1	41.5
8	ND	ND	ND	27.6	ND	ND	0.3	0.5	13.4	76.5
9	ND	0.3	0.5	52.9	ND	ND	ND	6.8	1.4	71.6
10	ND	ND	ND	26.8	ND	ND	0.3	ND	13.6	77.3
11	ND	ND	ND	1.2	ND	ND	ND	ND	0.1	8.8
12	ND	ND	ND	ND	ND	ND	ND	5.8	ND	7.5
13	ND	0.3	0.5	52.9	ND	ND	ND	1.1	1.1	73.1
14	ND	ND	ND	ND	ND	ND	ND	0.1	ND	2.1
15	ND	ND	ND	ND	ND	ND	ND	5.7	ND	5.7
16	ND	ND	ND	ND	ND	ND	ND	ND	13	15.0
17	ND	ND	ND	26.8	ND	ND	0.3	0.1	0.7	62.3
18	ND	ND	ND	ND	ND	ND	0.3	0.1	0.5	–

6.8 Kinetics studies

Modelling of the kinetics of vanadium, scandium, niobium and thorium dissolution in HCl using the chemical reaction control expression (equation 2.14) gave negative structural parameter (ψ) values, indicating that pore diffusion probably dominated the leaching kinetics. The fraction of metal extracted (α) vs. time (t) can therefore be described by eq. 6.7, which is derived from eqs. 2.17 - 2.19.

$$1 - 3(1-\alpha)^{\frac{2}{3}} + 2(1-\alpha) = \frac{6\mathscr{D}_e}{(1-\epsilon)\rho_m} C_{A,ave} R_p^{-2} t \tag{6.7}$$

In equation 6.7, $\mathscr{D}_e/(1 - \epsilon)\rho_m$ is determined by plotting $1-3(1-\alpha)^{\frac{2}{3}}+2(1-\alpha)$ against $[HCl]R_p^{-2}t$. The diffusivity ($\mathscr{D}_e$) can be calculated by linear regression and substituting the values for porosity and molar density.

6.8.1 Niobium dissolution

The variation of $1 - 3(1 - \alpha)^{\frac{2}{3}} + 2(1 - \alpha)$ with time (t) is plotted for leaching temperature (6.68), HCl concentration (6.69), solid-liquid ratio (6.70) and stirring speed (6.71) according to the random pore model.

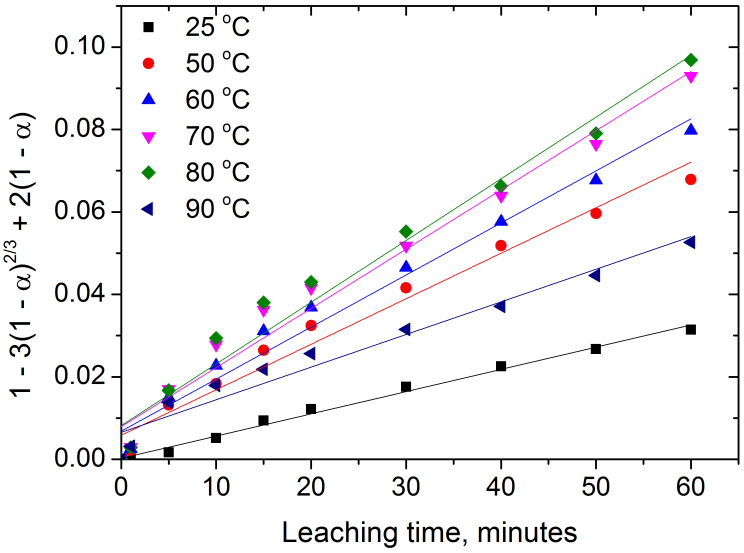

Fig. 6.68 Variation of $1 - 3(1 - \alpha)^{\frac{2}{3}} + 2(1 - \alpha)$ with t at different temperatures. Constant parameters: Stirring speed (300 rpm), solid-liquid ratio (50 g L^{-1}) and HCl concentration (1.5 M).

As is evident from the figures, the random pore model equation correlates well with experimental data ($R^2 > 0.99$ for all plots). Leaching temperature and

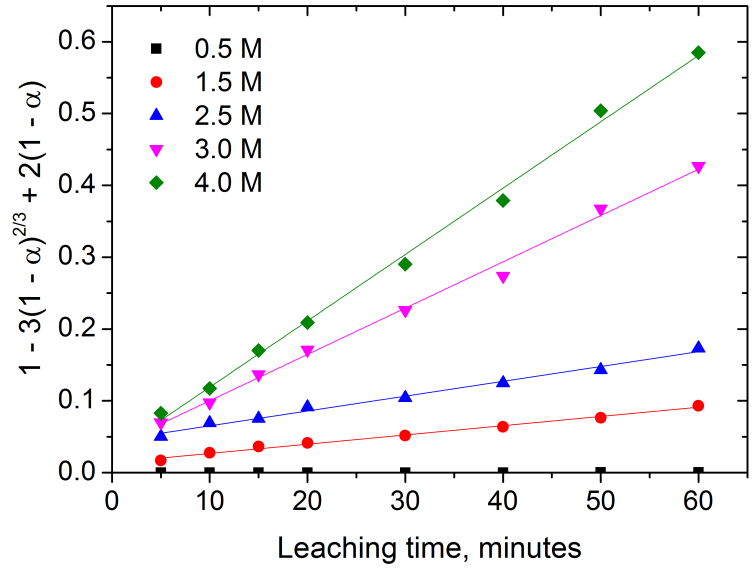

Fig. 6.69 Variation of $1-3(1-\alpha)^{\frac{2}{3}}+2(1-\alpha)$ with t at different HCl concentrations. Constant parameters: Stirring speed (300 rpm), solid-liquid ratio (50 g L^{-1}) and temperature (70 °C).

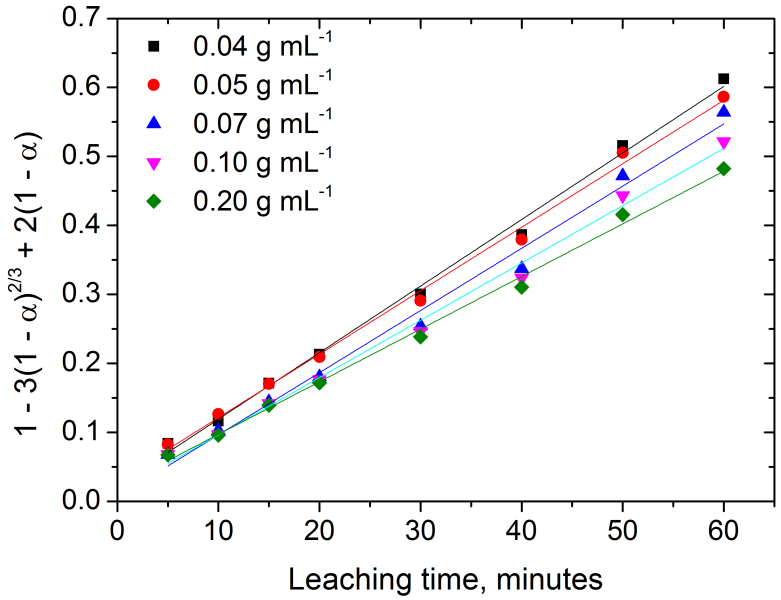

Fig. 6.70 Variation of $1-3(1-\alpha)^{\frac{2}{3}}+2(1-\alpha)$ with t at different solid-liquid ratios. Constant parameters: Stirring speed (300 rpm), temperature (70 °C and HCl concentration (4 M).

acid concentration show the most influence on niobium dissolution. The filter cake became more soluble at high temperature and high acid concentration, and the advantage of both high leaching temperature and concentration for the dissolution of niobium was demonstrated.

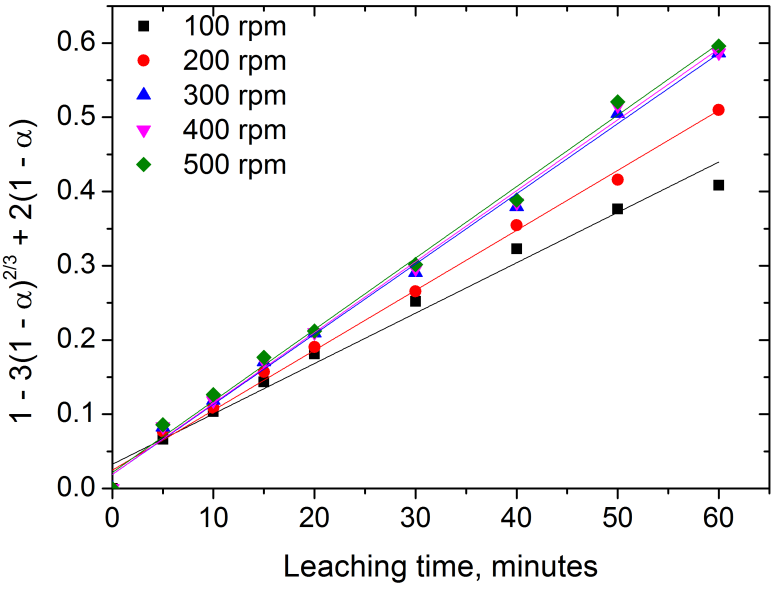

Fig. 6.71 Variation of$1 - 3(1 - \alpha)^{\frac{2}{3}} + 2(1 - \alpha)$ with t at different stirring speeds. Constant parameters: Temperature (70 °C), solid-liquid ratio (50 g L^{-1}) and HCl concentration (4 M).

Fig. 6.72 presents the activation energy for niobium dissolution in HCl.

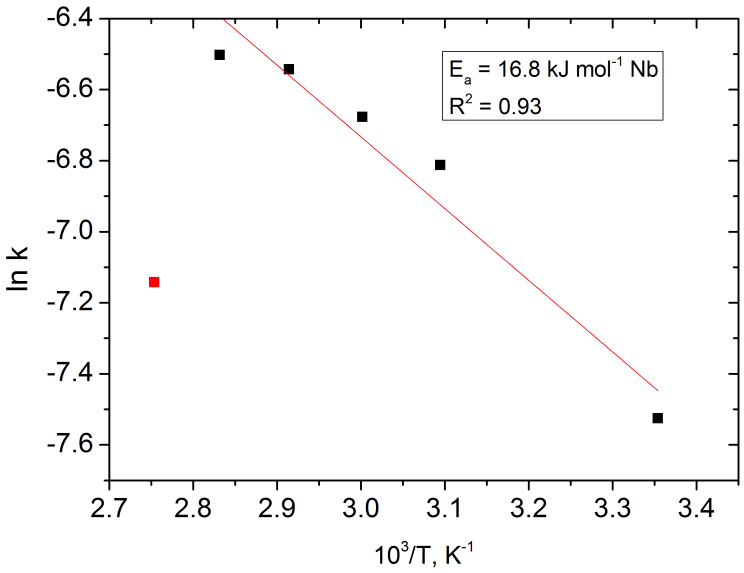

Fig. 6.72 Arrhenius plot for niobium dissolution in HCl

In section 6.3, the influence of leaching temperature on niobium dissolution was discussed, highlighting that at 90 °C, niobium undergoes hydrothermal precipitation from the acidic media leading to a lower than expected recovery. When calculating the activation energy, the $\ln k$ value for leaching at 90 °C is therefore not used. From the Arrhenius plot, the minimum energy required

for dissolution of niobium from the filter cake was calculated to be 16.8 kJ mol^{-1} Nb. The activation energy is well within the typical range for pore diffusion controlled reaction kinetics [182, 183]. Some researchers have obtained comparable values of activation energy for the acid dissolution of niobium ores, reporting figures in the region of 15 - 22 kJ mol^{-1} [184, 185].

6.8.2 Vanadium dissolution

Leaching of binary mixtures

Dissolution of vanadium from TiO_2 - V_2O_5 binary mixtures sintered at different temperatures is presented in figures 6.73 and 6.74. The dissolution process is governed by pore diffusion of the shrinking core model.

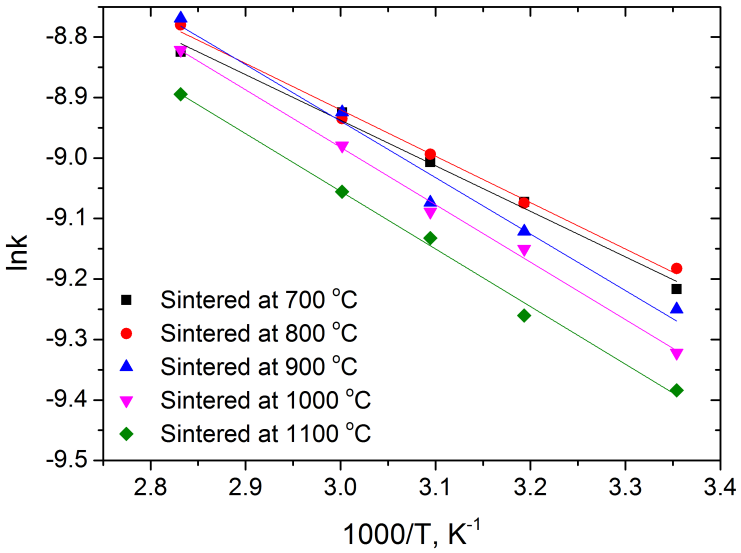

Fig. 6.73 Plot of $\ln k$ against $^1/_T$ for samples sintered at different temperatures. Constant parameters: Stirring speed (300 rpm), solid-liquid ratio (50 g L^{-1}), leaching temperature (60 °C) and NaOH concentration (2 M).

Fig. 6.74 shows that the solid solutions formed between 700 and 800 °C require similar amounts of activation energy (6.3 ±0.5 and 6.4 ± 0.5 kJ mol^{-1} vanadium respectively). Increasing the sintering temperature from 800 to 900 raises the activation energy requirement to 7.8 ± 0.7 kJ mol^{-1} vanadium and increasing further does not lead to significant increase in activation energy requirement.

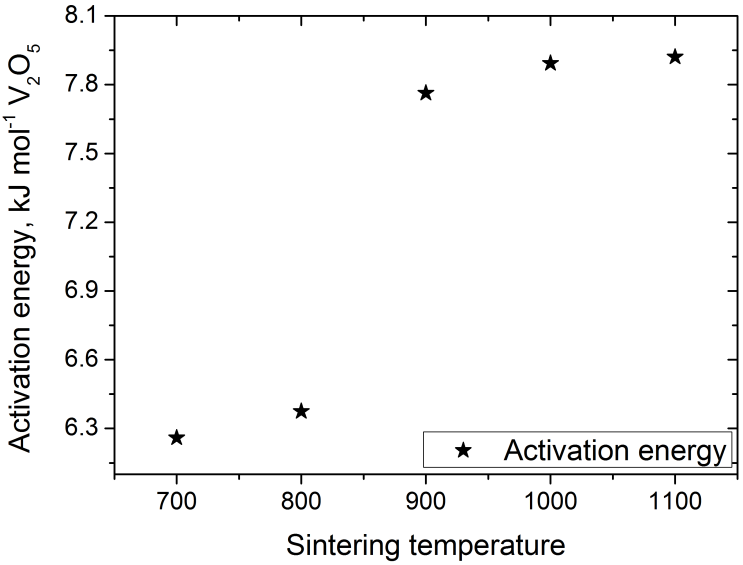

Fig. 6.74 Activation energies for dissolution of vanadium from binary mixtures.

Leaching of filter cake

The variation of $1-3(1-\alpha)^{\frac{2}{3}}+2(1-\alpha)$ with time (t) is presented for leaching temperature (Fig. 6.75), HCl concentration (Fig. 6.76), solid-liquid ratio (Fig. 6.77) and stirring speed (Fig. 6.78) to describe the kinetics of vanadium dissolution in HCl.

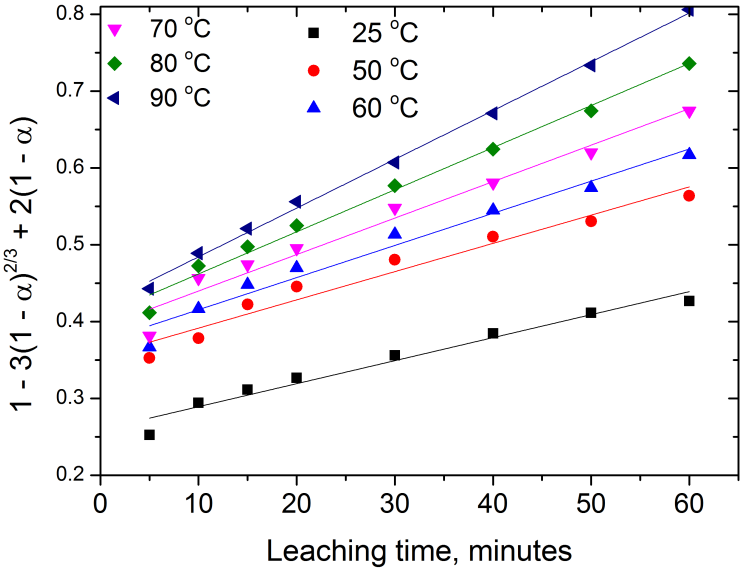

Fig. 6.75 Variation of $1-3(1-\alpha)^{\frac{2}{3}}+2(1-\alpha)$ with time. Stirring speed (300 rpm), solid-liquid ratio (50 g L^{-1}) and HCl concentration (1.5 M).

Figures 6.75 - 6.78 show that HCl concentration and leaching temperature have the most influence on vanadium dissolution and that there is good correla-

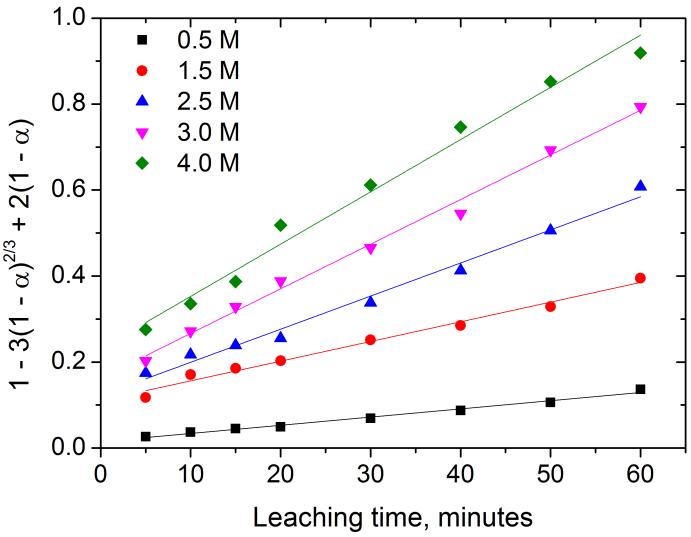

Fig. 6.76 Variation of $1-3(1-\alpha)^{\frac{2}{3}}+2(1-\alpha)$ with time. Constant parameters: Stirring speed (300 rpm), solid-liquid ratio (50 g L^{-1}) and temperature (70 °C).

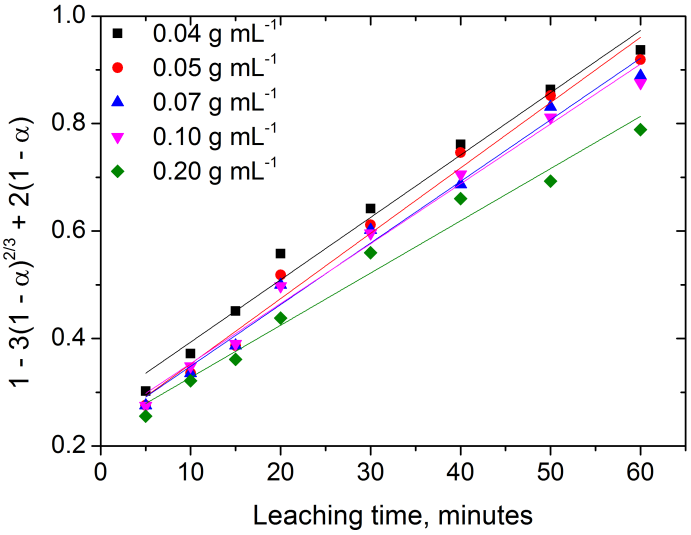

Fig. 6.77 Variation of $1-3(1-\alpha)^{\frac{2}{3}}+2(1-\alpha)$ with time. Constant parameters: Stirring speed (300 rpm), temperature (70 °C) and HCl concentration (4 M).

tion between the diffusion controlled random pore model and the experimental data ($R^2 > 0.95$ for all plots). Using the Arrhenius plot shown in Fig. 6.79, the activation energy was calculated to be 10.4 kJ mol^{-1} V, which is expected for pore diffusion controlled reaction kinetics. The activation energy is significantly lower than the values quoted in literature for dissolution kinetics of vanadium in acidic media, which ranges from 30 - 45 kJ mol^{-1} V [186–189]. Vanadium is dissolved from the filter cake by means of desorption from iron and titanium

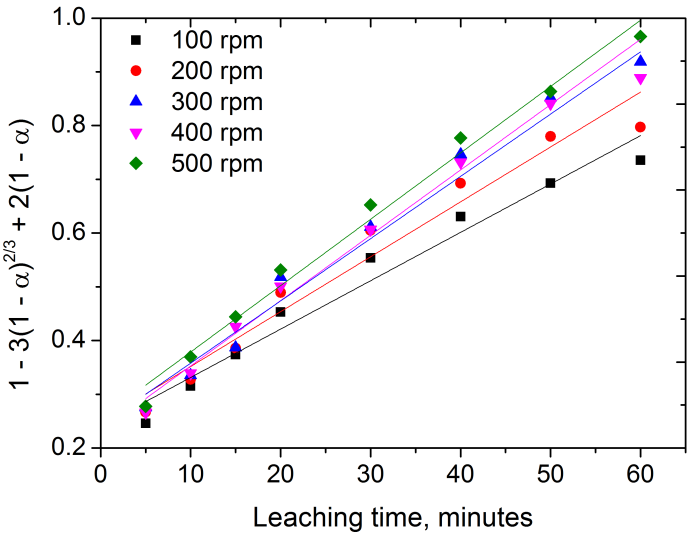

Fig. 6.78 Variation of $1-3(1-\alpha)^{\frac{2}{3}}+2(1-\alpha)$ with time. Constant parameters: Temperature (70 °C), solid-liquid ratio (50 gL^{-1}) and HCl concentration (4 M).

hydroxide surfaces hence the lower activation energy compared to literature values which are quoted for chemical reaction type of kinetics [145, 190–192].

Fig. 6.79 presents the Arrhenius plot used for determining the activation energy.

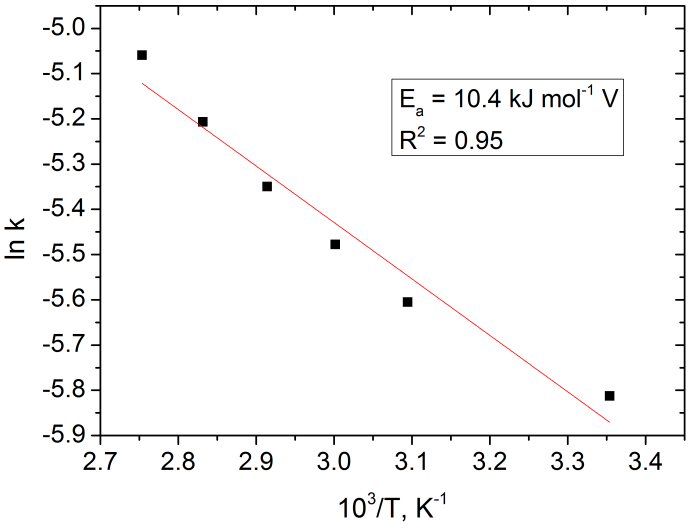

Fig. 6.79 Arrhenius plot for vanadium dissolution in HCl

6.8.3 Scandium dissolution

The variation of $1-3(1-\alpha)^{\frac{2}{3}}+2(1-\alpha)$ with time (t) is presented for leaching temperature (Fig. 6.80), HCl concentration (Fig. 6.81), solid-liquid ratio (Fig. 6.82) and stirring speed (Fig. 6.83) to describe the kinetics of scandium dissolution in HCl. As well as showing the good correlation between the diffusion controlled random pore model and experimental data ($R^2 > 0.90$ for all plots), figures 6.80 - 6.83 show that HCl concentration has the most significant influence on scandium dissolution from the filter cake. Leaching temperature also has a significant influence on dissolution of scandium while the significance of both solid-liquid ratio and stirring speed is not as obvious in the ranges investigated.

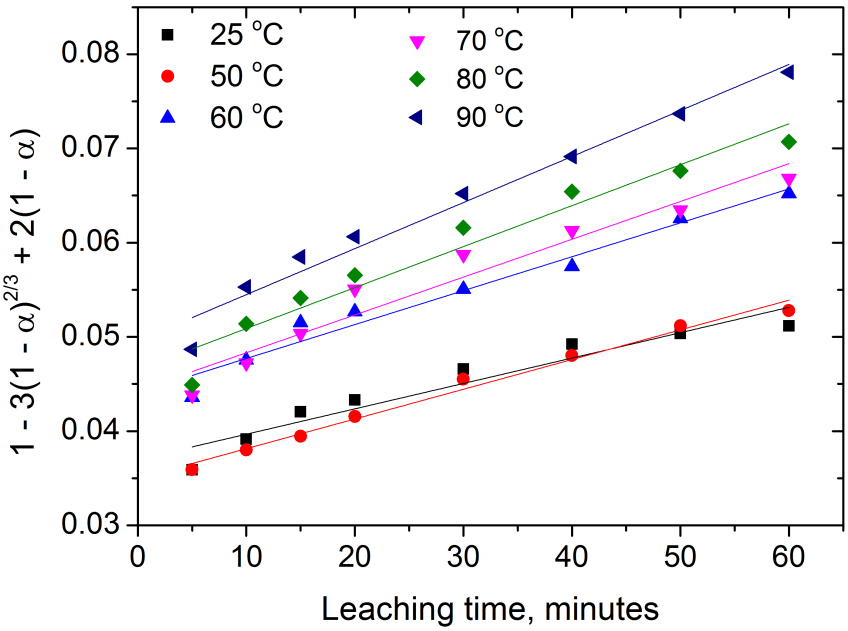

Fig. 6.80 Variation of $1-3(1-\alpha)^{\frac{2}{3}}+2(1-\alpha)$ with time. Constant parameters: Stirring speed (300 rpm), solid-liquid ratio (50 g L^{-1}) and HCl concentration (1.5 M).

Using the Arrhenius plot in Fig. 6.84, the activation energy for scandium dissolution in hydrochloric acid is determined to be less than 10 kJ mol^{-1} Sc, again confirming that the acid dissolution reaction kinetics are controlled by pore diffusion. There is no data in literature to compare with due to the limited number of studies on dissolution kinetics of scandium.

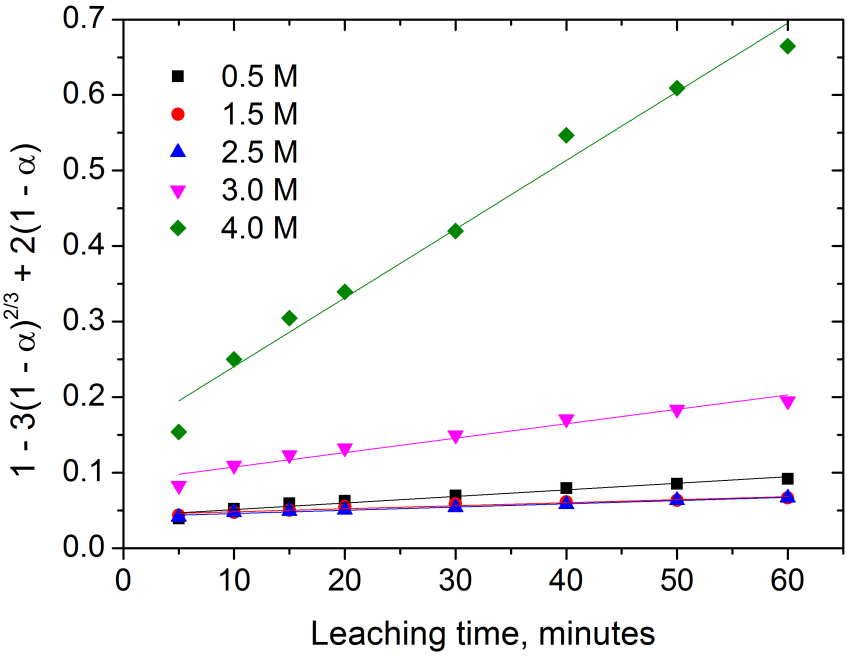

Fig. 6.81 Variation of $1-3(1-\alpha)^{\frac{2}{3}}+2(1-\alpha)$ with time. Constant parameters: Stirring speed (300 rpm), solid-liquid ratio (50 g L^{-1}) and temperature (70 °C).

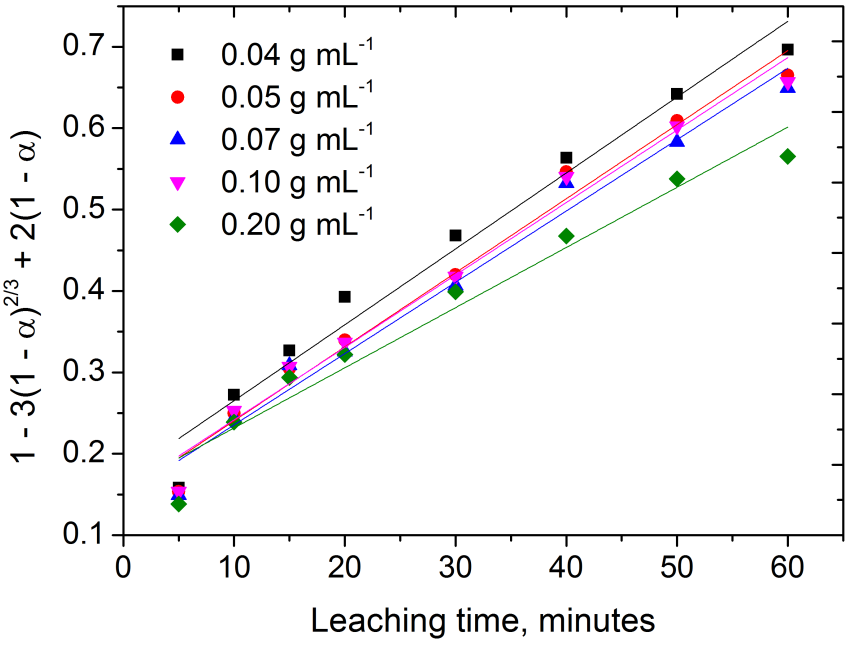

Fig. 6.82 Variation of $1-3(1-\alpha)^{\frac{2}{3}}+2(1-\alpha)$ with time. Constant parameters: Stirring speed (300 rpm), temperature (70 °C) and HCl concentration (4 M).

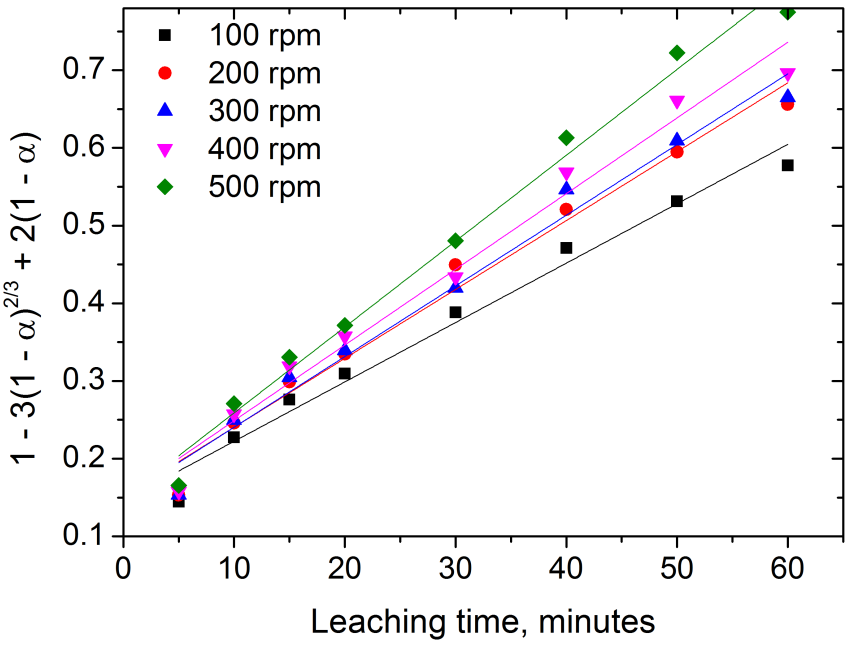

Fig. 6.83 Variation of $1-3(1-\alpha)^{\frac{2}{3}}+2(1-\alpha)$ with time. Constant parameters: Temperature (70 °C), solid-liquid ratio (50 g L^{-1}) and HCl concentration (4 M).

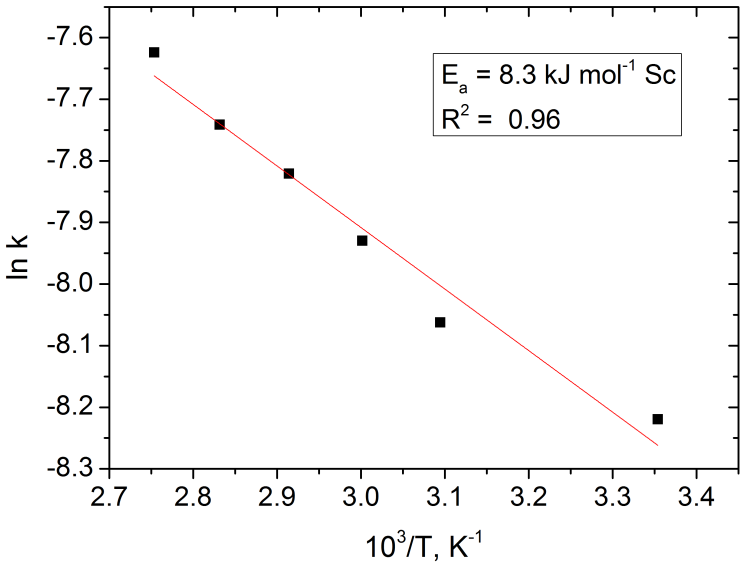

Fig. 6.84 Arrhenius plot for scandium dissolution in HCl

6.8.4 Thorium dissolution in HCl

Kinetics for thorium dissolution were studied in two parts because the dissolution is very fast in the first 15 minutes and then reaches equilibrium. Figures 6.85 - 6.88 present the graphs for variation of $1-3(1-\alpha)^{\frac{2}{3}}+2(1-\alpha)$ with time and calculations of activation energy for the first and second stages of thorium dissolution in HCl.

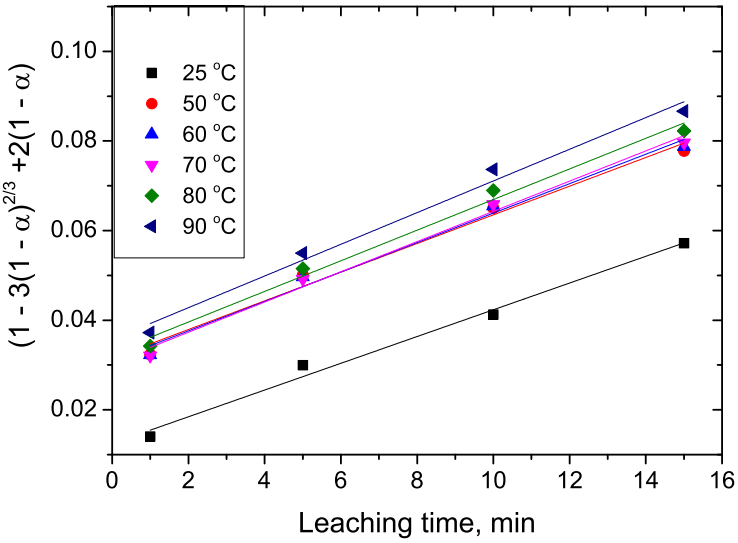

Fig. 6.85 Variation of $1-3(1-\alpha)^{\frac{2}{3}}+2(1-\alpha)$ with time (first stage). Constant parameters: Stirring speed (300 rpm), solid-liquid ratio (50 g L^{-1}) and HCl concentration (1.5 M).

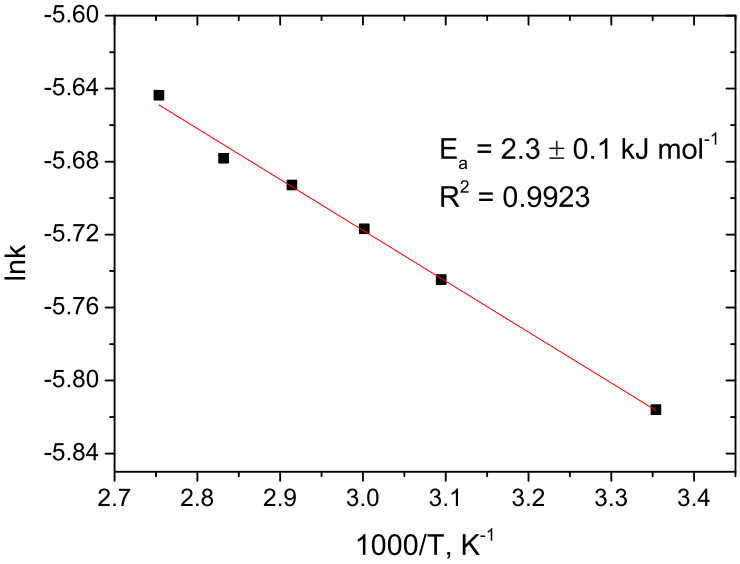

Fig. 6.86 Arrhenius plot of the dissolution process (first stage).

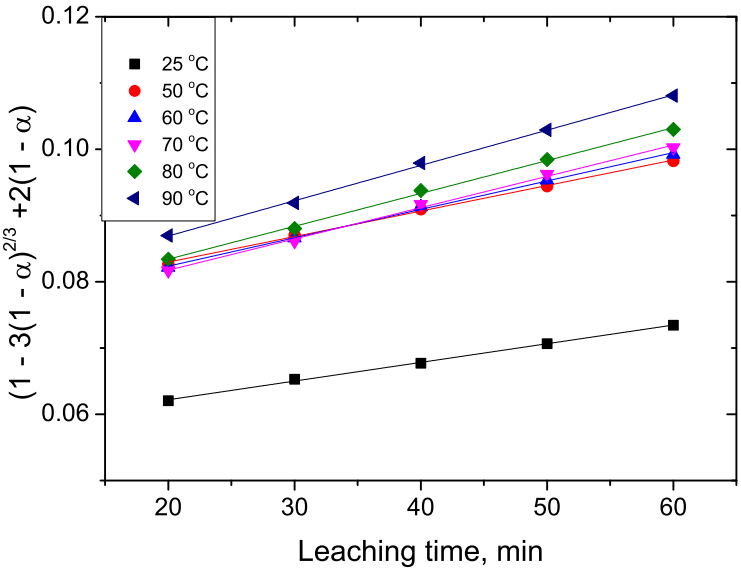

Fig. 6.87 Variation of $1-3(1-\alpha)^{\frac{2}{3}}+2(1-\alpha)$ with time (second stage). Constant parameters: Stirring speed (300 rpm), solid-liquid ratio (50 g L^{-1}) and HCl concentration (1.5 M).

The activation energies for the first and second stages of acid leaching are 2.3 ±0.1 kJ mol^{-1} and 9.2 ±0.5 kJ mol^{-1} respectively. Thorium dissolution in HCl is governed by the random pore model. Diffusion of HCl and thorium ions through filter cake pores seems to be the rate controlling step.

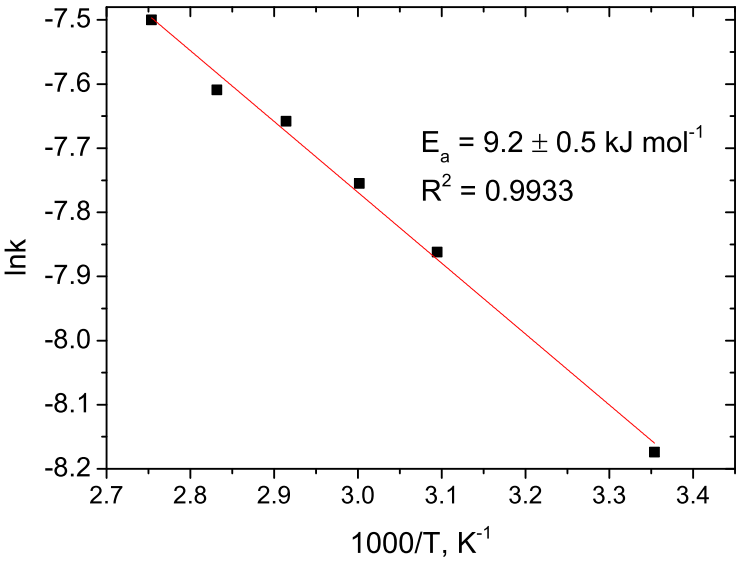

Fig. 6.88 Arrhenius plot of the dissolution process (second stage).

6.8.5 Removal of zirconium from pH 1 precipitates

Fig. 6.89 and 6.90 present the plots of $1-3(1-\alpha)^{\frac{2}{3}}+2(1-\alpha)$ against time for different leaching temperatures and alkali concentrations respectively.

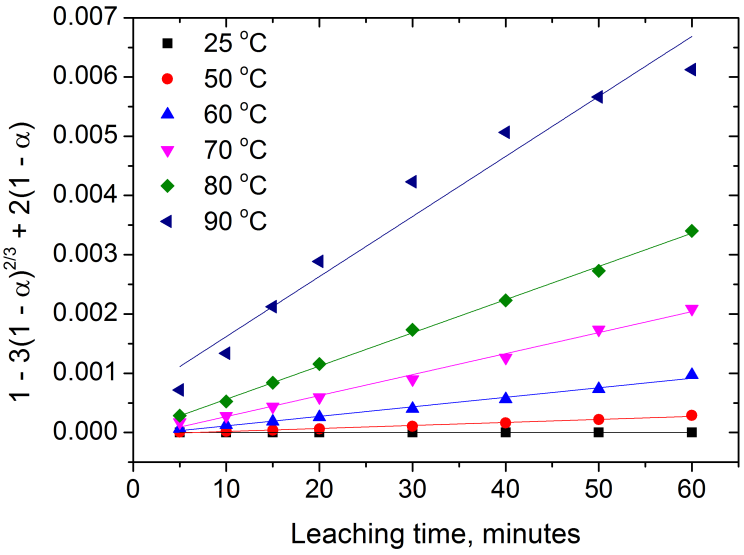

Fig. 6.89 Variation of $1-3(1-\alpha)^{\frac{2}{3}}+2(1-\alpha)$ with time at different temperatures. Stirring speed (300 rpm), solid-liquid ratio (50 g L^{-1}), $NaNO_3$ concentration (20 g L^{-1}) and Na_2CO_3 concentration (1 M).

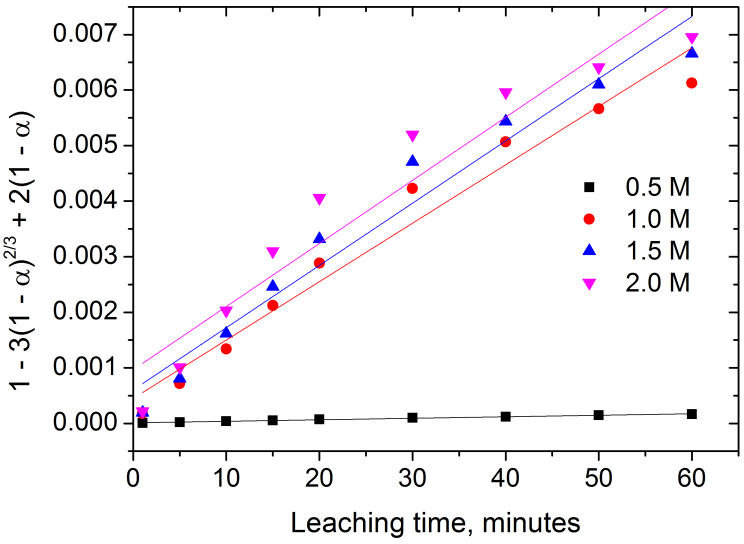

Fig. 6.90 Variation of $1-3(1-\alpha)^{\frac{2}{3}}+2(1-\alpha)$ with time at different alkali concentrations

Figs. 6.89 and 6.90 show that the pore diffusion model fits the data very well particularly for the influence of temperature on zirconium removal. Unlike

in the acid leaching process where the structural parameter has a large negative value, alkali leaching has small negative structural parameter values, close to zero. This means the influence of chemical reaction kinetics is relatively more significant in the alkali leaching processes. The parameters calculated for chemical reaction controlled kinetics are shown in the appendix. The activation energy for the zirconium removal was calculated based on the random pore model and is presented in Fig. 6.91.

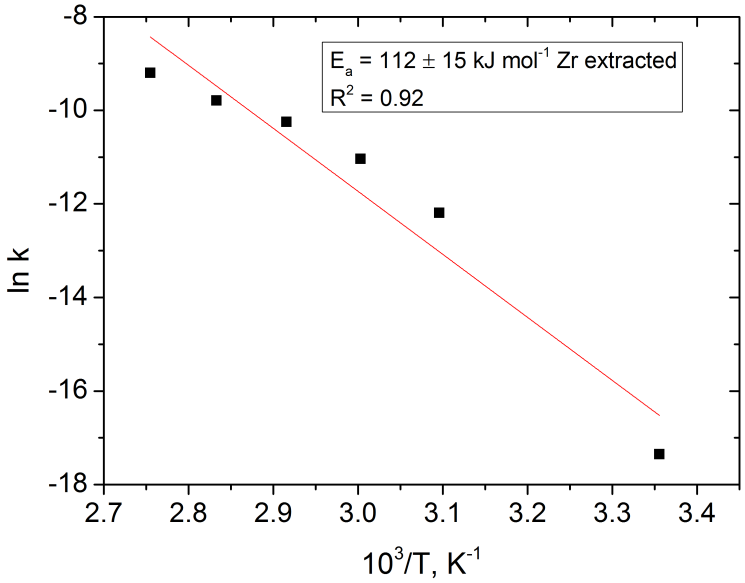

Fig. 6.91 Arrhenius plot for zirconium dissolution in a Na_2CO_3 - $NaNO_3$ system

Fig. 6.91 shows that an activation energy greater than 100 kJ mol^{-1} zirconium is needed for removal of zirconium from the niobium-rich precipitates. Although the fraction of zirconium removed from the residues is low, using the system at a higher temperature, perhaps by employing pressure leaching, could provide efficient separation of niobium and zirconium. There is no published literature on separation of zirconium and niobium by alkali leaching processes, therefore, if such a technique works, it could be a significant addition to available separation and purification technologies of zirconium and niobium.

6.8.6 Vanadium dissolution from pH 1.5 precipitates

Fig. 6.92 and 6.93 compare plots of $1-\exp[-k\alpha-\psi(k\alpha/2)^2]$ and $1-3(1-\alpha)^{\frac{2}{3}}+2(1-\alpha)$ against leaching time (t) for surface reaction and diffusion controlled reaction kinetics respectively. The structural parameter values are once again

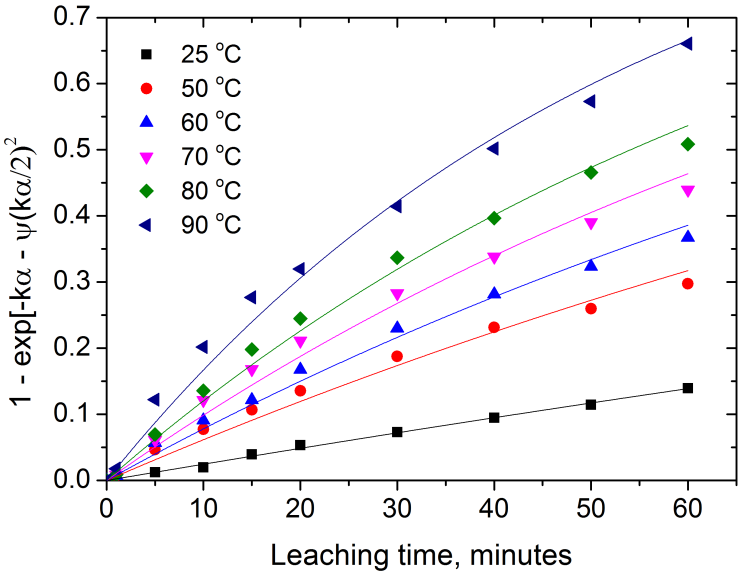

Fig. 6.92 Variation of $1-\exp[-k\alpha-\psi(k\alpha/2)^2]$ with time. Constant parameters: Stirring speed (300 rpm), solid-liquid ratio (50 g L^{-1}), $NaNO_3$ concentration (20 g L^{-1}) and Na_2CO_3 concentration (1 M)

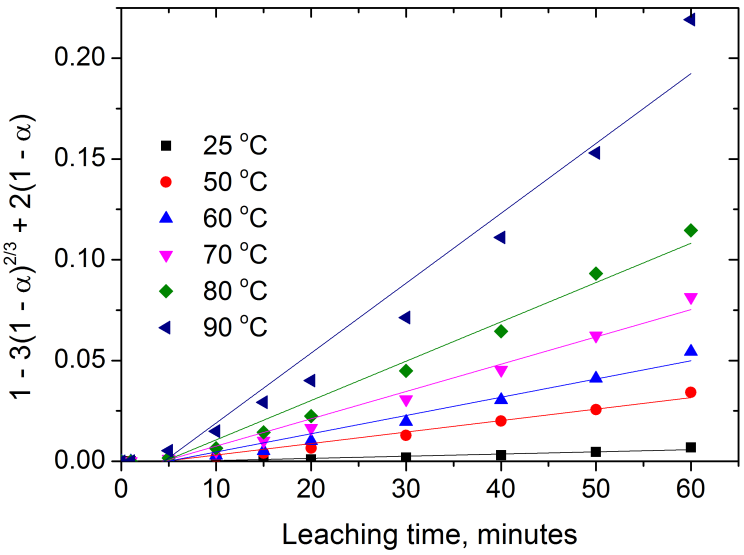

Fig. 6.93 Variation of $1-3(1-\alpha)^{\frac{2}{3}}+2(1-\alpha)$ with time. Constant parameters: Stirring speed (300 rpm), solid-liquid ratio (50 g L^{-1}), $NaNO_3$ concentration (20 g L^{-1}) and Na_2CO_3 concentration (1 M)

near-zero negative, meaning that the alkali leaching of vanadium from pH 1.5 precipitates is to some extent controlled by surface chemical reaction. Pore diffusion also contributes to the reaction rate, particularly at high temperatures (>70 °C).

The activation energy for the alkali dissolution of vanadium from pH 1.5 precipitates was calculated to be 46.6 ±1.8 kJ mol^{-1} V using the Arrhenius plot shown in Fig. 6.94.

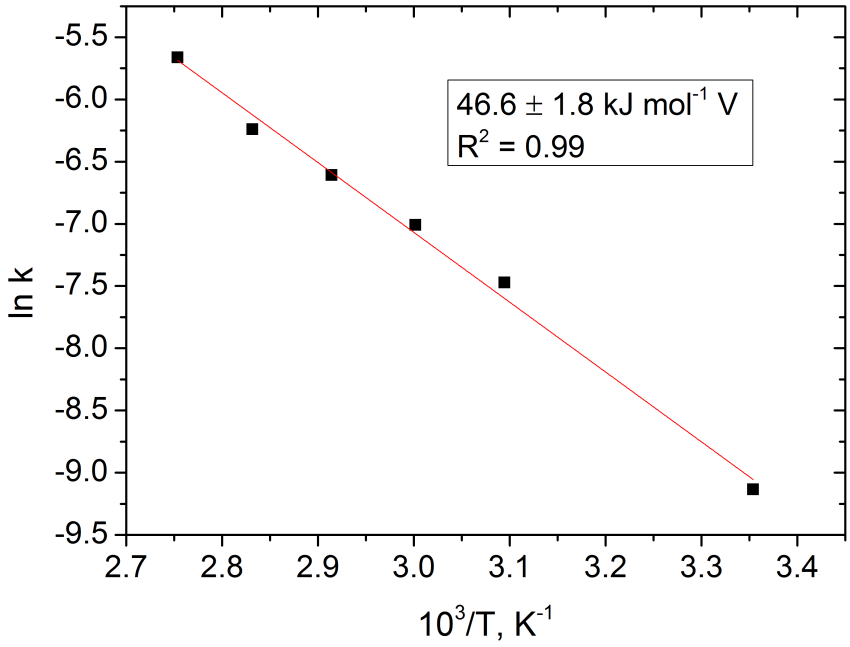

Fig. 6.94 Arrhenius plot for vanadium dissolution in a Na_2CO_3 - $NaNO_3$ system

The activation energy is in the range for reactions typically controlled by chemical reaction and compares well with activation energies recorded in literature for alkali leaching of various forms of vanadium [193–195].

Fig 6.95 and 6.96 compares the plots of $1 - \exp[-k\alpha - \psi(k\alpha/2)^2]$ and $1 - 3(1-\alpha)^{\frac{2}{3}} + 2(1-\alpha)$ against time for sodium carbonate concentration and affirms the conclusion that the alkali leaching reaction is at least to some extent chemical reaction controlled.

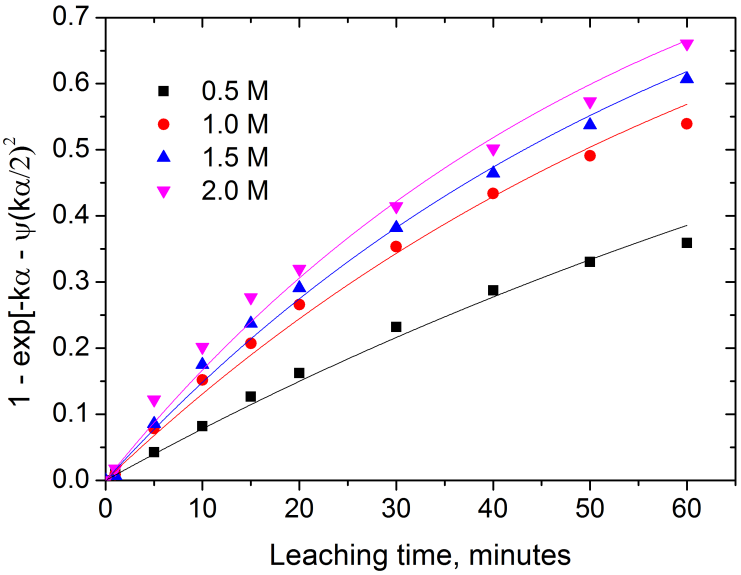

Fig. 6.95 Variation of $1 - \exp[-k\alpha - \psi(k\alpha/2)^2]$ with time. Constant parameters: Stirring speed (300 rpm), solid-liquid ratio (50 g L^{-1}), $NaNO_3$ concentration (20 g L^{-1}) and temperature (90 °C).

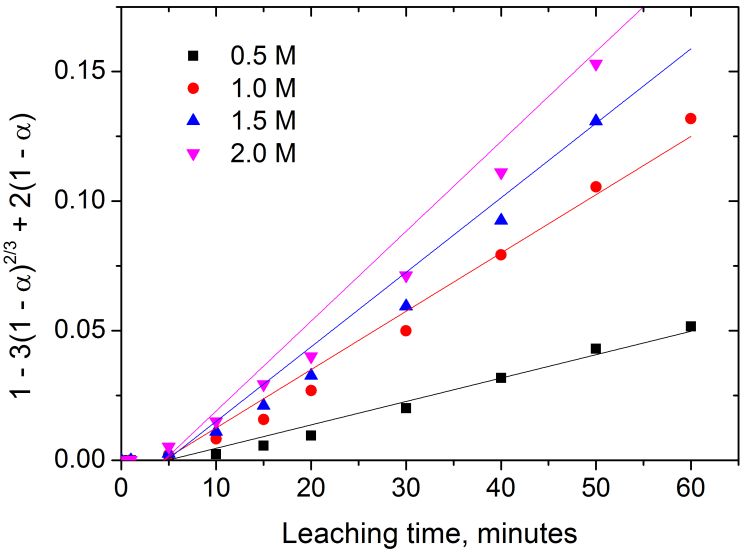

Fig. 6.96 Variation of $1 - 3(1-\alpha)^{\frac{2}{3}} + 2(1-\alpha)$ with time. Constant parameters: Stirring speed (300 rpm), solid-liquid ratio (50 g L^{-1}), $NaNO_3$ concentration (20 g L^{-1}) and temperature (90 °C).

6.8.7 Scandium re-dissolution from pH 5 precipitates

The kinetics of scandium dissolution in alkaline media were investigated using pH 5 precipitates. As shown in figures 6.97 and 6.98, scandium dissolution is controlled by both chemical reaction and pore diffusion. Results from dissolution studies presented in section 6.3 show that scandium is nearly insoluble in sodium

carbonate solutions when sodium nitrate is not present, suggesting that sodium nitrate plays a key role in the dissolution of scandium. It is therefore likely that scandium dissolves by forming relatively big complex ions with the lixiviant system, which diffuse slowly through the filter cake pores, hence the influence of both chemical reaction and pore diffusion kinetics on scandium dissolution.

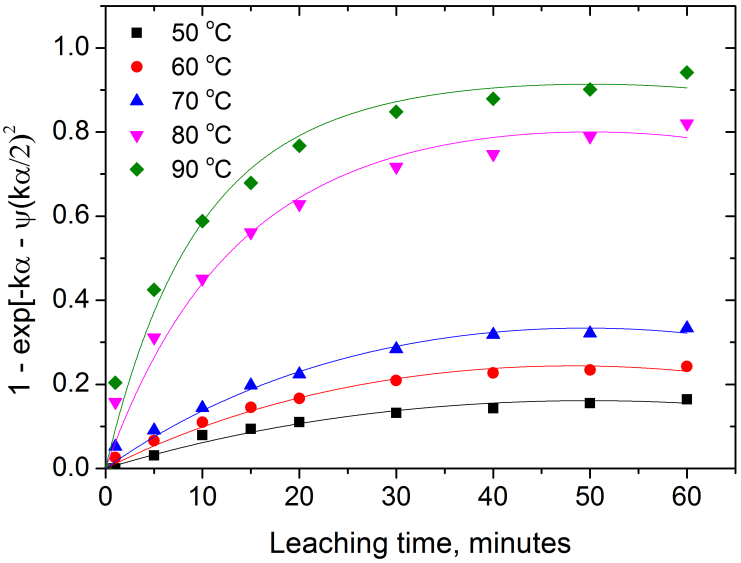

Fig. 6.97 Variation of $1 - \exp[-k\alpha - \psi(k\alpha/2)^2]$ with time. Constant parameters: Stirring speed (300 rpm), solid-liquid ratio (50 g L^{-1}), $NaNO_3$ concentration (20 g L^{-1}) and Na_2CO_3 concentration (1 M).

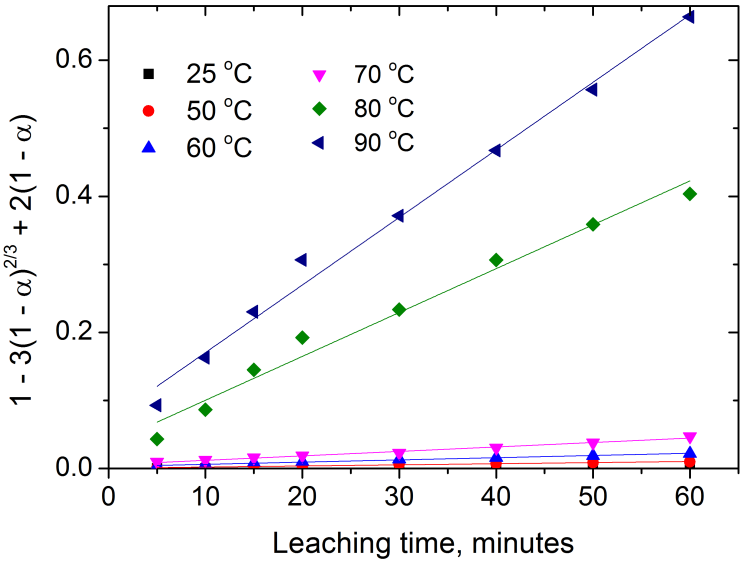

Fig. 6.98 Variation of $1 - 3(1-\alpha)^{\frac{2}{3}} + 2(1-\alpha)$ with time. Constant parameters: Stirring speed (300 rpm), solid-liquid ratio (50 g L^{-1}), $NaNO_3$ concentration (20 g L^{-1}) and Na_2CO_3 concentration (1 M).

Fig. 6.99 presents the Arrhenius plot for scandium dissolution in a Na_2CO_3 - $NaNO_3$ system, showing that the minimum energy required for scandium to dissolve from pH 5 precipitates into the oxidised alkali system is nearly 110 kJ mol^{-1} Sc. The activation energy for scandium dissolution in the alkali system is significantly higher than typical for diffusion controlled reactions, suggesting that surface reaction kinetics played a significant role in the extraction rate of scandium.

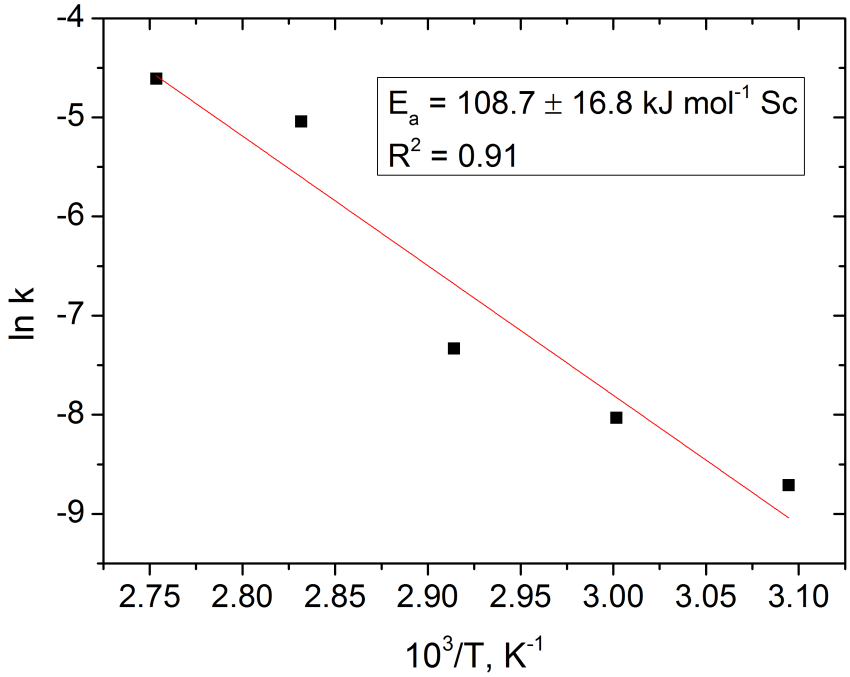

Fig. 6.99 Arrhenius plot for scandium dissolution in a Na_2CO_3 - $NaNO_3$ system

Plots of $1 - \exp[-k\alpha - \psi(k\alpha/2)^2]$ and $1 - 3(1-\alpha)^{\frac{2}{3}} + 2(1-\alpha)$ against leaching time for alkali leaching of pH 5 precipitates are presented for various lixiviant concentrations in Fig. 6.100 and Fig. 6.101 respectively. The plots show that both the pore diffusion controlled reaction and chemical reaction controlled kinetics fit the empirical data very well ($R^2 > 0.99$). Based on the high activation energy requirement, the reaction has been concluded to be largely chemical reaction controlled.

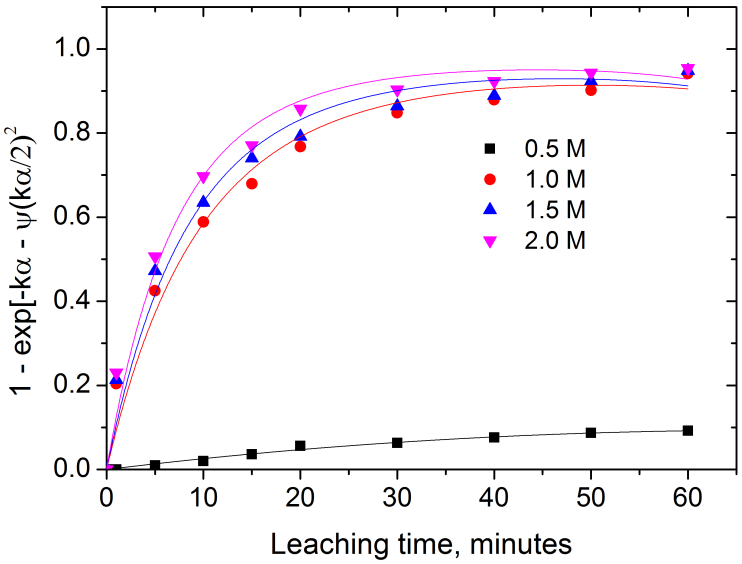

Fig. 6.100 Variation of $1 - \exp[-k\alpha - \psi(k\alpha/2)^2]$ with time. Constant parameters: Stirring speed (300 rpm), solid-liquid ratio (50 g L^{-1}), $NaNO_3$ concentration (20 g L^{-1}) and temperature (90 °C).

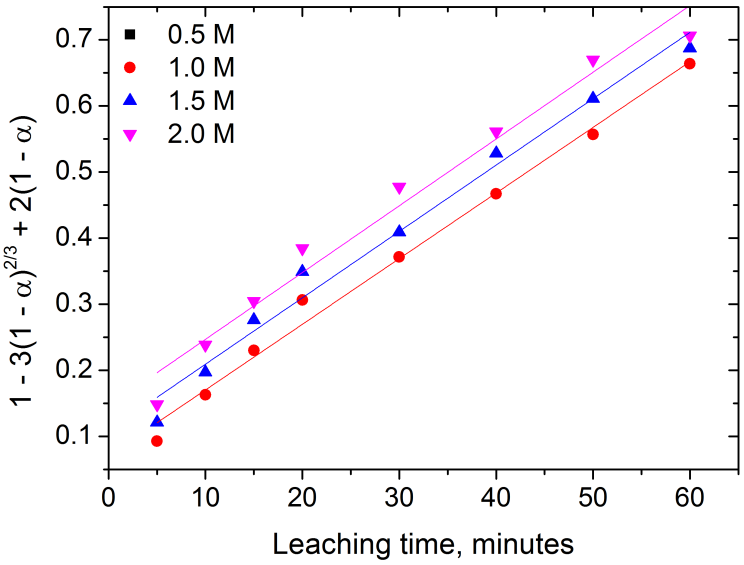

Fig. 6.101 Variation of $1 - 3(1-\alpha)^{\frac{2}{3}} + 2(1-\alpha)$ with time. Constant parameters: Stirring speed (300 rpm), solid-liquid ratio (50 g L^{-1}), $NaNO_3$ concentration (20 g L^{-1}) and temperature (90 °C).

6.9 Chapter summary

Chapter 6 has presented extensive data from studies on sequential optimisation of selective leaching and precipitation processes carried out using filter cake and synthetic binary mixtures of TiO_2 and V_2O_5. An integrated process for recovering 80 % vanadium with a grade of 99.5 % while concentrating niobium and scandium values for further purification has been demonstrated. Niobium is concentrated in pH 1 precipitates, with zirconium, titanium and thorium being the key impurities while scandium can be selectively re-dissolved from pH 5 precipitates, giving a relatively pure scandium solution, with REE as the main impurities. Attempts to precipitate organic scandium salts from the alkali solution by neutralising with organic acids were unsuccessful. This was attributed to the relatively high concentration of sodium ions in the system, which interfere with the precipitation of scandium. The recoveries and grades achieved from the 1 kg batch (**B3**) are presented in table 6.12. Key vanadium

Table 6.12 Recoveries and grades of the valuable metals

	Recovery (%)	**Grade (%)**	**Key impurities**
Vanadium	80.3	99.5	Cl^-
Niobium	82.3	15.7	SO_4^{2-}, Zr, Ti, Th
Scandium	≈100	> 50	REE (La, Ce)

losses were observed during initial precipitation from HCl media and during the salt roasting process. Niobium losses were significant in both the HCl leaching and selective precipitation stages.

Leaching temperature and HCl concentration significantly affect the dissolution rates of vanadium, scandium and niobium. Dissolution of thorium is mainly dependent on acid concentration, with extraction rates greater than 80 % achieved in about 15 minutes of leaching the residues in 4 M HCl.

Chapter 6 also presented kinetics studies for key leaching experiments. The activation energies for the dissolution processes are presented in table 6.13:

Table 6.13 Activation energies for dissolution of vanadium, scandium and niobium in HCl and Na_2CO_3

	V	Sc	Nb
HCl	10.4 kJ mol^{-1}	8.3 kJ mol^{-1}	16.8 kJ mol^{-1}
Na_2CO_3	46.6 kJ mol^{-1}	108.7 kJ mol^{-1}	insoluble

The dissolution of metals from filter cake is governed by the random pore model, with pore diffusion being the rate limiting step for HCl leaching and surface chemical reaction for alkaline leaching. From the results presented in this chapter, reactor design for a pilot plant and subsequently, detailed economics assessment can be carried out.

Chapter 7

Conclusions

The overall aim of this project was to design and develop an integrated process for recovery of vanadium, scandium and niobium from waste produced during TiO_2 production. This was done by initially studying the thermodynamics of the multi-metal system, followed by experiments to verify the theoretical work.

The main points of conclusion drawn from each investigation addressing the objectives are listed below.

7.1 Dissolution of vanadium in TiO_2 lattice

1. At 1100 °C, more than 8.6 mol% vanadium ions can occupy octahedral sites in TiO_2's rutile structure. This is in agreement with the predictions made using the Goldschmidt rules and the crystal field theory, both described in chapter 2. SEM-EDX analysis of as received cake presented in the materials characterisation chapter (Chapter 3) confirmed the presence of vanadium ions in solvent rutile lattice.

2. NaOH leaching at 60 °C for 3 hours is not sufficient for extracting vanadium from the rutile lattice. This may be because vanadium ions attain increased stability in the distorted rutile coordination sites compared to the NaOH aqueous solution. Leaching of vanadium ions from the rutile structure also depends on the ease with which the NaOH can penetrate into the environment around the vanadium ion and this may not be easy considering the size of the sodium ions.

7.2 Dissolution of metals in HCl

1. As predicted by Pourbaix diagrams in chapter 4 vanadium, scandium and niobium dissolve in HCl. Leaching temperature and HCl concentration have the biggest influence on dissolution of the metals. Extraction rates of vanadium and scandium increase with increasing temperature between 25 - 90 °C and HCl concentration between 0.5 - 4 M. Niobium extraction increases with leaching temperature up to 70 °C and decrease as temperature is further increased. Reduction in niobium extraction rate when temperature is raised above 70 °C has been attributed to hydrothermal precipitation of niobium.

2. Both stirring speed and solid-liquid ratio do not have a significant effect on the kinetics of filter cake dissolution in HCl.

3. Residues left after HCl leaching of the as-received cake are rich in TiO_2, contaminated mainly by SiO_2. All other metal hydroxides, including thorium, are dissolved in the acid, with some vanadium remaining dissolved in the crystal lattice of rutile.

7.3 Selective precipitation of valuable metals

The efficiency of selective precipitation is significantly reduced if the filter cake is oxidised before leaching in acid. The selective precipitation process relies on keeping iron, the major impurity, in the Fe (II) state to allow the valuable metals to precipitate before the iron is precipitated at pH > 5. When iron is oxidised before acid leaching, ferrihydrite begins precipitating at pH as low as 0.5, rendering the selective precipitation process ineffective.

7.3.1 Precipitation of niobium

1. Precipitation temperature and time have the biggest influence on selective precipitation of niobium.

2. As predicted by the Pourbaix diagrams in chapter 4, niobium precipitates at pH 1. At 90 °C, the precipitation rate is slow but can be catalysed by H_2SO_4. Zirconium, titanium and thorium are the key contaminants of the niobium-rich precipitates.

3. During the precipitation reactions, iron is continuously oxidised from Fe (II) to Fe (III), allowing ferrihydrite and goethite to co-precipitate. To minimise contamination of the niobium-rich precipitates with iron, a precipitation time in the region of 180 minutes was suggested.

7.3.2 Precipitation of vanadium

1. The precipitation rate of vanadium at pH 1.5 between 50 - 90 °C is not affected by temperature. The precipitates become more filterable with increasing precipitation temperature therefore a temperature of 70 °C is recommended. At lower temperatures, gelatinous ferrihydrite precipitation dominates while the filterable goethite precipitation dominates above 70 °C.

2. Fig. 4.2 and Fig. 4.3 show that vanadium is not expected to precipitate at pH as low as 2, yet it is nearly fully precipitated at pH 1.5. This can be attributed to co-precipitation/adsorption of vanadium ions on hydrated iron oxide precipitates. Moreover, the pH range for vanadium precipitation is consistent with observed precipitation of iron hydroxides, particularly $Fe(OH)_3$.

7.3.3 Precipitation of scandium

1. Precipitation temperature does not affect the precipitation rate of scandium at pH 5. As with vanadium precipitation, the filterability of the precipitated scandium is poor at low precipitation temperatures, suggesting that ferrihydrite precipitation still dominates at lower temperatures. A precipitation temperature of 70 °C is recommended.

2. Using selective precipitation, a concentrate containing up to 4000 ppm Sc_2O_3 has been obtained, with iron and aluminium being the major impurities.

3. From the SEM-EDX analysis, scandium is distributed evenly between the iron and aluminium phases, which may be indicating that scandium precipitated as the hydrated oxide as opposed to adsorption/co-precipitation. Precipitation of scandium as the hydrated oxide may also be the explanation for scandium remaining in solution even when iron started

precipitating at lower pH and the theory is supported by the Pourbaix diagrams for scandium (Chapter 4).

4. Rare earth oxides, particularly CeO_2, La_2O_3 and Y_2O_3 also concentrate with the scandium.

7.4 Purification of valuable metals

7.4.1 Niobium purification

1. Removal of zirconium and thorium impurities from niobium-rich precipitates (pH 1 precipitates) by alkali leaching is not effective. Purification of pH 1 precipitates for obtaining saleable niobium may require an ion exchange or solvent extraction process.

7.4.2 NaCl roasting of pH 1.5 precipitates for vanadium recovery

1. NaCl spontaneously reacts with vanadium to form water soluble sodium vanadates at temperatures above 800 °C.

2. Vanadium needs to be oxidised to the V(V) state before or during the purification process for effective recovery. Calcining the pH 1.5 precipitates at 450 °C for 60 minutes is adequate for oxidising the vanadium.

7.4.3 Na_2CO_3 leaching of pH 1.5 precipitates for vanadium recovery

1. Leaching temperature has a significant influence on vanadium recovery. A leaching temperature of 90 °C over a period of 60 minutes is required for a vanadium extraction rate of 65 %.

2. 20 g L^{-1} $NaNO_3$ can adequately oxidise vanadium from V(III) and V(IV) to V(V). Increasing the $NaNO_3$ concentration above 20 g L^{-1} does not have an effect on overall recovery of vanadium.

3. Vanadium purification by the alkali leaching route requires an impurity removal step prior to NH_4VO_3 precipitation. Removal of the impurities

is achieved by reducing pH of the pregnant liquor to 7 - 8, allowing impurities such as aluminium to precipitate leaving vanadium in solution.

7.4.4 Precipitation of near-pure vanadium from $NaVO_3$ solutions

1. The overall vanadium recovery from the salt roasting process is about 30 % higher than the recovery achieved through the alkali leaching route and this can be attributed to (I) the lower leaching efficiency achieved using alkali leaching and (II) the loss of vanadium by co-precipitation during removal of impurities from the loaded Na_2CO_3 solution.

2. Precipitation temperature lower than 30 °C is needed for the best vanadium recoveries from the loaded solutions. Higher temperatures increase the solubility of ammonium vanadate, hence lower the vanadium recovery.

3. Precipitation pH has little influence on overall vanadium recovery in the range 4 - 6.

4. Maximum vanadium recoveries require up to 6 hours of precipitation time at pH 5 and a temperature of 25 °C. Solutions richer in vanadium may require less precipitation times - 2 hours has been reported in literature.

5. Between 0.6 - 0.8 g NH_4 per gram of vanadium is required for maximum vanadium recovery. This value can vary depending on the concentration of vanadium as the solution has to be saturated before any precipitation takes place.

6. V_2O_5 with a purity of 99.5 % can be produced by decomposing the precipitated NH_4VO_3 at 450 °C. Na and Cl are the main impurities in the final V_2O_5 product. The Cl is most likely from residual NH_4Cl, hence can be removed by longer calcination times, while the Na can be removed by thoroughly washing the NH_4VO_3 precipitates with NH_4Cl before calcining.

7.4.5 Purification of scandium from pH 5 precipitates

1. A mixture of Na_2CO_3 and $NaNO_3$ can selectively leach out scandium from the pH 5 precipitates, leaving both iron and aluminium in the residues.

Rare earth elements are the only notable impurities in the scandium rich liquor.

2. Leaching temperature, Na_2CO_3 concentration and $NaNO_3$ concentration significantly affect the scandium extraction rate, although the influence of Na_2CO_3 concentration is not significant above 1 M and that of $NaNO_3$ is not significant above 20 g L^{-1}. Scandium extraction is negligible when there is no $NaNO_3$, suggesting that $NaNO_3$ may be aiding the dissolution by forming soluble carbonate/nitrate complexes.

3. Attempts to precipitate organic scandium salts from the Na_2CO_3 - $NaNO_3$ solutions were not successful.This may be because: (I) Organic scandium salts are usually precipitated from acidic media, the amount of sodium ions present in the alkaline solution may have interfered with formation of the salts or (II) The complexes formed by CO_3^{2-} and NO_3^- are very stable and hence limit formation of scandium salts.

7.5 Dissolution and precipitation of thorium

1. Thorium is quantitatively dissolved in HCl in a similar way niobium and scandium were dissolved. Above 25 °C, HCl concentration has a significant effect on the extraction rate of thorium and temperature has negligible influence.

2. As predicted by Pourbaix diagrams, thorium co-precipitates/adsorbs on hydrated iron and titanium oxides at pH < 1.

3. As much as 30 % thorium can be liberated from the pH 1 precipitates in a Na_2CO_3 - $NaNO_3$ system.

4. When utilising the Na_2CO_3 - $NaNO_3$ system, alkali concentration and leaching temperature have a significant influence on dissolution of thorium while solid-liquid ratio's influence is negligible.

7.6 Kinetics studies

1. The kinetics of vanadium, scandium and niobium dissolution from TiO_2 residues can be described by the random pore model.

2. Dissolution of niobium, vanadium and scandium in HCl is governed by pore diffusion and the activation energies are 16.8 kJ mol^{-1} Nb, 10 kJ mol^{-1} V and 10.4 kJ mol^{-1} Sc respectively.

3. The extraction of vanadium from pH 1.5 precipitates and scandium from pH 5 precipitates in sodium carbonate is governed by both surface chemical reaction and pore diffusion kinetics. The calculated activation energies for dissolution of vanadium and scandium from their respective precipitates are 47 kJ mol^{-1} V and 109 kJ mol^{-1} Sc respectively, which are both in the range of surface reaction controlled kinetics.

4. Dissolution of thorium in HCl is governed by pore diffusion (2.3 $\pm$ 0.1 kJ mol^{-1} Th for the first 15 minutes and 9.2 $\pm$ 0.5 kJ mol^{-1} Th for the second stage).

5. Dissolution of zirconium from pH 1 precipitates is governed by surface reaction kinetics (112 $\pm$10 kJ mol^{-1} Zr).

7.7 Major achievements of the project

1. The filter cake from TiO_2 production was fully characterised by XRD, XRF, AAS, ICP OES and SEM-EDX, allowing a good understanding of its mineralogy. The solution chemistry of the multi-metal system obtained from dissolving the filter cake in acid and alkali was subsequently predicted accurately using Pourbaix diagrams, allowing establishment of a metal recovery route.

2. Developing steps for an integrated process for recovery of vanadium, scandium and niobium from their respective streams is an important contribution not only to the TiO_2 industry, but also to sectors such as the aluminium production industry where waste (red mud) containing vanadium, scandium and niobium is often landfilled. The current market prices of vanadium, niobium and scandium, coupled with incentives for resource recovery available both at national and European level make recovery of the metals from wastes very attractive.

3. From the developed processing steps, opportunities for recovery of lower value metals such as iron, zirconium and titanium have been identified.

4. Thorium was monitored throughout the process development and its fate was established.

5. The developed processing steps did not require the use of the highly toxic hydrofluoric acid, which is conventionally used for niobium extraction.

6. Demonstrating that scandium can be concentrated in pH 5 precipitates and dissolved by a Na_2CO_3 - $NaNO_3$ system is also an important contribution to the research community as the method provides an alternative, more selective process that can potentially allow separation of scandium and rare earth oxides from impurities without the need for a solvent extraction process.

7. It was particularly interesting to discover that scandium, vanadium and the rare earths could dissolve in a Na_2CO_3 - $NaNO_3$ system. It means the three could be directly extracted from residues before employing acid leaching for niobium recovery.

8. The kinetics data presented in chapter 6 can be used for process design, particularly for sizing of chemical reactors and for assessing key features of process dynamics [196], which will subsequently allow a more detailed cost-benefit analysis to be carried out.

7.8 Recommendations for follow-up work

Working on this thesis has uncovered many areas worthy of further investigation. Some of the suggestions are highlighted herein and some preliminary work is presented in the appendix.

7.8.1 Separation and purification of niobium

Niobium was selectively precipitated at pH 1, with titanium, thorium and zirconium being the major impurities. An attempt to remove the impurities by an alkali leach process was not successful and an alternative approach is needed. The separation of niobium from titanium and zirconium is very difficult because their chemical behaviour is very similar owing to their atomic volumes, ionic and covalent radii [197]. Solvent extraction or ion exchange processes consisting of several extraction and stripping stages are typically used for separating the metals form solutions and it is very likely that similar processes will be required

for recovering saleable niobium. Optimised process control schemes should allow for recovery of the niobium as well as titanium, zirconium and thorium, in relatively pure saleable forms. Since the niobium-rich stream is relatively low on impurities, the potential of greener technologies such as ionic liquids and liquid membranes for separation and purification of the niobium could be explored.

7.8.2 Separation and purification of scandium

Scandium, lanthanum, cerium and yttrium are all concentrated in pH 5 precipitates, with iron and aluminium being the only significant impurities. Selective dissolution of scandium and the rare earths from the residues has been achieved using a Na_2CO_3 - $NaNO_3$ system but precipitation of the scandium from the solution could not be achieved. A process for recovering the scandium from the system should be investigated. Attempts to precipitate the scandium as an oxalate led to sodium oxalate precipitating instead, and this may be because of sodium saturation in the system. Removal of such sodium precipitates by filtration and drying the solutions followed by calcination should give a relatively pure rare earth oxide mixture, from which the individual oxides can be recovered by conventional processes such as solvent extraction and ion exchange. Again, use of ionic liquids and membrane technology could be explored as alternative greener approaches.

Leaching of the pH 5 residues with a NaOH solution led to nearly complete removal of aluminium from the residues, further concentrating the rare earths and scandium in the residues. Control of iron precipitation at pH 5 would lead to significant concentration enhancement of the rare earths and scandium. Leaching the residues in HCl followed by precipitation of scandium oxalate should then be possible.

7.8.3 Recovery of unreacted ore

Unreacted ore, SiO_2 and coke are removed from the metal recovery process during the acid leaching stage. The unreacted ore is too fine to feed back into the chlorinator, therefore, to recover the values, an alternative approach needs to be investigated. Preliminary investigations on recovery of the values were done using two approaches:

1. Sulphating the unreacted ore by:

   (a) Roasting the residues with ammonium sulphate followed by water leaching

   (b) Baking the residues with H_2SO_4 followed by water leaching

2. Roasting the residues with Na_2CO_3 followed by water leaching for removal of silica and other impurities.

Carbon dioxide gas was bubbled through the solutions from the sulphating processes and hydrated TiO_2 was precipitated with a purity of over 98 %. The purity of the TiO_2 in the residues formed from the Na_2CO_3 roasting route was over 90 %, the majority of the impurities being residual sodium. The recoveries achieved from such seemingly simple processes are very encouraging and the optimisation of the process parameters are worthy of further investigation.

7.8.4 Recovery of iron

Most of the iron present in solution is precipitated at near-neutral pH, with manganese being the main impurity. A process for purification of the iron and manganese values could be investigated and ferrovanadium and/or ferroniobium could be produced on site from the recovered vanadium and niobium. The removal of residual sodium from the iron rich precipitates should leave a relatively easy to separate and purify iron-manganese residue.

7.8.5 Recovery of reagents

According to preliminary thermodynamic calculations, regeneration of reagents such as the NH_4Cl used for ammonium vanadate precipitation process is possible. The ammonia gas evolved from conversion of ammonium vanadate to V_2O_5 can be reacted with sodium chloride from neutralisation reactions as shown in equation 7.1:

$$2NH_3 + 2NaCl + CO_2 + H_2O \leftrightharpoons 2NH_4Cl + Na_2CO_3 \tag{7.1}$$

The economical feasibility of such a system needs to be investigated.

7.8.6 Early interception

The metal chloride mixture coming out of the gas cyclone of the chloride process (before neutralisation) could be the feed for metal recovery process instead of

using neutralised filter cake. The material coming out of the gas cyclone could be slurried in water to dissolve all metal chlorides, leaving only the unreacted ore, coke and silica in the residues. Due to technical difficulties associated with intercepting the chloride process to recover unneutralised metal chlorides, the feasibility of such a system could not be explored but is certainly worth investigating as:

1. Early interception reduces the wastage of materials - No need for lime used for neutralising the metal chlorides and no need for the HCl used for re-dissolving the metals.

2. Early interception reduces the energy costs associated with filtration of filter cake after the water washing and acid leaching stages- two filtration steps are removed from the process.

7.8.7 Economics analysis

An indepth economics analysis needs to be conducted to determine feasibility of recovery of all metals of interest sustainably. The assessment should simultaneously look into the environmental impact of any proposed processes, particularly the disposal of thorium and sodium-rich effluents.

References

[1] U.S Geological Survey. *Mineral Commodity Summaries*. 2015. URL http://minerals.usgs.gov/minerals/pubs/mcs/2015/mcs2015.pdf.

[2] A D Wilson. *Surface Coatings—2*. Springer Netherlands, 2012. ISBN 9789400913516.

[3] V M Goldschmidt. The principles of distribution of chemical elements in minerals and rocks. *J. Chem. Soc.*, (0):655–673, 1937. doi: 10.1039/JR9370000655.

[4] "OHBA's Laboratory". Crystal structure. URL http://www.geocities.jp/ohba-lab-ob-page/structure6.html.

[5] Brian Mason. The enstatite chondrites. *Geochimica et Cosmochimica Acta*, 30(1):23–39, jan 1966. ISSN 00167037. doi: 10.1016/0016-7037(66)90089-5.

[6] K C Misra. *Introduction to Geochemistry: Principles and Applications*. Wiley, 2012. ISBN 9781444350951.

[7] R G Burns. *Mineralogical Applications of Crystal Field Theory*. Cambridge Studies in New Art History and Criticism. Cambridge University Press, 1993. ISBN 9780521430777.

[8] Pearson education. Crystal-field theory, 2010. URL http://wps.prenhall.com/wps/media/objects/3085/3159106/blb2406.html.

[9] Awan Asadullah, Truong Hong, and Robert. J Lancashire. Crystal Field Theory, 2015. URL http://chemwiki.ucdavis.edu/Inorganic{_}Chemistry/Crystal-Field-Theory/Crystal-Field-Theory.

[10] A Ghosh and H S Ray. *Principles Of Extractive Metallurgy*. Wiley, 1991. ISBN 9788122403220.

[11] W D Jamrack. *Rare metal extraction by chemical engineering techniques*. International series of monographs on chemical engineering. Pergamon Press, 1963.

[12] G. J Brimhall. Preliminary fractionaltion patterns of ore metals through Earth history. *Chemical Geology*, 64(1-2):1–16, 1987. ISSN 00092541. doi: 10.1016/0009-2541(87)90147-1.

[13] Scott Middlemas, Z. Zak Fang, and Peng Fan. A new method for production of titanium dioxide pigment. *Hydrometallurgy*, 131-132:107–113, jan 2013. ISSN 0304386X. doi: 10.1016/j.hydromet.2012.11.002.

[14] J Winkler. *Titanium Dioxide*. European coatings literature. Vincentz Verlag, 2003. ISBN 9783878701484.

[15] R A Gonzalez, C D Musick, and J N Tilton. Process for controlling agglomeration in the manufacture of TiO2, 1996.

[16] J C Deberry, M Robinson, M D Pomponi, A J Beach, Y Xiong, and K Akhtar. Controlled vapor phase oxidation of titanium tetrachloride to manufacture titanium dioxide, 2002.

[17] C K Gupta and N Krishnamurthy. *Extractive Metallurgy of Vanadium*. Process Metallurgy. Elsevier, 1992. ISBN 9780444882523.

[18] A.G. Chmielewski, T.S. Urbański, and W. Migdał. Separation technologies for metals recovery from industrial wastes. *Hydrometallurgy*, 45(3): 333–344, jul 1997. ISSN 0304386X. doi: 10.1016/S0304-386X(96)00090-4.

[19] Shigendo Akita, Tsuyoshi Maeda, and Hiroshi Takeuchi. Recovery of vanadium and nickel in fly ash from heavy oil. *Journal of Chemical Technology & Biotechnology*, 62(4):345–350, 1995. ISSN 1097-4660. doi: 10.1002/jctb.280620406.

[20] R Navarro, J Guzman, I Saucedo, J Revilla, and E Guibal. Vanadium recovery from oil fly ash by leaching, precipitation and solvent extraction processes. *Waste management (New York, N.Y.)*, 27(3):425–38, 2007. ISSN 0956-053X. doi: 10.1016/j.wasman.2006.02.002.

[21] Shang-Lin Tsai and Min-Shing Tsai. A study of the extraction of vanadium and nickel in oil-fired fly ash. *Resources, Conservation and Recycling*, 22(3-4):163–176, 1998. ISSN 09213449. doi: 10.1016/S0921-3449(98)00007-X.

[22] Sandra Vitolo, Maurizia Seggiani, Sara Filippi, and Cristina Brocchini. Recovery of vanadium from heavy oil and Orimulsion fly ashes. *Hydrometallurgy*, 57(2):141–149, sep 2000. ISSN 0304386X. doi: 10.1016/S0304-386X(00)00099-2.

[23] Sandra Vitolo, Maurizia Seggiani, and Francesco Falaschi. Recovery of vanadium from a previously burned heavy oil fly ash. *Hydrometallurgy*, 62(3):145–150, dec 2001. ISSN 0304386X. doi: 10.1016/S0304-386X(01)00193-1.

[24] Maurizia Seggiani, Sandra Vitolo, and Salvatore D'Antone. Recovery of nickel from Orimulsion fly ash by iminodiacetic acid chelating resin. *Hydrometallurgy*, 81(1):9–14, jan 2006. ISSN 0304386X. doi: 10.1016/j.hydromet.2005.09.005.

[25] Oriol Font, Xavier Querol, Roberto Juan, Raquel Casado, Carmen R Ruiz, Angel López-Soler, Pilar Coca, and Francisco García Peña. Recovery of gallium and vanadium from gasification fly ash. *Journal of hazardous*

materials, 139(3):413–23, jan 2007. ISSN 0304-3894. doi: 10.1016/j.jhazmat.2006.02.041.

[26] Jamal Stas, Dahdouh Ajaj, and Omar Al-Chayah. *Recovery of vanadium, nickel and molybdenum from fly ash of heavy oil-fired electrical power station*, volume 51, pages 67 – 70. 2007.

[27] Kuniaki Murase, Ken-ichi Nishikawa, Tetsuya Ozaki, Ken-ichi Machida, Gin-ya Adachi, and Taiichiro Suda. Recovery of vanadium, nickel and magnesium from a fly ash of bitumen-in-water emulsion by chlorination and chemical transport. *Journal of Alloys and Compounds*, 264(1-2): 151–156, jan 1998. ISSN 09258388. doi: 10.1016/S0925-8388(97)00247-8.

[28] Masud A Abdel-latif. Recovery of vanadium and nickel from petroleum flyash. *Minerals Engineering*, 15(11):953–961, nov 2002. ISSN 08926875. doi: 10.1016/S0892-6875(02)00134-6.

[29] C A Pickles and C B Alcock. Production of Ferronickel and Ferrovanadium from Fly Ash in an Extended Arc Flash Reactor. *JOM*, 35(12):40–45, 1983. doi: 10.1007/bf03339187.

[30] R.R Moskalyk and A.M Alfantazi. Processing of vanadium: a review. *Minerals Engineering*, 16(9):793–805, sep 2003. ISSN 08926875. doi: 10.1016/S0892-6875(03)00213-9.

[31] W. H Dresher. *A mechanism study of the formation of sodium vanadate compounds under the conditions of the salt-roast process*. St. Louis, 1961.

[32] E Hukkanen and H Walden. The production of vanadium and steel from titanomagnetites. 15:89–102, 1985.

[33] P Kanta Rao, P.V.R. Bhaskara Sarma, A.K. Tripathy, and P.K. Jena. Extraction of vanadium as high purity vanadium pentoxide from vanadium-bearing titaniferous magnetites. *Transactions – Institute of Mining and Metallurgy Mining, Section C*, 88:187 – 190, 1979.

[34] A Mahdavian, A Shafyei, E Keshavarz Alamdari, and D. F Haghshenas. Recovery of vanadium from Esfahan steel company steel slag; optimizing of roasting and leaching parameters. *International Journal of ISSI*, 3(2): 17 – 21, 2006.

[35] M. Aarabi-Karasgani, F. Rashchi, N. Mostoufi, and E. Vahidi. Leaching of vanadium from LD converter slag using sulfuric acid. *Hydrometallurgy*, 102(1-4):14–21, apr 2010. ISSN 0304386X. doi: 10.1016/j.hydromet.2010.01.006.

[36] S M J Mirazimi, Z Abbasalipour, and F Rashchi. Vanadium removal from LD converter slag using bacteria and fungi. *Journal of environmental management*, 153:144–51, 2015. ISSN 1095-8630. doi: 10.1016/j.jenvman.2015.02.008.

[37] Biao Liu, Hao Du, Shao-Na Wang, Yi Zhang, Shi-Li Zheng, Lan-Jie Li, and Dong-Hui Chen. A novel method to extract vanadium and chromium from vanadium slag using molten NaOH-NaNO 3 binary system. *AIChE Journal*, 59(2):541–552, feb 2013. ISSN 00011541. doi: 10.1002/aic.13819.

[38] A Helge and N Rolf. Process for the production of ferro-vanadium directly from slag obtained from vanadium-containing pig iron, 1971.

[39] T.K. Mukherjee, S.P. Chakraborty, A.C. Bidaye, and C.K. Gupta. Recovery of pure vanadium oxide from bayer sludge. *Minerals Engineering*, 3(3-4):345–353, jan 1990. ISSN 08926875. doi: 10.1016/0892-6875(90)90129-Y.

[40] G. Power, M. Gräfe, and C. Klauber. Bauxite residue issues: I. Current management, disposal and storage practices. *Hydrometallurgy*, 108(1-2):33–45, jun 2011. ISSN 0304386X. doi: 10.1016/j.hydromet.2011.02.006.

[41] C Schmitz. *Handbook of Aluminium Recycling*. Vulkan-Verlag, 2006. ISBN 9783802729362.

[42] S.V. Gladyshev, A. Akcil, R.A. Abdulvaliyev, E.A. Tastanov, K.O. Beisembekova, S.S. Temirova, and H. Deveci. Recovery of vanadium and gallium from solid waste by-products of Bayer process. *Minerals Engineering*, 74:91–98, 2015. ISSN 08926875. doi: 10.1016/j.mineng.2015.01.011.

[43] Mediha Demet Okudan, Ata Akcil, Aysenur Tuncuk, and Haci Deveci. Effect of parameters on vanadium recovery from by-products of the Bayer process. *Hydrometallurgy*, 152:76–83, 2015. ISSN 0304386X. doi: 10.1016/j.hydromet.2014.12.003.

[44] R.A. Abdulvaliyev, A. Akcil, S.V. Gladyshev, E.A. Tastanov, K.O. Beisembekova, N.K. Akhmadiyeva, and H. Deveci. Gallium and vanadium extraction from red mud of Turkish alumina refinery plant: Hydrogarnet process. *Hydrometallurgy*, 157:72–77, oct 2015. ISSN 0304386X. doi: 10.1016/j.hydromet.2015.07.007.

[45] R Navarro, J Guzman, I Saucedo, J Revilla, and E Guibal. Vanadium recovery from oil fly ash by leaching, precipitation and solvent extraction processes. *Waste management (New York, N.Y.)*, 27(3):425–38, jan 2007. ISSN 0956-053X. doi: 10.1016/j.wasman.2006.02.002.

[46] G Z Nasyrov and I V Ravdonikas. Method of preparing vanadium pentoxide, 1977.

[47] Karl. B Thews. Process of recovering vanadium, 1922.

[48] Rajeev, J. Pradhan, S. N. Das, and R. S. Thakur. Vanadium sludge : An useful byproduct of alumina plant. *Journal of scientific & industrial research*, 58(12):948–953, 1999. ISSN 0022-4456.

[49] D J Crouse, K B Brown, Oak Ridge National Laboratory. Chemical Technology Division. Chemical Development Section C., Union Carbide

Corporation, and U S Atomic Energy Commission. *Solvent extraction recovery of vanadium (and uranium) from acid liquors with di(2-ethylhexyl) phosphoric acid*. Oak Ridge National Laboratory, 1959.

[50] Minting Li, Chang Wei, Shuang Qiu, Xuejiao Zhou, Cunxiong Li, and Zhigan Deng. Kinetics of vanadium dissolution from black shale in pressure acid leaching. *Hydrometallurgy*, 104(2):193–200, sep 2010. ISSN 0304386X. doi: 10.1016/j.hydromet.2010.06.001.

[51] Zhi-gan Deng, Chang Wei, Gang Fan, Min-ting Li, Cun-xiong Li, and Xing-bin Li. Extracting vanadium from stone-coal by oxygen pressure acid leaching and solvent extraction. *Transactions of Nonferrous Metals Society of China*, 20(50874053):s118–s122, may 2010. ISSN 10036326. doi: 10.1016/S1003-6326(10)60024-6.

[52] Xingbin Li, Chang Wei, Zhigan Deng, Minting Li, Cunxiong Li, and Gang Fan. Selective solvent extraction of vanadium over iron from a stone coal/black shale acid leach solution by D2EHPA/TBP. *Hydrometallurgy*, 105(3-4):359–363, jan 2011. ISSN 0304386X. doi: 10.1016/j.hydromet.2010.10.006.

[53] D Schrötterová, P Nekovář, and T Dropa. Extraction of polyvanadates by means of amines. *Journal of Radioanalytical and Nuclear Chemistry Articles*, 183(1):73–84, 1994. doi: 10.1007/BF02043118.

[54] P Nekovář and D Schrötterová. Extraction of V(V), Mo(VI) and W(VI) polynuclear species by primene JMT. *Chemical Engineering Journal*, 79(3):229–233, oct 2000. ISSN 13858947. doi: 10.1016/S1385-8947(00)00207-2.

[55] E. M Ho, J Kyle, S Lallenec, D. M Muir, and A. J Parker. Recovery of vanadium from spent catalysts and alumina residues. *Hydrometallurgy '94*, pages 1105 – 1121, 1994.

[56] I A E Wilkomirsky, A Luraschi, and A Reghezza. Vanadium extraction process from basic steel refining slags. *Extraction Metallurgy*, pages 531–549, 1985.

[57] Donald C. Zipperian and Srini Raghavan. The recovery of vanadium from dilute acid sulfate solutions by resin ion exchange. *Hydrometallurgy*, 13(3):265–281, mar 1985. ISSN 0304386X. doi: 10.1016/0304-386X(85)90016-7.

[58] T. Soldi, M. Pesavento, and G. Alberti. Separation of vanadium(V) and -(IV) by sorption on an iminodiacetic chelating resin. *Analytica Chimica Acta*, 323(1-3):27–37, apr 1996. ISSN 00032670. doi: 10.1016/0003-2670(95)00612-5.

[59] Li Zeng, Qinggang Li, and Liansheng Xiao. Extraction of vanadium from the leach solution of stone coal using ion exchange resin. *Hydrometallurgy*, 97(3-4):194–197, jul 2009. ISSN 0304386X. doi: 10.1016/j.hydromet.2009.03.005.

[60] C Namasivayam and D Sangeetha. Removal and recovery of vanadium(V) by adsorption onto ZnCl2 activated carbon: Kinetics and isotherms. *Adsorption*, 12(2):103–117, 2006. doi: 10.1007/s10450-006-0373-3.

[61] Wayne. C Hazen. Method of recovery of vanadium from its ores, 1968.

[62] Xue-Pin Liao, Wei Tang, Rong-Qing Zhou, and Bi Shi. Adsorption of metal anions of vanadium(V) and chromium(VI) on Zr(IV)-impregnated collagen fiber. *Adsorption*, 14(1):55–64, 2007. doi: 10.1007/s10450-007-9045-1.

[63] K Kadirvelu. Removal of heavy metals from industrial wastewaters by adsorption onto activated carbon prepared from an agricultural solid waste. *Bioresource Technology*, 76(1):63–65, 2001. ISSN 09608524. doi: 10.1016/S0960-8524(00)00072-9.

[64] M Kobya, E Demirbas, E Senturk, and M Ince. Adsorption of heavy metal ions from aqueous solutions by activated carbon prepared from apricot stone. *Bioresource technology*, 96(13):1518–21, sep 2005. ISSN 0960-8524. doi: 10.1016/j.biortech.2004.12.005.

[65] M.O. Corapcioglu and C.P. Huang. The adsorption of heavy metals onto hydrous activated carbon. *Water Research*, 21(9):1031–1044, 1987. ISSN 00431354. doi: 10.1016/0043-1354(87)90024-8.

[66] Dinesh Mohan and Kunwar P. Singh. Single- and multi-component adsorption of cadmium and zinc using activated carbon derived from bagasse—an agricultural waste. *Water Research*, 36(9):2304–2318, may 2002. ISSN 00431354. doi: 10.1016/S0043-1354(01)00447-X.

[67] Caroline L. Peacock and David M. Sherman. Vanadium(V) adsorption onto goethite (α-FeOOH) at pH 1.5 to 12: a surface complexation model based on ab initio molecular geometries and EXAFS spectroscopy. *Geochimica et Cosmochimica Acta*, 68(8):1723–1733, apr 2004. ISSN 00167037. doi: 10.1016/j.gca.2003.10.018.

[68] A V Barker and D J Pilbeam. *Handbook of Plant Nutrition*. Books in soils, plants, and the environment. CRC Press, 2006. ISBN 9781420014877.

[69] M. Ochsenkühn, Th. Lyberopulu, and G. Parissakis. Direct determination of landthanides, yttrium and scandium in bauxites and red mud from alumina production. *Analytica Chimica Acta*, 296(3):305–313, oct 1994. ISSN 00032670. doi: 10.1016/0003-2670(94)80250-5.

[70] Weiwei Wang, Yoko Pranolo, and Chu Yong Cheng. Recovery of scandium from synthetic red mud leach solutions by solvent extraction with D2EHPA. *Separation and Purification Technology*, 108:96–102, 2013. ISSN 13835866. doi: 10.1016/j.seppur.2013.02.001.

[71] M. Ochsenkühn, Th. Lyberopulu, and G. Parissakis. Selective separation and determination of scandium from yttrium and lanthanides in red mud by a combined ion exchange/solvent extraction method. *Analytica Chimica Acta*, 315(1-2):231–237, oct 1995. ISSN 00032670. doi: 10.1016/0003-2670(95)00309-N.

[72] L Piga, F Pochetti, and L Stoppa. Recovering metals from red mud generated during alumina production. *JOM*, 45(11):54–59, 1993. doi: 10.1007/BF03222490.

[73] D.I. Smirnov and T.V. Molchanova. The investigation of sulphuric acid sorption recovery of scandium and uranium from the red mud of alumina production. *Hydrometallurgy*, 45(3):249–259, jul 1997. ISSN 0304386X. doi: 10.1016/S0304-386X(96)00070-9.

[74] M. Ochsenkühn, Th. Lyberopulu, K.M. Ochsenkühn, and G. Parissakis. Recovery of lanthanides and yttrium from red mud by selective leaching. *Analytica Chimica Acta*, 319(1-2):249–254, jan 1996. ISSN 00032670. doi: 10.1016/0003-2670(95)00486-6.

[75] H Zhou, D Li, Y Tian, and Y Chen. Extraction of scandium from red mud by modified activated carbon and kinetics study. *Rare Metals*, 27(3): 223–227, jun 2008. ISSN 10010521. doi: 10.1016/S1001-0521(08)60119-9.

[76] L Erdey, R Belcher, and L Gordon. *Gravimetric Analysis: International Series of Monographs on Analytical Chemistry*. Number v. 7. Elsevier Science, 2013. ISBN 9781483222677.

[77] C. Liao, G. Xu, J. Jia, Y. Zhang, S. Wu, and C Yan. Recovery and application of scandium-A strategic resource of new century. *J. Chin. Rare Earth Soc.*, 19(4):289 – 297, 2001.

[78] Deqian Li, Yong Zuo, and Shulan Meng. Separation of thorium(IV) and extracting rare earths from sulfuric and phosphoric acid solutions by solvent extraction method. *Journal of Alloys and Compounds*, 374(1-2): 431–433, jul 2004. ISSN 09258388. doi: 10.1016/j.jallcom.2003.11.055.

[79] Weiwei Wang, Yoko Pranolo, and Chu Yong Cheng. Metallurgical processes for scandium recovery from various resources: A review. *Hydrometallurgy*, 108(1-2):100–108, jun 2011. ISSN 0304386X. doi: 10.1016/j.hydromet.2011.03.001.

[80] L.D. Lash and J.R. Ross. Vitro chemical recovers costly scandium from uranium solutions. *Min. Eng.*, 13:966–969, 1961.

[81] J R Ross and J B Rosenbaum. *Reconnaissance of Scandium Sources and Recovery of Scandium from Uranium Mill Solutions*. Report of investigations / Bureau of Mines. U.S. Department of the Interior, Bureau of Mines, 1962.

[82] W J Rourke. Recovery of scandium and uranium, 1990.

[83] R J Feuling. Recovery of scandium, yttrium and lanthanides from titanium ore, 1991.

[84] Mineral Sands Industry. The mineral sands industry fact book. Technical report, 2014. URL http://www.zircon-association.org/Websites/zircon/images/The{_}Mineral{_}Sands{_}Industry{_}Factbook.pdf.

[85] Xu Shaoquan and Li Suqing. Review of the extractive metallurgy of scandium in China (1978–1991). *Hydrometallurgy*, 42(3):337–343, oct 1996. ISSN 0304386X. doi: 10.1016/0304-386X(95)00086-V.

[86] D Li and C Wang. Solvent extraction of Scandium(III) by Cyanex 923 and Cyanex 925. *Hydrometallurgy*, 48(3):301–312, 1998.

[87] Y.W. Gokhale and T.R. Bhat. Determination of scandium in wolframite and in the residues obtained after the extraction of tungsten. *Talanta*, 14(3):435–437, mar 1967. ISSN 00399140. doi: 10.1016/0039-9140(67)80020-1.

[88] C T Horovitz. *Scandium Its Occurrence, Chemistry Physics, Metallurgy, Biology and Technology*. Elsevier Science, 2012. ISBN 9780323144513.

[89] C D Vanderpool, J A Ladd, M B MacInnis, and M A Fedorchak. Recovery of tungsten, scandium, iron, and manganese from tungsten bearing material, 1989. URL http://www.google.co.uk/patents/US4808384.

[90] R C Vickery. The extraction and purification of scandium. *J. Chem. Soc.*, (0):245–251, 1955. doi: 10.1039/JR9550000245.

[91] Guo Gongyi, Chen Yuli, and Li Yu. Solvent Extraction off Scandium from Wolframite Residue. *JOM*, 40(7):28–31, 1988. doi: 10.1007/bf03258146.

[92] M. L. Navtanovich, A. S Chernyak, and Yu. E. Sutyrin. The Selective Extraction of Scandium With Alkyl Hydrogen Phosphates. *J. Appl. Chem. of the U.S.S.R. (English transl. of Zhurnal Prikladnoi Khimii [Journal of Applied Chemistry])*, 38(2):341–344, 1965.

[93] Yoshito Wakui, Hideyuki Matsunaga, and Toshishige M Suzuki. Selective recovery of trace scandium from acid aqueous solution with (2-ethylhexyl hydrogen 2-ethylhexylphosphonate)-impregnated resin. *Analytical Sciences*, 5(2):189–193, 1989. doi: 10.2116/analsci.5.189.

[94] Xue-ming Zhong, Zhou Tong, Xing-hua Tong, and Rui-yuan Cui. Technology of extracting scandium oxide by primary amine. *Chinese Journal of Rare Metals*, 6:527 – 529, 2002.

[95] A H W Kimura, K H W Murai, and H H W Yakushiji. Process for recovering scandium from nickel-containing oxide ore, 1997.

[96] D.D Harbuck and G.R Palmer. Scandium recovery from a tantalum waste residue. Technical report, The Metallurgical Society Inc., 1992.

[97] V.I. Kuzmin, V.G. Lomayev, and G.L. Pashkov. Processing of the ores weathered carbonatite crusts is the future of the rare metal industry of Russia. *Non-Ferrous Metals (Russ.)*, 12:62–68, 2006.

[98] C J Hartley, W W HAZEN, D R Baughman, C M A Bemelmans, P F Belits, T J Lanyk, B F Porter, L Liao, J Mcallister, and M S Y Yang. Methods of recovering scandium from titanium residue streams, 2014.

[99] A. Ditze and K. Kongolo. Recovery of scandium from magnesium, aluminium and iron scrap. *Hydrometallurgy*, 44(1-2):179–184, jan 1997. ISSN 0304386X. doi: 10.1016/S0304-386X(96)00041-2.

[100] P C Stevenson and W E Nervik. *The Radiochemistry of the Rare Earths: Scandium, Yttrium, and Actinium*. Number no. 3020 in National Academy of Sciences-National Research Council. Subcommittee on Radiochemistry, National Academy of Sciences, National Research Council, 1961.

[101] Feng Xie, Ting An Zhang, David Dreisinger, and Fiona Doyle. A critical review on solvent extraction of rare earths from aqueous solutions. *Minerals Engineering*, 56:10–28, feb 2014. ISSN 08926875. doi: 10.1016/j.mineng.2013.10.021.

[102] Dongbei Wu, Chunji Niu, Deqian Li, and Yan Bai. Solvent extraction of scandium(III), yttrium(III), lanthanum(III) and gadolinium(III) using Cyanex 302 in heptane from hydrochloric acid solutions. *Journal of Alloys and Compounds*, 374(1-2):442–446, jul 2004. ISSN 09258388. doi: 10.1016/j.jallcom.2003.11.058.

[103] C Wang and D Li. *Extraction mechanism of Sc(III) and separation from Th(IV), Fe(III) and Lu(III) with BIS(2,4,4-trimethylpentyl)phosphinic acid in n-hexane from sulphuric acid solutions*, volume 12. 1994.

[104] C Wang and D Li. *Solvent extraction of Sc(III), Zr(IV), Th(IV), Fe(III), and Lu(III) with thiosubstituted organophosphinic acid extractants*, volume 13. 1995.

[105] M Aguilar and J L Cortina. *Solvent Extraction and Liquid Membranes: Fundamentals and Applications in New Materials*. Ion exchange and solvent extraction. CRC Press, 2008. ISBN 9781420014112. URL https://books.google.co.uk/books?id=SuidWh6pKtEC.

[106] W J Rourke, W C Lai, and S Natansohn. Ion exchange method for the recovery of scandium, 1989.

[107] W J Rourke, W C Lai, and S Natansohn. Ion exchange method for separation of scandium and thorium, 1988.

[108] L A Herchenroeder and H R Burkholder. Ion exchange purification of scandium, 1990.

[109] F Habashi. *Handbook of extractive metallurgy: Primary metals; secondary metals; light metals*. Number v. 2. VCH, 1997. ISBN 9783527287925.

[110] British Geological Survey. Niobium - tantalum. Technical report, Natural Environment Research Council, Nottingham, 2011.

[111] I Gaballah, E Allain, and M Djona. Extraction of tantalum and niobium from tin slags by chlorination and carbochlorination. *Metall and Materi Trans B*, 28(3):359–369, 1997. doi: 10.1007/s11663-997-0102-7.

[112] C K Gupta and A K Suri. *Extractive Metallurgy of Niobium*. Taylor & Francis, 1993. ISBN 9780849360718.

[113] R Chidambaram and S Banerjee. *Materials Research: Current Scenario and Future Projections*. Allied Publishers, 2003. ISBN 9788177644500.

[114] Eduardo A. Brocchi and Francisco J. Moura. Chlorination methods applied to recover refractory metals from tin slags. *Minerals Engineering*, 21(2):150–156, jan 2008. ISSN 08926875. doi: 10.1016/j.mineng.2007.08.011.

[115] Richard Shaw, Kathryn Goodenough, Gus Gunn, Teresa Brown, and Debbie Rayner. Niobium–tantalum. Technical Report April, British Geological Survey, 2011.

[116] R E Kirk, J I Kroschwitz, D F Othmer, and M Howe-Grant. *Encyclopedia of chemical technology*. Number v. 17; v. 31 in Encyclopedia of Chemical Technology. J. Wiley, 1996. ISBN 9780471526865.

[117] NIIR Board of Consultants & Engineers. *The Complete Book on Glass and Ceramics Technology*. Asian Pacific Business Press, 2005. ISBN 9788178330334.

[118] Ernest. L Koerner and Morton Smutz. Separation of niobium and tantalum - a literature survey. Technical report, Ames Laboratory, 1956.

[119] F Cardarelli. *Materials Handbook: A Concise Desktop Reference*. Springer London, 2013. ISBN 9781447136484.

[120] C Subramanian and A.K Suri. Recovery of niobium and tantalum from low grade tin slag - A hydrometallurgical approach. *Environmental and waste management*, 831(07):100 – 107, 1998.

[121] S Gireesh, V Vinod, S Nair, and G Ninan. Recovery of Niobium and Zirconium from the Cyclone Discharge of Chlorination Plant Producing Titanium Tetrachloride. *Oriental Journal of Chemistry*, 30(1), 2014.

[122] Terence Makanyire, Animesh Jha, and Stephen Sutcliffe. A kinetics analysis of acid leaching of niobium and zirconium from titania waste residue stream - An energy efficient methodology for the reclamation of metal values. In *The Minerals, Metals and Materials Society*, pages 115 – 122. John Wiley & Sons, 2015.

[123] F Habashi. Niobium. In *Handbook of Extractive Metallurgy*, chapter 28, pages 1403–1416. WILEY-VCH, 1997.

[124] Hongming Zhou, Shili Zheng, and Yi Zhang. Leaching of a low-grade niobium–tantalum ore by highly concentrated caustic potash solution. *Hydrometallurgy*, 80(1-2):83–89, nov 2005. ISSN 0304386X. doi: 10.1016/j.hydromet.2005.07.006. URL http://linkinghub.elsevier.com/retrieve/pii/S0304386X05001726.

[125] Zhaowu Zhu and Chu Yong Cheng. Solvent extraction technology for the separation and purification of niobium and tantalum: A review. *Hydrometallurgy*, 107(1-2):1–12, apr 2011. ISSN 0304386X. doi: 10.1016/j.hydromet.2010.12.015.

[126] V.G Mayorov and A.L Nikolaev. Tantalum (V) and niobium (V) extraction by octanol. *Hydrometallurgy*, 66(1-3):77–83, oct 2002. ISSN 0304386X. doi: 10.1016/S0304-386X(02)00091-9.

[127] P D Bowerman. Metals recovery from hydrochloric acid solutions, 1976.

[128] T Pierau and O Gnotke. Separating high-valent metal ions from iron(II) chloride containing acidic solution, comprises adding aqueous solution of a phosphate compound or phosphoric acid into iron(II) chloride solution, and precipitating metal ions as phosphates, 2013. URL https://www.google.com.ar/patents/DE102011106750A1?cl=en.

[129] S. K. Bhatia and D. D. Perlmutter. A random pore model for fluid-solid reactions: II. Diffusion and transport effects. *AIChE Journal*, 27(2): 247–254, mar 1981. ISSN 0001-1541. doi: 10.1002/aic.690270211.

[130] S Svanberg. *Atomic and Molecular Spectroscopy: Basic Aspects and Practical Applications*. Advanced Texts in Physics. Springer Berlin Heidelberg, 2003. ISBN 9783540203827.

[131] R A Scott and C M Lukehart. *Applications of Physical Methods to Inorganic and Bioinorganic Chemistry*. EIC Books. Wiley, 2007. ISBN 9780470032176.

[132] D A Skoog, F James Holler, and S R Crouch. *Principles of Instrumental Analysis*. International student edition. Thomson Brooks/Cole, 2007. ISBN 9780495012016.

[133] J Cazes. *Analytical Instrumentation Handbook, Third Edition*. CRC Press, 2004. ISBN 9780849390395.

[134] C R Brundle, C A Evans, and S Wilson. *Encyclopedia of Materials Characterization: Surfaces, Interfaces, Thin Films*. Characterization Series. Butterworth-Heinemann, 1992. ISBN 9780750691680.

[135] T G Rochow and P A Tucker. *Introduction to Microscopy by Means of Light, Electrons, X Rays, or Acoustics*. Language of science. Springer US, 2013. ISBN 9781489915139.

[136] S Zhang. *Electric-Field Control of Magnetization and Electronic Transport in Ferromagnetic/Ferroelectric Heterostructures*. Springer Theses. Springer Berlin Heidelberg, 2014. ISBN 9783642548390.

[137] Andrew. R Barron. *Physical methods in chemistry and nanoscience*. 2015.

[138] W H Bragg and W L Bragg. The Reflection of X-rays by Crystals. *Proceedings of the Royal Society of London A: Mathematical, Physical and Engineering Sciences*, 88(605):428–438, 1913. ISSN 0950-1207. doi: 10.1098/rspa.1913.0040.

[139] Surfgroup.be. SEM EDX | SURF, 2015. URL http://www.surfgroup.be/semedx.

[140] J A Seigel and K Mirakovits. *Forensic Science: The Basics, Second Edition*. CRC Press, 2013. ISBN 9781439895054.

[141] M L Minges and A.S.M.I.H. Committee. *Electronic Materials Handbook: Packaging*. Electronic Materials Handbook. Taylor & Francis, 1989. ISBN 9780871702852.

[142] P C Hayes and P M J Gray. *Process Selection in Extractive Metallurgy*. Hayes Publishing Company, 1985. ISBN 9780958919715.

[143] A K SenGupta. *Environmental Separation of Heavy Metals: Engineering Processes*. Taylor & Francis, 2001. ISBN 9781566768849.

[144] Adegoke H, F Adekola, O Fatoki, and B Ximba. Sorptive interaction of oxyanions with iron oxides: A review. *Polish Journal of Environmental Studies*, 22(1):7 – 24, 2013.

[145] Paul C Aebersold. The Radiochemistry of vanadium. *Nuclear Sciences Series*, 1960.

[146] James Lawton Brownlee. *The Radiochemistry of Vanadium*. Number no. 3022 in National Acad. of Sciences. National Research Council. Nuclear Science Series. Subcommittee on Radiochemistry, National Academy of Sciences-National Research Council, available from the Office of Technical Services, Department of Commerce, 1960.

[147] C Chen. *Synthesis and Characterization of New Cathode Materials for Lithium Ion Batteries*. State University of New York at Binghamton, 2008. ISBN 9781109034776.

[148] C F Baes and R E Mesmer. *The hydrolysis of cations*. Wiley, 1976.

[149] Anubhav Jain, Shyue Ping Ong, Geoffroy Hautier, Wei Chen, William Davidson Richards, Stephen Dacek, Shreyas Cholia, Dan Gunter, David Skinner, Gerbrand Ceder, and Kristin A. Persson. Commentary: The Materials Project: A materials genome approach to accelerating materials innovation. *APL Materials*, 1(1):011002, 2013. ISSN 2166532X. doi: 10.1063/1.4812323.

[150] Ulla-Maija Levanto. *On the precipitation of ammonium polyvanadate*. The Finnish academy of technical sciences (Helsinki), 1969.

[151] B Sahoo, N Charan, Samantaray Asutosh, and P Kumar. *Inorganic Chemistry*. PHI Learning, 2012. ISBN 9788120343085.

[152] M.Th. Ochsenkühn, K S Hatzilyberis, L N Mendrinos, and C E Salmas. Pilot-plant investigation of the leaching process for the recovery of scandium from red mud. *Industrial and Engineering Chemistry Research*, 41 (23):5794–5801, 2002.

[153] Edouard Asselin, Tawfik M. Ahmed, and Akram Alfantazi. Corrosion of niobium in sulphuric and hydrochloric acid solutions at 75 and 95°C. *Corrosion Science*, 49(2):694–710, feb 2007. ISSN 0010938X. doi: 10.1016/j.corsci.2006.05.028.

[154] E P Steinberg. *The Radiochemistry of Niobium and Tantalum*. Number no. 3039 in National Academy of Sciences-National Research Council. Subcommittee on Radiochemistry, National Academy of Sciences-National Research Council; available from the Office of Technical Services, Department of Commerce, 1961.

[155] A J Bard, R Parsons, and J Jordan. *Standard Potentials in Aqueous Solution*. Monographs in Electroanalytical Chemistry and Electrochemistr. Taylor & Francis, 1985. ISBN 9780824772918.

[156] Earl K Hyde. *The Radiochemistry of Thorium*. Number no. 3004 in National Academy of Sciences-National Research Council. Subcommittee on Radiochemistry, National Academy of Sciences–National Research Council; available from the Office of Technical Services, Department of Commerce, 1960.

[157] M Altmaier, Volker Neck, Melissa A Denecke, R Yin, and Thomas Fanghnel. Solubility of ThO2xH2O(am) and the formation of ternary Th(IV) hydroxide-carbonate complexes in NaHCO3-Na2CO3 solutions containing 0-4 M NaCl. *Radiochimica Acta*, 94(9-11), 2006. doi: 10.1524/ract.2006.94.9-11.495.

[158] Aly M Abdel-Rehim. An innovative method for processing Egyptian monazite. *Hydrometallurgy*, 67(1-3):9–17, dec 2002. ISSN 0304386X. doi: 10.1016/S0304-386X(02)00134-2.

[159] R G Compton, C H Bamford, and C F H Tipper†. *The Theory of Kinetics*. Comprehensive Chemical Kinetics. Elsevier Science, 2012. ISBN 9780444600707. URL https://books.google.co.uk/books?id=KeetJpeb6vkC.

[160] J S Sanghera and J Williamson. TiO2-Nb2O5 solid solutions. *Journal of Materials Science Letters*, 6(4):449 – 450, 1987.

[161] L. Vegard. Die Konstitution der Mischkristalle und die Raumfüllung der Atome. *Zeitschrift für Physik*, 5(1):17 – 26, 1921.

[162] D M Roundhill and J P Fackler. *Optoelectronic Properties of Inorganic Compounds*. Modern Inorganic Chemistry. Springer, 1999. ISBN 9780306455575. URL https://books.google.co.uk/books?id=WCg5pOI39DkC.

[163] Liana Alvares Rodrigues and Maria Lúcia Caetano Pinto da Silva. Thermodynamic and kinetic investigations of phosphate adsorption onto hydrous niobium oxide prepared by homogeneous solution method. *Desalination*, 263(1-3):29–35, nov 2010. ISSN 00119164. doi: 10.1016/j.desal.2010.06.030.

[164] Z Marczenko and E Kloczko. *Separation, Preconcentration and Spectrophotometry in Inorganic Analysis*. Analytical Spectroscopy Library. Elsevier Science, 2000. ISBN 9780080541082.

[165] G.L.J.P. da Silva, M.L.C.P. da Silva, and Tatiana Caetano. Preparation and Characterization of Hydrous Zirconium Oxide Formed by Homogeneous Precipitation. *Materials Research*, 5(2):149–153, jun 2002. ISSN 1516-1439. doi: 10.1590/S1516-14392002000200011.

[166] Anna Szymczycha-Madeja. Kinetics of Mo, Ni, V and Al leaching from a spent hydrodesulphurization catalyst in a solution containing oxalic acid and hydrogen peroxide. *Journal of hazardous materials*, 186(2-3):2157–2161, feb 2011. ISSN 1873-3336 (Electronic). doi: 10.1016/j.jhazmat.2010.11.120.

[167] G Pfaff. *Special Effect Pigments: Technical Basics and Applications*. American coatings literature. Vincentz Network, 2008. ISBN 9783866309050.

[168] J Marsden and I House. *The Chemistry of Gold Extraction*. Society for Mining, Metallurgy, and Exploration, 2006. ISBN 9780873352406.

[169] A J Monhemius and P M Swash. Removing and stabilizing as from copper refining circuits by hydrothermal processing. *Journal of Materials*, 51(9):30 – 33, 1999.

[170] Evan J Jamieson. *Precipitation and characteristics of iron (III) oxyhydroxides from acid liquors*. PhD thesis, Murdoch University, 1995. URL http://researchrepository.murdoch.edu.au/id/eprint/111.

[171] J.O Claassen, E.H.O Meyer, J Rennie, and R.F Sandenbergh. Iron precipitation from zinc-rich solutions: defining the Zincor Process. *Hydrometallurgy*, 67(1-3):87–108, dec 2002. ISSN 0304386X. doi: 10.1016/S0304-386X(02)00141-X.

[172] American Geological Institute. *Geokhimiya Translations*. AGI Translations Office, 1968. ISBN 9780913312117.

[173] Xiao-Jin Yang, Zhong-Mao Gu, and De-Xi Wang. Extraction and separation of scandium from rare earths by electrostatic pseudo liquid membrane. *Journal of Membrane Science*, 106(1-2):131–145, oct 1995. ISSN 03767388. doi: 10.1016/0376-7388(95)00083-O.

[174] A K Karamalidis and D A Dzombak. *Surface Complexation Modeling: Gibbsite*. Wiley, 2011. ISBN 9781118063101.

[175] M Singh. *Vaccine Adjuvants and Delivery Systems*. Wiley, 2007. ISBN 9780470134924.

[176] S Seetharaman. *Treatise on Process Metallurgy, Volume 3: Industrial Processes*. Number v. 3 in Treatise on Process Metallurgy. Elsevier Science, 2013. ISBN 9780080969893.

[177] R C Vickery. Scandium oxalate and its ammine complexes. *J. Chem. Soc.*, (0):255–258, 1955. doi: 10.1039/JR9550000255.

[178] R W Boyle. *Geochemical Prospecting for Thorium and Uranium Deposits*. Developments in Economic Geology. Elsevier Science, 2013. ISBN 9780444597632.

[179] J M Kokosa, A Przyjazny, and M Jeannot. *Solvent Microextraction: Theory and Practice*. Wiley, 1st edition, 2009. ISBN 9780470278598.

[180] J Willebrand and D L T Anderson. *Modelling Oceanic Climate Interactions*. Nato ASI Subseries I:. Springer Berlin Heidelberg, 2013. ISBN 9783642849756.

[181] W E Harris and B Kratochvil. *Chemical Separations and Measurements: Background and Procedures for Modern Analysis*. Chemical separations and measurements. Saunders, 1974. ISBN 9780721645353.

[182] K N Han. *Fundamentals of Aqueous Metallurgy*. Society for Mining, Metallurgy, and Exploration, 2002. ISBN 9780873352154.

[183] A C Lasaga. *Kinetic Theory in the Earth Sciences*. Princeton Legacy Library. Princeton University Press, 2014. ISBN 9781400864874.

[184] S Ayanda, Olushola, A Adekola, Folahan, and S Fatoki, Olalekan. Dissolution Kinetics of Columbite in Nitric Acid. *Asian Journal of Chemistry*, 24(3):1087 – 1090, 2012.

[185] S Ayanda, Olushola and A Adekola, Folahan. Leaching of A Nigerian Columbite in Hydrochloric Acid: Dissolution Kinetics. *International Journal of Metallurgical Engineering*, 1(3):35 – 39, 2012.

[186] Shuang Qiu, Chang Wei, Minting Li, Xuejiao Zhou, Chunxiong Li, and Zhigan Deng. Dissolution kinetics of vanadium trioxide at high pressure in sodium hydroxide–oxygen systems. *Hydrometallurgy*, 105(3-4):350–354, jan 2011. ISSN 0304386X. doi: 10.1016/j.hydromet.2010.08.005.

[187] Minting Li, Chang Wei, Shuang Qiu, Xuejiao Zhou, Cunxiong Li, and Zhigan Deng. Kinetics of vanadium dissolution from black shale in pressure acid leaching. *Hydrometallurgy*, 104(2):193–200, sep 2010. ISSN 0304386X. doi: 10.1016/j.hydromet.2010.06.001.

[188] Maria Skyllas-Kazacos and Yuni Limantari. Kinetics of the Chemical Dissolution of Vanadium Pentoxide in Acidic Bromide Solutions. *Journal of Applied Electrochemistry*, 34(7):681 – 685, 2004.

[189] Xuejiao Zhou, Chang Wei, Wentang Xia, Minting Li, Cunxiong Li, Zhigan Deng, and Hongsheng Xu. Dissolution kinetics and thermodynamic analysis of vanadium trioxide during pressure oxidation. *Rare Metals*, 31 (3):296 – 302, 2012.

[190] D.P.T. Blackmore, J. Ellis, and P.J. Riley. Treatment of a vanadium-containing effluent by adsorption/coprecipitation with iron oxyhydroxide. *Water Research*, 30(10):2512–2516, oct 1996. ISSN 00431354. doi: 10.1016/0043-1354(96)00080-2.

[191] Philippe Poizot, Stéphane Laruelle, Marcel Touboul, and Jean-Marie Tarascon. Wet-chemical synthesis of various iron(III) vanadates(V) by co-precipitation route. *Comptes Rendus Chimie*, 6(1):125–134, jan 2003. ISSN 16310748. doi: 10.1016/S1631-0748(03)00015-8.

[192] A Naeem, P Westerhoff, and S Mustafa. Vanadium removal by metal (hydr)oxide adsorbents. *Water research*, 41(7):1596–602, apr 2007. ISSN 0043-1354. doi: 10.1016/j.watres.2007.01.002.

[193] Laila Guirguis, Maha Sharaf, Abu Rehab Mahmoud, and Magdy Zahran. Leaching Kinetics and Recovery of Vanadium from Egyptian Boiler Ash Under Alkaline Oxidizing Conditions. In *4th International Conference on Radiation Sciences and Applications.*, pages 67 – 73, Taba, 2014. The Egyptian Society of Radiation Science and Applications. URL http://www.esrsaeg.net/proceeding/8.pdf.

[194] Hui-bin Liu, Hao Du, Da-wei Wang, Shao-na Wang, Shi-li Zheng, and Yi Zhang. Kinetics analysis of decomposition of vanadium slag by KOH sub-molten salt method. *Transactions of Nonferrous Metals Society of China*, 23(5):1489–1500, may 2013. ISSN 10036326. doi: 10.1016/S1003-6326(13)62621-7.

[195] V I Cherkashin, V P Doroshenko, I A Goncharov, and G V Denisova. On vanadium oxide dissolution in sodium carbonate solutions. *Izv. Vyssh. Uchebn. Zaved., Tsvetn. Metall; (no.3)*, 15(4):54 – 55, 1983.

[196] A C Dimian and C S Bildea. *Chemical Process Design: Computer-Aided Case Studies*. Wiley, 2008. ISBN 9783527621590.

[197] A.K. Majumdar and A.K. Mukherjee. Separation of niobium, tantalum, titanium and zirconium from each other. *Analytica Chimica Acta*, 23: 246–247, jan 1960. ISSN 00032670. doi: 10.1016/S0003-2670(60)80060-8.

[198] Desmond McMahon. World Class Vanadium Deposits | Vanadium Investing News, 2015. URL http://vanadiuminvestingnews.com/vanadium/world-class-vanadium-deposits.

[199] Roskill. *Vanadium: Global Industry Markets & Outlook*. Roskill Reports on Metals and Minerals. 2013.

[200] J J McKetta. *Encyclopedia of Chemical Processing and Design: Volume 61 - Vacuum System Design to Velocity: Terminal in Setting: Estimation*. Chemical Processing and Design Encyclopedia. Taylor & Francis, 1997. ISBN 9780824726126.

[201] U.S Geological Survey. Mineral commodity summaries. Technical report, 2014. URL http://minerals.usgs.gov/minerals/pubs/mcs/2014/mcs2014.pdf.

[202] C Stewart. Study of By-Products of Copper, Lead, Zinc and Nickel. In *By-Product Metals in Non-Ferrous Metals Industry*, Wroclaw, 2013. URL https://connect.innovateuk.org/documents/2865354/3895467/Study+of+By-Products+of+Copper{%}2CLead{%}2CNickel+{%}26+Zinc/2703f24f-14c6-4038-abb4-fb4f215327c6.

[203] Zaki Ahmad. The properties and application of scandium-reinforced aluminum. *JOM*, 55(2):35–39, 2003. doi: 10.1007/s11837-003-0224-6.

[204] Dirk Küster. Granitoid-hosted Ta mineralization in the Arabian–Nubian Shield: Ore deposit types, tectono-metallogenetic setting and petrogenetic framework. *Ore Geology Reviews*, 35(1):68–86, mar 2009. ISSN 01691368. doi: 10.1016/j.oregeorev.2008.09.008.

[205] D Lupton, F Aldinger, and K Schulze. *Niobium in Corrosive Environments*. Technology of metallurgy series. Metallurgical Society of AIME, New York, 1984.

[206] K Eguchi, M Machida, and I Yamanaka. *Science and Technology in Catalysis 2006: Proceedings of the Fifth Tokyo Conference on Advanced Catalytic Science and Technology, Tokyo, July 23-28, 2006*. Studies in Surface Science and Catalysis. Elsevier Science Limited, 2007. ISBN 9780444532022.

[207] T Ichimura. *Niobium Oxide in Optical Glass Manufacture*. Technology of metallurgy series. Metallurgical Society of AIME, New York, 1984. URL http://books.google.co.uk/books?id=ZslQAAAAYAAJ.

Appendix A

Appendix

A.1 Sampling

The conning and quartering sampling method was applied to the three batches of filter cake obtained from Huntsman Pigments and Additives and residues obtained from leaching and precipitation experiments reported herein. It is a widely used method for materials up to 50 tonnes where particle diameter is $\leq$ 5 cm. Dried residues are ground using a motor and pestle and formed into the shape of a cone on a clean flat surface. The top of the cone is then flattened and divided into 4 roughly equal quarters and a pair of opposite quarters is removed. The remaining pair is formed into a new cone and the process of quartering and rejection continued until a suitable quantity for leaching or analysis remains.

A.2 Cost effectiveness of V, Sc and Nb recovery

A chloride plant producing 250 tonnes per day TiO_2 generates between 150 - 250 tonnes of neutralised waste per day and can in theory recover:

- about 2000 kg per day V_2O_5, currently trading at \$13 - 15 per kg
- about 2000 kg per day Nb_2O_5, currently trading at \$40 - 45 per kg
- about 100 kg per day Sc_2O_3, currently trading at \$3500 - 5000 per kg

The major costs expected from a selective precipitation process are:

1. Reagents
    (a) Acid for leaching the filter cake - plant acid could be used (HCl)
    (b) Alkali for neutralisation/selective precipitation - NaOH costs about \$350 per tonne while $Ca(OH)_2$ costs about \$120 per tonne
    (c) Other reagents which are used for selective precipitation of purified vanadium (NH_4Cl) and scandium (such as oxalic acid)
2. Energy costs such as
    (a) Pumping of fluids
    (b) Mixing
    (c) Filtration
    (d) Roasting/calcination for producing metal oxides as final products
3. Capital costs

Although usage of $Ca(OH)_2$ for acid neutralisation is the cheapest option available, it should only be used after niobium has been precipitated from solution as this minimises contamination of the pH 1 precipitates with calcium sulphate (Fig. B.4). Solution neutralisation up to pH 1 should be done using NaOH instead. The costs associated with reagents can be summarised as:

- \$ 6830 per tonne of vanadium for neutralisation of chloride solution using NaOH, roasting pH 1.5 precipitates using NaCl and precipitating pure vanadium using NH_4Cl
- \$ 4100 per tonne of vanadium for raising pH to 1 using NaOH, neutralising the chloride solution using $Ca(OH)_2$, roasting pH 1.5 precipitates using NaCl and precipitating pure vanadium using NH_4Cl
- \$ 1980 per tonne of vanadium for neutralisation the chloride solution using $Ca(OH)_2$, roasting the pH 1.5 precipitates using NaCl and precipitating pure vanadium using NH_4Cl .

The average cost of energy in the UK is about \$0.15 per kWh for non-domestic use and total cost of energy used in a recovery process can be calculated provided some key information such as materials of construction (equipment), reaction temperatures, pulp density, *etc.* is available.

The processing steps developed in this project demonstrated an overall vanadium recovery of over 80 % with a grade of 99.5 %, meaning about 800 kg vanadium could be recovered from the waste. Similar recoveries are expected for niobium and scandium, based on the recoveries achieved during concentration enhancement. Analysis of the operating costs alone show that the process for metal recovery is feasible.

A V_2O_5 market price in the region of $13 000 - $15 000 per tonne of vanadium therefore means vanadium alone will be able to at least offset the energy and material costs even for scandium and niobium recovery since they are already in concentrated forms and are readily soluble in cheap reagents. As mentioned in recommendations for further work section (Section 7.8), a thorough economics assessment of such a process needs to be conducted before investing in a full scale plant. A pilot plant treating 50 kg filter cake per day may be a good start for initial assessment.

A.3 Recovery of lower value materials

A.3.1 Recovery of TiO_2

Recovery of TiO_2 from residues formed by HCl leaching of as received cake was attempted by employing two methods:

1. Alkali roasting of the residues
2. Baking of the residues in H_2SO_4

Alkali roasting of the residues attempted to form the water soluble sodium silicate (silica is the main impurity in the residues) via the reaction A.1:

$$Na_2CO_3 + SiO_2 \leftrightharpoons Na_2SiO_3 + CO_2 \tag{A.1}$$

The reaction shown by equation A.1 is thermodynamically feasible above 400 °C therefore temperatures of 800 °C and 900 °C were employed for the roasting. As shown in Fig. A.1, the reactants melted at both temperatures, making the recovery of TiO_2 almost impossible.

The second method employed for recovery of TiO_2 values involved baking the residues with H_2SO_4 at 300 °C for 60 minutes and water leaching the baked sample. The dissolved TiO_2 was then precipitated by bubbling the water leach

(a) Residues roasted at 800 °C

(b) Residues roasted at 900 °C

Fig. A.1 Effect of roasting HCl leach residues with Na_2CO_3 at 800 and 900 °C for 60 minutes.

filtrates with CO_2. A white TiO_2 precipitate with more than 98 % purity was obtained - Fig A.2.

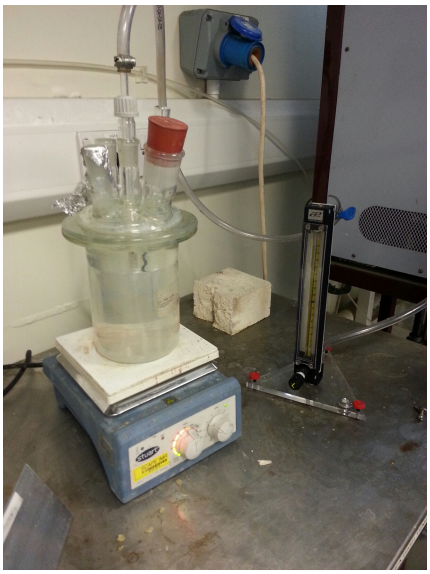

(a) Filtrates from H_2O leaching

(b) Precipitates from CO_2 bubbling

Fig. A.2 Recovery of TiO_2 from HCl leach residues by H_2SO_4 baking followed by H_2O leaching and CO_2 bubbling

A.3.2 Recovery of ZrO_2

Zirconium had a remarkably similar behaviour to niobium. The dependence of zirconium extraction on leaching temperature and time is presented in Fig. A.3.

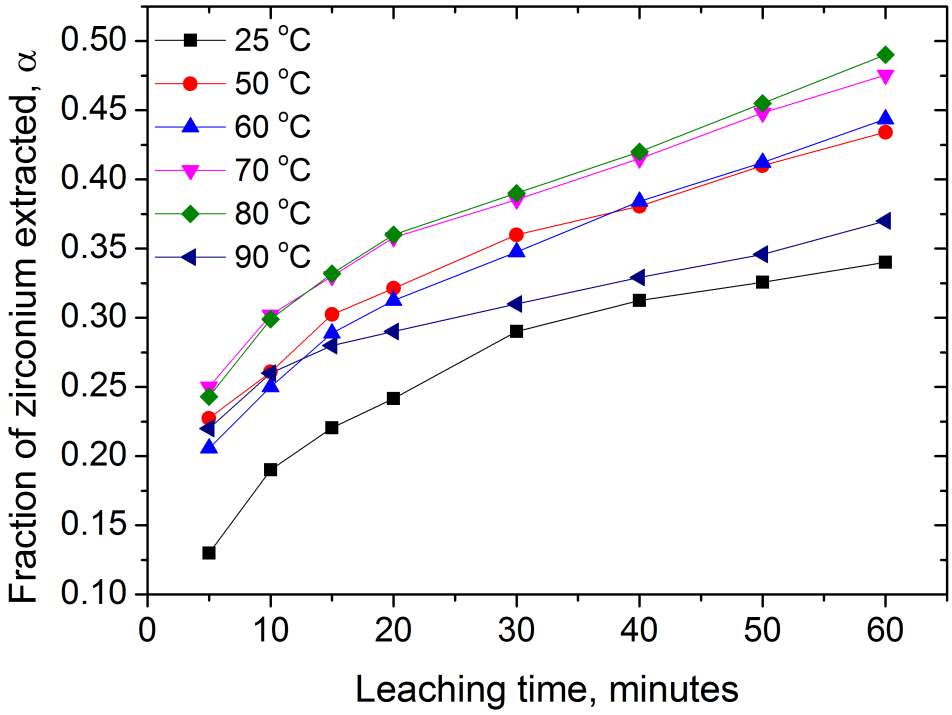

Fig. A.3 The extraction rate of zirconium in 1.5 M HCl at different temperatures over 60 minutes.

As with niobium extraction rate presented in Fig. 6.9, zirconium dissolution increased with temperature up to 80 °C and at 90 °C, the extraction rate decreased significantly.

Zirconium also precipitated at pH 1 with niobium and can be obtained from the precipitates using solvent extraction.

A.3.3 Recovery of Fe

Iron recovery was attempted by using an integrated metal recovery processing that employs alkali reduction instead of the selective precipitation approach. The alkali reduction process involved roasting the as-received filter cake with a predetermined amount of Na_2CO_3 at 900 °C under reducing conditions, followed by water leaching for recovery of the water soluble sodium vanadate. The reduced iron was magnetically separated from the 'slag'. Although the method showed great potential for recovery of iron and vanadium, the niobium and scandium values could not be recovered. It may be possible to recover iron from the final precipitates (pH $>$ 5) by washing residual NaCl off and employing a reduction process.

A.4 Conventional sources of V, Sc and Nb

In 2013, the European Commission identified 20 raw materials as critical to Europe's economy. Niobium was among the raw materials considered critical due to the risk in its supply security as well as its high economic importance within Europe. Although vanadium was not considered critical in Europe, it had the highest score in economic importance and scandium scored highly on supply security, making both worthy of continuous monitoring.

A.4.1 Vanadium

Sources and reserves

Vanadium is a relatively abundant trace element with a crustal abundance of 135 ppm, present in more than 65 different minerals [119] and fossil fuel deposits like crude oil, coal, and tar sands [198]. Due to the nature of vanadium mineralisation, there are currently no known mineral deposits in which vanadium occurs as a major constituent and therefore rarely gets mined and processed economically for vanadium recovery. Important naturally occurring sources of the metal include the hydrous potassium uranium vanadate, carnotite ($KU_4V_2O_{12}{\cdot}3H_2O$), the vanadium mica, rascoelite ($K_4(Mg, Fe)SiAl_4V_6O_{26}{\cdot}4H_2O$), the base metal vanadate, vanadinite ($Pb_{10}V_6O_{16}Cl_2$) and the complex sulphide, patronite (V_xS_y). Processing of the minerals or burning fossil fuels produces vanadium as a byproduct, but rarely in concentrations that can be economically exploited.

Figure A.4 illustrates the distribution of the four main types of vanadium sources. Nearly 50 % of the total vanadium is in titaniferous magnetites, almost 40 % in phosphorite and phosphatic shale deposits and the rest almost equally divided between Minnete type iron ores and crude petroleum. In minerals such as titaniferous magnetites, vanadium usually constitutes between 0.1 and 2 % of the host rock [198] and can therefore be produced as either a co-product or byproduct [17]. World reserves of vanadium have been reported to be in excess of 63 million tonnes [1], with China, South Africa and Russia supplying more than 99 % of the world's vanadium demand in 2014.

Key applications

The most important commercial property of vanadium is its ability to offer more performance (optimised balance of strength, weldability, toughness, ductility, corrosion resistance, and formability) per pound of steel. At least 90 % of the

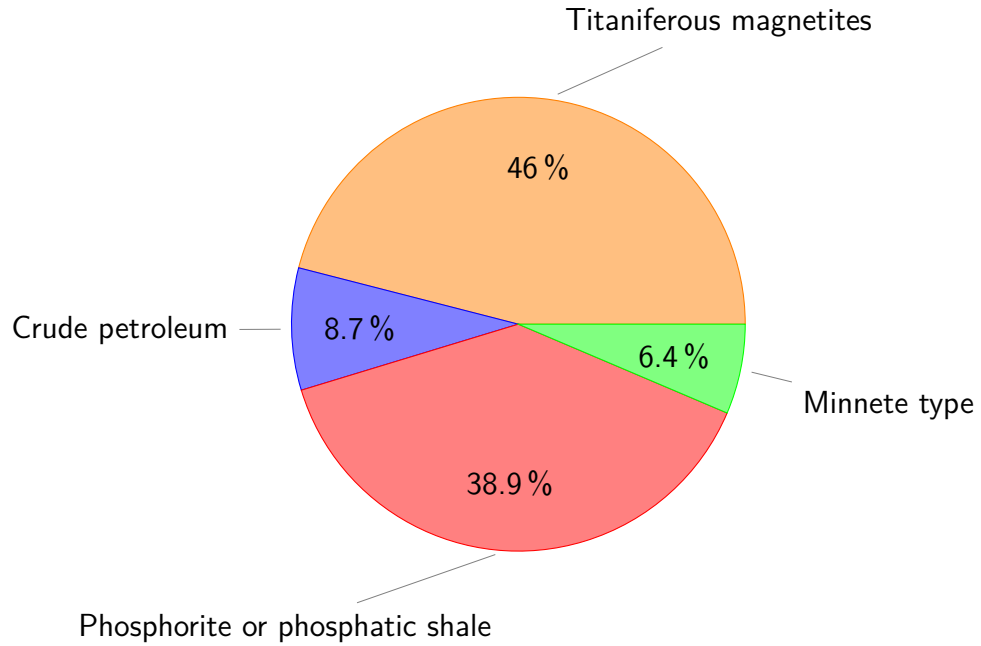

Fig. A.4 Distribution of vanadium in its major sources [17]

global end-use of vanadium is in the steel industry, with majority of remaining 10 % split between production of catalysts, chemicals and titanium alloys [199]. Global production of vanadium in 2014 was 78 000 tonnes [1] and the principal sectors consuming vanadium are summarised by Figure A.5.

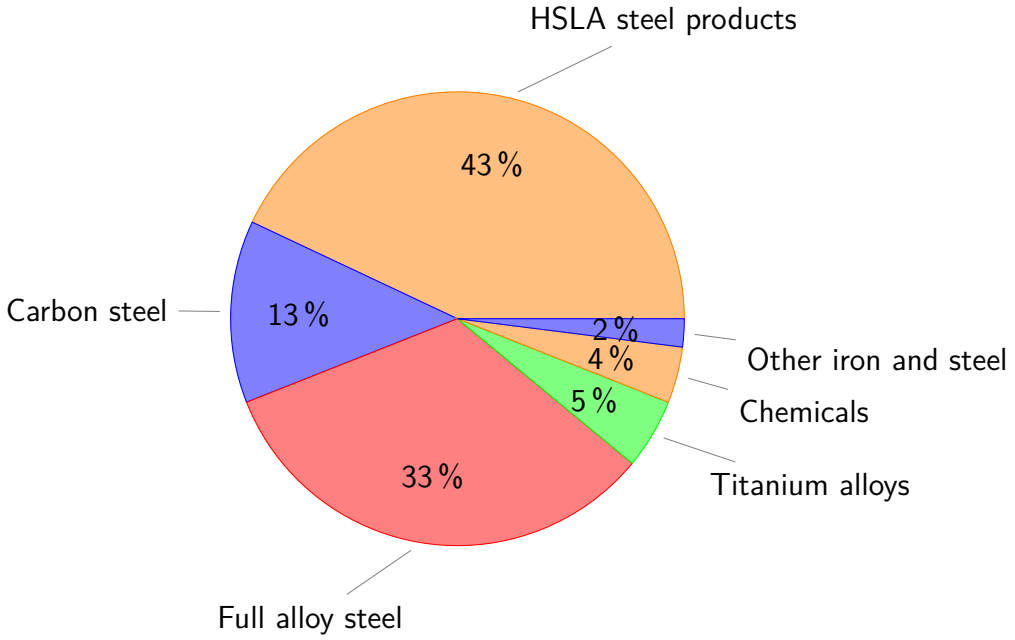

Fig. A.5 Global consumption of vanadium in various end-use categories in 2012 [199]

Due to their wear resistance, vanadium steels are used for making cutting tools. The steels also find usage in construction, iron and steel castings, springs, and ball bearings and in the chemicals industry, the major use of vanadium is as a catalyst in synthesis of sulphuric acid and oxidation of various organic compounds to commercial products [200].

A.4.2 Scandium

Sources and reserves

Scandium has a low affinity for the common ore-forming anions, and is therefore found distributed sparsely in trace amounts in rocks consisting of ferromagnesian minerals [79] and rarely concentrated [1]. It readily substitutes major elements such as iron and aluminium in minerals, forming solid solutions in more than 100 minerals. Primary ores with a scandium concentration of 20 - 50 ppm are considered worthy of exploitation [79]. As a consequence, scandium is exclusively produced as a byproduct from residues, tailings and waste liquors during production of other metals such as rare earths, aluminium and niobium.

Scandium is currently being produced as a byproduct in China (titanium and rare earths), Kazakhstan (uranium), Russia (apatite), and Ukraine (uranium). Like with many specialty metals, the scandium market is very small and decidedly opaque, making mapping of the supply chain very difficult. Making public the scandium pricing details would effectively 'set' the market and offer the competition and analysts a metric with which to compare various projects and the resulting economics. Global annual consumption is estimated to be in the region of 10 - 15 tonnes, based on 2013 figures [201]. Figure A.6 summarizes the key scandium producers. There are two pipeline projects in Australia which may supply scandium as either a byproduct from Ni-Co mining or as sole product [202].

Key applications

The principal use of scandium is in the making of aluminium-scandium alloys for minor aerospace industry components, where it limits the excessive grain growth that occurs in the heat-affected zone of welded aluminium components [203] thereby forming smaller crystals than those found in other aluminium alloys and reducing the volumes of precipitate free zones that are typical at the grain boundaries of age hardening aluminium alloys [203]. Another emerging

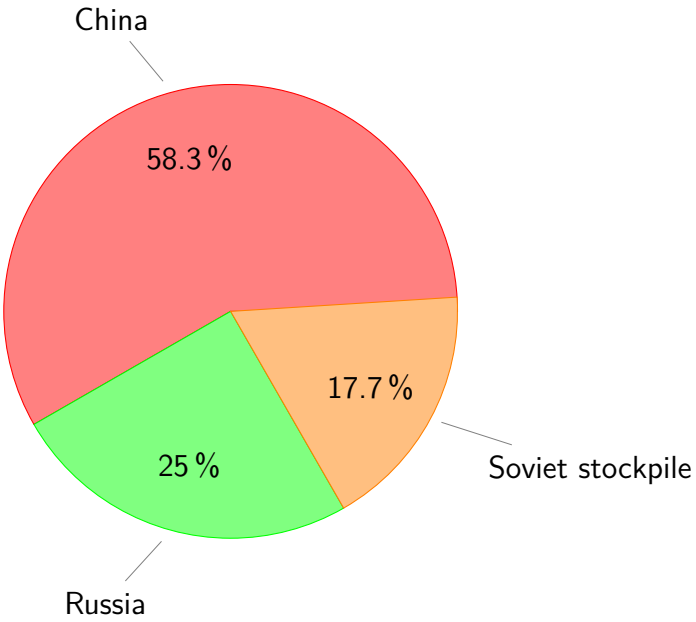

Fig. A.6 Global supply of scandium in 2012 [202]

use of scandium is in solid oxide fuel cells (SOFCs) which generate electricity directly by oxidising a fuel [1]. Scandium is also used in ceramics, electronics, lasers and lighting, but new supplies and market development are needed for full benefits of scandium usage to be realised [202]. Figure A.7 summarises the key applications of scandium.

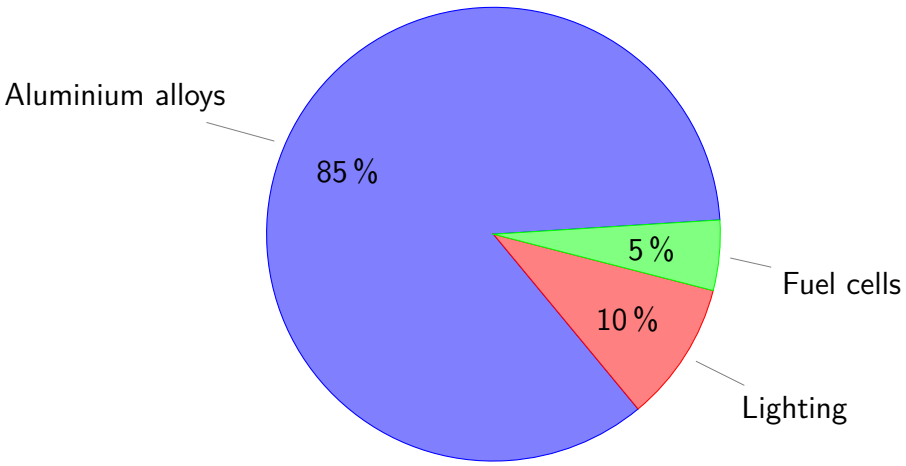

Fig. A.7 Key applications of scandium [202]

A.4.3 Niobium

Sources and reserves

Compared to a lot of metals, light rare earths included, niobium has a relatively low abundance (24 parts per million (ppm)) in the average continental crust [112]. Niobium mineral deposits are most commonly associated with igneous rocks, the most important mineral being pyrochlore, $(Ca,Na)_{2-m}Nb_2O_6(O,OH,F)_{1-n}xH_2O$ where the lattice positions of Ca and Na can also be occupied by elements such as Ba, Sr, rare earths, Th and U [109]. In primary deposits, pyrochlore is always inter stratified in carbonates containing between 0.5 and 0.7% niobium pentoxide. Depending on the type of igneous rock they are associated with, niobium deposits can be divided into three main types [204].

1. Carbonatites and associated rocks
2. Alkaline to peralkaline granites and syenites
3. Granites and pegmatites of the lithium (Li), caesium (Cs) and tantalum (Ta) (LCT family)

Although moderately high contents of niobium have been observed in some granites and pegmatites that are not part of the three categories mentioned above, there are no known economic examples [110]. Commercially important niobium deposits are in Brazil, Canada, Nigeria and Zaire, with the Brazilian ores containing the highest percentage of niobium (2.5 - 3%) from secondary deposits where the niobium has been enriched by weathering [109, 110]. Columbite, $(Fe,Mn)(Nb,Ta)_2O_6$ is the second most important niobium ore deposit. Niobium can also be present in rare earths (RE) such as stibiocolumbites $(Sb(Nb,Ta)O_4)$, fergusonites $(RENbO_4)$ and euxenites $((Y,Ca,Ce,U,Th)(Nb,Ta,Ti)_2O_6)$.

Figure A.8 summarises the world primary production of niobium in 2014. According to the U.S Geological survey [1], Brazil led the niobium production industry with 90 % of global production, followed by Canada with 9 % in 2014.

Key applications

Figure A.9 highlights the major applications of niobium in 2010. The steel industry represents almost 90 % of the global niobium demand. Metallic niobium has very high resistance to corrosion by chemicals [205] even at high

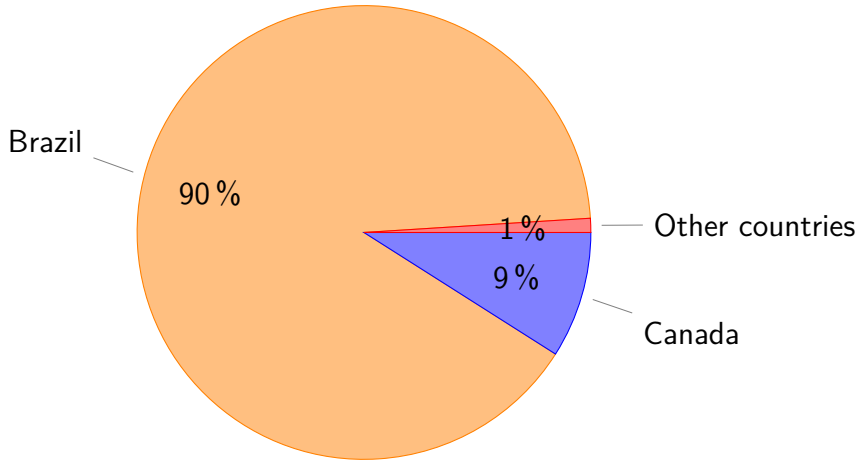

Fig. A.8 World primary production of niobium [1]

temperatures, hence has a major role in construction of chemical equipment. As much as 85 % of global niobium demand is used for making ferroniobium, which is subsequently used in the steel industry for manufacturing high strength low alloy and carbon steels. Addition of only 200 ppm niobium can significantly increase the yield and tensile strength of steel [116], providing qualities that are required for usage of the steels in construction, oil and gas pipelines and in the automotive industry.

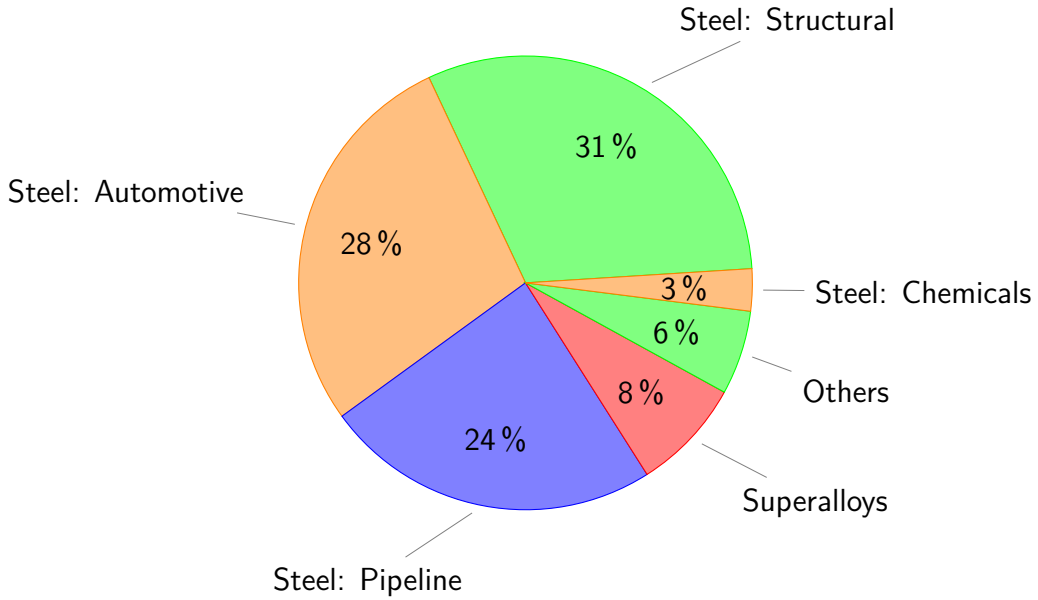

Fig. A.9 Key applications of niobium [1]

Hydrated Nb_2O_5 can be regarded as an isopoly acid with a high surface acidity and therefore has usage as a catalyst in the polymerisation of alkenes

[206]. Consumption of niobium for production of superconducting materials such as Nb_3Sn and NbTi is estimated to be between 60 and 70 tonnes per year around the globe [123]. Niobium can also be added to tantalum-aluminium alloys to improve on their ductility, hence improving their applicability in aircraft and space industry. NbC is primarily used as a grain growth inhibitor in tungsten carbide hard materials but can also be used with titanium carbide, tantalum carbide and tungsten carbide for cutting tools. Nb_2O_5 is added to molten glass to prevent devitrification and to control properties such as refractive index and light absorption [207].

Appendix B

Raw data and rate constants tables

Some of the data and results from qualitative analysis of samples summarised in main text is presented herein to highlight the variability of compositions reported.

B.1 Analysis of as-received cake

B.1.1 XRF analysis of as-received cake batches

Tables B.1, B.2 and B.3 show the raw data from XRF analysis of five samples from each of the as-received cake batches.

Table B.1 XRF analysis of batch 1 (B1)

	TiO_2	Fe_2O_3	V_2O_5	Sc_2O_3	Nb_2O_5	Al_2O_3	CaO	ZrO_2	ThO_2	LOI(%)
S1	27.1	37.3	1.7	720*	1.7	5.0	9.8	1.2	0.1	32
S2	27.3	36.9	1.8	786*	1.7	5.3	9.7	1.4	998*	31
S3	28.1	36.2	1.8	757*	1.6	5.2	9.4	1.3	0.1	30
S4	28.0	36.2	1.6	742*	1.6	5.3	9.5	1.4	986*	31
S5	27.5	37.4	1.6	729*	1.5	5.2	9.6	1.3	988*	29

*= ppm

Table B.4 shows that despite some vanadium dissolving in the solvent rutile matrix, majority of it is present in the iron-rich precipitates. Thorium and scandium were not detected by EDX analysis and this may be because their composition is lower than the instrument's limit of detection.

Table B.2 XRF analysis of batch 2 (B2)

	TiO_2	Fe_2O_3	V_2O_5	Sc_2O_3	Nb_2O_5	Al_2O_3	CaO	ZrO_2	ThO_2	LOI(%)
S1	33.1	25.9	2.0	820*	2.4	4.8	10.2	2.2	933*	28
S2	34.2	24.9	2.2	839*	2.2	4.9	9.9	2.3	0.1	27
S3	34.0	25.0	2.0	930*	2.2	4.9	9.8	2.5	992*	28
S4	33.0	25.5	2.0	932*	2.3	4.6	9.9	2.4	979*	29
S5	34.0	25.7	2.3	930*	2.4	4.8	9.7	2.5	998*	29

*= ppm

Table B.3 XRF analysis of batch 3 (B3)

	TiO_2	Fe_2O_3	V_2O_5	Sc_2O_3	Nb_2O_5	Al_2O_3	CaO	ZrO_2	ThO_2	LOI(%)
S1	28.9	24.5	2.2	340*	2.3	5.9	10.6	5.5	0.1	26
S2	29.5	23.9	2.1	430*	2.3	5.6	10.7	5.9	0.1	28
S3	29.4	24.5	1.9	322*	2.1	6.0	10.5	5.8	990*	28
S4	28.8	24.2	2.2	314*	2.0	5.3	10.4	6.0	0.1	25
S5	29.4	24.4	2.1	355*	2.3	5.8	10.7	5.7	0.1	29

*= ppm

Table B.4 SEM-EDX semiquantitative analysis (wt. %) of the as-received filter cake - obtained from points numbered 1, 2 and 3 in Fig. 3.2 and converted to oxide concentrations.

	TiO_2	SiO_2	V_2O_5	Nb_2O_5	Fe_2O_3	ZrO_2	Al_2O_3	ThO_2
1	97.3	0	1.6	0	1.1	0	0	0
2	5.8	0.7	3.8	1.5	69.9	2.3	16.0	0
3	3.8	0	4.6	1.2	75.5	1.6	13.3	0

B.1.2 SEM analysis of as-received cake batches

As-received cake batches (B1, B2 and B3) were analysed by SEM-EDX and the results are presented in Figs. B.1, B.3 and B.2.

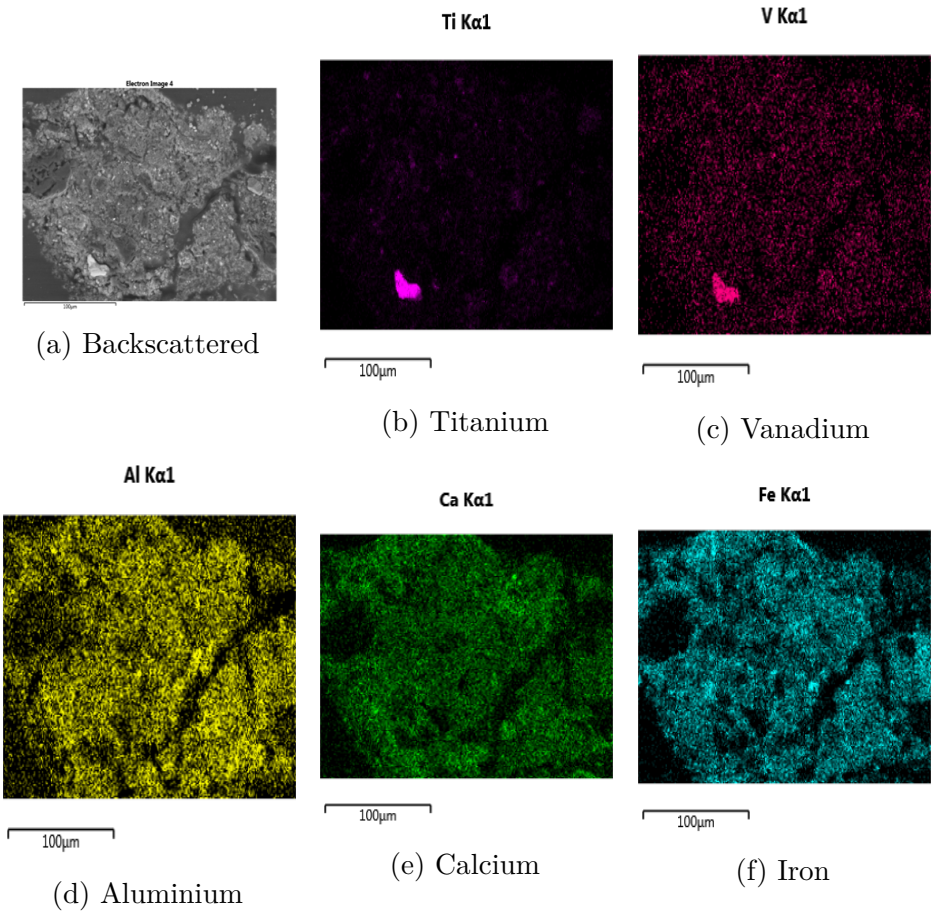

(a) Backscattered (b) Titanium (c) Vanadium

(d) Aluminium (e) Calcium (f) Iron

Fig. B.1 Elemental mapping of the as-received filter cake (Batch 1)

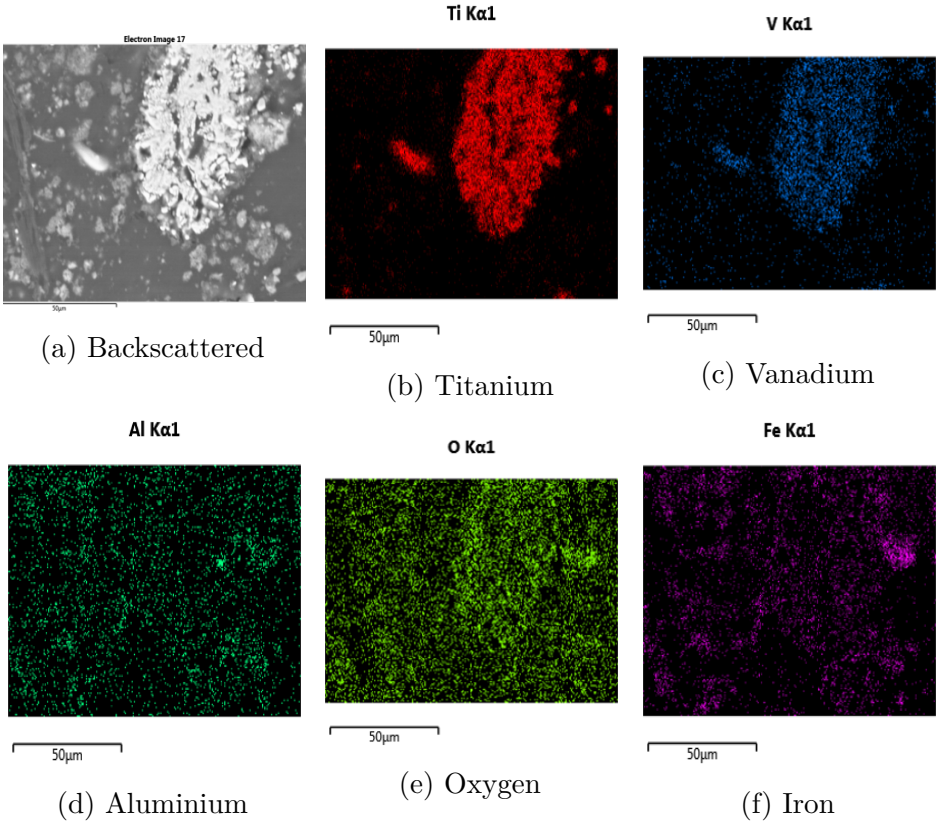

(a) Backscattered (b) Titanium (c) Vanadium

(d) Aluminium (e) Oxygen (f) Iron

Fig. B.2 Elemental mapping of the as-received filter cake (Batch 2)

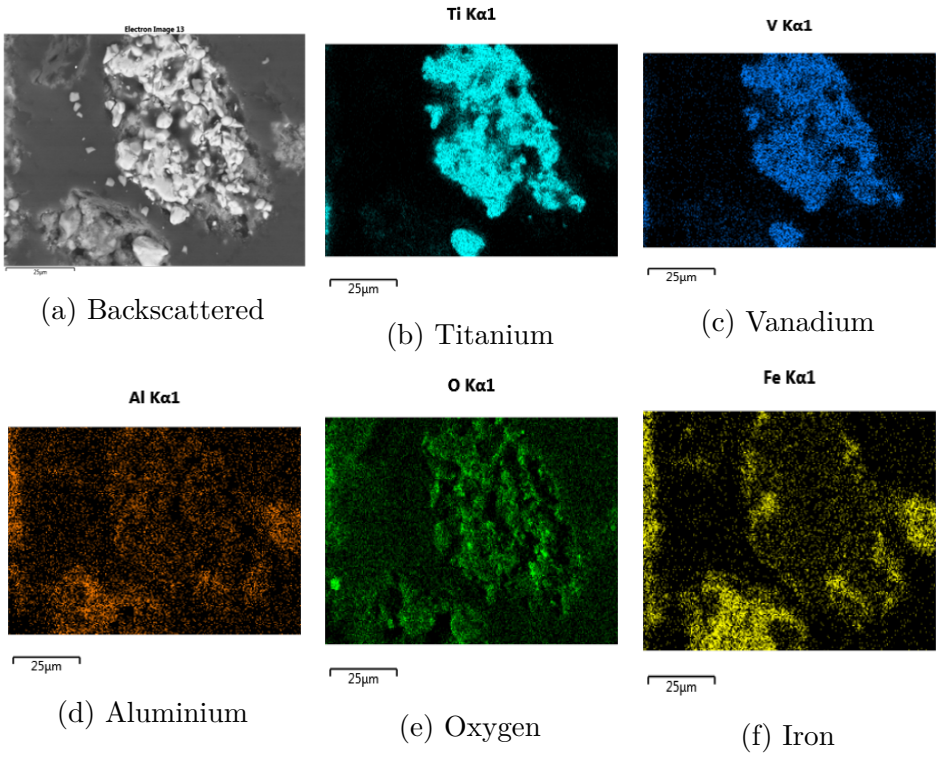

(a) Backscattered (b) Titanium (c) Vanadium

(d) Aluminium (e) Oxygen (f) Iron

Fig. B.3 Elemental mapping of the as-received filter cake (Batch 3)

B.2 Analysis of treated cake samples

B.2.1 EDX analysis of HCl leached cake - from Fig. 6.22

Table B.5 summarises the semi-quantitative analysis results for the sample presented in Fig. 6.22.

Table B.5 SEM-EDX semiquantitative analysis (wt. %) of the residues after leaching filter cake under optimised conditions - obtained from Fig. 6.22b.

	TiO_2	SiO_2	V_2O_5	Nb_2O_5	ThO_2
1	96.6	0.57	1.2	1.6	ND
2	97.7	0.58	1.1	0.6	ND
3	65.9	30.3	2.6	1.2	ND
4	14.0	85.7	0.3	0	ND

ND= Not Detected

B.2.2 EDX analysis of niobium-rich precipitates from Fig. 6.26

Table B.6 presents the EDX analysis of points 1, 2, 3 and 4 marked on the SEM migrograph presented in Fig. 6.26.

Table B.6 Compositions of precipitates formed at 90 °C and pH 1 over a total time of 180 minutes.

	TiO_2	Fe_2O_3	V_2O_5	Nb_2O_5	ZrO_2	Al_2O_3	ThO_2
1	35.2	19.3	3.0	27.9	13.5	1.0	0.2
2	32.9	32.2	3.0	20.9	9.6	1.0	0.3
3	32.1	29.2	3.0	24.2	10.4	0.8	0.4
4	33.1	28.8	2.9	22.4	11.5	0.9	0.3

B.2.3 XRD analysis of pH 1 precipitates

Fig. B.4 presets the XRD graph from analysis of pH 1 precipitates.

B.2.4 EDX analysis of vanadium-rich precipitates

Table B.7 presents the EDX analysis of points 1, 2 and 3 marked on the SEM migrograph presented in Fig. 6.30 and A, B and C as marked on Fig 6.29.

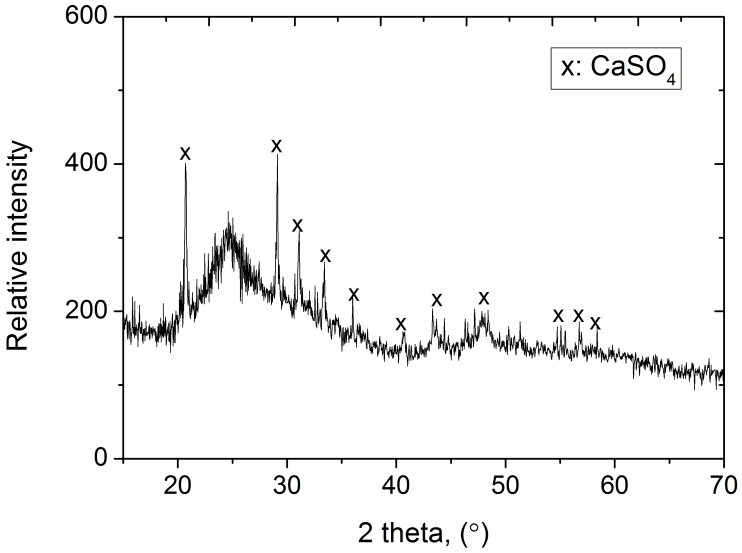

Fig. B.4 XRD analysis of pH 1 precipitates for phase determination.

Table B.7 SEM-EDX semiquantitative analysis (wt. %) of the pH 0.5 and pH 1.5 precipitates - obtained from Fig. 6.30 and Fig 6.29 respectively.

	TiO_2	Fe_2O_3	V_2O_5	Nb_2O_5	ZrO_2	Al_2O_3	ThO_2
1	17.3	38.2	35.8	2.9	4.8	0.9	0.2
2	32.4	51.6	4.5	5.3	4.7	1.2	0.2
3	20.4	46.9	4.4	15.2	13.0	ND	0.2
A	0.2	79.6	16.2	0.5	0.8	2.6	ND
B	1.6	78.5	14.8	0.7	1.4	3.0	ND
C	0.4	80.9	14.2	0.6	1.1	2.9	ND

ND= Not Detected

B.2.5 EDX analysis of pH 5 precipitates

Table B.8 presents the EDX analysis of points 1, 2 and 3 marked on the SEM migrograph presented in Fig. 6.36.

Table B.8 SEM-EDX semiquantitative analysis (wt. %) of the pH 5 precipitates - obtained from points numbered 1, 2 and 3 in Fig. 6.36.

	Al_2O_3	Fe_2O_3	MnO_2	CaO	Sc_2O_3	TiO_2	ThO_2
1	53.1	24.0	17.9	4.5	0.5	ND	ND
2	59.6	16.1	19.7	4.0	0.6	ND	ND
3	17.0	67.2	14.8	0.7	0.3	ND	ND

B.2.6 EDX analysis of impurities formed during NH_4VO_3 precipitation steps

Table B.9 presents the EDX analysis of points 1 and 2 marked on the SEM migrograph presented in Fig. 6.51a.

Table B.9 SEM-EDX semiquantitative analysis (wt. %) of the precipitated pH 8 impurities - obtained from points numbered 1 and 2 in Fig. 6.51a.

	Al_2O_3	ZrO_2	CaO	Na_2O	Sc_2O_3	V_2O_3	ThO_2
1	85.0	1.8	1.6	0.3	ND	11.1	ND
2	82.2	3.0	3.1	2.3	ND	9.5	ND

B.2.7 EDX analysis of sodium-rich precipitates (pH 1)

Table B.10 presents the EDX analysis of points 1 and 2 marked on the SEM migrograph presented in Fig. 6.58.

Table B.10 SEM-EDX semiquantitative analysis (wt. %) of the pH 1 precipitates - obtained from Fig. 6.58.

	TiO_2	V_2O_5	CaO	Na_2O	Sc_2O_3	Al_2O_3	ThO_2
1	ND	ND	ND	100	ND	ND	ND
2	92.1	3.6	ND	4.3	ND	ND	ND

B.3 Analysis of precipitates by XRF

Analysis of some of the precipitates formed during the processing of filter cake are presented in tables B.11, B.12 and B.13.

Table B.11 presents the compositions of precipitates formed from leaching washed and dried cake in HCl followed by pH adjustment to 0.5 using NaOH.

Table B.12 summarises the compositions of precipitates formed from leaching fresh as-received cake in HCl followed by selective precipitation at pH 1.5 using NaOH.

Table B.13 summarises the compositions of pH 5 precipitates where the scandium and REE precipitate.

Table B.11 XRF analysis of pH 0.5 precipitates -

	TiO_2	Fe_2O_3	V_2O_5	Nb_2O_5	Al_2O_3	ZrO_2	ThO_2
S1	16.3	32.7	5.5	13.1	0.3	13.3	0.5
S2	16.7	32.8	6.1	12.7	0.4	12.7	0.4
S3	16.8	33.4	5.9	12.6	0.7	12.8	0.5
S4	16.2	33.5	5.3	12.3	0.5	13.1	0.6
S5	16.5	33.0	5.7	12.4	0.7	12.6	0.5

Table B.12 XRF analysis of pH 1.5 precipitates -

	TiO_2	Fe_2O_3	V_2O_5	Nb_2O_5	Al_2O_3	ZrO_2	ThO_2
S1	ND	73.6	9.5	0.6	2.3	0.3	ND
S2	ND	72.4	9.9	0.9	1.8	0.6	ND
S3	ND	74.3	9.6	0.7	1.9	0.5	ND
S4	560*	74.6	9.3	0.6	2.1	0.4	ND
S5	500*	74.4	9.4	0.6	1.9	0.4	ND

*= ppm

Table B.13 XRF analysis of pH 5 precipitates

	TiO_2	Fe_2O_3	V_2O_5	Sc_2O_3	Y_2O_3	CeO_2	Al_2O_3	ThO_2(%)
S1	ND	34.5	ND	0.6	0.3	0.4	18.6	ND
S2	ND	33.9	ND	0.6	0.3	0.6	18.7	ND
S3	ND	35.7	ND	0.3	0.1	0.5	17.9	ND
S4	ND	34.7	ND	0.3	0.2	0.2	18.3	ND
S5	ND	34.8	298*	0.3	0.1	0.3	18.4	ND

*= ppm

B.4 NaOH usage

The average amounts of NaOH used for recovery of niobium, vanadium and scandium from the 1 kg batch experiment are summarised in Fig. B.5.

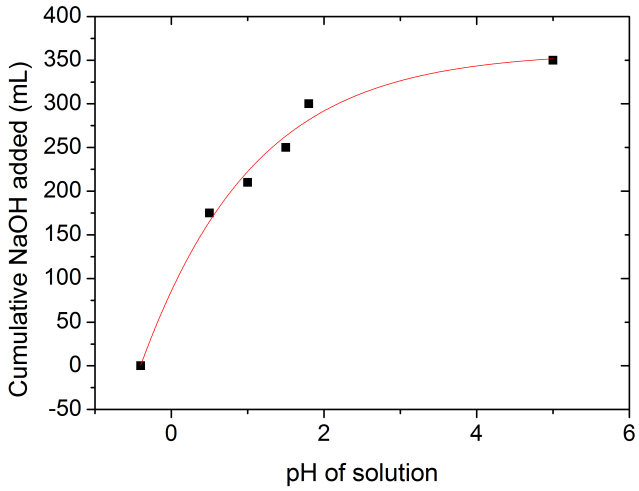

Fig. B.5 Cumulative amount of NaOH required for selective precipitation

B.5 Kinetic parameters

Parameters for kinetics of metal dissolution form filter cake (Acid) and from relative precipitates (Alkali) are presented in tables B.14 - B.16.

B.5.1 Niobium leaching

Table B.14 presents the pore diffusion and surface reaction controlled kinetics parameters for niobium leaching in HCl and in Na_2CO_3 - $NaNO_3$

Table B.14 Parameters for pore diffusion and surface reaction controlled kinetics for niobium leaching in HCl and in Na_2CO_3 - $NaNO_3$

Temp	Acid leach Parameters			Alkali leach parameters		
	P.D	S.R		P.D	S.R	
	k	ψ	k*	k	ψ	k*
25	2.44×10^{-4}	-1.61×10^{1}	6.28×10^{-4}	2.93×10^{-8}	-4.45×10^{2}	6.04×10^{-5}
50	5.85×10^{-3}	-1.38×10^{1}	1.84×10^{-3}	5.09×10^{-6}	-3.23×10^{1}	7.61×10^{-4}
60	6.84×10^{-3}	-1.16×10^{1}	2.07×10^{-3}	1.61×10^{-5}	-1.94×10^{1}	1.66×10^{-3}
70	7.91×10^{-3}	-9.70×10^{0}	2.31×10^{-3}	3.54×10^{-5}	-1.30×10^{1}	2.55×10^{-3}
80	8.17×10^{-3}	-9.40×10^{0}	2.42×10^{-3}	5.60×10^{-5}	-1.02×10^{1}	3.61×10^{-3}
90	6.55×10^{-3}	-1.93×10^{1}	1.47×10^{-3}	1.01×10^{-4}	-7.05×10^{0}	6.04×10^{-3}

P.D = Pore Diffusion; S.R = Surface reaction

B.5.2 Vanadium leaching

Table B.15 presents the pore diffusion and surface reaction controlled kinetics parameters for niobium leaching in HCl and in Na_2CO_3 - $NaNO_3$

Table B.15 Parameters for pore diffusion and surface reaction controlled kinetics for vanadium leaching in HCl and in Na_2CO_3 - $NaNO_3$

Temp	Acid leach Parameters			Alkali leach parameters		
	P.D	S.R		P.D	S.R	
	k	ψ	k*	k	ψ	k*
25	2.99×10^{-3}	-	-	1.08×10^{-4}	-1.15×10^{0}	2.58×10^{-3}
50	3.68×10^{-3}	-7.39×10^{-1}	6.70×10^{-2}	5.69×10^{-4}	-2.99×10^{0}	9.35×10^{-3}
60	4.18×10^{-3}	-6.60×10^{-1}	7.43×10^{-2}	9.05×10^{-4}	-2.03×10^{0}	1.08×10^{-2}
70	4.75×10^{-3}	-5.86×10^{-1}	8.25×10^{-2}	1.35×10^{-3}	-1.36×10^{0}	1.28×10^{-2}
80	5.48×10^{-3}	-5.52×10^{-1}	9.10×10^{-2}	1.95×10^{-3}	-9.72×10^{-1}	1.52×10^{-2}
90	6.35×10^{-3}	-4.57×10^{-1}	1.00×10^{-1}	3.47×10^{-3}	-6.47×10^{-1}	2.12×10^{-2}

P.D = Pore Diffusion; S.R = Surface reaction

B.5.3 Scandium leaching

Table B.16 presents the pore diffusion and surface reaction controlled kinetics parameters for niobium leaching in HCl and in Na_2CO_3 - $NaNO_3$

Table B.16 Parameters for pore diffusion and surface reaction controlled kinetics for scandium leaching in HCl and in Na_2CO_3 - $NaNO_3$

Temp	Acid leach Parameters			Alkali leach parameters		
	P.D	S.R		P.D	S.R	
	k	ψ	k*	k	ψ	k*
25	2.69×10^{-4}	-4.34×10^{3}	-1.59×10^{3}	-	-	-
50	3.15×10^{-4}	-4.34×10^{3}	-1.59×10^{3}	1.65×10^{-4}	-5.68×10^{0}	7.06×10^{-3}
60	3.60×10^{-4}	-4.17×10^{3}	-1.53×10^{3}	3.26×10^{-4}	-3.57×10^{0}	1.16×10^{-2}
70	4.01×10^{-4}	-4.16×10^{3}	-1.53×10^{3}	6.55×10^{-4}	-2.46×10^{0}	1.64×10^{-2}
80	4.35×10^{-4}	-4.14×10^{3}	-1.52×10^{3}	6.45×10^{-3}	-6.21×10^{-1}	6.44×10^{-2}
90	4.88×10^{-4}	-4.06×10^{3}	-1.49×10^{3}	9.93×10^{-4}	-4.08×10^{-1}	9.79×10^{-2}

P.D = Pore Diffusion; S.R = Surface reaction

B.5.4 Thorium leaching

Table B.17 presents the pore diffusion controlled kinetics for thorium leaching in HCl.

Table B.17 Parameters for pore diffusion controlled kinetics for thorium leaching in HCl

Reaction Temp (°C)	Diffusion controlled kinetics			
	First stage		Second stage	
	k (min^{-1})	R^2	k (min^{-1})	R^2
25	2.98×10^{-3}	0.9853	2.82×10^{-4}	0.9979
50	3.20×10^{-3}	0.9775	3.85×10^{-4}	0.9977
60	3.29×10^{-3}	0.9826	4.29×10^{-4}	0.9980
70	3.37×10^{-3}	0.9867	4.72×10^{-4}	0.9964
80	3.42×10^{-3}	0.9842	4.96×10^{-4}	0.9979
90	3.54×10^{-3}	0.9812	5.33×10^{-4}	0.9987

B.6 Precision and measurement uncertainties

Tables B.18 (Niobium), B.19 (vanadium) and B.20 (scandium) present the data from repeat analysis of 4 samples drawn from reactor after 60 minutes of leaching.

Table B.18 Repeat analysis of three niobium samples drawn after 60 minutes of leaching filter cake at 70 °C. Values reported as fraction extracted.

Repeat analysis	Sample 1	Sample 2	Sample 3	Sample 4
1	0.93	0.88	0.93	0.90
2	0.89	0.91	0.92	0.89
3	0.90	0.90	0.94	0.90
4	0.91	0.93	0.93	0.91
5	0.90	0.89	0.92	0.89

Table B.19 Repeat analysis of three vanadium samples drawn after 60 minutes of leaching filter cake at 70 °C. Values reported as fraction extracted.

Repeat analysis	Sample 1	Sample 2	Sample 3	Sample 4
1	0.99	0.97	0.96	0.98
2	0.98	0.98	0.98	0.96
3	0.98	0.98	1.0	0.98
4	1.0	0.99	0.99	0.97
5	0.99	0.96	0.97	0.99

Table B.20 Repeat analysis of three scandium samples drawn after 60 minutes of leaching filter cake at 70 °C. Values reported as fraction extracted.

Repeat analysis	Sample 1	Sample 2	Sample 3	Sample 4
1	0.93	0.94	0.95	0.94
2	0.95	0.93	0.94	0.95
3	0.92	0.95	0.94	0.95
4	0.91	0.92	0.93	0.93
5	0.95	0.91	0.95	0.94